United States
Environmental Protection
Agency

Great Lakes National
Program Office
536 South Clark Street
Chicago, Illinois 60605

EPA-905/4-79-016

EPA

An Experimental Study of Lake Loading by Aerosol Transport and Dry Deposition in the Southern Lake Michigan Basin

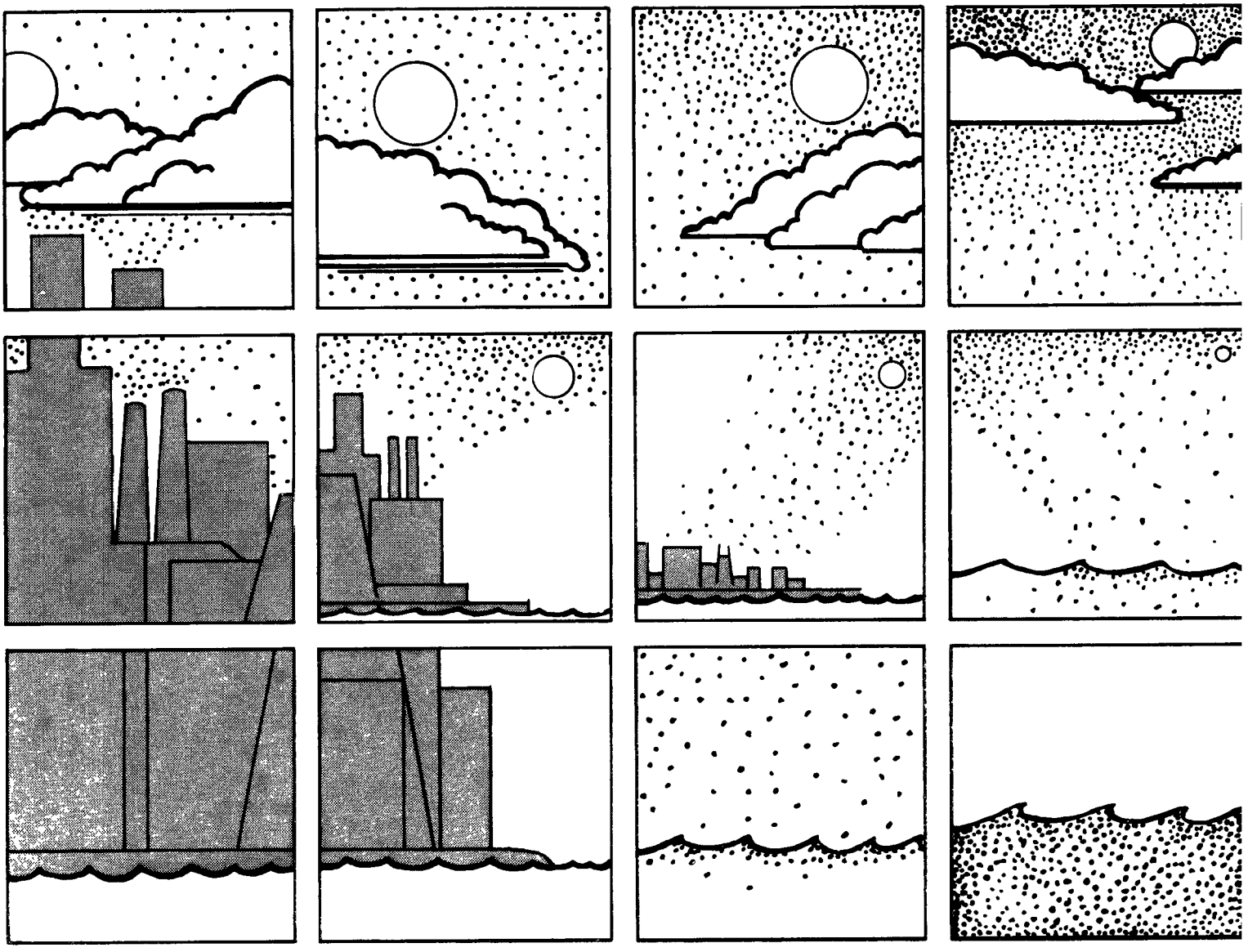

EPA-905/4-79-016
July, 1979

AN EXPERIMENTAL STUDY OF LAKE LOADING BY AEROSOL TRANSPORT AND DRY DEPOSITION IN THE SOUTHERN LAKE MICHIGAN BASIN

by

Herman Sievering
Mehul Dave'
Donald A. Dolske
Richard L. Hughes
Patric McCoy

U. S. EPA Grant Number
R005301 01

Project Officer

J. Regan, Chief
Air Surveillance Branch
U.S. Environmental Protection Agency

Final Report for the Period June 1976-July 1979

GREAT LAKES NATIONAL PROGRAM OFFICE
U.S. ENVIRONMENTAL PROTECTION AGENCY
536 SOUTH CLARK STREET, ROOM 932
CHICAGO, ILLINOIS 60605

DISCLAIMER

This report has been reviewed by the Great Lakes National Program Office, Region V, U.S. Environmental Protection Agency, and approved for publication. Approval does not signify that the contents necessarily reflect the views and policies of the U.S. Environmental Protection Agency, nor does mention of trade names or commercial products constitute endorsement or recommendation for use.

FOREWORD

This study was supported by a Great Lakes National Program grant to Governors State University for investigating the rate of deposition of atmospheric transported pollutants to southern Lake Michigan as a result of the industrial complex located on the southern shores of Lake Michigan. The R/V Simons, a laboratory and lake water quality sampling ship, operated by this office, was used to support this project. Data in this report covers a period from June 1976 to July 1979.

Madonna F. McGrath
Director
Great Lakes National Program Office

PREFACE

The enclosed document represents our best description of a three year effort to gather field data, analyze the collected data by computer as well as manually, and interpret the results in the context of Lake Michigan climatology. Data base interpretation is far from complete at this writing for the field program generally met with good and, often, excellent weather conditions. Coupled with a superior field crew, conditions were ripe for a rich bounty of data. Even in poor weather the crew succeeded upon the seas of Lake Michigan. Mehul Davė, Don Dolske, Mike Eason, Jil Forst, Vic Jensen, Pat McCoy, Rich Rupert, Nell Sutton, Keith Walther and Ebbe Ward are all to be thanked for making possible the great success achieved. Their collective spirit was the equal of this unknown sailor's:

> A strong nor'wester's blowin, Bill
> Hark! don't ye hear it roar now?
> Lord help 'em, how I pities them
> Unhappy folks on shore now!

No less spirited were grant secretaries Cindy Overton and B.J. Yates, who created readable English out of often unintelligible scribblings. Research Associate Richard Hughes brought order and coherence to this document as its Editor. Special thanks go to all the Research Associates, Mehul Davė, Don Dolske, Pat McCoy and Richard Hughes for their computer and laboratory analysis efforts and help in every other respect of grant activity over these past three years.

Many persons among the Governors State University support staff were extremely helpful to the completion of this effort. Don Douglas and Ted Andrews were especially helpful. Staff members of the USEPA are also to be thanked: Bob Bowden and Jerry Regan for their administrative support; Capt. McLain and the crew of the R/V Simons for bringing us through those storms; and the staff at EPA's Central Regional Laboratory. Aircraft support of the project was gratefully supplied by the Research Aviation Facility (RAF) at the National Center for Atmospheric Research. To Paul Spyers-Duran and Pete Orum of RAF special thanks.

As Principal Investigator of this grant I accept full responsibility for any errors of omission or commission.

July, 1979

Herman Sievering
Park Forest South, Illinois

EXECUTIVE SUMMARY

A Lake Michigan experimental program to assess the contribution to Great Lakes loading by atmospheric transport and dry deposition has been completed. The first midlake trace metal and nutrients data base with associated meteorology capable of establishing a climatology for both midlake aerosol mass concentrations and mass transfer to Lake Michigan was collected during May to October 1977. Trace metal concentrations were determined by atomic emission spectroscopy for seventeen elements. Of these, nine elements were significantly above instrumental detection limits, filter blank concentrations, and laboratory contamination, viz., Al, Ca, Cu, Fe, Mg, Mn, Pb, Ti and Zn. Nutrient species phosphate, nitrate, and sulfate were determined by standard USEPA automated spectrophotometric techniques. A mid-Lake Michigan concentration climatology was estimated for each of these twelve aerosol constituents. A strong linear dependence of the variability in all these concentrations upon atmospheric thermal stability and, thus, season of the year was found. No linear dependence on wind speed was found, but event analysis suggests a strong dependence of concentration variability on wind direction changes. Source region dependence was found to cause as much as an order of magnitude change in concentrations. Source type identification has been successful to the extent that soil, lake, and anthropogenically derived components have been specified. The percentage considered to be anthropogenically derived for each of the nine trace elements above is: Al, 0; Ca, 0; Cu, $\geq$ 90%; Fe, $\geq$ 65%; Mg, 0; Mn, $\geq$ 80%; Pb, $\geq$ 95%; Ti, 0; and Zn, $\geq$ 75%. A detailed case study of aircraft data taken on September 30, 1977 has investigated the change in aerosol size distribution as a function of traverse over the lake and meteorological conditions.

The rate of aerosol deposition from the atmosphere to the lake by dry processes is taken to be approximately equal to the deposition velocity just above the lake's surface. A value for the deposition velocity was estimated by a product of wind speed and diabatic momentum drag coefficient, accounting for thermal stability effects. This parameterized deposition velocity, $\tilde{v}_d$, is compared to a small number of directly measured deposition velocities, $\bar{v}_{dp}$, calculated by a limited profile method. The ratio of $\tilde{v}_d$ to $\bar{v}_{dp}$ for these case studies is generally less than two and suggests that the momentum parameterization is not unreasonable. Because of the simplicity in $\tilde{v}_d$ measurement, a mass transfer climatology could be estimated. Indeed, the simultaneous measurement of aerosol constituent mean concentrations, $\bar{C}$, and $\tilde{v}_d$ make possible the calculation of constituent mass flux; that is, mass transferred per unit area of the lake's surface per unit time (as the product of $\tilde{v}_d$ and $\bar{C}$). This mass flux is considered to be representative of more than 80 percent and possibly 90 percent of Lake Michigan's southern basin area. A nearshore experimental data base collected in 1978 is presently being reviewed to better establish the representativeness of midlake data for the lake basin as a whole.

Annual loadings of twelve aerosol constituents to the southern basin were determined by a method which accounts for the dependence of both $\tilde{v}_d$ and $\overline{C}$ upon changing meteorological conditions. Data sets were aggregated by similarity of wind speed, atmospheric thermal stability, or aerosol source region observed during sampling. A mass flux for each aggregation of sets was weighted according to the climatological frequency of occurrence for the conditions prevailing during these data sets. These mass fluxes were then summed to give total annual loadings. Less than 25 percent variation in the results of the three aggregation-scheme calculations was found, suggesting that the midlake data base was fairly representative of southern basin climatology. Minimum (lower confidence) estimates for dry deposition loadings are given in the table below in addition to the mean loadings. A comparison of minimum dry deposition loadings to estimates of precipitative loading and surface run-off inputs shows that the atmospheric inputs by dry loading are at least 60 percent of the total Pb input, 30 percent of the total Zn input, 20 percent of the total Fe input, and probably well over half the total sulfate and nitrate input. It was also found that phosphorus input by dry deposition is about equal to precipitation deposition and that possible contaminant or otherwise anomolous data for Cu and Ti make the results for these two elements suspect. The atmospheric dry deposition Pb inputs could be 75 percent or more of the total loading, and the input for Zn 50 percent or more, were the mean dry deposition estimates considered. All loadings are expressed as 10^3 kg-yr^{-1}.

	Dry Deposition (1)				
Element	Minimum	Mean	% Total	Precipitation (2)	Run-Off (3)
Al	300	650	$\geq$ 2	560	13,000
Ca	1000	2900	< 1		490,000
Cu	{10}	{20}	{6}	20	140 (4)
Fe	600	1200	$\geq$ 20	950	1450
Mg	400	730	< 1		134,000
Mn	30	60	$\geq$ 10	50	250
Pb	300	520	$\geq$ 60	90	100
Ti	{15}	{30}	{10}	60	100
Zn	100	200	$\geq$ 30	50	180 (4)
Total P	75	150		100 (5)	~ 3,000 (6)
NO_3^-/NO_2^- - N	2000	4350			
$SO_4^=$ - S	3500	7850			

Brackets {} enclosing results indicate caution should be used in interpretation -- see Section 5.

(1) This work.
(2) Gatz, D.F., 1975, Water, Air and Soil Pollution, 5, pp. 239-251.
(3) Winchester, J.W. and G.D. Nifong, 1971, Water, Air and Soil Pollution, 1, pp. 50-64.
(4) Robbins, et al., 1972, Proc. 15th Conf. Great Lakes Res. International, Assoc. Great Lakes Res. pp. 270-290.
(5) Murphy, T.J. and P.V. Doskey, 1976, J. Great Lakes Res., pp. 60-70.
(6) International Joint Commission on The Great Lakes, 1977 Water Quality Board Report, Appendix B, Surveillance Subcommittee Report.

Atmospheric loadings by dry deposition to the southern basin of Lake Michigan are clearly a significant part of the overall inputs of Pb, Zn, other metals, and sulfate to the lake ecosystem. This is especially true because atmospheric loading contributes directly to the biologically active surface waters. Accurate quantification of the atmospheric input to the Great Lakes is an important continuing research endeavor. The identification of source types for Great Lakes atmospheric inputs will require a still closer scrutiny of existing data. Only then can management and control objectives to meet Great Lakes water quality goals be realized.

This report was submitted in fulfillment of Grant No. R005301012 under sponsorship of the U.S. Environmental Protection Agency, with additional support from the research aviation facility and the computing facility of the National Center for Atmospheric Research, Boulder, CO 80301. This report covers the period June 1, 1976 to July 31, 1979, and work was completed as of July 31, 1979.

CONTENTS

FIGURES

LIST OF TABLES

LIST OF SYMBOLS

SYMBOL	MEANING	UNITS
A	area of southern Lake Michigan basin	m^2
b_{scat}	aerosol light scattering coefficient	$10^{-4}m^{-1}$
C_D	neutral drag coefficient for momentum	
C_{DD}	diabatic momentum drag coefficient	
C_{DF}	momentum form drag coefficient	
C_E	neutral drag coefficient for water vapor	
C_H	neutral drag coefficient for heat	
C	elemental concentration in aerosol	$ng\text{-}m^{-3}$
C_b	concentration in filter blank	$\mu g\text{-}l^{-1}$
C_m	total aerosol mass concentration	$ng\text{-}m^{-3}$
C_{ref}	concentration of a reference element	$ng\text{-}m^{-3}$
D	molecular diffusion coefficient	$m^2\text{-}s^{-1}$
d	aerosol diameter	μm
E_t	transfer efficiency	
EF	aerosol elemental enrichment factor	
F_o	frequency of occurrence for range of climatological conditions	
FC	fine to coarse particulate fractional ratio	
g	acceleration due to gravity	$m\text{-}s^{-2}$
H	depth of mixed layer	m
h	height above mean water level	m
I_t	intensity of turbulence	

K_D	eddy diffusion coefficient	m^2-s^{-1}
K_m	momentum diffusion coefficient	m^2-s^{-1}
L_d	instrumental detection limits	μg-l^{-1}
N	aerosol number concentration	m^{-3}
Ri_B	Bulk Richardson number	s^{-1}
R	resistance to mass transfer	s-cm^{-1}
R_{TL}	resistance to mass transfer in turbulent layer	s-cm^{-1}
r	radius	μm
S	stop distance	m
Sc^L	molecular Schmidt number, defined as ν/D	
Sc^L	turbulent Schmidt number, defined as Km/K_D	
S_o	atmospheric stability parameter	^oC-s^2-m^{-2}
T_h	air temperature at height h	^oC
T_5	air temperature at 5 m height	^oC
T_o	water surface temperature	^oC
T_w	bulk water temperature	^oC
ΔT	atmospheric thermal stability	^oC
t	time	s
u_h	windspeed at height h	m-s^{-1}
u_5	wind speed at 5 meter height	m-s^{-1}
u_o	surface water current	m-s^{-1}
u_*	friction velocity	cm-s^{-1}
V	aerosol volume concentration	μm^3-m^{-3}
v	velocity	m-s^{-1}
v_d	deposition velocity	m-s^{-1}

$\tilde{v}_d$	bulk parameterized deposition velocity	$cm\text{-}s^{-1}$
$\bar{v}_d$	mean bulk deposition velocity	$cm\text{-}s^{-1}$
v_{dp}	profile method deposition velocity	$cm\text{-}s^{-1}$
$\bar{v}_{dp}$	mean profile deposition velocity	$cm\text{-}s^{-1}$
W_5	vertical wind at 5 m height	$cm\text{-}s^{-1}$
WD	wind direction	^{o}magnetic
X_m	mass transfer	$cm\text{-}s^{-1}$
X_R	remainder mass transfer	$cm\text{-}s^{-1}$
X_{TL}	turbulent layer mass transfer	$cm\text{-}s^{-1}$
α	empirical exponent	
β	filter blank correction factor	$\mu g\text{-}l^{-1}$
γ	a constant	
δ	laminar sublayer thickness	μm
ε	a constant	
ζ	a constant	
η	a constant	
λ	wavelength	m
ν	kinematic viscosity of air	$m^2\text{-}s^{-1}$
Π	elemental mass percent of aerosol	
ρ	density of air	$kg\text{-}m^{-3}$
σ	standard deviation	
τ	time of year with no precipitation overlake	s

SECTION 1

INTRODUCTION

The densely populated and heavily industrialized southwestern shore of Lake Michigan represents a significant and expanding source of anthropogenic aerosol to the atmosphere. The combustion of fossil fuels in residential, industrial, and transportation activities, as well as manufacturing processes such as steel and cement making, are principal sources. Pollutant aerosol emitted in near shore urban/industrial areas provides an input potential for loading of Lake Michigan via wet and dry removal. 50 percent or more of the time, prevailing winds give rise to greater than 80 km long trajectories over the lake for air masses passing through the Chicago/Gary area (e.g. Sievering and Williams, 1975). Not only the well being of the urban population, but also the well being of the lake ecosystem, may therefore be linked to atmospheric pollution by wet and dry deposition. The transfer of atmospheric pollution constituents to land and water surfaces in the Great Lakes region by precipitation has been extensively documented in the literature (e.g. Murphy and Doskey, 1976; Torrey, 1976; and Eisenreich, Emmling and Beeton, 1977). Air pollution, and particularly dry deposition of atmospheric aerosol, was long assumed to be a negligible fraction of the total mass flux of most trace elements to the lake. Increasing concern for water quality of the Great Lakes led to re-examination of that assumption. Estimates of trace element loadings to Lake Michigan by aerosol deposition have often been made by using a transfer efficiency (E_t) approach. Winchester and Nifong (1971) calculated an emission inventory for the Milwaukee, Chicago, and northwest Indiana region and assumed an E_t of 0.10 where:

$$E_t = \frac{\text{pollutant loaded to lake}}{\text{pollutant emitted at source}}. \qquad (1)$$

Skibin (1973) suggested that 0.10 may be too low a value for E_t; consideration of mesoscale circulation effects on aerosol trajectories, as well as temperature stability and wind speed effects on aerosol deposition, made a value of 0.25 seem more probable. Sievering (1976) presented an overlake aerosol transport and deposition model, and proposed an E_t of 0.20 to 0.40 for total aerosol mass transfer to Lake Michigan and 0.01 to 0.15 for trace elements, dependent upon elemental aerosol size distribution and season of the year. Gatz (1975a and 1975b) calculated an emission inventory based on the chemical composition of Chicago area aerosol and showed precipitation and dry deposition to be about equal contributors to trace element loadings of the lake. Very large uncertainties in the emission inventory calculations and E_t models of these studies pointed to the need for overlake measurements of aerosol concentration, composition, and deposition.

Very little has appeared in the literature regarding measurements of overlake aerosol composition and deposition. Eisenreich, Emmling, and Beeton (1977) and the International Joint Commission review (1978) used primarily shore-collected bulk precipitation samples, i.e. wet and dry removal combined, to estimate atmospheric inputs to the lake. However, the bulk samples give no better than an order of magnitude idea of the dry depositional component of total deposition (Cadle, 1975). Schmidt (1977) gathered overlake aerosol trace element data and applied wind tunnel measurements of the dry deposition velocity (Sehmel and Sutter, 1975) to estimate loadings. Other workers investigated nutrient inputs to the Great Lakes from the atmosphere (Delumyea and Petel, 1977; Murphy and Doskey, 1976) by precipitation and dry deposition. The level of uncertainty in estimates of trace element deposition to Lake Michigan remained at nearly an order of magnitude. This research has sought to reduce that uncertainty by observation of aerosol composition and deposition velocity as part of an intensive midlake data collection experimental program, described in Section 3.

The large uncertainty in the aerosol dry deposition velocity at and above the air/water interface is usually not stated in dry loading estimates found in the literature. At a particular sampling height, h, the deposition velocity, v_{dh}, can be defined as a function of aerosol radius, r, by:

$$v_{dh} = \text{Flux}_h(r)/C_h(r) \qquad (2)$$

where the upward or downward mass flux of aerosol through a unit area at h is divided by the mass concentration $C_h(r)$ of aerosol at h. Uncertainty may be introduced by not considering the variation in v_d with aerosol radius. Using theoretical arguments, Sehmel (1971) has shown that v_d (0.5 μm) is approximately equal to 10 • v_d (0.05 μm). Yet wind tunnel data by Sehmel and Sutter (1974) on deposition to a water surface indicated that v_d (0.5 μm) is approximately equal to v_d (0.05 μm). Thus, an order of magnitude uncertainty concerning loading estimates for this size range could be introduced by v_d (r) variability. One possible explanation for the difference between theoretical predictions and wind tunnel data is the degree of turbulence in the air just above the water surface. If a relatively large turbulence effect is included in the theoretical analysis, the finding from wind tunnel studies that v_d (0.5 μm) is approximately equal to v_d (0.05 μm) is understandable. Nevertheless, it should be emphasized that there is no generally accepted theoretical explanation of these findings, and the variation of v_d with aerosol radius under field conditions remains uncertain.

Given the potential uncertainty, any method used to measure v_d (r) and the values resulting must be carefully scrutinized for applicability to the air/water interface over Lake Michigan. Thermal stability of the lowest air layers above the lake's surface varies greatly by season. During spring and summer months warm, land-based air moving over the cold lake creates extremely stable atmospheric temperature profiles, and thus a very small turbulence contribution to v_d can be expected. During late fall and winter unstable conditions enhance turbulence and larger values of v_d can be expected. The conditions occurring over Lake Michigan require a deposition velocity measurement which accommodates

climatological variability. Most theoretical models of dry deposition do not consider this variation with thermal stability. There are two direct measurement methods -- the eddy correlation and concentration gradient or profile methods -- which can be used to experimentally measure v_d. However, neither method is well suited to routine use in the field, especially overlake. The use of a limited profile method, along with a parameterized measurement which simplifies the experimental demands, was found to be a good compromise approach. In particular, a drag coefficient parameterization for mass transfer was used here, with wind speed and thermal stability as parameters. Hess and Hicks (1975) have shown that these two parameters dominate the steady state consideration of meteorological variables for Great Lakes mass transfer. By this method a bulk deposition velocity at a measurement height, h, ($\tilde{v}_{dh}$) is determined by

$$\tilde{v}_{dh} = (\bar{u}_h - \bar{u}_o) \cdot C_{DD}, \qquad (3)$$

where $\bar{u}_h$ is the mean wind speed over the sampling time at the height of measurement, $\bar{u}_o$ is the water surface speed, and C_{DD} is the diabatic momentum drag coefficient. A complete discussion of the use of C_{DD} appears in Section 4.3. Note that this method does not give v_d as a function of both r and h. The data base obtained by the limited profile method (described in Section 4.4) was used in conjunction with data from an aerosol size spectrometer to consider the variation of $\tilde{v}_{dh}$ with aerosol radius.

Of greater significance to Great Lakes atmospheric loading estimates than variability in v_{dh} alone is the possibly synergistic interaction of the temporal variabilities in C_h and $\tilde{v}_{dh}$. As equation (2) indicates, the flux of aerosol to the lake surface is depending upon the product of two factors: v_{dh} and C_h. Both factors are quite variable across the range of meteorological conditions prevailing at midlake throughout the year. Wind speed and thermal stability have a strong influence upon aerosol transport and deposition processes. In order to estimate annual total loadings from data collected during a necessarily limited sampling effort, some means of relating changes in v_d and C to meteorological variation must be included in the sampling and analysis (see Section 4.3). Moreover, other environmental factors, such as wind direction (WD) changes which transport aerosol from differing source regions overlake, affect the loading rate (see Section 4.2). Aerosol of varying chemical and physical characteristics must also be considered in transport and deposition calculations (see Sections 4.1 and 4.2). In this research, the approach used was to simultaneously collect meteorological data and aerosol samples. Sampling was performed around the clock during four several-day-long sojourns at a midlake station, during which distinct aerosol samples were collected in many successive 3-to 6-hour periods. This restricted length of exposure time for the aerosol collection media resulted in each sample, i.e. each value of C, being identified with a value of v_d which was based upon data collected within a period of well defined and fairly constant meteorological conditions. Annual loading estimates were then made, using meteorological parameters as weighting factors in calculations, and extrapolating the results by reference to the expected overlake climatology (NOAA, 1975). These loading estimates are considered in Section 5. It is concluded that a 2-to-3-fold uncertainty in loading estimates remains.

SECTION 2

CONCLUSIONS AND RECOMMENDATIONS

A major conclusion of this work is that at least 60 percent of the total Pb input, 30 percent of the total Zn input, and 20 percent of the total Fe input to the southern basin of Lake Michigan is by dry deposition of atmospheric aerosol. It was also found that major inputs of sulfate and nitrate are by dry loading. Phosphorus input by dry loading is about equal to precipitation inputs.

The percentage of anthropogenically derived aerosol at the sampling point near the middle of the southern basin of Lake Michigan for each of nine trace elements was calculated to be: Al, 0; Ca, 0; Cu, $\geq$ 90 percent; Fe, $\geq$ 65 percent; Mg, 0; Mn, $\geq$ 80 percent; Pb, $\geq$ 95 percent; Ti, 0; and Zn $\geq$ 75 percent. Aerosol trajectory considerations show that more than 75 percent of the anthropogenically derived aerosol are from the Chicago/Northwest Indiana source region.

The application of a factor analysis technique (Appendix A) to the midlake aerosol chemistry and meteorological data base specifies six uncorrelated factors. Physical significance was attached to each factor, resulting in several general conclusions:

1. The variance in midlake aerosol metal concentrations is linearly independent of wind speed, but strongly dependent upon temperature stability of the surface layer.

2. The variance in midlake mass concentration is more dependent upon fine particulate mass (with high Pb, Zn, and Mn content) than upon coarse particulate mass.

3. Midlake aerosol metal concentration is more dependent upon nearshore sources than upon long range transport.

Determination of the rate of dry deposition to the lake surface by a bulk parameterization technique (Appendix B) resulted in values for deposition velocities which were no worse than a factor of three removed from direct measurement and generally within a factor of two. Accuracy of the bulk parameterization was identified by simultaneously measuring the deposition velocity by direct aerosol profile (i.e, number concentration gradient) measurement.

Midlake sampling necessitated the use of an anchored ship platform. As a result, sampling took place during only 2 percent of the year. Overlake clima-

tological data were used to estimate annual loading rates. Thus, the results above are not specific to the year of sampling but rather are extended to a climatologically averaged year.

Elemental analysis of the nearshore samples has only recently been completed. Tentative interpretation shows a three-fold higher concentration for most trace elements than at midlake, with a major portion being in the soluble phase.

IT IS RECOMMENDED THAT:

1. A materials balance analysis be carried out, using the midlake data base in conjunction with emission inventory data on mass, trace elements and sulfate differentiated by source region and source type in the greater Lake Michigan basin region. This analysis should afford the identification of coal and oil burning sites, automotive and other source types, and an estimation of their percentage contribution to atmospheric dry loading.

2. Further interpretation of the combined midlake and nearshore data base using factor analysis and aerosol characterization analysis techniques should be pursued. The gross effects of transport and transformation upon source region and source type emissions would be significantly clarified by these analyses.

3. Aircraft aerosol data used on a case study basis will further clarify the transport and transformation processes. In addition, aerosol number and volume distribution analysis and interpretation can help identify synoptic and mesometeorological effects upon aerosol and trace element concentrations as a function of location over the lake.

4. Numerical modeling should be applied to reduce the uncertainty in the extension of results to other geographical areas and time frames. It is expected that modeling will also play an important role in the understanding of the process of aerosol transfer near the air/water interface. A model of turbulent inertial deposition in the buffer layer and laminar sublayer may provide a clear picture of aerosol mass transfer at the interface.

5. Direct measurement of aerosol deposition to the Great Lakes by either the profile or eddy flux method under varying meteorological conditions should be supported.

6. Future Great Lakes atmospheric studies should be performed in the context of year-round meteorological sampling at several sites on the lakes to establish the representativeness of ship-based meteorology, both from a temporal and spatial viewpoint. Temporally, it is necessary to verify that sampling aboard ship fits the climatological data for the Great Lakes. Spatially, a confirmation that single site sampling represents the majority of a Great Lake's surface must be further considered.

SECTION 3

DESCRIPTION OF EXPERIMENTAL PROGRAM

3.1 GENERAL PROCEDURES

In order to compile a data base for the estimation of annual dry deposition loadings, investigations in two general categories were concurrently pursued. These categories were: 1) meteorological conditions, both at the mesoscale (affecting aerosol transport) and microscale (affecting aerosol deposition); and 2) the physical (aerosol size distribution and mass concentration) and chemical (trace element and nutrient content) nature of overlake aerosol. Meteorological data and aerosol samples were gathered from sampling sites at midlake (87^{o} 00' W by 42^{o} 00' N) aboard the United States Environmental Protection Agency (USEPA) R/V Roger R. Simons during 1977, and nearshore (87^{o} 32' W by 41^{o} 47' N) at the City of Chicago 68th Street water intake crib during May through November, 1978 (see Figure 1). Aircraft overflights were made during June and September, 1977 and May, 1978 by a National Center for Atmospheric Research (NCAR) Beechcraft Queenaire, for collection of meteorological and aerosol size spectrometry data from near surface up to 2000 m. Surface meteorological reports from the National Weather Service (NSW), Argonne National Laboratory, and U.S. Coast Guard were gathered from various stations around southern Lake Michigan. NWS low-level soundings at Chicago's Midway Airport complemented the soundings taken by the NCAR Queenaire.

At the sampling sites, a portable array of meteorological sensors was operated (Table 1). Analog output from the five meter height wind speed and direction (u_5 and WD), temperature (T_5) and relative humidity (RH) sensors was scanned at 1 Hz by a signal conditioner/data acquisition system (Weather Measure Corp. (WMC), Sacramento, CA, model SC601). The 1 Hz readings were stored and fifteen-minute means and standard deviations (σ) in all parameters calculated by a microprocessor (WMC #M733). These mean and σ values, along with manually measured water surface temperature (T_0) readings were hardcopy printed and recorded on magnetic tape (Texas Instruments Inc., Houston, TX, model ASR/KSR 733). Surface current (u_0) and bulk water temperature (T_W) were observed and recorded at 4 to 7 hour intervals.

Data collection was done around the clock. In order to divide each sampling day into manageable time segments, data collection was done within 3 to 6 hour periods, referred to as "data sets." Each data set, because of its limited duration, corresponds to a period of fairly constant meteorological conditions. The occurrence of rain or fog events precluded any sampling,

since this study was directed at dry deposition only. At the beginning of each data set, aerosol sampling media were replaced and water samples were taken. Thus, aerosol and water samples can be classified according to values of meteorological parameters which prevailed during each data set. In general, a minimum of three hours elapsed time was required per data set to provide sufficient loading of the Hi-Volume filters to be above detection limits of the chemical analysis procedure used. Past that minimum time, rapid and persistent changes in u_5, WD, T_5, or T_0 were cause for the termination of a data set. Such changes were defined as two successive 15-minute mean values for a given parameter being more than 1σ removed from the running mean. A maximum time of about 8 hours was allowed so that no data set was biased by a widely differing run time. Additional constraints upon data set initiation/termination, unique to each sampling site, will be discussed as part of each site's description.

Aerosol samples were taken with standard Hi-Volume samplers (General Metal Works, Inc., Cleveland, OH #GMW 2000). Samples for gravimetric analysis of total aerosol mass concentration were collected on 20 by 25 cm glass fiber filters (Sierra-Misco, Carmel Valley, CA, #C305); samples for chemical analyses were collected on cellulose fiber substrates (Sierra-Misco #P252A) and 20 by 24 cm filters (Sierra-Misco #810A). The three-part cellulose media were exposed at 1.18 $m^3 - min^{-1}$ (40 SCFM) in a modified cascade impactor (Sierra 5-stage #230), using the #1, #3, and backup stages only. Collection efficiency curves for this configuration were determined by Sievering, et al. (1978) and were found to resolve well two aerosol size fractions. A coarse particulate fraction(diameter, $d > 1.0$ µm, 90% confidence) is collected on the first impactor stage substrate, while a fine particulate fraction ($d < 1.0$ µm, 90% confidence) is collected on the backup filter. The third stage acts as an intermediate step which improves the separation between size fractions collected on the other two filter stages (see Figure 2). Two such cascades of three-stage cellulose filter media were simultaneously exposed on separate Hi-Vols during each set. One cascade of filters was prepared for trace element analyses, while the other was analyzed for aerosol nutrient content.

Aerosol samples collected on one of each pair of three-stage cascades were analyzed for trace elements at the USEPA Central Regional Laboratory in Chicago. The filters were placed in acid-washed fused quartz trays and low temperature ashed in O_2 at 75 watts. The residue was then dissolved in HNO_3 and distilled deionized water. Trace element analysis was done by Inductively Coupled Argon Plasma atomic emission spectroscopy (ICAP-AES) (Jarrell-Ash, Pittsburgh, PA, Plasma AtomComp 750). In more than 85 percent of the data sets, concentrations of Ca, Mg, Cu, Fe, Mn, Pb, Ti, and Zn were above ICAP-AES instrumental detection limits (L_d). The limited 3 to 8 hour exposure time of the filters resulted in concentrations of Na, Ba, Cd, Co, Mo, Ni, and V which were below L_d in at least 50 percent of the data sets (Table 2). Therefore, loading calculations for these metals are of limited validity. Post-analysis statistical review of the data revealed contaminant or otherwise anomalous data for B, so that this element was not used in loading estimates. Filter blanks were subjected to all handling and analysis procedures, except the

collection of ambient aerosol. The blank correction (β) applied to the ICAP-AES results for the exposed filters was defined as:

$$\beta = C_b + 1\sigma \qquad (4)$$

where C_b is the mean concentration of the element in filter blanks, and σ is the standard deviation in that mean value. For those elements which were above L_d in more than 85 percent of the data sets, the expected reproducibility of the concentrations reported here is ± 20 percent for ICAP-AES analyses (USEPA, 1974).

The nutrient analyses for total phosphorus (P), sulfate (SO_4) and nitrate/nitrite nitrogen (NO_2/NO_3) were done by first leaching the particulate-loaded cellulose media in three successive baths of boiling distilled water for a total of 3 hours. The degree to which the soluble and insoluble particulates were removed in this process was investigated by Sutton (unpublished data, 1977) at USEPA-CRL. Recovery of P was found to be $\geq$ 95 percent. The combined extracts of the 3 hour leaching process were divided into separate aliquots for analyses for P, SO_4, and NO_2/NO_3. The P subsamples were digested in $(NH_4)_2\ S_2\ O_8$ and CH_2SO_4 to convert all phosphorus to orthophosphate. The digestate was then colorimetrically analyzed for orthophosphate by an automated molybdate method. The SO_4 subsamples were passed through a Na - form cation-exchange column to remove multivalent metal ions. Sulfate content was then determined by an automated methylthymol blue method. The NO_2/NO_3 subsamples were passed through a Cd/Cu column, reducing all nitrate to nitrite. Nitrite was then colorimetrically determined by an automated diazotization-coupling method. The automated colorimetric analyses were performed following standard autoanalyzer methods (Jirka, et al.; USEPA, 1974; Technicon Instruments Corp.).

Several optical particle size and concentration measuring instruments were used to collect information on the physical character of overlake aerosol. An integrating nephelometer (Meteorology Research, Inc., Altadena, CA, #1550) continuously monitored the aerosol light-scattering coefficient and thus, variations in aerosol mass concentration. Condensation nuclei counters (Environment One Corp., Schenectady, NY, models #E1012E and Rich 100) were also used to routinely observe submicron particle concentrations.

The behavior of aerosol in the diameter size range, $0.1 < d < 1.0$ μm is of particular interest, since trace elements are strongly associated with this fine particulate fraction. This is especially true at a midlake sampling site which is substantially removed from sources of large aerosol. Information concerning aerosols in this size range was obtained from an Active Scattering Aerosol Spectrometer (ASAS, Particle Measuring Systems, Boulder, CO, #PMT300). This instrument measures in situ aerosol number by detection of scattering internal to the cavity of a Helium-Neon laser. Ambient air is drawn through a mini-wind tunnel in which the laser resides. Number concentration separated into 60 size channels was recorded on magnetic tape. Accurate flow rate control (better than 1%) and low coincidence error provided high reproducibility and precision. If an average density is assumed, mass information can be obtained.

During sampling on board ship and at the crib, a 730 cm^2 cross sectional area entry tube facing into the wind at the tip of the boom was tapered to match the 20 cm^2 ASAS sampling cylinder. A 4.6 $m\text{-}s^{-1}$ entry speed allowed nearly isokinetic sampling from ~3 to ~6 $m\text{-}s^{-1}$ ambient winds. The 2 m long tube was grounded to minimize loss of electrically charged aerosol to the wall. Results from a wind tunnel test were used to correct for the tube wall loss that was observed. The instrument gathered data in the range $0.09 < d < 3.53$ μm in size intervals from almost 0.01 μm for the smallest sizes to 0.2 for the 1 μm and larger sizes. The ASAS returned measurements of sufficient precision to provide vertical profiles of surface layer aerosol concentrations in some circumstances.

Besides being based at the crib and on board the ship, an ASAS was mounted on the NCAR Beechcraft Queenaire research aircraft. Also on board were sensors for temperature, dewpoint, pressure, height, and other meteorological parameters. Instrumentation for the analysis of atmospheric turbulence was included in the September 1977 and May 1978 flights. The air sampled by the ASAS on the aircraft was drawn from the Pennsylvania State University isokinetic intake (Pena, Norman and Thomson, 1977) through copper tubing and flow-controlled to produce a variation in the aircraft monitoring sample volume flow rate of about 2 percent. Corrections for aerosol loss to tubing walls was again based on wind tunnel data which was gathered using the actual field instruments and set-up. The instrument used in the 1977 flights provided data in the range $0.23\ \mu m < d < 2.8\ \mu m$ in size intervals of 0.01 μm - 1.0 μm. The aircraft platform provided data which could be used to investigate vertical and horizontal distributions of meteorological conditions as well as aerosol concentration. Also on board for these 1977 flights was the Classical Scattering Aerosol Spectrometer (CSSP), a device very similar to the ASAS, which gathered data in the range $1.1\ \mu m < d < 30\ \mu m$ in intervals of 0.1 μm - 1.0 μm. The instrument used in the May 1978 flights was the same ASAS used on board ship and at the crib, described earlier.

Water samples were taken of "bulk" water, i.e., at 3, 5, and 7 m depths, with a neoprene and polyvinylchloride Kemmerer bottle. The 2ℓ samples from all three depths were combined in a 20ℓ polyethylene container; T_w and pH were determined. A 400 ml subsample was withdrawn and acidified with 4 ml 6N HNO_3, then frozen. Surface water samples were taken using the polyethylene screen technique (Elzerman, 1976) during some of the sampling periods. The surface water samples were also acidified and frozen. All water samples were analyzed at the USEPA-CRL by ICAP-AES for the same 17 trace elements as were the aerosol samples.

3.2 MIDLAKE SAMPLING PROCEDURES

During four several-day-long periods in the summer and autumn of 1977, 48 aerosol samples and meteorological data sets were collected from the USEPA R/V Roger R. Simons, anchored at a mid-Lake Michigan station (see Figure 1). The site was chosen to be fairly representative of most of the southern basin lake surface. The nearest shore is 40 km distant, so that effects upon loading rates due to point sources and the land-water boundary zone are minimized.

The 40 km or greater upwind fetch allows a 10 to 30 m thick "surface layer" of air, just above the water, to approach equilibrium with respect to surface effects. As long as the lake surface appears constant to the air passing over it, the mass flux within the surface layer is constant throughout its vertical extent (Dyer and Hicks, 1970; Kraft, 1977). Thus, under most conditions, the aerosol is well-mixed within the atmospheric surface layer by the time it is sampled at the midlake site (Gillette and Winchester, 1972). The site is also well away from heavily travelled shipping lanes.

Aboard the R/V Simons, meteorological sensors were mounted at the tip of a 6 m aluminum boom, which extended ahead of the ship's bow at a mean height of 5 m above the water (Figure 3). The results of bluff-body turbulence effects studies by Hunt (1973) and Hunt and Mulhearn (1973) indicate that a boom length of only 3.5 to 4 m would have been sufficient to avoid any turbulence effects due to the ship's presence. The undisturbed ambient wind field presented to the meteorological sensors is also evidenced by the intensity of turbulence (I_t), which is calculated as

$$I_t = \sigma/\bar{u}_5 \qquad (5)$$

where σ is the standard deviation about $\bar{u}_5$, and $\bar{u}_5$ is the 15-minute mean of 1 Hz wind velocity values. Overall I_t at midlake was observed to be 0.10 ± 0.05, which is comparable to the 0.02 to 0.14 range of I_t observed by SethuRaman and Tichler (1977) from an air-sea interaction tower. Thus, no significant increase in I_t due to the location shipboard of the sensors could be detected.

Two Hi-Volume samplers were also located on the boom, approximately 3.5 and 4.5 m ahead of the bow. The filter holders and heads were carefully sealed to the pump motor assemblies, and the pump exhausts were vented through 4 m long, 11 cm diameter hoses (see Figure 3). This was done to prevent possible contamination of aerosol samples by the sampler pump motors. Sampling was conducted with the ship bow-anchored on station; therefore, the boom pointed upwind and the likelihood of contamination by the ship's effluent was reduced (Moyers, Hoffman, and Duce, 1972). Whenever local WD at the ship shifted quickly or u_5 decreased to the point where the upwind orientation of the boom was uncertain, the Hi-Vols were stopped. WD data from the boom-tip wind vane shows that the boom pointed to within $\pm 40^{o}$ of directly upwind during sampling periods. The ASAS was located at the proximal end of the boom, and aerosol number concentration was usually measured at the 5 m mean height above water. When vertical ship motion was minimal, attempts were made to measure vertical gradients in the aerosol number concentration. The intake of the ASAS was alternately placed at heights of 3.7 and 6.4 m during successive counting periods of from 3 to 15 minutes. In a certain number of cases, the measurement of number concentration differences between the two heights met an expected logarithmic law criterion and was then used to estimate aerosol deposition velocities by the profile method (Gillette, 1972).

The Hi-Vol used with glass-fiber filters for total aerosol mass concentration determination was run on the upper foredeck of the R/V Simons. The

integrating nephelometer and condensation nuclei counter also were operated upon the foredeck. Observers, using a hand-held infrared thermometer, measured T_0 by scanning an area of the lake surface directly below the boom. Bulk, and when feasible, surface water samples, were taken from a platform on the upwind side or from a fiberglass launch (when feasible) well away from the ship.

3.3 NEARSHORE SAMPLING PROCEDURES

At the City of Chicago 68th Street Crib, two different configurations of the sampling equipment were used. During the last two weeks of May 1978, when the NCAR aircraft was also collecting data, the first configuration was used in collecting 9 data sets. Later in the summer and fall, the second configuration was used for an additional 15 data sets. Initially, the meteorological sensors and Hi-Volume samplers were located on the upper steel-beam bridge between the two masonry buildings which make up the crib site (Figure 4). The samplers in that position were located about 13 m above the water surface and 20 m from either building. Because of the proximity of these buildings, one of which is occupied by a crib maintenance crew, WD sampling windows were defined. Sampling was only conducted when WD $\pm 2\sigma$ was within the directional sectors $40^0 < WD < 130^0$ or $210^0 < WD < 330^0$ (see Figure 4). Sampling other than within these windows increases the probability of local contamination of aerosol samples and of turbulent disturbance of the observed windfield. Infrared thermometer T_0 observations were made from the lower bridge at about 5 m above the water. The integrating nephelometer and vertical wind sensor were operated on a small boom which extended 2 m towards the upwind sector from the lower bridge. Water samples were taken from a fiberglass boat, well away (0.75 to 1 km upwind) from the crib, again using the Kemmerer bulk sampler and surface screen.

During the June through November period, 15 data sets were collected at the 68th Street crib site. The Hi-Volume samplers were relocated to the lower bridge (5 m above water) level, and the meteorological sensors were installed on a portable mast. Sampling was conducted at irregular times, usually one or two data sets per day in bi-weekly intervals. The movable mast for the meteorological sensors was set up on the windward side of the seawall around the north (crew quarters) building. Meteorological data could then be collected at the 5 m height from all WD sectors except for $130^0 < WD < 210^0$; WD windows for the Hi-Vol samples remained the same as for the May 1978 sampling period. The integrating nephelometer, condensation nuclei counter, and ASAS were also made portable and operated at the upwind point of the seawall. The ASAS intake was fitted to a 6 m boom, and the vertical wind sensor was mounted at the tip of this boom. Measurements of the vertical wind field at distances from 1 to 6 m upwind of the 1 m high seawall at heights from 0.5 to 4 m above water were made to verify that the ASAS intake was sampling the ambient aerosol distribution. Aerosol number concentration vertical gradients were observed with the ASAS during the June through November period. Bulk and surface water samples were taken for each set.

SECTION 4

DATA, ANALYSIS, AND BASIC RESULTS

4.1 RESULTS OF CHEMICAL ANALYSIS

1. Water Samples

Bulk water, composited from samples taken at 3, 5, and 7 meter depths, was collected once during each data set at the midlake site. Table 3 is a compilation of the ICAP-AES trace element analyses of these samples. Nutrient analyses were not run for any water samples. Geometric mean elemental concentrations for each sampling period indicate the degree of temporal variability in trace metal levels at the midlake site. The data do not provide adequate resolution to infer any seasonal pattern; however, the trace element levels at that single site are shown to be far from constant over the summer through fall season. The "overall" mean includes all of the 40 bulk samples collected during the entire May through September, 1977 period. The overall mean concentrations for all elements appear to fall well within ranges summarized from the literature by Torrey (1975). The water trace element data form the basis for assessing the contribution of the lake as a source of atmospheric aerosol, particularly of those with metallic content.

Surface-water samples were taken concurrently with the bulk samples during the September, 1977 sampling period only. For the September group of 16 samples, concentrations in the 100 to 200 μm depth surface sample (Garrett, 1965) can be compared to the underlying bulk water concentrations. A convenient method of expressing this comparison is by a surface-enrichment value, E_{sb}, given by

$$E_{sb} = \frac{C_{surface}}{C_{bulk}} - 1.0 \qquad (6)$$

Thus, the sign of E_{sb} gives the direction of increased concentration; E_{sb} being positive when $C_{surface} > C_{bulk}$. In Table 3, then, it is noteable that all the E_{sb} values, except that for B, are positive. The magnitude of E_{sb} indicates the extent of surface enrichment.

The E_{sb} values listed in Table 3, however, probably do not indicate the actual magnitude of enrichments in the surface microlayer. This is partly due to the sampling technique, which collects water from a surface layer about 10^2 to 10^3 times the depth of the surface organic microlayer (Andren,

et al., 1975). Also, it is partly due to the fact that the surface samples were collected during each data set, whether or not a surface organic microlayer was present (Elzerman, 1979). However, the E_{sb} results in Table 3 strongly suggest that the surface water is at least slightly enriched relative to the underlying bulk water. Due to the small number of samples represented in these results, and the fact that the E_{sb} values are not statistically different from zero, any extension or application of the surface water results must be considered tentative (Owen, et al., 1979). Current models of gas transfer across the air/water interface (Brtko and Kabel, 1976) do not adequately apply to the case of aerosol particle transfer. The E_{sb} data, however tentative, may prove to be of value for development and evaluation of models of aerosol transfer across the interface. Bulk water temperature and pH were measured during each data set; the results are included at the bottom of Table 3. The pH measurements of the bulk samples are typical of open-lake waters (Torrey, 1976). These pH values may be viewed as an indication of the buffering capacity of the lake, in light of the inputs of acid aerosols, i.e., SO_4 and NO_3 loadings (see Section 5). No measurement of surface water pH was attempted in the 1977 or 1978 sampling. It is, however, conceivable that atmospheric inputs of acid aerosol may create a reduced pH in the surface microlayer. This could in turn enhance the solubility of other aerosol constituents at the time of deposition to the lake's surface. Such a reduced pH microenvironment at the interface could enhance the availability to the ecosystem of toxic aerosol constituents, and should be assessed in ongoing research.

2. Aerosol Samples

Three-stage cascade impactor filter sets were exposed on Hi-Volume samplers during each data set. The results of ICAP-AES trace element and autoanalyzer phosphorus, nitrite/nitrate, and sulfate analyses are listed in Table 4. The mean concentrations for each element show a wide range of variability over the summer through fall season. This is primarily due to the atmospheric thermal stability. A detailed discussion regarding this variability will appear in Section 5. For the trace element results, a general filter blank correction from equation (4) was applied after the analysis of all 48 data sets and eight filter blanks was complete. The P, NO_2/NO_3, and SO_4 blank corrections were generated for each sampling period's group of filters as they were analyzed by USEPA-CRL. The B values were, in general, small compared to typical sample values for the majority of analyses (see Table 2). The mean values of chemical parameters reported are given as geometric means. Rahn (1976) has suggested that geometric means tend to better represent distributions of environmental parameters, as compared to simple arithmetic means. Figures 5, 6, 7, 8, 9, 10, 11, and 12 also strongly suggest this. Each of these figures is a histogram plot of elemental concentration distribution for those data sets in which $C > 0$. The entire range of C measured for each element was divided into 60 increments; the number of data sets for which C values within a particular increment were observed was then plotted. For the elements Al, Ca, Fe, Mg, Mn, Pb, Ti, and Zn, shown in these figures, the concentration distributions are seen to tend toward log-normal frequency

distributions, for which a geometric mean is appropriate. There are data in the literature with which to compare the midlake aerosol trace element and nutrient mean concentration data. Schmidt (1977) presented trace element concentration data for samples collected over southern Lake Michigan which generally correspond with the ranges of values reported here. The results of Table 4 represent a midlake aerosol chemistry data base which has been collected at a single site under a wide range of meteorological conditions.

Over the entire May through September, 1977 period, a total of 48 aerosol samples were collected. In the various data set aggregation schemes used in this work, it has often been necessary to exclude some data sets from some calculations. For example, due to handling and analysis problems, such as internal reference element (Yttrium) spiking inaccuracy in the ICAP-AES procedure, or some obvious contamination, nine of the trace metal samples have been eliminated from further consideration. Similarly, seven samples for P, NO_2/NO_3, and SO_4 are unusable. Wherever mean concentrations or other mean values are reported in this work, those results are based upon only those data sets which appear to be consistent with the entire data base for that parameter.

A chemical characterization of atmospheric aerosol over southern mid-Lake Michigan can be made using the $\bar{C}$ data of Table 4. The geometric mean total aerosol mass concentration, $\bar{C}_m$, observed at the midlake site was 32 $\mu g - m^{-3}$; the range of values measured was $10 < C_m < 94$ $\mu g - m^{-3}$. Trace element composition is thus expressed in Table 5 by three ratios of concentrations:

$$\Pi = \frac{\bar{C}}{\bar{C}_m} \cdot 100 \qquad (7)$$

$$FC = \frac{\bar{C}\ (d < 1.0\ \mu m)}{\bar{C}\ (d > 1.0\ \mu m)} \qquad (8)$$

$$EF = \frac{\bar{C}/\bar{C}_{ref}\ (\text{in aerosol})}{C/C_{ref}\ (\text{in soil})} \qquad (9)$$

The first of these ratios, Π, from (7), represents the percentage of total aerosol mass contributed by the concentration of a particular element. Gatz' (1975a) composite model of Chicago/Northwest Indiana aerosol corresponds closely to the Π values observed at midlake. This suggests that trace element composition of the aerosol is not drastically altered during overlake transport (see Appendix C). The second ratio, FC, from (8), gives an indication of the degree to which the fine particulate ($d < 1.0$ μm) contributes to the total concentration of a particular element. In this calculation, fractional concentrations from the first cascade impactor stage ($d > 1.0$ μm) and backup filter ($d < 1.0$ μm) are used (Figure 2). The intermediate impactor stage serves to improve resolution between the fine and coarse particu-

late fractions. The intermediate stage concentration is included, however, in all total concentration calculations. The third ratio in Table 5, aerosol Enrichment Factor, EF, from (9), relates the concentration of an element to the concentration which might be attributed to a reference natural source material. In this work, the composition of midwestern soil described by Bowen (1966) is used, with Al concentration defined as the soil source reference, C_{ref}. EF values close to unity for a given element indicate that the element is present in aerosol in soil-derived proportions; large EF values indicate other major sources for that element (Rahn, 1976). From Table 5, it appears that at least Cu, Zn, and especially Pb are greatly enriched in mid-lake aerosol, i.e., come from other than midwestern soil sources.

Disaggregation of the grand average EF values by filter set is facilitated by the use of scatter diagrams (Rahn, 1976). Metal enrichment factors (ordinate) are plotted versus Al concentration (abscissa) by filter set on a log-log scale. The scatter diagram shows how the enrichment factor of a given element varies with the concentration of soil material in sampled aerosol. Points at the high-Al end of the diagram are usually from nearshore, polluted urban areas; points at the low-Al end are from long over lake trajectory areas (or are otherwise low in Al). Scatter diagrams for Pb, Zn, Mn, Fe, Ti, and Mg are shown in Figures 13, 14, 15, 16, 17, and 18 respectively. The dashed straight lines on each scatter diagram are lines of constant concentration in the metal plotted.

Overall comparison of the scatter diagrams with those in a compilation of over 100 data sources (Rahn, 1976) shows a higher enrichment factor trend (except for Fe) for the Lake Michigan site than many urban sites. Disaggregation by filter set also shows greater variability in the enrichment factors for Fe, Mg, Ti, and Mn, than most other field sites. This suggests a variable depletion mechanism not only for Al but also for these four additional metals.

The scatter diagram for Pb (Figure 13) falls within the range of data reported (Rahn, 1976). However, there are two regimes of data points which are somewhat unique. The first is in the upper left where enrichment factors of 3×10^3 to 1×10^4 are associated with Al concentrations less than 35 ng/m^3. These data points are generally related to sampling of air with north winds and long over water trajectories. The second unique regime of data points is that with enrichment factors less than 1×10^3. These data are all related to northeast to east winds with intermediate to long over water trajectories.

The Zn scatter diagram (Figure 14) shows no peculiarities. It is quite consistent with the reported literature (Rahn, 1976), although greater variability in the enrichment factor is present. The Mn scatter diagram (Figure 15) presents a different picture. The data not only convey a larger enrichment factor than other data sources (Rahn, 1976) but there is a rather wide scatter in their magnitude. This may be due to a combination of variability in source region concentrations and variable over water depletion in Mn.

The Fe scatter diagram (Figure 16) shows variability in enrichment factors similar to that of Mn but without a large average enrichment factor. The same pattern is present in the Ti and Mg scatter diagrams (Figures 17 and 18) although the average Mg enrichment factor is very likely high due to lake source contributions of this metal. The Ti scatter diagram has a strong trend toward constant concentration. It appears that contamination from shipboard and laboratory handling probably contributes to the Ti midlake concentration data. It appears that shipboard and laboratory handling probably contributed to the Ti midlake concentration data. The enrichment factor scatter diagrams support the notion that differences in source region is not the only major factor influencing the variability in enrichment factors. The unique over water trajectory of an air mass must also be considered to explain this variability.

Results of correlation coefficient determinations are shown in Table 6. Non-chemical parameters included in this Table are total aerosol mass, C_m, as well as $\bar{u}_5$ and $\overline{\Delta T}$. Also shown are the squared multiple correlation coefficients (underlined) which give the percentage linear variation that can be explained for the specified variable by all the others combined. Clearly, little of the Mo and Ti concentrations and wind speed variability are linearly dependent upon the other variables.

The individual element dependencies of Table 6 also suggest that Ti is anomalous, since it has only moderate correlation with two or three other metals. Al, is strongly correlated with other soil derived metals: Ca, Mg, Fe, and Mn. Ca and Mg have similar correlations to that of Al. Fe is strongly correlated with all three of these metals but is also highly correlated with Mn, Pb, and Zn. In fact, Fe seems well correlated with more variables than any other metal. Mn, Pb, and Zn are also strongly correlated with several other metals. Mn shows the highest correlation with mass. Mo correlates only moderately with Pb.

The trace element concentrations in aerosol observed at the City of Chicago 68th Street Crib are summarized in Table 7a. For most elements, $\overline{C}$ is usually increased three-fold in the nearshore area. However, a close scrutiny of the Π and FC results suggests that the trace element composition of nearshore aerosol (predominantly Chicago/Northwest Indiana source) is not significantly altered (see Table 4) during transport to the midlake region. That is to say, although the gross concentration of aerosol is reduced by dispersion and deposition during overlake transport, the composition and proportion of fine and coarse particulates do not appear to change. This is evidence supportive of the contention that v_d overlake is not a strong function of aerosol size. Use of the nearshore data in the loading estimate calculations of this work is precluded by the state of development of the loading model. The priority application of these data will lie in the development of loading models which integrate nearshore and midlake data, and in the source area/source type resolution calculations, discussed in succeeding sections of this report.

A passive aqueous extraction procedure (see Appendix D) was used on two 9 cm by 9 cm sections of crib backup filters. The filter sections rested on the surface of deionized water for 24 hours. The extraction liquid (i.e., soluble aerosol fraction) along with the samples generated from the extracted section (i.e., insoluble aerosol fraction) and from the unextracted remaining portion of the backup filter were analyzed for trace metal. The ambient air concentrations of 17 trace metals were calculated and compared for each of the three fractions. The percent soluble and the sum of the soluble and insoluble fractions (the total recovery from the extraction procedure) are listed in Table 7b for five important trace metals. With the exception of copper, the extraction procedure accounted for, on average, the trace metal concentration determined from the unextracted portion. The mean value of the "percent soluble" column indicates the range of solubility of the trace metal. Iron and lead were found to be very soluble, 80-85 percent, whereas copper, manganese, and zinc were found to be only partially soluble, approximately 50 percent.

Filter sets 70740 through 70810 present anomalous results. The analysis of the extracted portion of these filters indicated a lack of trace metal. The results for the five metals in Table 7b are typical of the rest of the elements analyzed. All or a large percentage of the trace metal recovered in the extraction procedure was found in the soluble portion. The absence of material in the insoluble fraction could not be traced to a procedural or operator error. The source region of the aerosol appears as a first explanation of the anomalous results. The wind directions for these filter sets were west to southwest -- from the Chicago urban area. The filter sets with measurable, insoluble, small aerosol had wind directions from the east-northeast. Secondary particle generation by acid gas dissolution into and reaction within liquid aerosol could possibly account for the preponderance of soluble aerosol found near the Chicago urban source.

4.2 PHYSICAL CHARACTERISTICS OF AEROSOLS

The chemical composition data were not presented in the context of mass concentration by data set since the cellulose filter medium is quite hygroscopic and, therefore, not conducive to gravimetric analysis. A standard Hi-Volume sampler with type A glass fiber filter was run for 8 to 24 hours to collect sufficient aerosol on the glass fiber filter. Eighteen mass concentration samples were obtained this way. In addition, integrating nephelometer scattering coefficient data (b_{scat}) was linearly regressed against the Hi-Vol mass concentration data ($\overline{C}_m$) with the result:

$$b_{scat} = 0.298 + 0.0138\ \overline{C}_m \qquad (10)$$

An extremely good correlation of 0.97 was found. The importance of the correlation is that b_{scat} values can be averaged across each cellulose filter sampling period to accurately reflect the associated aerosol mass concentration by using equation (10). The 49 mass concentrations determined in this way have a normal distribution mean of 34 $\mu g/m^3$, but are a better fit to the log-normal distribution with a geometric mean of 31 $\pm$ 19 $\mu g/m^3$. The mean of 31 is clearly

below typical urban and even rural concentrations but above the 15 to 25 $\mu g/m^3$ found at remote, land-based sites (Rahn, 1976) and 10 to 15 $\mu g/m^3$ found at remote oceanic sites (Windom and Duce, 1976).

The size distribution of this midlake mass concentration was monitored by the ASAS -- at least that mass fraction in the $0.1 < d < 3.5$ μm aerosol size range. The ASAS directly monitors the number of aerosol in each of 60 size fractions. Table 8 shows the 50 percent collection efficiency diameters for the ASAS with a comparison to those for the Hi-Volume sampler and integrating nephelometer. The ASAS counts aerosol over the entire range of sizes observed by the nephelometer, but only a portion of the sizes collected on the Hi-Volume sampler. The aerosol particles which are detected are electronically sized and the number of particles falling within each of the 60 size ranges is accumulated. Aerosol distributions are normally displayed on plots having d or log d as the abscissa, and $\Delta N/\Delta$ (log r) as the ordinate, where ΔN is the number of particles counted in a size range and Δ (log r) is the difference between the logs of the upper and lower limits of the range.

Figures 19, 20, 21, and 22 display this plotting of the average number concentration for each of the four midlake sampling periods: 17-20 May 77; 7-9 June 77; 14-19 August 77; and 26-30 September 77. The average slope of the data points is -2.3, -3.4, -3.3, and -3.8 for May, June, August, and September, respectively. September data are representative of unstable air over the lake. As a result, large aerosol are indeed depleted at the midlake sampling point. In fact, the -3.8 slope is rarely encountered in surface layer air unless the air resides several hundred kilometers from pollution or natural primary aerosol sources. The August data is representative of a neutral surface layer. The slope of -3.3 suggests less depletion of large aerosol than in September. During the June sampling period, though slightly stable air prevailed, heavy rains washed out a significant number of aerosol in all size ranges. Possibly due to the greater washout efficiency of primary aerosol, the slope of -3.4 is slightly more than that in August. During the May sampling, a very stable surface layer prevailed. The stable layer clearly "held" more large aerosol during the May sampling period. Overall, the slope of -2.3 indicates that the $d > 1$ μm aerosol are enhanced when compared to urban and even many rural concentrations of these primary aerosols.

Similar distributions of particle volume can be obtained by multiplying the number counted in each size bin by $4/3\pi r^3$. The ordinate for those plots, then, is $\Delta V/\Delta$ (log r). These plots are shown in figures 23, 24, 25, and 26. Each figure also shows "typical" urban and continental background volume distributions for comparative purposes. The May period data (Figure 23) show aerosol volume distributed approximately as found in urban environments except for the relatively large midlake contribution by the $r = 0.5$ to 1.0 μm aerosol sizes. This may be attributed to a relatively poor depositional loss of this size fraction. The close proximity of the remainder of midlake aerosol volume to that of the typical urban air mass may be caused by the slow rate of depositional loss during transport from the predominantly Chicago source of May period aerosol. During June sampling, the heavy rains just prior to the

period are the major cause for the aerosol volumes encountered (Figure 24). The August and September periods both show a pronounced volume peak in the $r = 0.1$ to 0.2 μm size range (Figures 25 and 26). Since the $r = 0.1$ μm aerosol number concentration was ~3 x 10^{10}-m^{-3}, an order of magnitude greater than it was during May, coagulative transfer of aerosols from the $r < 0.1$ μm size to the $r > 0.1$ μm size could occur within a 4-hour period as against a 25-hour period in May. The coagulative aerosol transfer from any one smaller size range to the next larger size range in a unit time increment is proportional to the square of the number of aerosols present in the smaller size range. To illustrate, the time in which an initial concentration of 3 x 10^{10}-m^{-3} aerosols falls to one-half that value due to coagulative loss is less than 4 hours, whereas a concentration of 4 x 10^{9}-m^{-3} takes more than 25 hours to reach one-half its initial value. If an aerosol population is sampled after the $r < 0.1$ μm aerosol concentration falls to half its initial value, it may be referred to as an "aged" aerosol population. The aerosol populations sampled in August and September can then be described as partially aged, and some enhancement of certain trace metal concentrations sampled on a Hi-Vol filter may have occurred. Gillette (1972b) found a 10 percent or more enhancement of Pb concentrations in aerosol populations which underwent aging during transit over Lake Michigan. The August volume distribution carries more volume overall than September, with substantially more in the $0.1 < r < 1.0$ μm size range. Wind speeds were not too dissimilar: August, $\bar{u}_5 = 4.9 \pm 1.3$ m-s^{-1}; September, $\bar{u}_5 = 5.9 \pm 1.6$ m-s^{-1}. In both periods, air downwind from the Chicago/Gary source area was sampled for less than 10 percent of the total sampling time. Neutral to slightly unstable temperature conditions prevailed more often in September. A data set by data set analysis showed that a thermally stable surface layer prevailed in August for the time when Chicago/Gary source aerosols were traversing to the midlake sampling site. Order of magnitude aerosol volume in the $0.1 < r < 1.0$ μm size was present for only two data sets thereafter, but this was sufficient to cause the substantially greater volume in August sampling compared to September. This last point indicates volume distributions averaged over data sets are valuable analysis tools.

Several sequences of data set average ASAS volume distributions were considered. The most significant outcome to date from this sequencing analysis is the often controlling influence which wind direction shifts seem to have upon midlake mass concentration. That is, wind direction shifts have a strong influence upon aerosol deposition to the lake in addition to bringing differing source region aerosols to bear on the total mass flux of aerosol.

Figures 27-33 show the sequence including the data sets numbered 20050-20110 (elsewhere referred to as sets 5-11) and covering the period 17 May 77, 22:15 CDT to 19 May 77, 06:15 CDT. The wind speed was relatively constant on the evening of the 17th, but a wind direction shift of 60° to 70° occurred between 18:00 and 21:00 CDT. An extremely stable surface layer prevailed throughout the entire sequence of 7 data sets with the difference between air and surface temperatures (ΔT) being a minimum of 5.9°C, and a maximum of 13.3°.

Data set averaged wind speeds were as low as 1.7 $m\text{-}s^{-1}$ and as high as 4.6 $m\text{-}s^{-1}$. Table 9 shows the data set start and stop times, the meteorological data averaged across each set's sampling time, and the aerosol parameters also averaged across the set sampling times.

The value for $\bar{C}_m$ averaged across the 7 sets, as determined by integrating nephelometry (equation 10) is 129 ± 54 $\mu g\text{-}m^{-3}$, whereas the standard Hi-Volume sampler, run across all 7 data sets, gave a value of 132 $\mu g\text{-}m^{-3}$. The nephelometer primarily responds to the $d < 1$ μm aerosol and should give a value somewhat below the Hi-Volume sampler. The b_{scat} values suggest variations in aerosol mass concentrations from set to set. This is substantiated by the ASAS volume distributions. The area under each volume distribution curve in Figures 27-33 has been producted by a size-independent aerosol density of 2 $g\text{-}cm^{-3}$ to give the values in the last column of Table 9. The mean of these equivalent mass concentrations is 120 $\mu g/m^3$ with a large standard deviation of 113 $\mu g\text{-}m^{-3}$. The second to last column gives the equivalent mass concentration measured by the ASAS in $d < 1$ μm aerosol sizes. The mean of 84 ± 64 $\mu g\text{-}m^{-3}$ shows somewhat less fluctuation from set to set than does the total ASAS mass, but the extreme values of 19 and 174 $\mu g\text{-}m^{-3}$ show that very wide fluctuations in midlake fine particulate concentration are possible. A consideration of the meteorology related to each set may help explain why such large variability is possible.

The first set in this sequence, 20050, had a moderate 51 $\mu g\text{-}m^{-3}$ ASAS mass concentration with nearly all of that mass in the $d < 1$ μm size range. Strong thermal stability, moderate wind speeds and winds from the Chicago source area with each meteorological variable rather steady all lead one to expect the concentration to be substantially higher. However, a wind direction shift of 60^o to 70^o had occurred only two hours prior to sampling. Since the Chicago source aerosol would be expected to reach midlake during the subsequent data set (20060), it is not surprising that the mass concentration determined from ASAS data more than tripled at that time. The smaller ΔT due to cooler nighttime air still maintains a very stable surface layer while wind speed and direction do not change at all. During set 20070, wind speeds drop off a bit, ΔT increases again, but an unchanged wind direction allows midlake air to become thoroughly populated by Chicago source area aerosol. During set 20080, wind speed continues to decrease to a value 1.9 $m\text{-}s^{-1}$, whereas the thermal stability continues to increase with daytime heating. However, a 60^o wind direction shift to southerly flow probably accounts for the six-fold fall-off in the ASAS mass concentration. The southern shore area is a weaker aerosol source region than the Chicago area, but far from six-fold weaker. Since stronger thermal stability and lower wind speeds prevail, aerosol deposition to the lake should be reduced during the 20080 set when compared to the 20070 set. However, the wind direction shift before and the relatively large σ of 46^o during set 20080 sampling appear to be strongly increasing depositional loss. Note, too, that σ on wind speed was 30% of

$\bar{u}_5$ during 20080 sampling, but only 8 percent of $\bar{u}_5$ during 20070 sampling. Another 35° wind shift with a 40° deviation during the 20090 set, along with a doubling of wind speed contributes to the maintenance of the ASAS-derived mass at about 30 $\mu g\text{-}m^{-3}$. By set 20100 the Chicago/Gary source is again upwind but too little time has elapsed for Chicago-derived aerosol to reach midlake. If anything, the wind shift, along with the 25 percent σ on wind speed, appears to have caused still more depositional loss to the lake, for the lowest ASAS and b_{scat} mass concentration for this seven set sequence was observed during set 20100. By the 20110 set the 212° wind direction has brought aerosol from the Gary area to the midlake site. The source types in Gary produce a substantial amount of coarse particulate mass ($d > 1$ μm). Combined with a shorter fetch (40 km, as compared to 55 km for the Chicago source) this resulted in a dramatic increase of total and especially of $d > 1$ μm aerosol mass.

This sequence of seven May sets indicates that wind direction change is an important Great Lakes loading factor in its own right, i.e., direction shifts can result in strong depositional loss of aerosols to the lake independent of the differing aerosol source regions presented to the lake by these direction changes. Donelan (1977) contends that the size and state of development of wind generated waves are important and occasionally controlling factors for momentum transfer at the air/water interface of the Great Lakes. In particular, the ratio of wind speed to the speed of the wave edges and the angle between their respective directions are critical parameters. When the waves are "young" they will not be in equilibrium with the wind field. As the waves "age" they approach an equilibrium with the wind field, the difference in speed reaches a minimum, and the angle between the wind direction and wave propogation direction usually approaches a minimum. Donelan (1977) has measured momentum drag coefficients (C_D) 5-to 10-times those observed under steady state conditions (see Figure 34). It is quite reasonable to expect aerosol transfer to increase several fold, if not by an order of magnitude during these same conditions. In fact, the large loss of aerosol mass between set 20070 and 20080 and again between sets 20090 and 20100 seems to exemplify the large mass transfer increase associated with young waves. The fact that the ASAS mass was at a minimum during set 20080 despite $\bar{u}_5$ of only 1.9 $m\text{-}s^{-1}$ is another indicator of substantial mass transfer due to wind diviation shifts and associated young waves. Since the majority of filter/data sets on Lake Michigan were collected during steady state conditions and not soon after large wind direction shifts, the majority of sampling occurred with aged waves present. As a result, the aerosol concentration measured may be high while the deposition velocities used do not represent young wave conditions. The resultant loadings found in this study do not reflect these non-steady state conditions. Though the consideration of non-steady state conditions would likely increase lake loadings, this is not obvious or even certain.

One sampling day during which non-steady conditions were followed by unusually high loadings was 30 September 77. Such occurrences are best investigated by a case-by-case approach, integrating all available data sources.

On 29 Sept 77, three weakly coupled low pressure areas were located in the Texas panhandle, over Lake Superior, and over New England. The Lake Superior low pressure system moved Southwest and eventually formed an elongated trough By 2 October 77, there was a cold front stretching from Louisiana to Maine. While it was in its early stages of formation, the front passed through the sampling site. Pre-frontal rain was observed at the ship the night of the 29th, and moderate to heavy rain followed the front, though no further precipitation was observed at the sampling site. Prior to frontal passage, there were broken clouds at 4000 m, while after the passage, the broken clouds were at 3000 m and the sky was generally overcast. The relative humidity on 30 September 77 was 70 to 90 percent. Winds at 300-600 m (1000-2000 ft.) were from the South to South-Southwest ahead of the front, at 1900 CDT and by 0700 CDT were from the West to West-Southwest. To analyze the effect of these occurrences, it is necessary to estimate the time of frontal passage through the sampling site. There was a 40° windshift at the ship between 0500 CDT and 0530 CDT. The pressure reached a local minimum at the same time. The pressure minimum was reached at Midway Airport between 0300 and 0500 CDT. However, wind shifts were observed at Midway, the 68th Street water intake crib, Argonne National Laboratory and Governors State University in the period 0900-1300 CDT. Because of reduced surface roughness, it is not unusual for an over-water system to be retarded upon land fall. This conjecture is borne out by consideration of the subjectively drawn streamlines for this period which show that at 0700 Milwaukee, WI, Muskegon, MI, and the midlake Sampling Site had undergone windshifts while Chicago, Michigan City, MI, and Benton Harbor, MI were still reporting southerly flow. The front had apparently formed a bulge over the lake so that the front approximately paralleled the Southern Lake Michigan shore, approximately 15-30 km from shore.

The loading on 30 September 77 was so heavy an odor could be detected at the midlake sampling site. Aerosol concentration detected by Hi-Vol sampling, by the ASAS, and by the IN were all substantially larger (2-to 3-fold) than the concentrations of the previous day. This is despite the fact that precipitation occurred overnight, which normally has the effect of depleting aerosol concentrations. The ASAS data taken during this period show that there was a significant drop in the concentration of aerosol in the size range $0.1 < d < 10$ μm somewhere between 100 and 160 m above the surface. There was also a depletion of aerosol concentration in the size range $0.5 < d < 1$, between 50 and 100 m above the surface, though this had little effect on the total volume concentration.

Soundings over the lake were taken by the NCAR Queenaire on this day. These reveal an inversion extending from 100 m to 200 m above the surface, with a lapse rate of nearly 20°C/km in this layer. This is consistent with the ASAS data. The height to which surface air would penetrate if heated 3°C was only about 200 m, while the comparable mixed layer for the previous day was 400-700 m. This inversion certainly prevented extensive vertical mixing over the lake. The lake surface was a modest 0.1°C (± 0.3°C) warmer than the near surface air, which is not particularly conducive to mixing. Another event which may have contributed to the heavy loading is apparent

upon consideration of the back trajectories calculated for this period. Since the surface wind speed was near 4 $m\text{-}s^{-1}$ during the sampling period, the air samples left shore 3-5 hours earlier. During this period, the wind shifted in such a manner that the volume, which was eventually sampled, swept through the heavily industrialized area along the south shore. It is these types of occurrences which make the gathering of data which is representative of a large area very difficult.

4.3 METEOROLOGICAL AND CLIMATOLOGICAL CONSIDERATIONS

The bulk deposition velocity was shown in equation 3 to be determined by the product of wind speed and the diabatic drag coefficient. The mean wind speed at the nominal sampling height of 5 meters was quite steady over a filter sampling set. Values ranged from a low of 1.7 ± 0.6 $m\text{-}s^{-1}$ to a maximum of 8.3 ± 0.6 $m\text{-}s^{-1}$. These values are not entirely representative of conditions over Lake Michigan since the local climatology indicates that wind speeds higher than 8.5 $m\text{-}s^{-1}$ occur one-fourth of the year (see Figure 35). However, the observed range of wind speeds results in an underestimate of annual average loading, provided, of course, that the low wind speed regime is carefully considered. It is well known that the condition of smooth flow over a water surface is established at wind speeds below 2 $m\text{-}s^{-1}$ and possibly below 3 $m\text{-}s^{-1}$. The smooth flow condition is one in which laminar (non-turbulent) flow prevails just above the air/water interface. When this laminar sublayer is spatially continuous, the transfer of aerosols to the water is impeded. With higher wind speeds, the roughness elements at the surface begin to protrude beyond the sublayer. Turbulent transport pathways may then strongly enhance aerosol transfer across the interface. Data of Kondo, et al. (1973) show that high frequency wave components cause 30 percent of the measured surface roughness elements to extend outside the laminar sublayer at wind speeds of 2 $m\text{-}s^{-1}$. Although these protrusions into the turbulent zone may give rise to substantial aerosol transfer, wind speeds of 2.0 $m\text{-}s^{-1}$ or less are assumed here to allow a continuous laminar sublayer to be established. This essentially blocks all aerosol transfer to the water surface, i.e., $v_d = 0$. It is felt that this may again be an assumption which leads to underestimates of loadings. Further, it obviates the determination of C_0, since C_0 for almost any constituent will be a significant fraction of C_5 only when the continuous laminar sublayer is present.

For wind speeds in the 2.0 to 8.5 $m\text{-}s^{-1}$ range, a neutral drag coefficient is graphically determined from Figure 34. The drag coefficients for neutral momentum (C_D), heat (C_H) and water vapor (C_E) are presented for wind speed measurement at the 5 m height. An analogy between water vapor transfer and mass transfer is sometimes suggested to support the use of C_E. However, the momentum drag coefficient was used because of a possibly still better analogy between momentum and aerosol transfer to be described later in this section. The results of several experiments (Sheppard, 1963; Hicks, 1972; and Kondo, 1975) were used to identify the C_D curve of Figure 34. Note the weak dependence of C_D on wind speed. Indeed, some micrometeorologists claim C_D to be independent of wind speed (Wu, 1969).

Having obtained a value for C_D, a correction for thermal stability can be incorporated by determining the diabatic drag coefficient, C_{DD}. This coefficient is usually determined experimentally by monitoring both the wind speed and temperature profiles in the lowest ten meters above the surface of interest. This regime is referred to as the surface layer. A Monin-Obukhov length is then calculated (Montieth, 1973). In the case of sampling on board an anchored ship, the temperature profile can be measured with reasonable accuracy, but the wind speed profile cannot be monitored (Donelan, 1977). A simplification of the Monin-Obukhov length determination must then be used if C_{DD} is still to be calculated.

The surface layer can be considered as a constant flux layer (here, the aerosol mass flux). Hicks (1972) and Kraft (1977) have shown the constant flux assumption to be valid to at least one meter of height for every several hundred meters of constant fetch. Fetch is here defined as that distance across which an invariant surface condition is presented to the wind field. As long as no sharp wind direction changes occur within five kilometers of the ship sampling site for the duration of a data set, a sufficient fetch and thus constant flux surface layer prevails. The determination of sufficient fetch is simply based on the absence of fronts within 5 km upwind of the ship. If this condition was not met, the data set was not considered for loading estimates.

In essence, then, the use of the drag coefficient method as stated here assumes a steady state condition during sampling. This assumption results in an underestimate of the annual average bulk deposition velocity, $\bar{v}_d$. Donelan (1977) has shown that the drag coefficient may at times be two to five times the neutral steady state C_D. This may be primarily due to wind direction shifts which then cause the wind flow lines to cut across the wave edges. Of course, a rapid 180^o wind direction change gives the most dramatic increase in drag coefficient--at least for momentum transfer.

Whether such large deposition velocities are appropriate for aerosol mass transfer when compared to momentum transfer as determined by C_{DD} directly is uncertain. This point will be further considered later in this section. Under the condition of adequate fetch, then, an analysis suggested by Kondo (1975) can be performed, as in Appendix B, to give the ratio of the diabatic drag coefficient to the neutral drag coefficient, C_{DD}/C_D. This ratio is expressed as a function of a stability parameter S_o, which for h = 5 is given by

$$S_o = \frac{\bar{T}_o - \bar{T}_5}{1.3\ \bar{u}_5^2} \tag{11}$$

The dependence of C_{DD}/C_D on temperature stability is developed more fully in Appendix B. For thermally stable conditions, i.e., $\Delta T = T_5 - T_o > 0$

$$C_{DD}/\ C_D \simeq 0.1 + 0.03\ S_o + 0.9\ \exp\ (4.8/S_o) \tag{12}$$

and for thermally unstable conditions, i.e., $\Delta T = T_5 - T_o < 0$

$$C_{DD}/C_D \simeq 1.0 + 0.47\sqrt{S_o} \tag{13}$$

These equations are plotted in Figure 35 as a function of S_o. The reduction in C_{DD}/C_D with increasing thermal stability is quite evident. For $\bar{u}_5$ = 5 m-s^{-1} C_{DD}/C_D equals 0.22 when $\Delta T = 8^oC$. These conditions prevail over southern Lake Michigan 12 percent and 3 percent of the average year, respectively. Unstable air prevails more often. ΔT of -4^oC and -8^oC occur on the average 30 percent and 13 percent, respectively. Yet the increased C_{DD}/C_D does not compare to the reduced C_{DD}/C_D under stable air conditions. This ratio is 1.07 and 1.15 for ΔT of -4^oC and -8^oC, respectively. Thus, for conditions over southern Lake Michigan, thermal stability may cause a 5-fold or greater variation in the deposition velocity, but the frequency of occurrence of this wide variability is not very high. Figure 37 is a cumulative frequency of occurrence plot for ΔT between -16^oC and $+16^oC$ over southern Lake Michigan. These climatological data were derived from the National Oceanic and Atmospheric Administration (NOAA) Summary of Synoptic Meteorological Observations for the Great Lakes Areas, Vol. 3: Lake Michigan (1975). These data were obtained from edited observations reported in the period 1961-1973 by ships in passage. It should be noted that since such ships attempt to avoid bad weather, the data are thereby biased.

Having estimated the deposition velocity as a function of micrometeorology, it is important to consider synoptic and mesometeorological effects (especially on $\tilde{v}_d$) in conjunction with micrometeorology. An additional factor in this discussion is the fact that source region and source type may contribute substantially to aerosol concentration variability, even at a midlake sampling point. Trajectory analyses -- especially back trajectory analyses -- based on meso- and synoptic meteorology can be used to establish source regions for each data set.

A simple back trajectory calculation followed aerosol sampled at the ship back toward shore horizontally and upward through first an assumed 50 m deep surface layer and then into the mixed layer. Upon reaching shore the trajectory was stopped and the time to reach shore was obtained to within ± 20 percent. The back trajectory procedure during traverse within the surface layer used the at-ship horizontal wind speed and direction averaged across the time of sampling for each data set and a vertical velocity estimated by $\tilde{v}_d$. Although not a real velocity, $\tilde{v}_d$ represents the time-averaged vertical motion of aerosols within the surface layer, so long as it is truly a constant flux layer. Within the mixed layer, vertical velocities are estimated by the mass continuity equation, whereas horizontal velocities are estimated by a weighted average of the sampling ship's horizontal velocity and a triangulation average of National Weather Service upper level sounding data. The horizontal spread in the completed trajectory was assumed to be determined by trajectories using two standard deviations about the mean wind direction. The vertical spread was determined through use of stability category dispersion coefficients determined as a function of the bulk Richardson number (Ri_B) (Nagib, 1978).

Although this simple trajectory procedure may be criticized on several counts -- especially regarding its accuracy -- the results are used simply to identify five horizontal source regions. In addition, the predominance of

nearshore mesoscale and long range macroscale sources can usually be identified. The five source regions are shown in Figure 1 and are defined as:

1) An overlake source with a long fetch across the northern and upper part of southern basin of Lake Michigan, referred to as L. It encompasses the ship to trajectory-at-shore angles 325^{o} to 30^{o}.

2) A west shore source of moderate to light industrial and residential development (nearshore) and largely forested land (longer range). Encompassing the ship to trajectory-at-shore angles 270^{o} to 325^{o}, it will be referred to as WS.

3) A southwest shore source of heavy industry and dense population. This source takes in Gary, Indiana with its heavy steel industry by beginning at 190^{o} and the entire Chicago source except its northern suburbs by ending at 270^{o}. Nearshore contributions from the source region will in most instances mask any long range contributions. It will be referred to as C/G for the Chicago-Gary source.

4) A southeast shore source of moderate industrial and residential development (nearshore) and agriculture (longer range). Encompassing the ship to trajectory-at-shore angles 90^{o} to 190^{o}, it will be referred to as SES.

5) An east shore source encompassing the ship to trajectory-at-shore angles 30^{o} to 90^{o}. This source is largely agricultural (nearshore) and industrial (longer range). It will be referred to as ES.

As to nearshore mesoscale vs. long range macroscale source identification, whenever the mean trajectory remains within the 50 m deep surface layer and the dispersion maximum trajectory within a 200 m deep layer all the way to shore, the nearshore source contributions are assumed to be predominant. Whenever the mean trajectory projects above a 100 m height before reaching shore, both nearshore and long range sources are assumed to contribute to midlake aerosol concentrations.

Some of the data sets cannot be analyzed by this trajectory approach because synoptic scale fronts were present on southern Lake Michigan or because the variation in wind direction across the data set was too great to identify any one source region.

Certain days during which interesting or anomalous conditions may have prevailed were subjected to a case study analysis. In the case of data set 50560, this has resulted in a strong suspicion that data taken were not truly representative of the indicated source region. These data were excised from source region consideration.

The possibility that coagulation of d < 0.1 μm aerosols may be an indirect source of sampled aerosol is addressed by the time the aerosol takes to reach shore. Gillette and Winchester (1972) found that coagulative aging of 6 hours or more does contribute to Hi-Vol filtered Pb concentration; however, for less than 4-hour aging no coagulative source for Pb is present. Given the fact that only five data sets had times-to-reach-shore of more than 6 hours, it is not very likely that a coagulative source contributes to sampling except for a few sets from the overlake source sector.

The determination of a Richardson number (Ri_B) can be calculated from $\overline{u}_5$ and $\overline{\Delta T}$, measured ahead of the ship's bow. The smaller this number, the more turbulent is the surface layer air. Several of the May and one each of the June and September data sets have large Ri_B. These sets were obtained, then, during conditions of reduced turbulence. One indication of synoptic effects is obtained by identification of the air mass type in which the sampling took place. Rossby diagrams were used to identify air mass types. Only about half of the sampling periods could be clearly associated with an air mass type. Continental polar (cP) air masses prevailed during 15 of the sampling periods, and maritime tropical (mT) air masses prevailed during 7 of the sampling periods.

Though the processes that directly determine the interfacial aerosol removal rate are microscale in nature, these processes are to some degree energetically parasitic on larger scales of motion. A complete understanding of microscale events requires some knowledge of the effect of measured synoptic scale phenomena. Because of the complex and non-linear nature of the interaction of synoptic scale events with the meso and micro-scales and with the climatology, a quantifiable relationship has not been sought. Nevertheless, a general consideration of the synoptic situation during sampling periods is necessary for several reasons.

It is not to be expected that events of a single year will parallel a regional climatology exactly, but significant anomalous events may indicate certain periods or types of data for which scepticism is appropriate when climatological extrapolations are made. Precipitation events were excluded since this study focused on dry deposition removal of atmospheric constituents to the lake. Frontal effects were also avoided as much as possible so that a relative constancy in meteorological conditions prevailed during each filter sampling data set. From a climatological viewpoint this does introduce anomalies since the greater mass transfer to the lake associated with frontal turbulence is not considered. Conservative estimates of atmospheric loading should result.

In the absence of frontal or precipitation events, the process most directly influenced by the synoptic scale which is of interest in this study is aerosol transport. The advective history of an air parcel will largely determine the character of the background aerosol it contains. The interaction of synoptic and mesoscale influences determines the short-to-mid-range vertical and horizontal transport of aerosol.

The direction of the near-surface winds reflected in the backward-in-time trajectory manual calculation revealed significant differences when aggregated by outing. If a mean is taken of all May, 1977 sampling-period-averaged wind directions, a value of 202°, with a σ of 40° is obtained. The climatology shows the two major wind directions in May are northerly or southerly. Thus, this outing is not particularly anomalous, but is lacking in representation of a major (and presumably "cleaner") source region characteristic of this period. The 300-600 m (1000-2000 ft.) winds were observed to be generally from the southwest during this period, as revealed by streamlines based on NWS data. A comparison of NWS upper air soundings taken at Midway Airport with those of standard air-mass types indicates that May, 1977 air in this region was most similar to maritime tropical (mT) air masses, consistent with the conclusion that this outing sampled air which arrived from the south.

A synoptic-scale vertical velocity was crudely calculated from one-dimensional divergences based on several NWS surface observations. The magnitude of the vertical velocities is not considered reliable, but these calculations do provide some indications of whether the synoptic situation tended to support rising motion or subsidence during the outings. The May, 1977 outing was characterized by a tendency toward subsidence, probably related to the not uncharacteristic residence of a high pressure area over the Great Lakes.

The June, 1977 outing mean wind direction was 203° (σ = 24°), which is quite consistent with the southern Lake Michigan climatology. However, the 300-600 m streamlines indicate a North-Northwest source for this level. This is substantiated by the persistent presence of continental polar (cP) air mass types. This air mass type typically has experienced a trajectory over relatively non-industrualized land. One would expect the "background" values of aerosol for this outing to be somewhat depleted compared to, say, the May outing.

The divergence-derived vertical velocities for this outing were positive (upward) on the average, indicative of the influence of two low pressure system passages during this time. As a general expectation, this should effectively increase the mixing depth and lower surface concentrations. The occurrence of substantial precipitation just prior to the outing resulted in the lowest concentrations experienced throughout the entire field program.

The back-trajectory source regions for the August, 1977 outing seems to be divided on the morning of August 16 by the passage of a low pressure system and associated developing front. Before this point, the winds were variable, but generally from the East (91°, σ = 44°). After frontal passage, the winds were from the northwest (327°, σ = 20°). The 300-600 m streamlines were from the northwest throughout the period, except during the frontal passage. As might be expected, the air mass type was cP after the evening of the 16th and mT before that. These occurrences are sharply in contrast with the climatology for the month, which indicates a strong tendency for south-southwest winds with a rather sharp "roll-off" of probability outside of these wind directions. Because of the strong and proximate aerosol sources that an air

mass with a traverse from the South would encounter, one would expect that the air sampled during August 1977 was atypically "clean." The calculated vertical velocities before the frontal passage were ambiguous, but afterwards the indications were for general subsidence.

The September outing is also seemingly divided into two regimes. Weather of the period before the evening of September 28 is dominated by a low pressure area which was to the East of Lake Michigan at the beginning of the outing and moved eastward. The combination of this system and a high pressure area to the West induced generally northerly winds (308^{o}, $\sigma = 19^{o}$) during this time. On the evening of the 28th, the low had moved far enough off shore to allow the high to establish itself southeast of Lake Michigan. This induced southerly winds for the remainder of the outing (181^{o}, $\sigma = 37^{o}$). The 300-600 m winds were westerly to northwesterly for the first portion of the outing and southerly thereafter. The air mass type was cP throughout. The climatology shows a general tendency for southerly winds in September, so that once again the outing-averaged concentrations for September might be looked upon as conservative estimates, with respect to the climatology. The calculated vertical velocity was quite variable, largely due to the synoptic disturbance, but the overall tendency was for subsidence.

A common mesoscale event is the lake breeze. Because of the large perturbation a lake breeze event has on transport, it is fruitful to attempt to assess the frequency of lake breezes during the sample periods. A major complicating factor is the uncertainty in whether to call certain events lake breezes. Past concern with lake breezes has stemmed from their effect on populated shorelines, so that occurrence criteria normally include a substantial degree of penetration inland. Objective indices are usually calibrated to those types of observations which are not necessarily of prime interest to this study, but still should provide at least a general guideline. Lyons and Olsson (1973) have documented the southern Lake Michigan lake breeze climatology. Lake breezes are observed overland approximately 35 percent of all days during May through August, and occasionally in March, April and September. Of the 15 days on which midlake samples were taken, one would expect slightly over five observations of lake breezes. In fact, only one day, 19 May 77, developed a lake breeze strong enough to be observed at Midway Airport (approximately 12 km inland). The 68th Street Crib observations show two additional days, 7 June 77 and 18 Aug 77 which had significant lake breezes.

A recent index was discussed by Lyons (1972) which is based on water-land temperature differences and pressure gradients. He reported a hindcast accuracy of 90-95 percent, if cloudiness and gradient flow influences were considered. An index which is perhaps more easily calculated from the data routinely gathered during the field program was developed by Hall (1954). This index is principally based on pressure differences. Hall found this index, in conjunction with other criteria, produced a hindcast accuracy of 92 percent but an overprediction of 65 percent. Using the Hall criterion, 18 May 77, 19 May 77, 7 June 77, 18 Aug 77, and 28 Sept 77 were identified as days with high lake breeze potential. The occurrence of lake breezes was confirmed for 7 June77 and 28 Sept 77.

Considering the paucity of over-lake data, lack of confirmation does not necessarily indicate non-existence.

The lack of roughness over the lake's surface, especially in comparison to that present over the Chicago/Gary source region, will tend to reduce the frictional turning effect on aerosol trajectories. Pilot-balloon (pibal) releases from the midlake sampling point tend to confirm this expectation for the August and September outings. Of 12 pibal releases during the August outing, only 2 were not straight line trajectories. Of 11 pibal releases during the September outing, only 1 was not a straight line trajectory. This would suggest that the August 18 and September 28 field days were not affected by the lake wind or gustfront phenomena. In contrast, the May 19 lake effect appears to have met classical lake breeze criteria, having a return flow layer aloft. Lyons (1975) has shown this return flow to bring more large aerosol ($d > 1$ μm) to the midlake surface layer than would otherwise be expected. This is exactly what the ASAS data shown in Table 9 indicates. The mass concentration of total aerosol increases from 23 to 333 $\mu g/m^3$ between the morning and afternoon of May 19 according to the ASAS data and from 47 to 141 $\mu g/m^3$ according to the b_{scat} of the IN. The increase is greater for the ASAS since it responds to $d > 1.0$ μm aerosol.

SethuRaman (1976) has considered the air mass modification caused by the change in surface characteristics from the rough, warm overland surface to the smooth, cool overlake surface. In addition to the mesoscale wind effects stated above, a pronounced thermal internal boundary layer (TIBL) often develops. This TIBL reduces the vertical dispersion of aerosol overlake and may cap off the vertical mixing. The height to which mixing occurs (H) may have considerable horizontal variation and is difficult to deduce from a single measurement. One semi-empirical calculation of H is given by Raynor, et al. as:

$$H \approx \frac{u_*}{u} \sqrt{\frac{F(T_U - T_D)}{-\Delta T/\Delta z}} \qquad (14)$$

where u_* is the friction velocity, F is the fetch in meters, $\Delta T/\Delta z$ is the lapse rate in $^oC\text{-}m^{-1}$, T_U is the upwind (land-based) surface temperature, and T_D is the downwind (lake) surface temperature. A calculation of this TIBL height, H, gives 235 ± 100 m for the May outing as a whole, with August and September having too small a percentage of cases with $T_D < T_U$ and June being inappropriate for application of equation (14) due to non-steady synoptic conditions. The 325 m TIBL for May is substantially less than the 1200 to 1500 m mixed layer height for the spring/summer midwestern area (Holzworth, 1972) which would otherwise be the best available estimate of mixing depth for aerosol over Lake Michigan.

Mesoscale events such as gust front passages and lake breezes can change the character of the wind field on a very short time scale -- on the order of a few minutes or less. The interaction of a new wind direction or speed with a previously established lake wave-train effectively presents a much altered and presumably rougher surface layer. This is part of the rationale behind the attempt to sample only during constant wind conditions. The change in sea state

following a wind shift can also be expected to affect the upward flux of aerosols. This is assumed to be of minor importance for the elements analyzed except Ca and Mg.

Windshifts are often accompanied by rapid changes in air temperatures. Besides having the obvious effect of changing stability conditions, this temperature change and any associated moisture change will affect the evaporation rate. It will always be somewhat simplistic to view these various atmospheric changes as independent effects. The amount of moisture in the air will affect the air buoyancy and, more importantly, can affect both the surface reactivity and the chemical characteristics of aerosol particles. Since changes in cloud cover are often associated with air mass changes, the effect of solar radiation on many atmospheric chemical reactions, particularly those involving nitric oxide, ozone and various organic materials, may provide another link between synoptic events and aerosol characteristics.

The air mass changes resulting from synoptic flow have effects similar to mesoscale air mass changes. They are generally on a longer time scale and are more easily identifiable. This may not be the case, however, when the front is weak, or undergoing formation or dissolution. Indeed an instance of the first effect was only discerned for the case of September 30, 1977 by post-analysis.

Besides estimates of uncertainty based on temporal variability or meteorological parameters, spatial variability must be considered. The midlake $\tilde{v}_d$ values obtained can be considered locally valid within a factor of 2 or 3. The process of extrapolation of these results to the whole of the southern lake or to an entire year may introduce even more uncertainty. At several points in this analysis, an effort is made to determine what is the minimum reasonable annual loading. Since these values are rather uncertain, an investigation of the sources of uncertainty and methods of increasing the degree to which the results may be trusted is in order.

The deposition of aerosols over the surface of the lake is considered to be uniform and to vary principally with distance from the shore -- probably in a non-linear fashion. It is likely, however, that most of the gradient occurs near-shore. The principal factors to consider are the short but increasing fetch as an air parcel moves away from shore, as well as the change in wind field and its effect on surface roughness and on ΔT with increasing distance from shore. The surface layer of constant mass flux will be nonexistent at the sharp discontinuity that is the shore (Vugts and Businger, 1977). In the first few kilometers from shore the reduced friction over water often causes a wind direction and speed change which, along with the temperature instability nearshore, causes a slow growth in the surface layer depth. However, between 5 and 10 kilometers from shore the surface layer can be expected to have reached 50 to 90 percent of its midlake depth (Hess and Hicks, 1975). The temperature difference between air and water surface stabilizes within a few kilometers distance from shore. In over 20 cases of NCAR aircraft overflights, the air temperature at 15 to 35 meters above the lake's surface always came to equilibrium with lake effects within 5 to 10 kilometers of shore. The water surface

temperature itself decreased in the first few kilometers, but also came to an equilibrium temperature, usually within the first 5 kilometers from shore. Water surface temperature anomalies did appear occasionally even at midlake -- very likely due to upwelling of warm, or cold, water from below the surface. It is safe to say, however, that the ΔT observed at the midlake sampling point is generally representative of 70 to 90 percent of the southern basin's lake surface -- unless synoptic scale or strong mesoscale fronts are present. The subsequent spatial variation of wind speed and direction could interact with aerosol concentrations in such a way as to make a plume either more or less diffuse, or far-reaching (Lyons, Keen, and Northhouse, 1974). Indeed the spatial variations in concentration found in plumes or even more diverse gradients bring into question the representativeness of sampling. Nearshore wind speed changes can be expected but should come to equilibrium with the relatively constant roughness of the lake's surface at least as rapidly as the air temperature. Thus again, unless synoptic conditions are dominant, the wind speed measured at the midlake sampling site should be representative of 70 to 90 percent of the southern basin's lake surface.

Changes in wind direction and in the variability in wind direction can be expected to affect not only the transport of aerosol, but the drag coefficient, since it takes some time for a wave regime to come into equilibrium with a new wind direction (Donelan, 1977). Though there is insufficient data to verify that directions measured at midlake were representative, the lack of large roughness elements on the lake and the care taken to restrict sampling periods to a constant wind regime suggests that the $\pm \sigma$ envelopes used were sufficient for the purposes to which the back trajectory method was applied.

Since the steady state 3-to 6-hour averaged bulk deposition may be considered reasonably constant over most of the lake's surface, the midlake concentration of any one constituent is a fraction of the source region concentration given by

$$C_{midlake} = C_{shore}\left[1 - \tilde{v}_d \cdot \frac{\Delta T}{H}\right] \qquad (15)$$

where $C_{midlake}$ varies only as a function of source concentration, shore to midlake travel time (t), ΔT, and the mean depth (H) to which mixing of that constituent occurs. When considering long range transport, H is usually chosen as the average mixed layer height of approximately 1000 m. However, transport of warm air from Chicago over the cold lake surface in spring and early summer creates the TIBL discussed previously, which sharply reduces mixing in the lowest few hundred meters above the surface and allows almost no mixing above the TIBL (Lyons, et al., 1974). If Equation (14) is used to estimate the TIBL height and u_* is taken to be 10 cm-s^{-1}, H is 150 m for the period of May 18-20, 1977. The wind direction was $225^o \pm 15^o$, and as a result C_{shore} was the Chicago source concentration. Using H = 150 m, the previously estimated ΔT and $\tilde{v}_d$ by data set and knowing $C_{midlake}$, an estimate of C_{shore} can be obtained by equation (15). Sievering, et al. (1979) then used Chicago's 22 sampling station average sulfate, Pb, Fe, and Mn concentrations to confirm the validity of H $\simeq$ 150 m and of the use of the bulk deposition velocity $\tilde{v}_d$ as being representative of the actual deposition velocity prevailing.

This confirmation assumes the aerosol size distribution remains essentially invariant with distance from shore. In an effort to assess the effects of short-range overlake transport, the aircraft data taken on 30 Sept 77 for the period 06:45-06:57 CDT were examined. During this time, the aircraft was headed directly from Midway Airport toward the midlake sampling site at an altitude of 310 m prior to 06:48 CDT (shore) and 30m after 06:49 CDT. There was a steady, persistent tailwind. Although these circumstances augered well, there were some complicating circumstances. A front was just forming and passing through the area, as described above, but exact time of passage could not be determined. Additionally, the flight path passed over a tanker about 20 km from shore at 6:50 CDT. A large increase in aerosol concentration was observed (Figure 38) throughout the size range measured ($0.1 < d < 10.0$ μm). Since this occurred immediately after overlake traverse began, relative contributions are not clear. The remainder of the leg was characterized by a general increase in aerosol concentration with fetch, particularly at 06:53 CDT. The only significant depletion of aerosol occurred in the size range $0.8 < d < 1.0$ μm, nearly 50 km from shore. There are several possible explanations. The measurement platform might have simply outrun the tanker plume, or it may have passed through the developing front.

The rate of decrease in number concentration with log d has been found -- worldwide -- to remain relatively constant. For this reason, the slope of the $\Delta N/\Delta$ (log r) plots (see Figures 19-22) is generally found to be near -3. On 30 Sept 77, the slope near shore (before 6:48 CDT) was slightly greater than -3. For much of the leg (06:48-06:52 CDT) the slope generally matched the expected -3 slope. After 06:52, near midlake, there was a decrease in the slope. It should be noted that the ASAS can give unrealistic data during conditions of high humidity, such as those observed on this day. This comes about not only from the possibility that water droplets will be counted as aerosols, but also because aerosols themselves often act as a nucleus for the formation of water droplets, which will obviously distort the size distribution. Although the case was chosen because of the fortuitous wind direction, the overwhelming contribution of other conditions prevented the discernment of a clear effect of overlake fetch. The examination of other appropriate cases will be pursued.

4.4 REMOVAL OF AEROSOLS AT AIR/WATER INTERFACE

Calculation of the bulk deposition velocity, $\tilde{v}_d$, described earlier in this section, is based on several assumptions which, strictly speaking, must remain in effect throughout the sampling time of each filter set. First, if momentum transfer is to be equated with aerosol mass transfer, sedimentation must be a negligible contribution to aerosol motion. Since the ASAS data showed essentially all the aerosol volume to be in the $d < 2$ μm size fraction -- except in very unusual circumstances -- this assumption is valid. Second, a constant flux layer must prevail. The criteria for data set beginning/ending resulted in this assumption being true for all but a few discarded sets. It becomes apparent that this sampling technique will bias the results toward low deposition velocities when one considers that non-steady state conditions will increase v_d. Third, in using $\tilde{v}_d$ one assumes the air/water interface concentration of a constituent

of interest to be a small fraction of the sampling height concentration. Only if this is true will the mass transfer coefficient, X_m, to be equal to v_d. It is felt that as long as the surface microlayer (Andren, 1975) is not present, this assumption is likely to be valid. The validity of this assumption is integrally tied to a fourth assumption; that a spatially continuous laminar sublayer prevails only with wind speeds of less than 2.5 m-s^{-1} and probably only for 2 m-s^{-1} or less. It is very likely that high concentration surface microlayers occur primarily when the laminar sublayer disallows transfer to the lake surface. Wind speed measurements in conjunction with surface microlayer studies are not entirely consistent for Lake Michigan samples (Andren, 1975; Eisenreich, 1978), but certainly the vast majority of cases with surface microlayer enrichment of trace elements or nutrients occur in very light winds. If the ratio of surface to bulk water trace element concentration is near one, the microlayer is probably not present and the laminar sublayer is also likely not to be present. Thus, the concentration of trace elements or nutrients at the air/water interface will be much less than their respective concentrations at the 5 m sampling height.

Support for the assumption that $X_m \simeq \tilde{v}_{d5}$ (i.e., that $C_0 \approx 0$) in higher winds -- when the laminar sublayer is discontinuous -- is given by Stulov, et al. (1978), who considered the collision efficiency of aerosols at water surfaces. At a clean water surface all collisions are effective and lead to aerosol transfer into the liquid. When aerosols collide with other aerosols previously deposited on that water surface, they usually rebound. Aerosol-aerosol collisions might occur when the surface microlayer is present, but the probability is otherwise extremely low. Further, Meszaros (1977) has found that 90 percent of summer continental aerosols not unlike those found over Lake Michigan are water-soluble, and in winter months 50 percent or more are water-soluble. As long as the laminar sublayer and surface microlayer are not present, it appears that the air/water interface constituent concentrations are indeed a small fraction of 5 m height concentrations. By assuming $\tilde{v}_d$ to be zero for wind speeds of ≤ 2.0 m-s^{-1}, the strong reduction in aerosol mass transfer in the presence of either of these layers should yield conservative estimates of total loading.

One final assumption -- a most important one -- must be considered. The use of the momentum drag coefficient to estimate $\tilde{v}_d$ carries with it the implicit assumption that the momentum drag coefficient, K_m, is equal to the eddy diffusion coefficient, K_D. This equality is usually referred to as the Reynolds analogy. Since much more is known about momentum transfer than mass transfer in the atmosphere, correlations of mass transfer based on momentum transfer have been developed by Reynolds and others. The Reynolds analogy simply states that in a turbulent regime mass and momentum are transferred in an analogous way and, thus, $K_D = K_m$. This analogy can be restated for the experimental conditions over Lake Michigan as:

$$\frac{\text{Momentum Flux}}{\text{Momentum at 5 m}} = \frac{\text{Aerosol Flux}}{C_5} \qquad (13)$$

The deposition velocity given by the latter ratio can then be equated to the former ratio which is identically $C_{DD} \cdot \bar{u}_5$. Does the Reynolds analogy, $K_D \simeq K_m$, hold for sampling conditions over Lake Michigan? This question cannot be simply answered; it requires a significant digression by careful consideration of mass and momentum transfer near the air/water interface. The reader to whom this is of little concern is advised to omit this discussion and resume at the beginning of Section 5.

A diagramatic representation of conditions near the interface is shown in Figure 39. Two quite different conditions can be expected to prevail within the surface layer above and at the lake's surface. A smooth flow regime is shown on the left. Here, the surface layer is seen as three separate ones: a turbulent layer, a buffer layer, and a laminar sublayer. The turbulent layer constitutes the largest portion of the surface layer depth of several meters to several tens of meters. A continuous laminar sublayer enveloping all or nearly all of the surface roughness elements follows the gross observable contour of the lake's surface.

Mass transfer within the laminar sublayer is dominated by molecular transport, i.e. Brownian motion. The buffer layer is a transition zone in which turbulence is reduced due to the close proximity of the surface. Both turbulence-induced eddies and Brownian motion contribute to mass transfer in the buffer layer. Turbulent transfer may be characterized by the eddy transfer coefficient (K_D) (cm^2-sec^{-1}), whereas molecular transport due to Brownian motion is characterized by the molecular diffusion coefficient (D) (cm^2-sec^{-1})

The molecular Schmidt number, Sc^L, is the ratio of the kinematic viscosity of air, ν(cm^2-sec^{-1}) to d and gives a measure of the rate of mass transfer to be expected due to molecular diffusion within the laminar sublayer. When $Sc^L < 1$ or $D > \nu$, a condition of relatively good transfer will prevail, whereas $Sc^L > 1$ or $D < \nu$ is a condition of relatively poor transfer. ν for air at 20° C and 1 atm pressure is 0.15 cm^2-sec^{-1}, while D for spherical aerosols of diameter 0.1 and 1.0 μm is 6.75×10^{-6} and 2.77×10^{-7} cm^2-sec^{-1} respectively. The molecular Schmidt number is clearly much greater than one for the 0.1 to 1.0 μm and larger aerosol size range. Thus, the continuous laminar sublayer of the smooth flow regime blocks the transfer of aerosols and associated trace elements and nutrients.

As higher wind speeds and less stable air prevail within the surface layer, a rough flow regime is eventually met (shown on the right of Figure 39) in which many of the surface roughness elements protrude outside of a now discontinuous laminar sublayer resulting in a more efficient path for mass transfer. The wind speed and stability at which this rough flow regime is actualized is quite uncertain. Yet it is certain that turbulent transfer will increase the overall mass transfer substantially. Turbulent transfer dominates the mass transfer of aerosols in both smooth and rough flow regimes for the majority of the surface layer which constitutes the turbulent layer. A turbulent Schmidt number, Sc^T, is defined as K_m/K_D and is applicable to the turbulent layer where K_m and K_D are the momentum and eddy transfer coefficients as before. Of course, when $Sc^T = 1$

or $K_m = K_D$ the Reynolds analogy holds. Businger, et al. (1971) found $Sc^T = 0.74$ in neutral conditions within the turbulent portion of the surface layer. Blackader (1975) estimated Sc^T to be 0.85 in neutral conditions. Unstable conditions within the turbulent portion of the surface layer could result in Sc^T values of 0.75 to no less than 0.67 times the neutral Sc^T or 0.50 (Kraft, 1977). Stable conditions could result in Sc^T values of no more than 1.17 times the maximum neutral value, or 0.99 (Kraft, 1977). Because of sedimentation effects, mass transfer is usually more efficient than momentum transfer in the turbulent layer. The Reynolds analogy holds, and the momentum drag coefficient is an accurate parameter for use in mass transfer calculations. The buffer layer is a layer of transition between turbulent transfer and molecular transfer. As such, mass transfer may be reduced relative to momentum transfer. However, this reduction is very much dependent upon whether the smooth or rough flow regime, i.e. a continuous or discontinuous laminar sublayer, prevails.

Given that the turbulent layer may be characterized in the same way regardless of whether smooth or rough flow prevails, the total surface layer mass transfer, X_m, can be split into two parts: a turbulent layer mass transfer, X_{TL} and a remainder mass transfer, X_R. Since the resistance to mass transfer, $R(h)$, is additive in the surface layer

$$R(h) = R_{TL}(h) + R_R(h) = \frac{1}{X_{TL}} + \frac{1}{X_R} \tag{16}$$

where h is the height of measurement, $R_{TL}(h)$ is the resistance to mass transfer in the turbulent layer, and $R_R(h)$ is the remainder mass transfer resistance.

It can be shown (Slinn, 1978) that

$$R_{TL}(h) = \frac{1}{X_{TL}(h)} = \frac{u_*}{\bar{u}_h^2} \equiv C_D \tag{17}$$

Kraft (1977) has shown that a more accurate statement must account for the combined thickness of the buffer layer and laminar sublayer and that Sc^T may not be assumed equal to one. As a result

$$R_{TL}(h) = \frac{1}{X_{TL}(h)} = \frac{\bar{u}_h - \gamma \cdot u_*}{\bar{u}_h^2} \cdot Sc^T \tag{18}$$

where γ is a constant between 2 and 10.

In most cases (and certainly over the lake) $\gamma \cdot u_*$ is much less than $\bar{u}_h$ so that $X_{TL} \simeq [\bar{u}_h \cdot C_D \cdot Sc^T]^{-1}$. Since $X_{TL} \propto C^{-1}$, the mass concentration (or that

of an aerosol constituent) is proportional to $\bar{u}_h \cdot C_D \cdot Sc^{\frac{1}{3}}$. The resistance to mass transfer for the turbulent layer is then approximately proportional to $\bar{u}_h$ since, as Figure 34 shows, C_D is a weak function of wind speed. This suggests that the midlake mass and trace element concentrations should vary with wind speed in a nearly linear fashion. The correlation coefficient between wind speed and mass was -0.12, and the percentage of linear variation in all chemical constituents explained by wind speed was 9 percent. However, a strong linear dependence of mass and trace elment concentrations on ΔT was found. The correlation coefficient between ΔT and mass was 0.52. Since the dispersion of aerosols in the vertical as well as the intensity of vertical velocity fluctuations is inversely proporational to ΔT in neutral to nearly all conditions of thermally stable surface layer air (Izumi and Caughey, 1976), the aerosol concentration may be expected to be directly proportional to ΔT. All but two or three concentration data sets were collected in neutral to stable air, and the correlation coefficient shows the direct proportionality expected. Thermally controlled turbulence within the turbulent and buffer layers must be contributing significantly to aerosol mass transfer in the overlake surface layer as these aerosol traverse from shore to midlake. The manner in which thermally generated turbulence is reduced in the buffer layer may then be an important research question. K_D in the buffer layer will be somewhat reduced relative to K_M as a result, but it is unknown by how much. Binkowski (1979) has shown that $K_D \propto \lambda \cdot \sigma_w$ in the surface layer where λ is the wavelength of the peak in the vertical velocity spectrum and σ_w is the standard deviation of the fluctuating vertical velocity component. As theory or experiments determine the difference between λ and σ_w in the turbulent surface layer from that in the buffer layer, a proportionality constant ε in $K_D = \varepsilon K_m$ may be estimated and the degree and conditions under which the Reynolds analogy holds approximated.

The lack of any linear dependence of the measured midlake concentration upon wind speed strongly suggests mass transfer may be largely independent of sublayer presence. Fewer than 10 percent of the data sets were obtained in wind speeds of 2 $m\text{-}s^{-1}$ or less. Kondo, et al. (1973) found that 30 percent of the roughness elements related to high-frequency components of ocean waves protrude outside the laminar sublayer at 2 $m\text{-}s^{-1}$ wind speeds. At 8 $m\text{-}s^{-1}$ over 99 percent of the high-frequency roughness elements protrude outside the remaining discontinuous sublayer. Schlichting (1968) observes that "from a physical point of view it must be concluded that the ratio of the height of the protrusions to the laminar sublayer thickness should be the determining factor" for smooth or rough flow. Since 30 percent of the high frequency ocean wave components protrude outside the sublayer at 2 $m\text{-}s^{-1}$ and the mean sea-surface roughness height equals the laminar sublayer thickness at 3 $m\text{-}s^{-1}$, smooth flow conditions will probably not prevail above 2 $m\text{-}s^{-1}$ and certainly not above 3 $m\text{-}s^{-1}$. Thus, a continuous sublayer was likely present for no more than 10 percent of the data sets collected.

Fully rough flow for momentum transfer is usually assumed to prevail at u_{10} = 7 to 8 $m\text{-}s^{-1}$ and above (Wu, 1972), whereas one may expect a transition flow between ~ 3 $m\text{-}s^{-1}$ and 7-8 $m\text{-}s^{-1}$, and smooth flow below ~ 3 $m\text{-}s^{-1}$. It has been stated that momentum transfer or K_m can be expected to be larger (possibly much larger) than K_D in the buffer layer during transition and smooth flow due to what is known as the bluff body effect (Chamberlain, 1968). In the

immediate vicinity of the surface, momentum is transferred to the surface by skin friction and pressure forces, which are due to fluid impacting on the roughness elements of the surface. Momentum transferred by pressure forces at the surface is known as form drag, and since there is no analogue in mass transfer a possibly severe limitation of the Reynolds analogy is encountered within the buffer layer. As a result, it is uncertain at what wind speeds the smooth, transition, and rough flow regimes apply to mass transfer.

The form drag force depends on the shape and orientation of the bluff body -- here, the roughness elements at the air/water interface. Maximum form drag is experienced by surfaces at right angles to fluid flow and the force can be estimated by assuming ρu_h to be the momentum transferred per unit volume of air at a point on the surface where fluid is brought to rest after being decelerated from a velocity u_h. Since $u_h/2$ is the mean velocity of the bulk fluid, the rate at which momentum is lost is $\rho u_h \cdot u_h/2$. In fact, fluid slip around the sides of the bluff body results in a force $< \rho u_h^2/2$. It can be expected that there is sufficient eddy formation in the vicinity of roughness elements to produce a form drag less than the theoretical maximum per unit area of $C_{DF} \cdot u_h^2 \cdot \rho/2$, where C_{DF} is the form drag coefficient.

Even though the form drag force is not at its maximum, it still contributes to the momentum transfer coefficient, K_m, with no analogous contribution to K_D. The wind speed regime for which smooth, transition, and rough flow prevails may therefore differ in addition to $K_m \simeq K_D$. There is, however, the aerosol mass transfer mechanism of turbulent inertial deposition in the buffer layer. Suppose aerosols in an idealized circular eddy are deflected through 90^o around the circular arc at the radius of this eddy, r. The centrifugal acceleration involved is $r\,(d\theta/dt)^2$, where $d\theta/dt$ is the angular velocity. This produces a radial "skid" of the aerosols relative to the accelerating air. This implies that aerosols immediately above the laminar sublayer will travel a finite distance before coming to rest. This finite distance is called the stop-distance, S, and is given by (Friedlander, 1977):

$$S = \frac{\rho_p\, d^2\, v_o\, \rho}{18\, \nu} \qquad (19)$$

where: ρ_p is the aerosol density

ν is the kinematic viscosity of air

ρ is the air density

v_o is the initial velocity imparted to the aerosol, and

d is the aerosol diameter.

Note the strong d^2 dependence of S on aerosol diameter. Clearly, when S is greater than or equal to the laminar sublayer thickness, δ, the combined mechanisms of turbulence and inertia of the aerosol or turbulent inertial deposition will cause an aerosol to traverse the sublayer. It can be shown (Twomey, 1977) that the collection efficiency of the water surface beneath the sublayer is in fact $S/\delta \simeq S/r$, or that the ratio of aerosol stop-distance to the mean radius of eddies determines their collection efficiency. As before, a knowledge of the wavelength spectrum of buffer layer turbulence would add greatly to understanding of mass transfer at the lake's surface.

Owen and Thomson (1963) have shown that horseshoe eddies wrap themselves around the individual roughness elements for those that are closely spaced. Such eddies can be expected to result from the high frequency wave components referred to earlier. Numerical models (Batchelor, 1967) and wind tunnel experiments (Taneda, 1956) of the flow past a circular cylinder (somewhat like an individual high frequency wave component when protruding outside the laminar sublayer) for neutral conditions and at $2 < u_{10} < 5$ m/s show the formation of closed streamlines downstream of the cylinder from 0.2 to 2.0 times the cylinder diameter. This eddy formation may well occur in the space between the closely packed roughness elements at the lake's air/water interface. Since the eddies are smaller than the roughness elements themselves and the roughness element heights measured by Kondo, et al. (1973) at u_{10} = 2 to 3 m-s^{-1} were about 1000 μm, the mean eddy radius may be 500 μm or less. Turbulent inertial deposition could then be a contributor (due to roughness element created eddies) to deposition at the lake's surface despite the low wind speeds of 2 to 3 m-s^{-1} for the half-micron and larger aerosol.

If we now reconsider the data of Kondo, et al. (1973), it is likely that turbulent inertial deposition in the 2 to 5 or 6 m-s^{-1} range and turbulent impaction to the roughness elements directly in the ~4 m-s^{-1} range or greater wind speed ranges induce a low resistance path for aerosol transfer when compared to molecular diffusion transfer through the laminar sublayer. At 2 m-s^{-1}, 30 percent of the roughness elements protrude outside the sublayer so that direct impaction due to turbulence-induced aerosol velocities and turbulent inertial deposition across the sublayer combine to provide a "short-circuiting path around" the laminar sublayer. This path may be available to half or fewer of the aerosols in the buffer layer but will be an efficient transfer path despite the 2 m-s^{-1} wind speed.

Thus, the transition from smooth to rough flow for aerosol mass transfer may have already begun at 2 m-s^{-1}. At 3 m-s^{-1} and more the mean height of the roughness elements is equal to or greater than the sublayer thickness, and the aerosols may follow the low resistance turbulent impaction or inertial deposition pathway to the lake's surface. At 8 m-s^{-1}, the mean roughness element height is probably five times the mean laminar sublayer thickness of < 0.08 cm and over 99 percent of the roughness elements protrude through a very discontinuous sublayer. At this wind speed the buffer layer itself -- usually estimated to be five times the sublayer thickness -- is only about equal to the mean roughness element height. Fully rough flow in the sense of turbulent eddies controlling

mass and momentum transfer prevails. In this case the data of Businger, et al. (1971) and Blackader (1975) can certainly be applied and $K_D \simeq K_m$. Though it cannot be stated with certainty, K_m will likely become no more than 2-to 3-fold K_D as smooth flow conditions become established. It is only below 2 $m\text{-}s^{-1}$ (and possibly 3 $m\text{-}s^{-1}$ under thermally stable surface layer conditions) that large discrepencies between K_m and K_D are realized. The Reynolds analogy certainly holds for aerosol mass transfer in rough flow conditions and may well be valid within a factor of two or three at wind speeds above 2-ms^{-1}.

All of the above digression into buffer layer and laminar sublayer dynamics argue for a rather small resistance to aerosol mass transfer for those layers. In particular, X_m becomes equal to X_{TL} as the rough flow condition is approached, leaving only the mass transfer resistance in the turbulent layer, $R_{TL}(h)$, as the total resistance to transfer. As smooth flow conditions are approached, X_R passes through a point of equality with X_{TL} and may become an order of magnitude less than X_{TL} for wind speeds of < 2 $m\text{-}s^{-1}$.

If the vertical gradient in aerosol number concentration can be measured, a field experiment to test the above theoretical discussion is feasible. It was stated in Section 3 that this was found possible using the ASAS when vertical ship motion was minimal. The vertical velocity measured at a height of 5 m (W_5) as detected by a Gill anemometer, was used to monitor the ship's vertical motion. Wind speeds above 6 to 7 $m\text{-}s^{-1}$ and/or wind direction changes causing ship instability usually forced aerosol vertical gradients to be disregarded -- simply due to the large vertical motions encountered. There were two notable exceptions in the 7 to 8 $m\text{-}s^{-1}$ wind speed range. Wind speeds above 6 $m\text{-}s^{-1}$ also usually generated sufficient lake spray that the logarithmic criterion for the aerosol vertical concentration gradient was not met to within the 90 percent confidence expected. That is, the aerosol concentration profile with height should be logarithmic -- if no lake source contributes. Only those concentration profiles that were logarithmic at the 90 percent confidence level or better were considered for analysis. Heights of 3.7 ± 0.2 m and 6.4 ± 0.2 m at the ship and 4, 2, and 1 m to within $\pm$ 0.05 m at the crib site were used here to estimate deposition velocities.

The profile (or gradient) method has been used by Gillette (1972a) to estimate aerosol deposition velocities above a soil surface. Garland (1974) and Whelpdale (1974) have used the method to estimate sulfur dioxide gas deposition over land and water surfaces. When possible, wind speed and concentration profiles are simultaneously measured in the lowest 10 to 20 meters above the surface of interest. The profile method deposition velocity, v_{dp} at h is then given by:

$$v_{dph} = \frac{\rho \cdot C_{DD} \cdot u_h^2 \cdot \left[C_{h_1} - C_{h_2}\right]}{\left[u_{h_1} - u_{h_2}\right] \cdot C_h} \qquad (20)$$

where: $h_2 < h < h_1$

Since a certain time must pass before sufficient aerosol are sampled by the ASAS at each of the two heights, the concentrations, wind speeds and profile method deposition velocities, v_{dp}, are, in actuality, average values. Sequential rather than simultaneous monitoring is essential for the few percent intercalibration accuracy required of two separate aerosol sampling instruments is not possible. Precision and reproducibility of ASAS aerosol number concentration counting was found to be better than 2 percent for the relatively low concentrations at midlake. Thus, equation 20 becomes for the 5 meter mean height of measurement, with $h_1 = 6.4$ m and $h_2 = 3.7$ m and air density, $\rho \simeq 1$ kg-m^{-3}

$$\bar{v}_{dp5} = \frac{C_{DD} \cdot \bar{u}_5^2 \left[\bar{C}_{6.4} - \bar{C}_{3.7}\right]}{\left[\bar{u}_{6.4} - \bar{u}_{3.7}\right] \cdot \bar{C}_5} \qquad (21)$$

Because the ship sampling platform is not sufficiently stable to allow wind speed profile measurement, a power law, $\bar{u}_h = \bar{u}_5 \cdot (h/5)^{\alpha}$, can be used as an estimator of the 6.4 and 3.7 m wind speeds in the surface layer. The power law can be used in equation 21 to estimate the difference in 6.4 and 3.7 m wind speeds as $u_5 \left[(6.4/5)^{\alpha} - (3.7/5)^{\alpha}\right]$. α was determined by first calculating the bulk Richardson number, Ri_B, as:

$$Ri_B = \frac{g \left[\overline{\Delta T} + \Gamma (h_1 - h_2)\right]}{(\bar{T}_5 + 273) \left[\bar{u}_5^2 \cdot (h_1 - h_2)^{-1}\right]} \qquad (22)$$

The Richardson number has been related to the Monin-Obukhov length for Great Lakes conditions by Donelan, Birch and Beesley (1974), and finally Irwin (1979) has related the Monin-Obukhov length to values of α. For the conditions encountered on Lake Michigan, $0.14 < \alpha < 0.65$ values were obtained. The overall uncertainty introduced by not directly measuring wind speed was found to be 20 to 40 percent of the calculated wind speed difference. Finally, $\bar{v}_{dp5}$ can be stated in terms of actually measured parameters at the ship by

$$\bar{v}_{dp5} = \frac{C_{DD} \cdot \bar{u}_5}{(6.4/5)^{\alpha} - (3.7/5)^{\alpha}} \cdot \frac{\bar{C}_{6.4} - \bar{C}_{3.7}}{\bar{C}_5} \qquad (23)$$

where the uncertainty introduced by $\bar{C}_{6.4} - \bar{C}_{3.7}$ has been somewhat reduced by sequentially sampling several times at the 6.4 at the 3.7 m heights. However, an additional uncertainty of 10 to 30 percent was found. Overall uncertainty in $\bar{v}_{dp5}$ estimates are then 30 to 70 percent. Profile measurements at the crib site were more accurate due to the fixed platform. Aerosol number concentration measurements at 4, 2, and 1 m heights gave an estimated 2 m reference deposition velocity $\bar{v}_{dp2}$ with 10 to 40 percent uncertainty.

Since the bulk momentum drag coefficient-estimated deposition velocity is $\tilde{v}_h = C_{DD} \cdot \bar{u}_h$, a correction factor for the difference between momentum transfer and aerosol mass transfer can be stated as

$$\frac{\bar{v}_{dph}}{\tilde{v}_d} = \frac{\bar{C}_{h_1} - \bar{C}_{h_2}}{\bar{C}_h} \cdot \frac{1}{\left(\frac{h_1}{h}\right)^{\alpha} - \left(\frac{h_2}{h}\right)^{\alpha}} \qquad (24)$$

This calculation affords a way to use the experimental data to test the theoretical arguments made earlier. Four field profile data sets will be considered here. These profile data sets were selected to demonstrate variation of $\bar{v}_{dp}/\tilde{v}$ with light, moderate, and high wind speeds, and lastly with a rapid change in wind speed. Finally, the average results of nine additional moderate wind speed profile data sets will be considered.

Table 10 shows the basic data and the $\bar{v}_{dp}/\tilde{v}_d$ ratios. The first profile set was taken at the crib site and gave the smallest ratio of $\bar{v}_{dp}/\tilde{v}_d$ for any wind speed greater than 2 m-s^{-1}. This may very well be due to the 25^o to 30^o shift in wind direction during the last 30 minutes before the profile set began. During the set itself, wind direction was extremely steady (this was a criterion for "good" profile sets), wind speed was 4.0 ± 0.2 m-s^{-1} and a slightly stable surface layer of $\overline{\Delta T}$ = 2.0 ± 0.3^o obtained. The bulk deposition velocity, $\tilde{v}_d$, was 0.6 cm-s^{-1}, whereas $\bar{v}_{dp} = [0.7 \pm 0.3]\tilde{v}_d$ for 0.6 < d < 1.5 μm, $\bar{v}_{dp} = [0.2 \pm 0.1]\tilde{v}_d$ for 0.3 < d < 0.6 μm and $\bar{v}_{dp} = [0.4 \pm 0.1]\tilde{v}_d$ for 0.1 < d < 0.2 μm. Notice that although the ASAS counts aerosols of d up to 3.5 μm, too few counts in the d > 1.5 μm were observed to be statistically significant. For the half micron aerosol, the $\bar{v}_{dp}/\tilde{v}_d$ ratio of 0.2 was one of the smallest values of the entire profile data sets. At the other extreme, the 16 Aug 77 ship profile set with a wind speed of 7.9 ± 0.3 m/s has the extreme high $\bar{v}_{dp}/\tilde{v}_d$ value of the entire profile data sets. For all sizes of aerosol 0.1 < d < 2.0 μm the $\bar{v}_{dp}$ is larger than $\tilde{v}_d$, despite the calculated 1.3 cm-s^{-1} bulk deposition velocity for momentum transfer. Note also the relative independence from aerosol size as compared to the case of 23 June 78 which had lower wind speeds, yet had similar temperature stability.

The 28 Sept 77 profile set had one of the lowest average wind speeds, 1.3 ± 0.3 m-s^{-1}, but still about the same temperature stability as the 23 June 78 and 16 Aug 77 cases. This low wind speed most certainly has brought on the smooth flow case since the ratio of high to low position counts is one or less than one throughout the 0.1 < d < 2.6 μm size range.

The most interesting profile set may be the sequence on 19 May 77, when unseasonably warm air over land brought about a $\overline{\Delta T}$ = 8.5^{o}C or more at midlake. This extremely stable surface layer was observed at 13:30 to 16:30 CDT to be in a state of near microscale stagnation since the wind speed was only 1.6 ± 0.5 m-s^{-1} and wind direction was extremely steady (105^o ± 5^o) during the four hour sampling period. As a result, the lowest ratios of high to low position counts for any profile set were recorded. This, despite a 180^o wind direction shift in the 12:00 to 13:00 CDT period. The laminar sublayer and buffer layer apparently combine to totally block aerosol mass transfer. Since the wind speed is below 2 m-s^{-1}, this is also the result expected for momentum transfer. Since Ri_B is 0.22, turbulence within the surface layer as a whole can be expected

to be substantially suppressed. The average ratio of aerosol counts at the 6.4 m height to that at the 3.7 m height is less than 0.9, with a range from 0.75 to 0.95. Thus, aerosol were actually being "stacked up" in the lowest few meters, with gravitational settling possibly having an effect on the ratio for 1 μm and larger aerosols.

Between 16:30 and 17:00 CDT, a rather unusual sharp increase in wind speed unaccompanied by any noticeable wind direction or ΔT change was observed. Thereafter, for over one hour the wind speed was steady at 4.2 ± 0.3 m/s. The surface layer during the 17:00 to 18:30 CDT period was clearly one in which mass (and momentum) transfer took place. This is exemplified by the count ratio for $0.6 < d < 2.6$ μm aerosol being 1.34, as compared to 0.77 before the wind speed increase. However, the ratio of $\bar{v}_{dp}/\tilde{v}_d$ is quite small with $\bar{v}_{dp}$ $(0.1 < d < 2.2$ μm$) = [0.05 \pm 0.02]\tilde{v}_d$. Since $\tilde{v}_d = 0.25$ cm-s^{-1}, $\bar{v}_{dp} \simeq 0.01$ cm-s^{-1}. The gravitational settling contribution to $0.6 < d < 2.6$ μm aerosol still appears to be present. A comparison with the 23 June 78 profile set shows an eight-fold smaller $\bar{v}_{dp}$ for this 19 May 77 17:00 to 18:30 period for the $0.1 < d < 0.2$ μm aerosols. The much stronger temperature stability on 19 May 77 probably reduces the actual deposition velocity. Given the short-lived micrometeorological change from 17:00 to 18:30 CDT on 19 May 78, the laminar sublayer so well established during the 13:30 to 16:30 time period was very likely a much more significant factor during the 17:00 to 18:30 time period than on 23 June 78, when the wind speed was approximately 4 m/s that entire day. Although the data cannot conclusively argue the point, it is likely that turbulent impaction and turbulent inertial deposition are both substantially reduced for the 17:00 to 18:30 period of 19 May 77, as compared to the 23 June 78 case.

By 20:00 CDT on 19 May 77, the strong thermal stability of the surface layer appears to have blocked most aerosol transfer again. Despite the 40° wind direction shift which has occurred, the strong stability, along with somewhat lower wind speeds, results in $\bar{v}_{dp} \simeq 0$ for $d \geq 0.3$ μm aerosol, as well as a small value for the ratio $\bar{v}_{dp}/\tilde{v}_d$ of 0.1 to 0.2. This does not seem unusual except that the small aerosol now are depositing, whereas during the 17:00 to 18:30 period the large aerosol had five-fold larger $\bar{v}_{dp}$ than did the small aerosol. The large aerosol concentration was depleted relative to small aerosol concentration by 20:00 CDT. Note that the lake source (WD = 105°) did not contain a high concentration of large aerosol, and that the wind direction change did not bring replacement large aerosol to the sampling site. A possible explanation for the deposition of small aerosol during the 20:00 to 21:15 CDT period, despite the lack of large aerosol, is that there had been little previous deposition of small aerosol. Their high concentrations, in conjunction with the wind direction change, finally brought about deposition of small aerosol even though wind speeds diminished. Finally, by the 22:45 to 24:00 CDT period, $\bar{v}_{dp}$ is zero, and steady state conditions were obtained with aerosol mass transfer completely blocked. Even though the wind speed is essentially the same as during the 23 June 78 profile set, no deposition occurs because of the extreme temperature stability.

Consideration of nine moderate wind speed ($2.4 < \bar{u}_5 < 8.2$ m/s) profile sets results in a $\bar{v}_{dp}/\tilde{v}_d$ ratio of 0.48 ± 0.19. The mean $\tilde{v}_d$ for the nine sets was 0.7 cm-s^{-1} and $\Delta\bar{T} = 2.6^{o}$C. The dependence of $\bar{v}_{dp}$ upon aerosol size is somewhat variable from profile set to set. However, no more than a three-fold, and only occasionally more than a two-fold difference, in $\bar{v}_{dp}$ across $0.1 < d < 2.5$ μm was observed. The 23 June 78 data set was the only exception among steady state profile sets. Both these results support the suggestion that turbulent impaction and turbulent inertial deposition contribute to aerosol mass transfer in the transition from smooth flow to rough flow. Indeed, since the $\bar{v}_{dp}/\tilde{v}_d$ ratio for this transition wind speed range was found to be about one-half, the Reynolds analogy is only mildly violated with $K_D \simeq K_m/2$ for these nine profile sets. A hypothesis might then be set forth: turbulent inertial deposition plus impaction may be for aerosol mass transfer what form drag is for momentum transfer at the air/water interface of large lakes. This can only be stated as a hypothesis at this point for too few data have yet been obtained by the profile method. Further, other transfer mechanisms such as phoretic effects may also contribute to aerosol mass transfer.

On a climatological basis, the Reynolds analogy may hold to better than the factor of two suggested by the nine steady state profile sets. As the 19 May 77 sequence pointed out, non-steady state conditions will tend to increase mass transfer. Of course, momentum transfer will also be increased. Donelan (1977) has shown that C_D approaches a minimum as the wave field approaches maturity. In contrast, "during a rising wind or near an upwind shore higher C_D are encountered." There is every reason to believe aerosol transfer may also be increased by five-to ten-fold, for the laminar sublayer could not have established itself in the early stages of wave development and turbulent eddies will then cause aerosol impaction upon the developing waves. Perhaps more significant for mass transfer to the Great Lakes is that by having sampled aerosol concentrations only under steady state conditions, the use of only steady state drag coefficients in $\tilde{v}_d$ estimation errs on the conservative (low estimate) side and thus contributes to Great Lakes loading estimates also on the conservative or low side of the probable mean.

SECTION 5

INTERPRETATION OF RESULTS

Two approaches were followed in the calculation of estimated annual dry loadings to the southern basin of Lake Michigan. The most basic approach is the overall-average method:

$$\text{dry loading} = \bar{v}_d \cdot \bar{C} \cdot A \cdot \tau \qquad (25)$$

where $\bar{v}_d$ is the mean bulk deposition velocity for all data sets ($m\text{-}s^{-1}$), $\bar{C}$ is the mean concentration of a given element ($kg\text{-}m^{-3}$), A is the total water surface area of the southern basin of Lake Michigan (2.9×10^{10} m^2), τ is that part of the year when no precipitation occurs overlake ($s\text{-}yr^{-1}$), and loading is in $kg\text{-}yr^{-1}$. Equation (25), although straightforward, entails an underlying assumption that deposition at the midlake point represents deposition over the entire southern basin. For single-site sampling, this is an unavoidable assumption. However, the surface layer conditions at midlake are certainly more similar to the majority of the lake surface than are conditions on shore or near to shore (see Section 4.3). Moreover (25) assumes that the data sets which made up the mean $\tilde{v}_d$ and C values were representative of the entire year's variability in $\tilde{v}_d$ and C. The values of $\tilde{v}_d$ and C are, however, strongly dependent upon surface layer meteorological conditions and aerosol source region. Overlake climatology is thus an important factor in the determination of annual loading rates (see Section 4.3). In order to relate the limited number of sampling hours (approximately two percent of the year) to the annual total loading, data sets taken in periods of similar surface layer conditions are computationally grouped into "bins". Each bin is defined by a range of values for one of three parameters: ΔT, u_5, or source region, identified through back-trajectory analysis. For each of the j bins the annual frequency of occurrence, F_o, is determined for the range of the defining parameter from climatological data (NOAA, 1975). Annual loadings which account for the climatological dependence of $\tilde{v}_d$ and C are then calculated from:

$$\text{dry loading} = \sum_j \bar{v}_{dj} \cdot \bar{C}_j \cdot F_{oj} \cdot A \cdot \frac{\tau}{\sum_j F_{oj}} \qquad (26)$$

In applying equation (26), it is assumed that the year in which sampling is done is a climatologically representative one. How well the data fits prevailing climatology is at least partially accounted for by the inclusion of the F_{oj} values (see Section 4.3). It is assumed, however, that the $\bar{v}_{dj}$ and $\bar{C}_j$ values for each bin do indeed represent the conditions of that bin averaged

over a year. Even so, (26) is a refinement over (25) in that the variations in v_d and C due to surface layer meteorology and source region are taken into consideration.

Two factors in the loading estimate calculations, (25) and (26), were quantified through field observations and related to overlake meteorological variability: $\tilde{v}_d$ and C. Because the results here are based upon sampling done at a single site, temporal variations within data-set-mean $\bar{v}_d$ and $\bar{C}$ are important factors in viewing the resultant loading estimates. The time-scale resolution afforded by the 3 to 6 hour data set duration eliminates short-term "patchiness" in the observed parameters, yet provides definition of the prevailing surface-layer meteorological regime. The data set initiation/termination criteria give priority consideration to the constancy of meteorological observations. As a consequence, the sets used in loading estimations generally had standard deviations about the data set means of: $\sigma WD < 15^o$, $\sigma u_5 < 0.6$ m-s^{-1}, and $\sigma\Delta T < 1^oC$. However, this degree of steadiness does not conclusively point to a similar aerosol concentration steadiness. Analysis of the ASAS data indicates that variation about the set-averaged number concentration was generally less than twenty percent (see Section 4.2). The IN-monitored aerosol mass concentration also showed a similar degree of steadiness. Each data set thus represents a period of fairly homogeneous meteorological and aerosol concentration conditions. The data set mean $\bar{v}_d$ and $\bar{C}$ were then used as input values for the loading calculations of this work.

The emphasis, during sampling, upon constancy of parameters within each set, necessitated relatively short Hi-Vol filter run times. The gross amount of aerosol collected was thus such that 7 elements which were analyzed for by ICAP-AES failed to appear above L_d in many data sets (Table 2). Contamination, probably introduced by the analytical procedure, makes the data for B unreliable. This leaves 9 elements and 3 nutrient species as candidates for the loading calculation; however, data for 2 of the elements must be used with caution. Because the Hi-Vol sampler pumps use Cu-alloy commutators which are known to produce Cu-aerosols (Moyers, Duce, and Hoffman, 1972), precautions were taken in setting up the samplers to avoid re-entrainment of the pump exhaust. At the 1.8 m^3 - min^{-1} flow rate, given the short run times and low filter matrix load, back-pressure contamination through the sampler head is unlikely. There is nothing in the Cu results to directly suggest that any significant contamination actually occurred. To the contrary, the percent of total aerosol mass, Π, and the ratio of elemental concentrations associated with fine and coarse aerosol, FC, for Cu appear to be consistent with other elements (Table 5). Even so, any Cu data from Hi-Vol sampling should be used with caution, and the loading results for Cu are so indicated. Finally, the Ti data shows some anomalous behavior that indicates probable contamination. Sievering, et al. (1979a) showed that while all other elements in this data base correlated inversely with u_5, Ti was positively, though weakly, correlated. By plotting Ti enrichment factors versus Al concentration (Figure 17), Ti is seen to tend somewhat towards constant concentration (dashed diagonal line). All this indicates the probability of contamination for Ti in collecting, handling, or analyzing the aerosol samples. The loading results for Ti are nevertheless

presented, but caution in interpretation is suggested. For the remaining 7 elements (Al, Ca, Fe, Mg, Mn, Pb, and Zn), the uncertainty introduced to the loading calculation by the concentration, C, factor is expected to be the ICAP-AES instrumental reproducibility confidence of less than 20 percent.

The binned data sets of Tables 11 and 12 demonstrate clearly that both $\tilde{v}_d$ and $\bar{C}$ are functions of the prevailing meteorological regime overlake. As much as a six-fold range in $\tilde{v}_d$ and an order of magnitude range in $\bar{C}$ for most elements were observed during the conditions sampled from May to September. Using the overall mean $\tilde{v}_d$ and $\bar{C}$, estimates of loading were calculated from equation (25). That calculation, however, does not take into account the wide range of observed $\tilde{v}_d$ anc $\bar{C}$. A better approach, in which the range and concurrent variability of both factors are applied, is the use of (26) to estimate loading. Also, from trends observed in the binned $\tilde{v}_d$ and $\bar{C}$ data, one can infer some qualitative information about the bias in loading resulting from the summer-season only sampling. The F_0 values provide a simple weighting factor for each bin in the averaging process of (26), relating observed data to southern basin climatology (NOAA, 1975). All loading results are normalized to $\tau = 2.7 \times 10^7$ s-yr^{-1}, i.e., the 85 percent of a year when no precipitation occurs overlake (Sievering and Williams, 1975). This entails the conservative assumption that no dry deposition occurs during precipitation. In fact, most estimates of atmospheric loadings assume dry deposition to occur throughout the year. F_0 values for the bins with the greatest $\tilde{v}_d$ values ($\overline{\Delta T} < -0.9^oC$; $\bar{u}_5 > 7.0$ m-s^{-1}) extrapolate the data to more unstable-air and high wind speed periods which were not sampled in the summer season. If winter season data had been available, the values of $\tilde{v}_d$ for these extreme-case bins would likely have been somewhat larger. Extrapolation through the F_0 values thus tends to make loading values apparent underestimates of annual loadings. At the other end of the bins, the assumption that $\tilde{v}_d$ is zero for all cases with $\bar{u}_5 < 2.0$ m - s^{-1} also leads to underestimation of annual loadings. For such low wind speed cases (which include some very stable-air cases), the laminar sublayer exists at the interface which impedes, but probably does not completely block (Sievering, 1979), aerosol deposition (see section 4.3). Both the $\overline{\Delta T}$ (Table 11) and $\bar{u}_5$ (Table 12) data set aggregations reveal that meteorological conditions which lead to high $\tilde{v}_d$ values were not sampled. The most unstable bin F_0 accounts for the 0.38 year with $\overline{\Delta T} < 0.9^oC$; yet, the single most unstable case sample was $\overline{\Delta T} = -2.0^oC$. Values of C_{DD}, and thus $\tilde{v}_d$ from (26) increase markedly as $\overline{\Delta T}$ becomes more negative. If more unstable ($\Delta T < -2.0^oC$) data had been collected, the $\tilde{v}_d$ for this bin would likely have been somewhat higher. Similarly, the bin for high u_5 values has an F_0 which accounts for the 0.41 year with $\bar{u}_5 > 7.0$ m-s^{-1}. The highest case sampled was $\bar{u}_5 = 8.3$ m-s^{-1}. Again, the available data sets miss the cases where higher $\tilde{v}_d$ values might have been determined. The F_0 values used in the extreme-case bins thus apply the available data to periods of the year when loading rates would be greater. Because of this, and despite the reduced $\bar{C}$ in the winter season, the loadings calculated here very likely are underestimates. Given this consideration and the 2-to 3-fold uncertainty in the C_{DD}-based $\tilde{v}_d$ determination, the lowest loading estimate from the overall-mean (25) and bin-method (26) calculations is divided by 2 and reported as a "minimum" loading.

The binned data of Tables 11, 12, and 13 reveal several kinds of general trends in the $\tilde{v}_d$ and $\bar{C}$ results which have direct bearing upon interpretation of the loading results. In Table 11, $\bar{C}$ for almost all elements generally increases as ΔT becomes more stable (positive); at the same time, $\tilde{v}_d$ decreases by a factor of 5. That is, for the stable-air cases when $\bar{C}$ is relatively higher, $\tilde{v}_d$ tends to be reduced. Because loading depends upon the product of these two factors, a summertime "self-protection" mechanism of the lake surface from stable-air (increased $\bar{C}$) periods is implied. For the late fall and winter unstable-air season, this mechanism is reversed; even though lower $\bar{C}$ values might be expected, increased $\tilde{v}_d$ would still result in significant cold season loadings. In Table 12, similar seasonal trends appear. Although less clearly apparent in the $\bar{C}$ data, $\tilde{v}_d$ varies strongly with increased wind speed. This is due not only to the use of the C_{DD}-based $\tilde{v}_d$, which increases somewhat with u_5 directly (Figure 34), but also the incidence of more unstable air ($\Delta T < 0$) during higher wind speed regimes. Thus, the winter season overlake being the increased $\bar{u}_5$ season (NOAA, 1975), the summer "self-protection" of the lake is reversed in winter. These trends in ΔT and $\bar{u}_5$, then, appear to indicate that while winter season, i.e. unstable air and high wind, conditions may lead to lower $\bar{C}$ expectations overlake, a partially compensatory trend toward increased $\tilde{v}_d$ during that season tends to continue loadings at a significant rate. It should be stressed here that these data were collected during the May through September 1977 period and therefore do not include any winter season data. The actual frequency of observance of ΔT and $\bar{u}_5$ ranges during sampling does, however, correspond to the climatologically expected values of F_o. Trends in these data are thus probably quite valid. The source region bin data in Table 13 point to another aspect of dry deposition loading. Although climatological expectations of ΔT and u_5, and thus, $\tilde{v}_d$ are only weakly variable with source sector, a $\bar{C}$ maximum is clearly indicated from the Southeast Shore and Chicago/Gary areas (Figure 1); not an unexpected result. The sum of F_o values show that 53 percent of the year these two high-air pollution regions are sources of increased $\bar{C}$ at the midlake site. As a consequence, the Chicago/Gary and Southeast Shore areas contribute from 60 to 85 percent of the total dry deposition loading to the southern basin.

The significance of atmospheric inputs of trace elements to the Lake Michigan ecosystem is not well known (IJC, 1978). Dry deposition appears to be a major contributing source of at least four elements on a percentage of total loading basis (Table 14). 10 percent of Mn, 20 percent of Fe, 30 percent of Zn, and at least 60 percent of Pb inputs to the lake are by dry deposition of atmospheric aerosol. Only for those elements which have very large natural land run-off inputs are atmospheric loadings seen to be negligible. The trace element loading estimates are discussed in detail in Appendix C.

The quantitative minimum estimates for annual dry deposition of nutrients, such as P, NO_2/NO_3, and SO_4 loading of the southern basin pose the immediate qualitative questions of relative significance of dry deposition and ecological impact. Unfortunately, there is to date no data regarding atmospheric nitrate inputs to the lake. Gatz and Changnon (1976) estimate atmospheric aerosol N input to be 20 to 45 times that of P, which agrees well with the result here of input N/P = 26. Eisenreich, Emmling, and Beeton (1977) summarized current data

from the literature on the relative importance of various P loading routes. Based on their analyses of monthly bulk samples collected around the shore of Lake Michigan in 1976, the atmospheric route accounts for 15.7 percent of all P inputs. They estimate P loading to the southern basin to be 1.05×10^6 kg/yr. Shoreline data may, however, overestimate total loading to the lake due to the close proximity of sources to P sampling sites. For comparison, earlier modeling estimates of P loading to the southern basin of Lake Michigan suggest 9-18 $\times 10^3$ kg/yr by the atmospheric route (Winchester and Nifong, 1971). The present estimate of dry deposition loading is then seen to be an order of magnitude above modeling estimates and an order of magnitude below bulk sampler estimates. Also, dry deposition of gaseous components, such as NO_x and SO_2, are not accounted for in the annual loading estimates of this work. Removal of gas phase pollutants in raindrops would be included in bulk precipitation measurements. There are no extensive wet deposition data from the midlake area to support this contention, however, and the bulk P loading of 1.05×10^6 kg/yr. remains a best available estimate. Based on this, the particulate dry deposition estimates account for at least 15 percent of atmospheric inputs of nutrients to the southern basin. Of more importance than this percentage implies, however, is the direct particulate deposition input of nutrient materials to the open waters of the lakes, far removed from shore sources. As Delumyea (1977) has pointed out, all atmospherically input nutrients must enter the surface water, i.e. the zone of photosynthetic activity. This is not the case for runoff water and direct discharge. Not only the total amounts of nutrients atmospherically input, but also the relative proportions of biologically active chemicals in aerosol, are of significance. As Kilham and Titman (1976) point out, a nutrient supply of changed composition can have disruptive effects upon the lake's biota.

Appendix A describes the basic theory and use of factor analysis in the identification of air pollution sources. Factor analysis is a technique which provides a way of recognizing and aiding in the interpretation of the underlying patterns of interrelationships in any multiple-parameter data base. Besides ascertaining the relationships, it condenses large sets of data into uncorrelated sets of factors. These factors can then be subjectively labeled or classified with a physical significance attached to the group of variables that constitute that factor.

The application of factor analysis to the midlake data base results in the specification of 6 uncorrelated factors, as shown in Table 15. The labeling or classification of the 6 factors, as well as a statement of primary and secondary member variables, is shown. A primary member is one for which that factor explains 75 percent or more of the variable's variance. A secondary member is one for which that factor explains 25 percent or more of the variable's variance. The percent variation row in Table 15 states the percentage of total variance in the midlake data base that is explained by each factor. In factor 1, the trace metals Ca, Mg, Al, Fe, Mn, Pb, Ti and Zn are primary members. The Chicago/Gary source region (C/G) and thermal stability (ΔT) over the lake enhance the concentrations measured at midlake for the trace elements above. This is the basis for the interpretation given to factor 1. Notice that despite the nutrients' secondary membership in factor 1, they are primary members of factor 4,

along with aerosol mass. The fine particulate metals Pb, Mn, and Zn are secondary members of this factor, but there is no wind direction association. This strongly suggests a longer range transport of the nutrients and that this factor is best described as fine particulate aerosol mass, unrelated to any one shore source region. The fact that mass is a primary member of this factor also suggests that the variance in midlake mass (not the mean itself but mass variability) is largely controlled by fine particulate ($d < 1$ μm) aerosols. Factor 3 shows that wind direction (but not necessarily change in wind direction) is not a controlling variable for metals' and nutrients' concentration variability at midlake. The elements associated with the coarse particulate fraction, viz., Ca, Mg, and Al are, however, shown to be mildly dependent upon wind direction by the factor 5 result. Temperature stability is shown in factor 5 to have a controlling influence over NO_2/NO_3 concentration variability and is of secondary importance to SO_4 and soil-derived coarse particulate. Finally, the second factor points out a negative though secondary dependence of Ti on wind speed. Upon closer scrutiny (Sievering, et al., 1979a) this appears to be attributable to ship contamination under light wind speed conditions. More importantly, factor 2 suggests that no other metals data is contaminated by ship effluent.

A more in-depth interpretation of several different midlake data base factor analyses is found in Sievering, et al. (1979a). The degree of surface layer turbulence, the time to reach shore, and air mass type are additional data (see Table 16) available for characterization of meteorological effects upon midlake elemental concentrations. The bulk Richardson number, Ri_B, was calculated to parameterize turbulence by data set as shown in Table 16, column 4. Data sets were then aggregated into 19 sets, having $Ri_B > 0.03$ and 20 sets, having $Ri_B < 0.03$. Factor analysis results are shown in Tables 17 and 18. Since larger Ri_B values indicate a surface layer reduced in turbulence and mixing, whereas smaller Ri_B values indicate enhanced turbulence and mixing, the results are quite reasonable. It was instructive to reintroduce Ti in this factor analysis by bulk Richardson number. In the case of reduced turbulence (Table 17), all the metals are members of factor 1, which explains over 50 percent of the variance in the 19 filter sets' data. Only Pb is more strongly a member of factor 4 and then along with Zn. Factor 3 and 1 together suggest that so long as turbulence is reduced, higher wind speeds are not necessary for high metal-related aerosol concentrations at midlake. Factor 2 shows that even with reduced turbulence, strong surface layer temperature stability is additionally necessary before mass concentrations and the concomitant large aerosol Al and Mg concentrations can be substantial. Table 18 shows that under conditions of enhanced turbulence mass is a member with the small aerosol Pb, Zn, and Mn, as well as Fe and Al. Given enhanced turbulence situations, neither surface layer wind speed nor temperature stability alone affect this 20 filter set metals' data base. Rather, the increased turbulence, along with lower wind speed, allows (as factor 3 points out) backwash of ship effluent to contribute to Ti loadings. Factor 2 shows that large aerosol, probably soil derived Al, Ca, Fe, and Ti, is present but does not contribute to mass concentration variance. Factor 4 suggests that Mg has its own unique source -- during enhanced turbulence conditions. The lake appears to be that source although it is unclear why Ca is not also a member of this factor. This may be because only 33 of the 40 data sets have Ca

concentrations above analytical detection limits. The lake source region data sets also suggested Mg to be lake derived. In Table 15, ΔT stands alone. It does not affect the metals' data during these enhanced turbulence conditions.

The third column of Table 16 indicates the average trajectory time for aerosols to reach shore for each of the 35 data sets for which trajectories could be drawn. By splitting the sets' data base into 15 with 3.5 hr. or greater trajectory times and 17 with 3.0 hr. or shorter trajectory times, the factor analysis results of Tables 19 and 20 are obtained.

In the case of the long travel time trajectories, Ca, Mg, Mn, Pb and Zn metal concentration variations explain over 40 percent of the variation in the data base. The third factor suggests Al, Fe, and much of the Mg and Mn concentrations are dependent upon stability but without contribution to mass variance. There is some contradiction for Mg and Mn relative to the first factor. Wind speed again stands alone. For the 17 short travel time trajectory data sets no significant subgroupings were found. Wind speed is a factor on its own, not contributing to any of the other variables. Factor analysis as a function of the air mass type designations of column 5, Table 16, showed no difference between cP and mT air masses.

Together, the factor analyses as a function of Richardson number and travel time show that higher midlake concentrations will generally be observed with increased temperature stability except under conditions of enhanced turbulence. It was verified for this data base that wind speed is not linearly related to midlake concentration variations.

Several general conclusions can be drawn from the factor analyses of the midlake data base:

1. The variance in midlake metal concentrations are linearly independent of wind speed. The only apparent exception is the possible dependence of fine particulate Pb and Zn upon high wind speeds under the condition of several hundred kilometers over lake fetch.

2. Midlake metal concentration variability is strongly and directly dependent upon temperature stability of the surface layer.

3. Midlake mass concentration variability is usually more dependent on fine particulate aerosol with high Pb, Zn and Mn content than on the coarse particulate fraction. The Chicago/Gary and southeast shore source regions are close enough to the sampling site to occasionally negate this conclusion.

4. The processes of sedimentation and aerosol aging appear to be of secondary consequence when compared to temperature stability of the surface layer as regards aerosol concentration variability within that surface layer.

5. Source region related metal concentrations clearly show that midlake metal concentration is more dependent upon nearshore sources than upon long range transport.

The third and fifth conclusions together are most interesting in that the fine particulate fraction dominates midlake mass concentration despite the fact that nearshore sources also dominate midlake mass concentration. Of greatest significance, however, are conclusions 1, 2 and 4. The controlling influence of temperature stability has implications for the consideration of resistance to transport across the air/water interface. For example, the unusually large scatter in the enrichment factor diagrams (Figures 13 through 18) can be attributed to the variance in Al concentration caused by variations in temperature stability. Additional factor analysis results can be found in Sievering, et al. (1979a).

The method of factor analysis, coupled with trajectory analysis, has sufficed to determine some general aerosol/meteorological relationships and to provide some information concerning the physical and chemical types of aerosol associated with each. If this method were to be used to provide much greater specificity of results, a vastly larger data set would be needed. An identification of the source of aerosol by an examination of the physical and chemical characteristics found is a tantalizing, nearly direct method, but requires more knowledge of transport, deposition and transformation mechanisms than is currently available.

A promising source typing method may be numerical modeling. Trajectory models could increase the specificity of source typing, at least on a case-study basis. The reliability of these methods are highly dependent on the density of the data available for initialization and testing of models, and the most useful models tend to be expensive of computation and programming time. Many of the atmospheric processes directly involved in transport, particularly turbulence, are not well understood. Nevertheless, these methods should provide more specificity and reliability than the manual methods used. Further source region/type information may be gathered from the consideration of chemical characteristics of aerosol. A materials balance calculation (Gatz, 1975) can give gross estimates of the natural and anthropogenic fractions of the midlake concentrations, by first calculating:

$$\text{Soil derived percentage} = \frac{\zeta\ C/C_{ref}\ (\text{in soil})}{C/C_{ref}\ (\text{in aerosol})} \cdot 100 \qquad (27)$$

$$\text{Lake derived percentage} = \frac{\eta\ C/C_{ref}\ (\text{in lake water})}{C/C_{ref}\ (\text{in aerosol})} \cdot 100 \qquad (28)$$

and then finally subtracting the results of equations (27) and (28) from 100. The remainder can be considered of "non-natural" origin, for soil derived and lake derived metal concentrations should constitute all of the natural sources of these metals. The remaining percentage should then, indeed, be "non-natural" and, very likely, anthropogenic. This assumes no unknown natural causes for higher atmospheric surface layer concentrations. One rather uncertain natural cause is represented by ζ and η of equations (27) and (28) respectively: ζ represents the fractionation that can occur in the process of soil breakup to

aerosol generation; η represents the fractionation that can occur in the generation of atmospheric aerosol from the bubble bursting process at a sea or lake air/water interface (Windom and Duce, 1976). Only rarely has ζ been found to be greater than one (Rahn, 1976). However, the fractionation in the transfer process from bulk water to the air/water interface (especially when a surface microlayer is present) and to an atmospheric aerosol can enrich certain metals from 5-to 25-fold and in rare instances 100-fold or more. For example, Bloch, et al. (1966) found an enrichment for Pb of 2-to 7-fold in water-generated atmospheric aerosol. ζ will here be assumed to be 1 and η to be 25 or less.

An estimate of the "non-natural" or anthropogenic percentage of midlake atmospheric surface layer metal concentrations is shown in Table 21. Bowen's average midwestern soil metal concentrations were used. The average Lake Michigan bulk water metal concentrations were based on over 40 samples taken at the ship sampling site. Each lake water sample was actually a mixture of 3, 5 and 7 m depth samples. Although this bulk water metal concentration should be more representative for the analysis at hand, the water concentrations measured differ insignificantly from previously reported values (Torrey, 1976). Al is used as the soil reference metal and Ca is used analogously for bulk lake water. The significance of Table 21 results is that a majority of Pb, Zn, Mn and probably Fe at the 50-100 km offshore sampling site are very likely anthropogenic in origin. The tabulation additionally shows the lake not to be a significant source for Ti.

Source type contributions to the remaining anthropogenic component of midlake aerosol mass shown in the last column of Table 21 may be estimated by materials balance analyses performed on the chemical composition of the collected aerosol samples (Gartrell and Friedlander, 1975). The method consists of (1) estimating certain primary source contributions at a point (here midlake) using chemical elements as tracers, and (2) supplementing these estimates with emission inventory data for those primary sources for which no characteristic tracers are available. Step (1) was used above in calculating the percent soil-derived (with Al as the tracer) and percent lake-derived (with Mg or Ca as the tracer) contributions to the overall midlake mass. Emission inventory data on the utility, transportation, steel, and smelter industries could be used as chemical composition fingerprints. Kowalcyzk, Choquette and Gordon (1978) have done this using emission inventories on the coal, oil, refuse and motor vehicle source types in Washington, D.C. with Fe, V, Zn and Pb as the respective source type reference metals. The method was found to identify source types better than in any previous urban materials balance calculation. This was attributed to the fact that monitoring stations were removed from any one source type. These findings suggest that the 1977 midlake data base, also well removed from the influence of any single source type, has potential for this method. This approach also seems promising since the relative percentage of each element is essentially invariant with transport from source to midlake as shown in Appendix C. The observed 2-to 3-fold variation in v_d values with aerosol size could, however, change source type fingerprints. Use of this balance approach will then have to await the presently ongoing analysis and

interpretation of aircraft size distribution data as a function of downwind distance from sources, as well as the accession of the available emission inventory data for the Lake Michigan basin.

A graphic approach to identification of aerosol from different source regions (and possibly types) has been suggested by Stolzenburg and Andren (1979). Figures 40, 41, 42, 43, 44, and 45 are plots of the elemental mass fraction in aerosol, normalized to the most abundant in the overall mean $\bar{C}$ data, sulfur:

$$\text{Relative mass fraction} = \frac{\Pi \text{ (element of interest)}}{\Pi \text{ (sulfur)}} \qquad (29)$$

The order of the elements along the abscissa is that of decreasing abundance in the overall-mean data, with no other significance implied by the abscissa labeling. Because of a lack of other mid-Lake Michigan aerosol data, nothing has yet appeared in the literature with which to directly compare these figures. In light of this, Figure 40 might be defined as a "baseline" plot, since it represents the overall-mean $\bar{C}$ for all data collected during the 1977 sampling. The slope of the line segment between two elements corresponds to the relative abundance between two elements, but no particular significance is assigned to the value of this slope. What is of importance in these figures is the general "shape" of the plots. In the baseline plot, Figure 40 , note that the trend (by definition, since the order of the elements was chosen for that to be true) is from upper left to lower right. Contrast that regularity to Figure 42, the plot of $\bar{C}$ data from the West Shore source region (see Figure 1). Clearly, for the West Shore aerosol, ratios of N/S, Mg/Fe, P/Zn, and Ti/Mn are quite different from the baseline trend. For the overlake transport (Figure 41) and East Shore (Figure 43) region aerosol, the plots differ noticeably from the baseline. The Southeast Shore (Figure 44) and Chicago/Gary (Figure 45) source region plots show much similarity to the trend of the baseline plot. This similarity points to the fact that, for over 50 percent of the year, aerosol from those two regions passes overlake, and was thus an important fraction of the "baseline" determination plot. This graphic method, or refined and subsequent developments based on it, may hold promise of becoming a source type identification tool. The largest obstacle to fulfillment of this promise is definition of a suitable baseline aerosol composition and of uniquely different source type compositions in the Lake Michigan basin. Beyond that, an expanding aerosol data base in the Great Lakes literature will allow for better comparison between aerosol from more than five source regions; comparisons to source type plots are an avenue for future research efforts

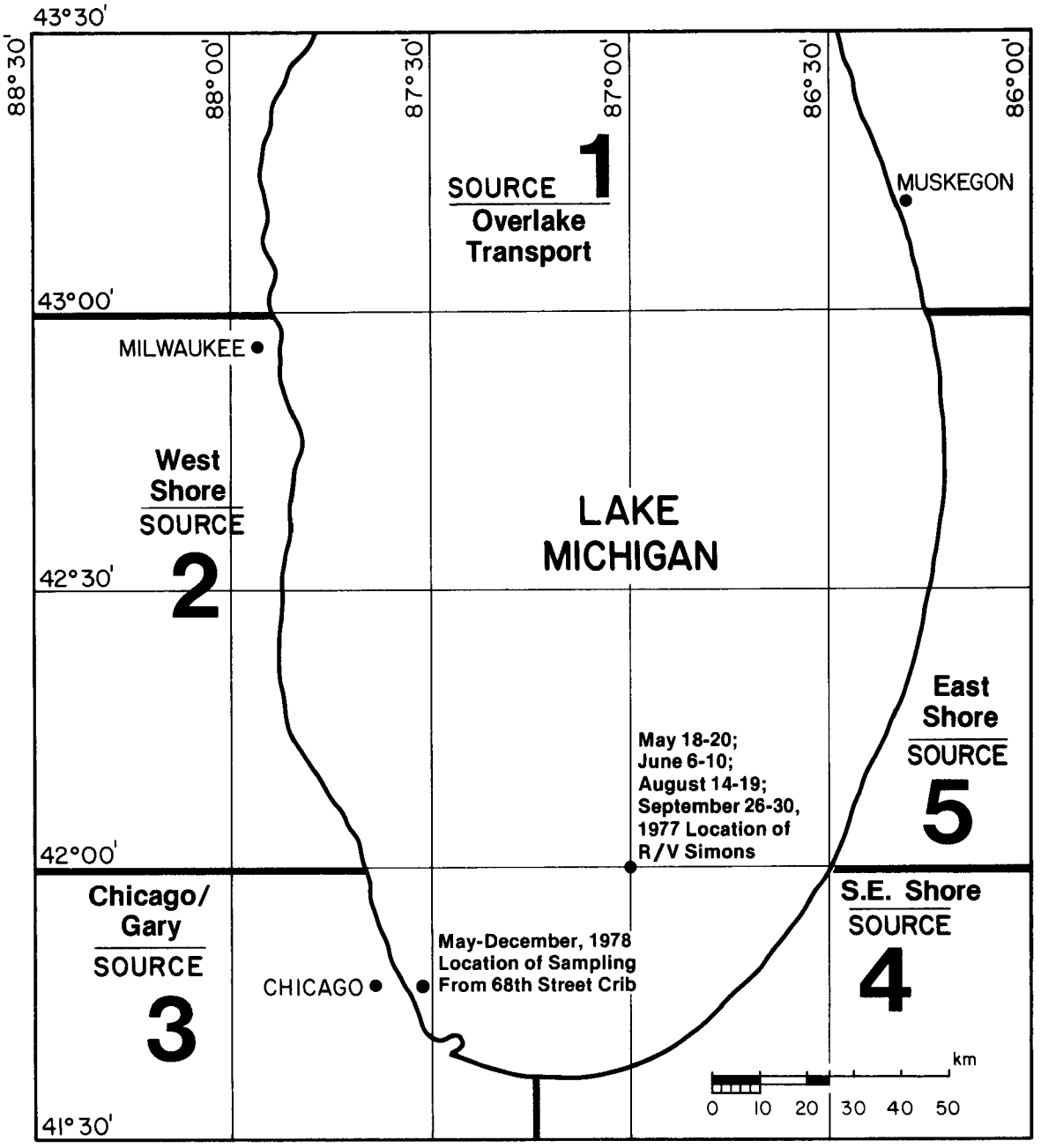

FIGURE 1. Location of Source Regions and Sampling Data.

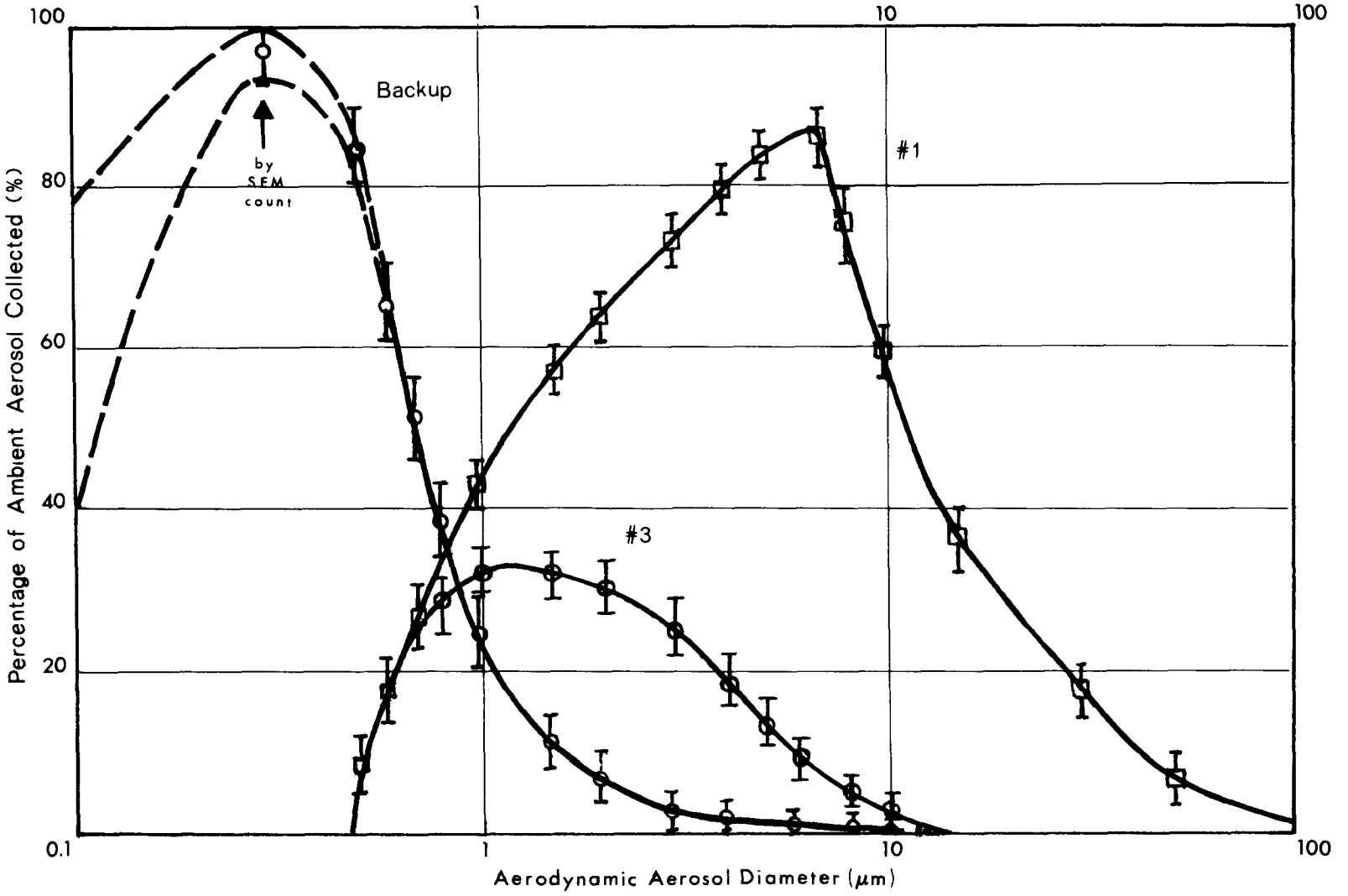

FIGURE 2. Aerosol Collection Efficiencies for Three-Stage Cascade Impactor.

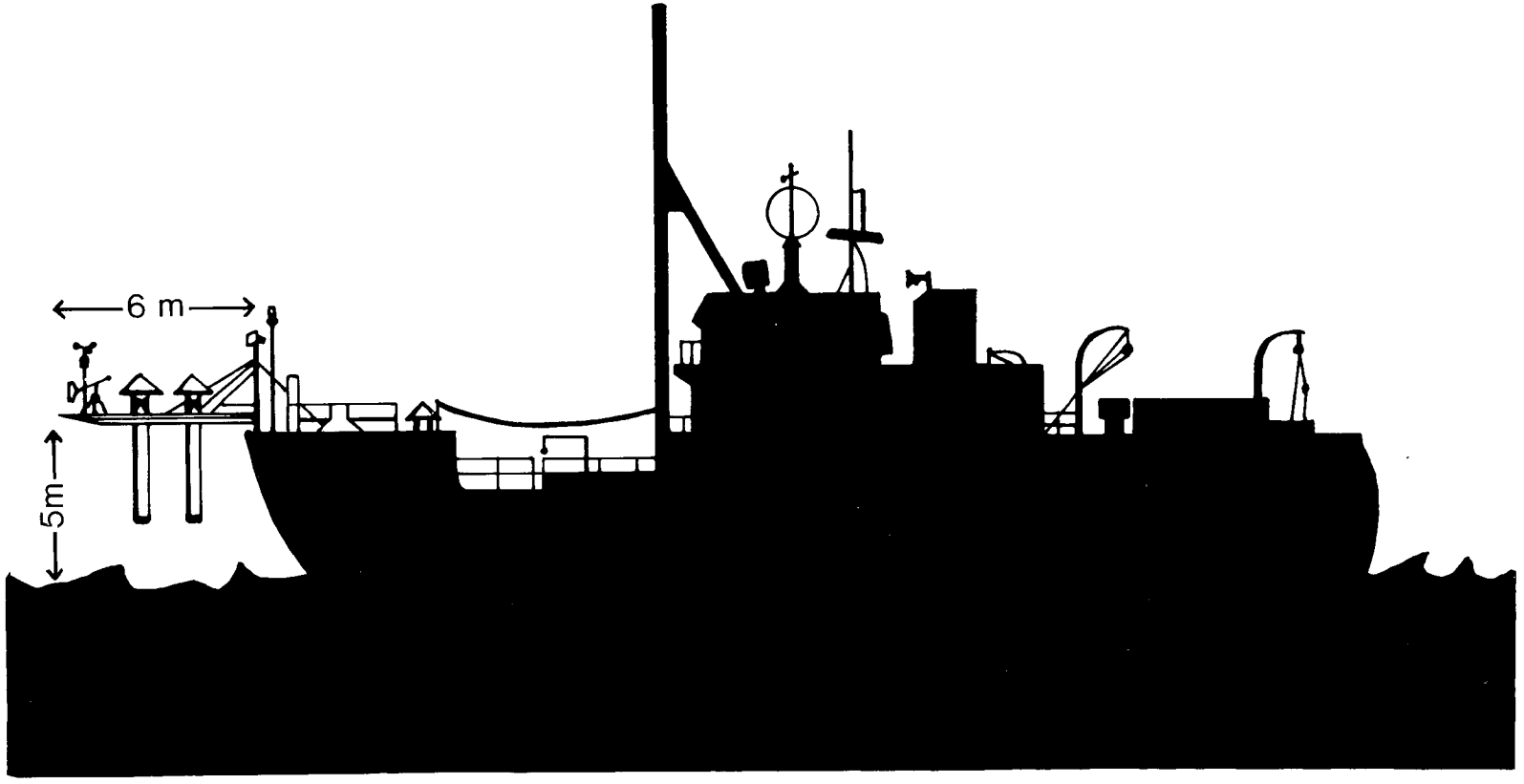

FIGURE 3. R/V Simons and Sampling Boom.

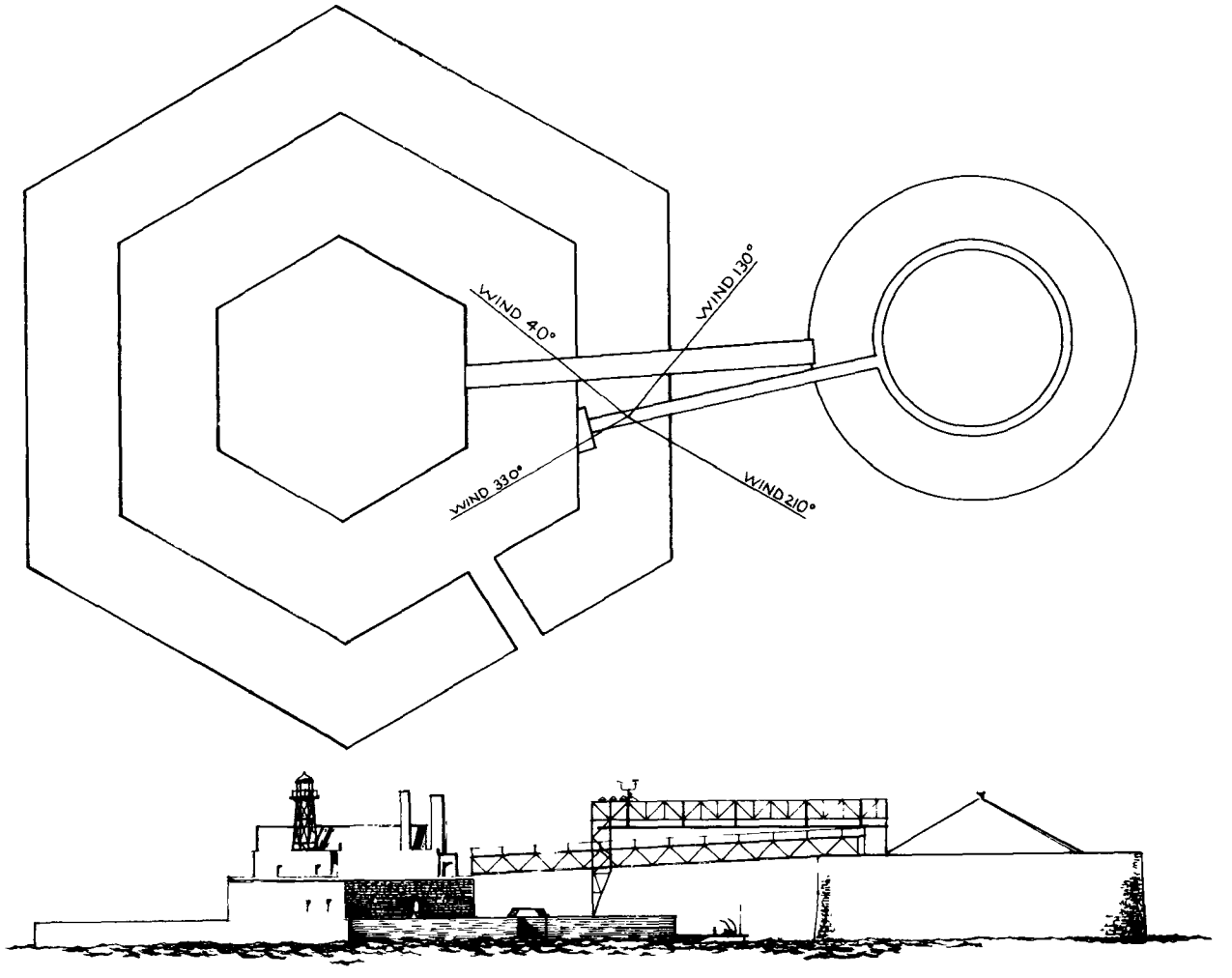

FIGURE 4. 68th St. Water Intake Crib and Sampling Windows.

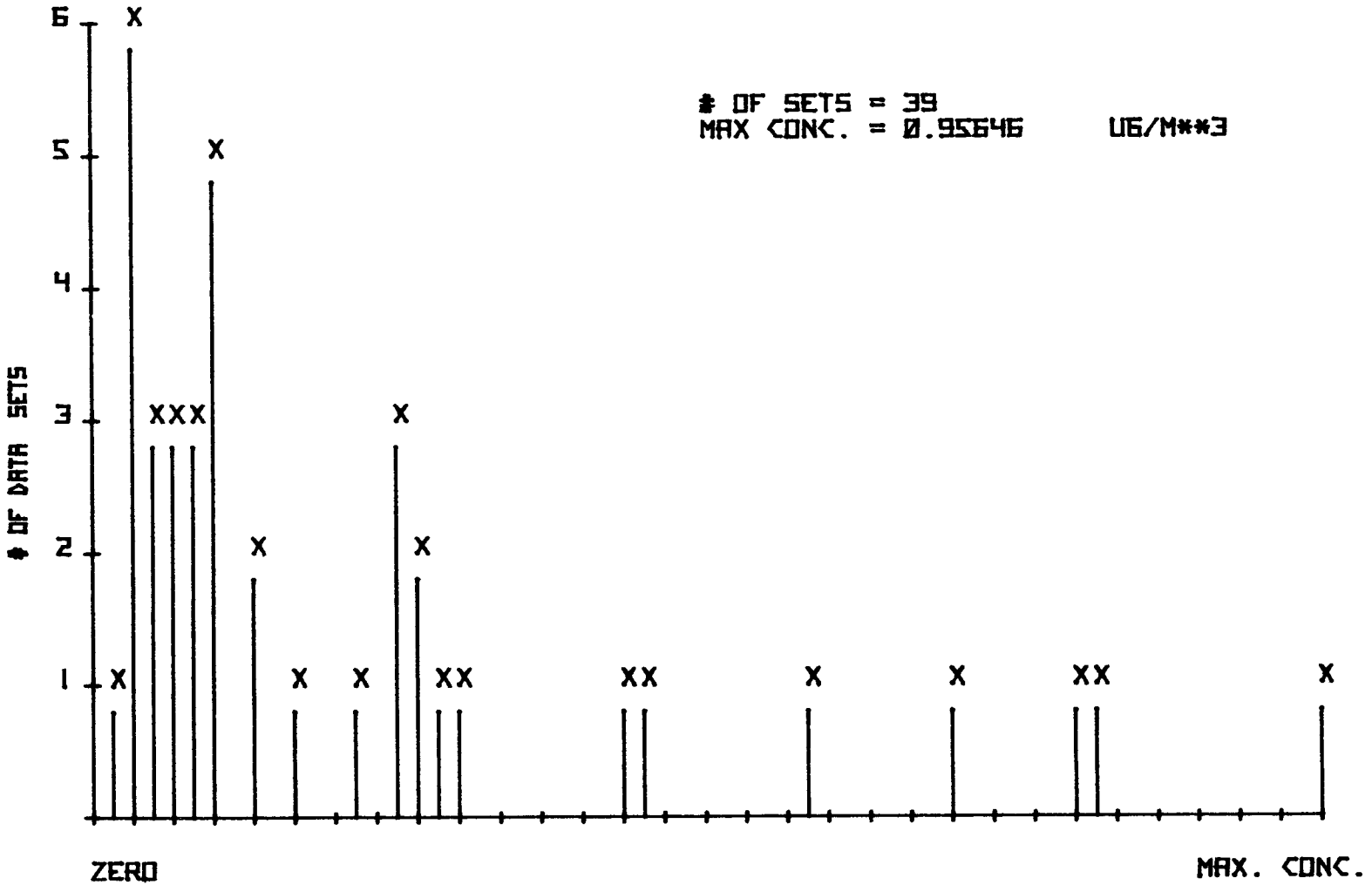

FIGURE 5. Distribution of Occurrences of Al Concentrations.

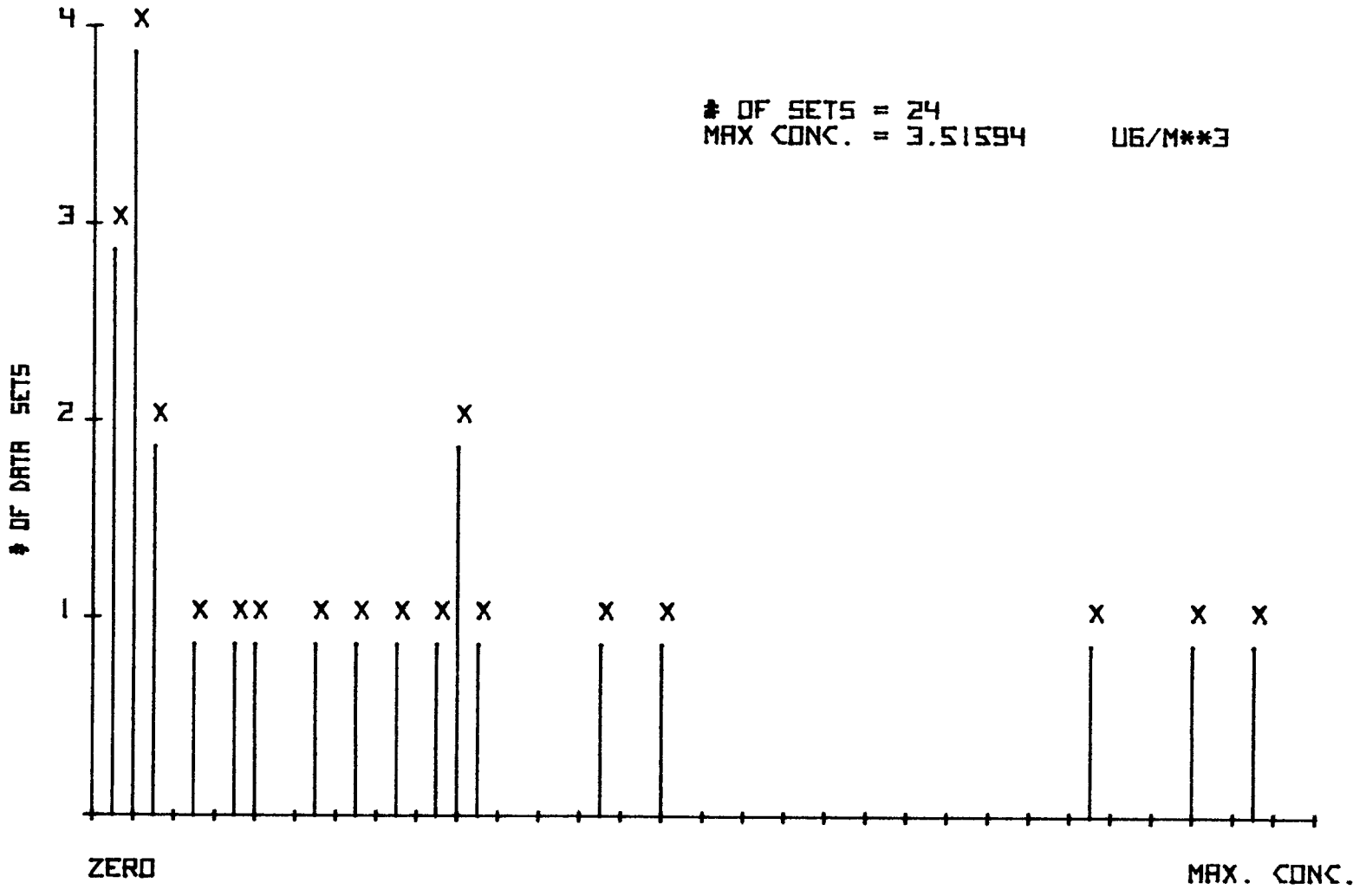

FIGURE 6. Distribution of Occurrences of Ca Concentrations.

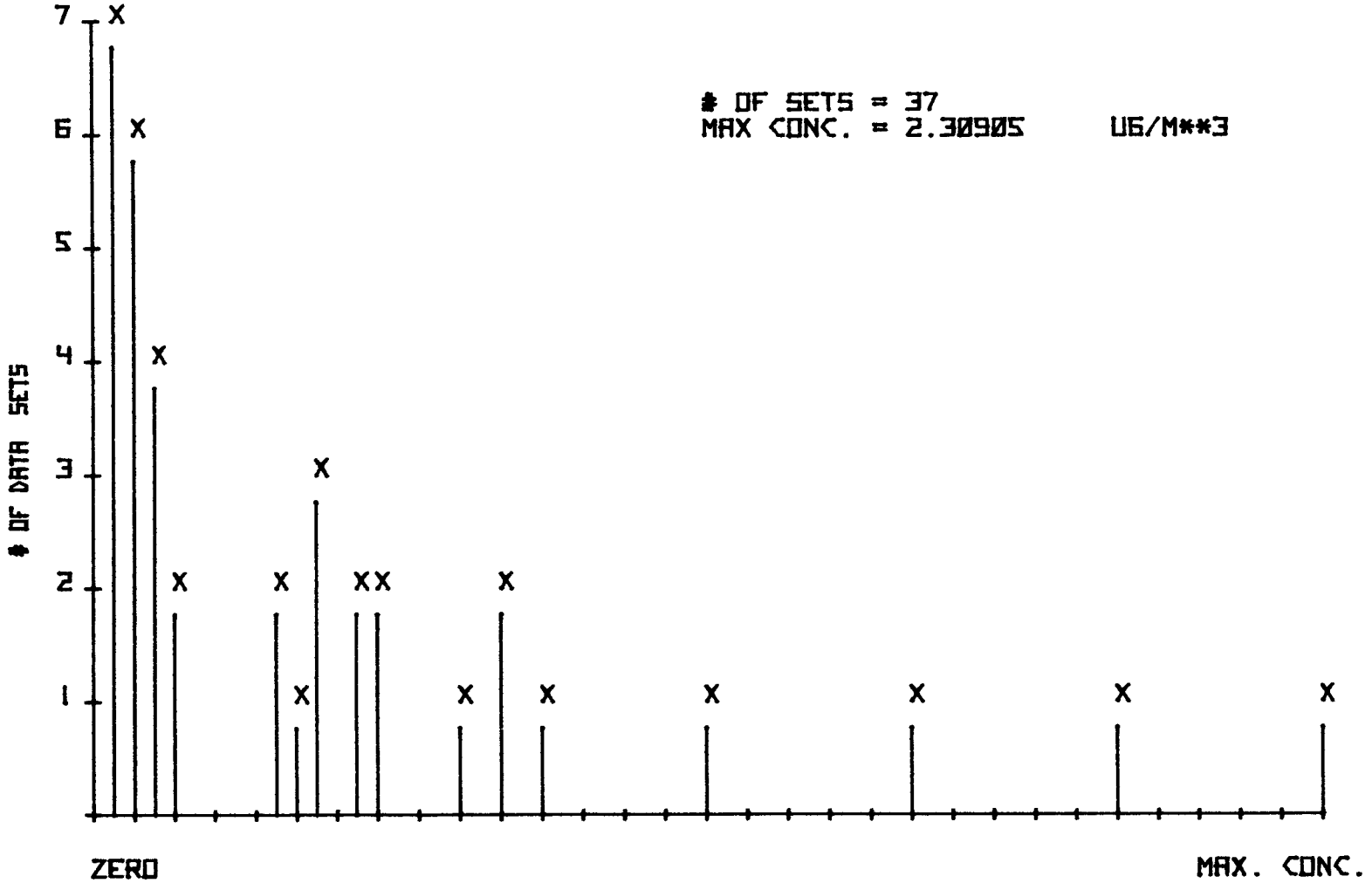

FIGURE 7. Distribution of Occurrences of Fe Concentrations.

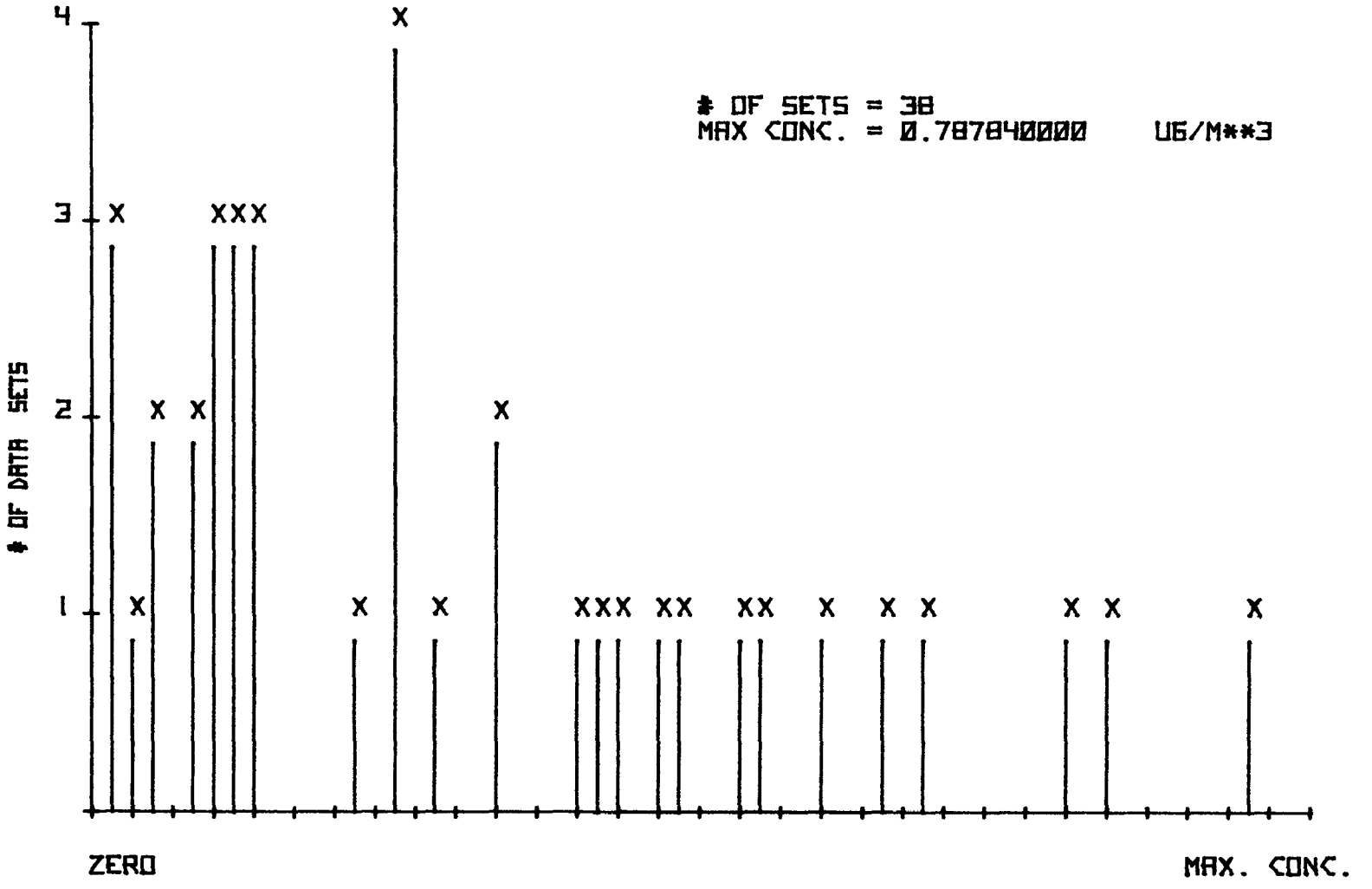

FIGURE 8. Distribution of Occurrences of Mg Concentrations.

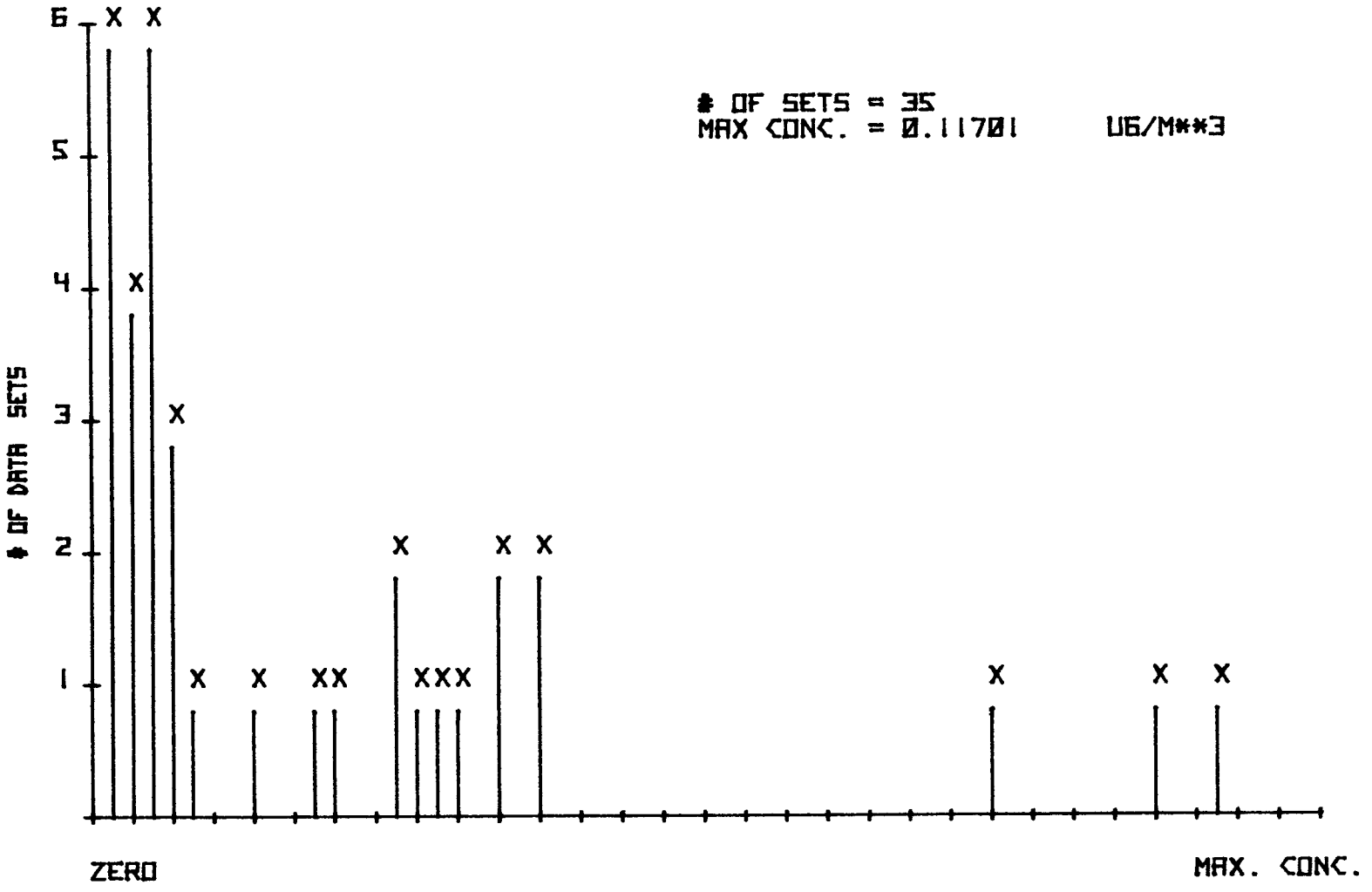

FIGURE 9. Distribution of Occurrences of Mn Concentrations.

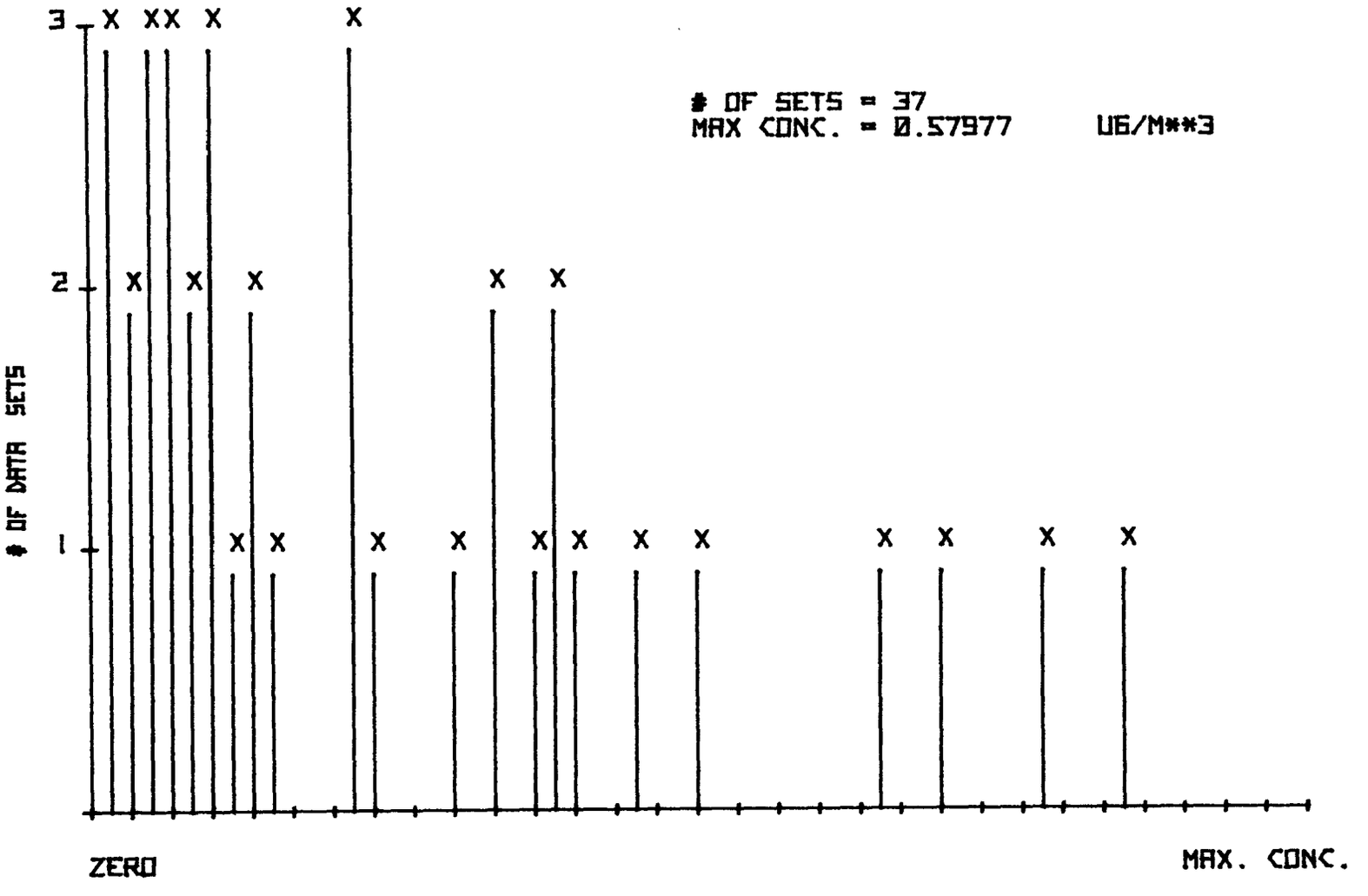

FIGURE 10. Distribution of Occurrences of Pb Concentrations.

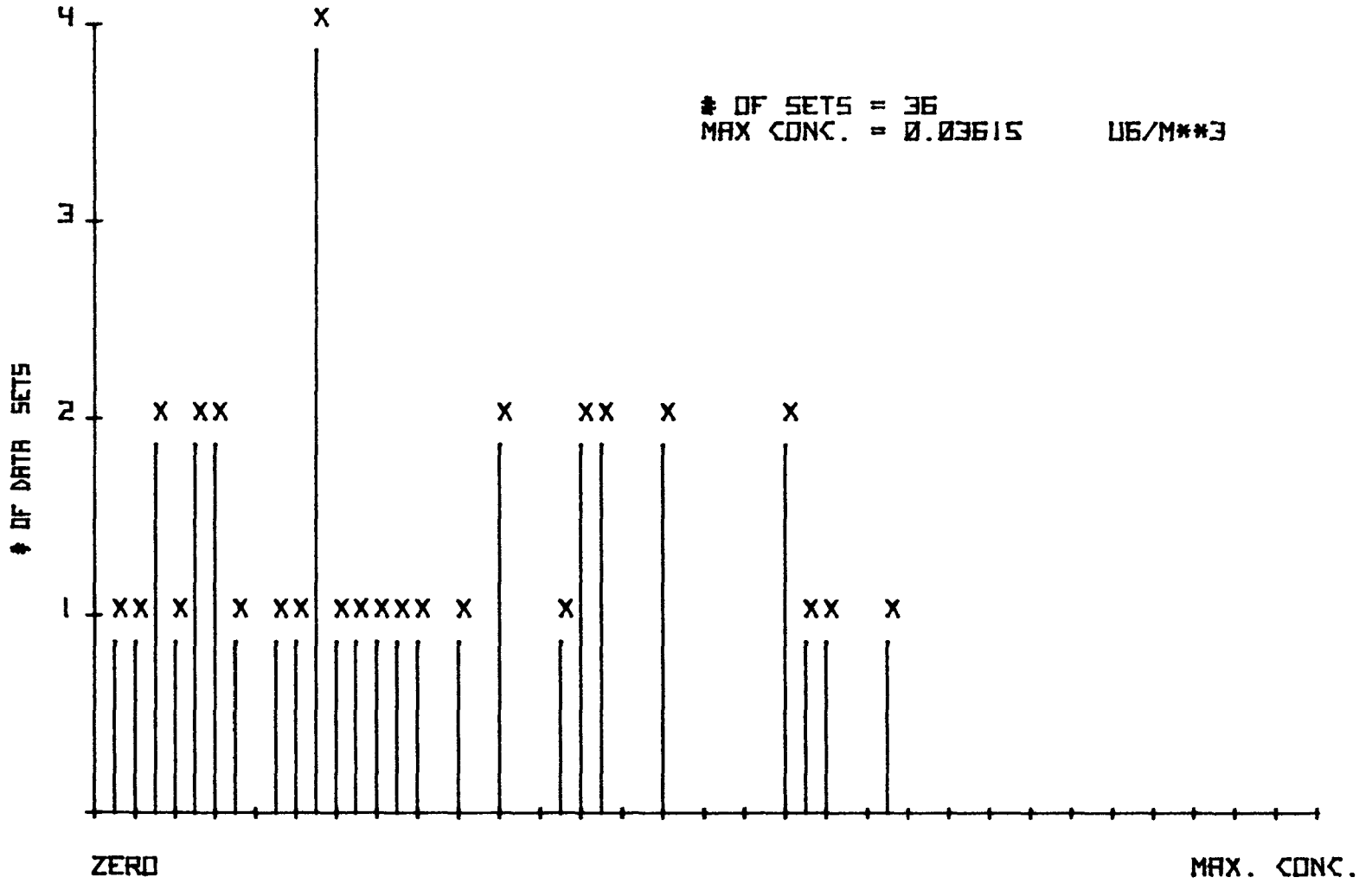

FIGURE 11. Distribution of Occurrences of Ti Concentrations.

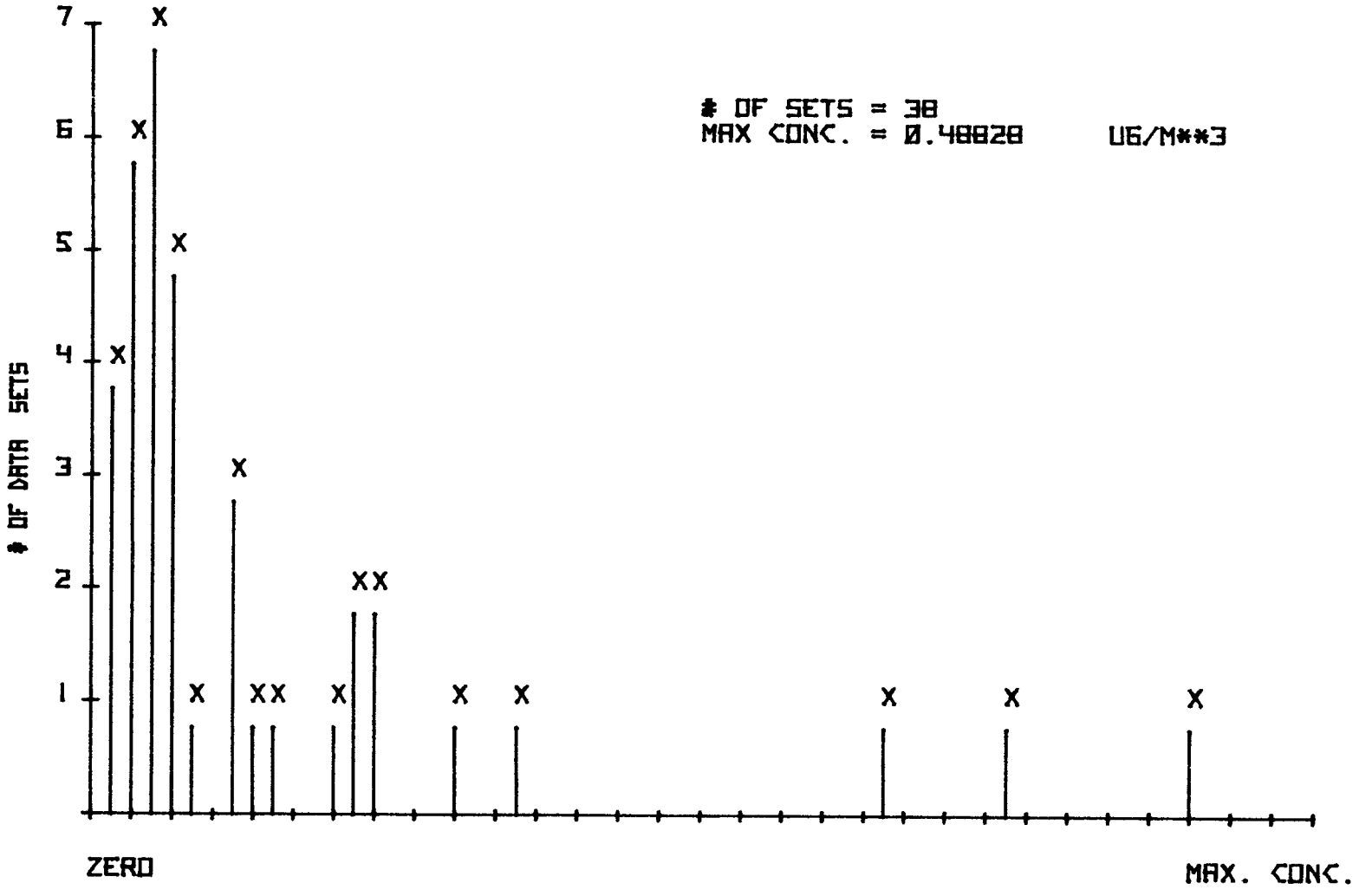

FIGURE 12. Distribution of Occurrences of Zn Concentrations.

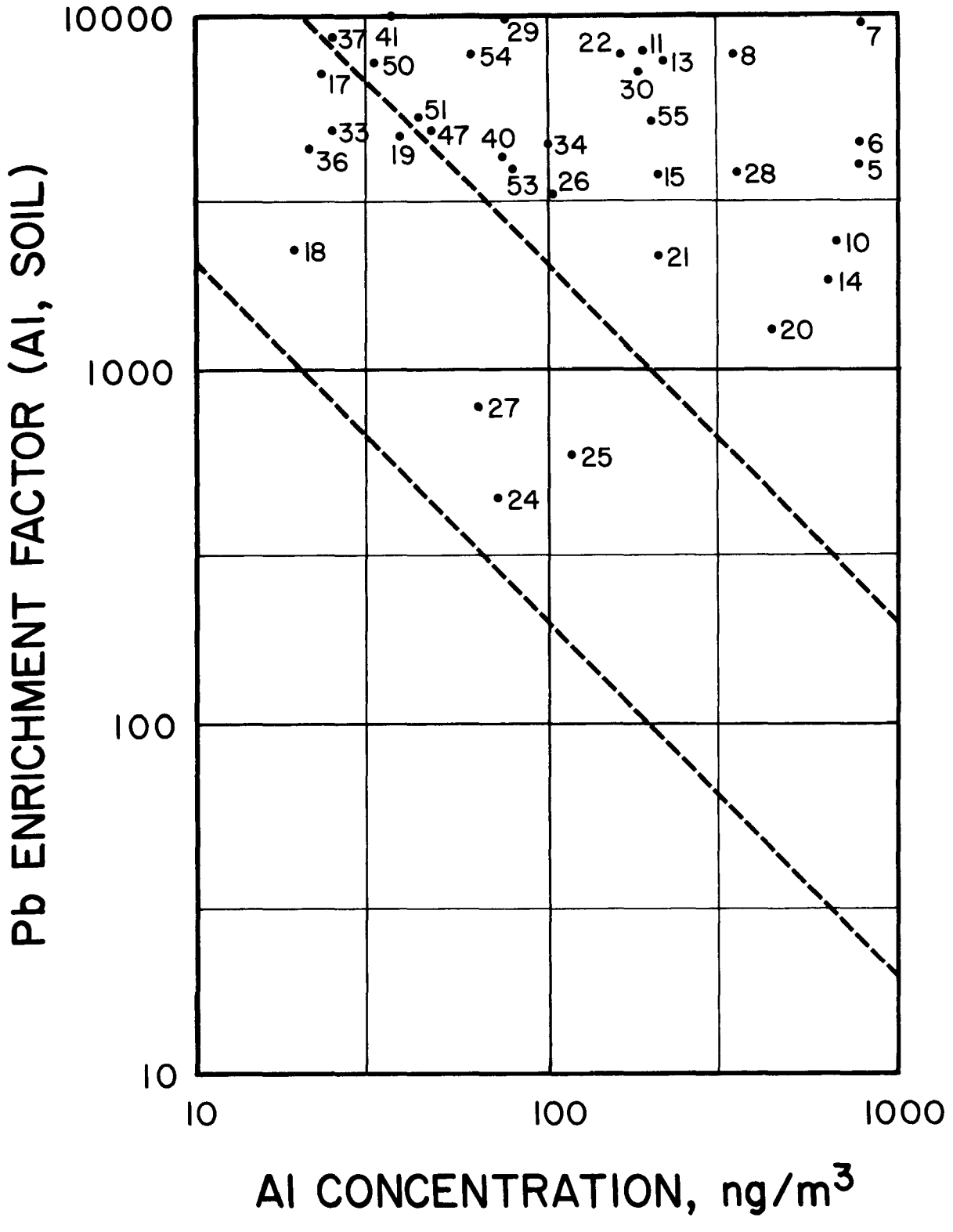

FIGURE 13. Pb Enrichment Factor vs. Al Concentration.

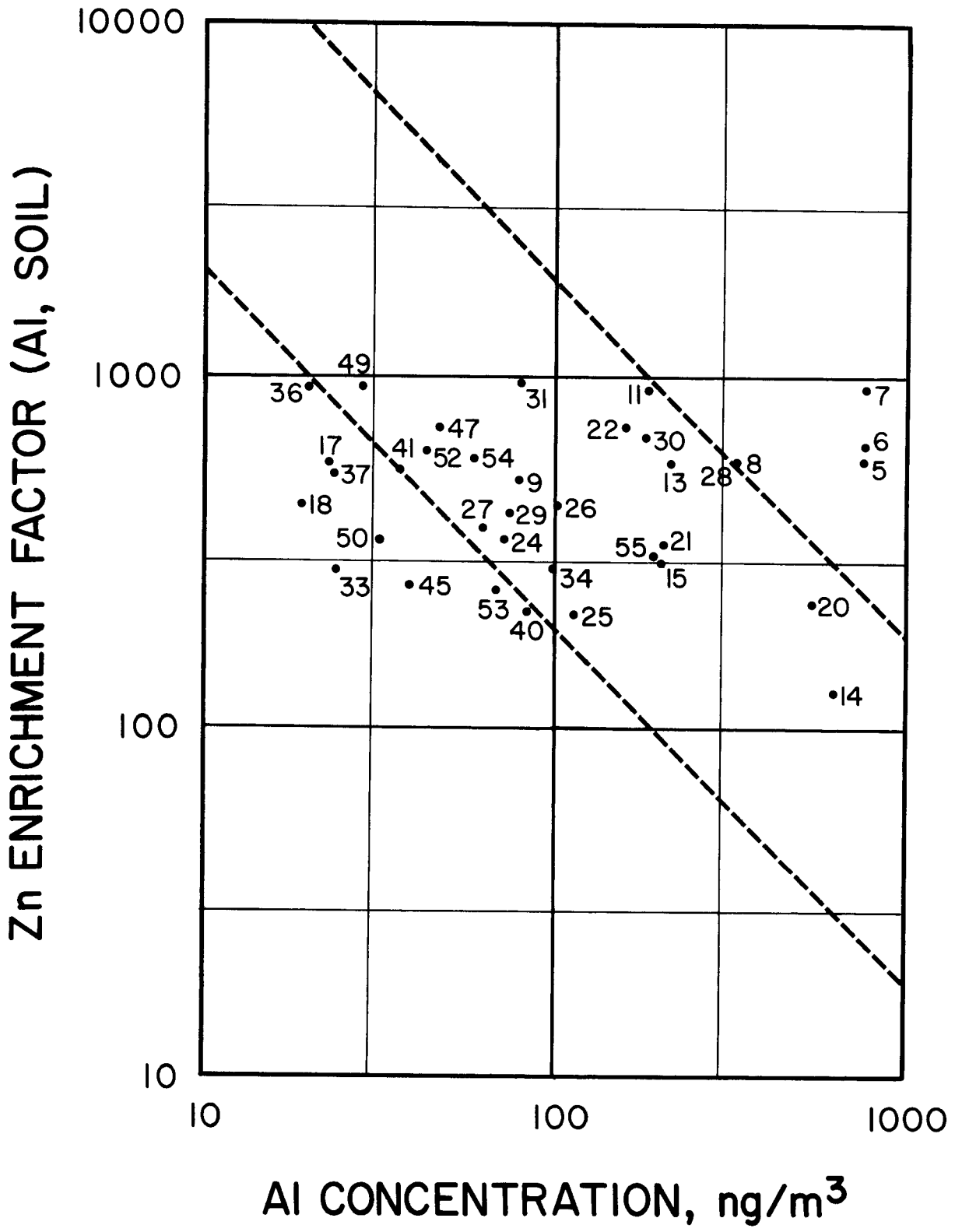

FIGURE 14. Zn Enrichment Factor vs. Al Concentration.

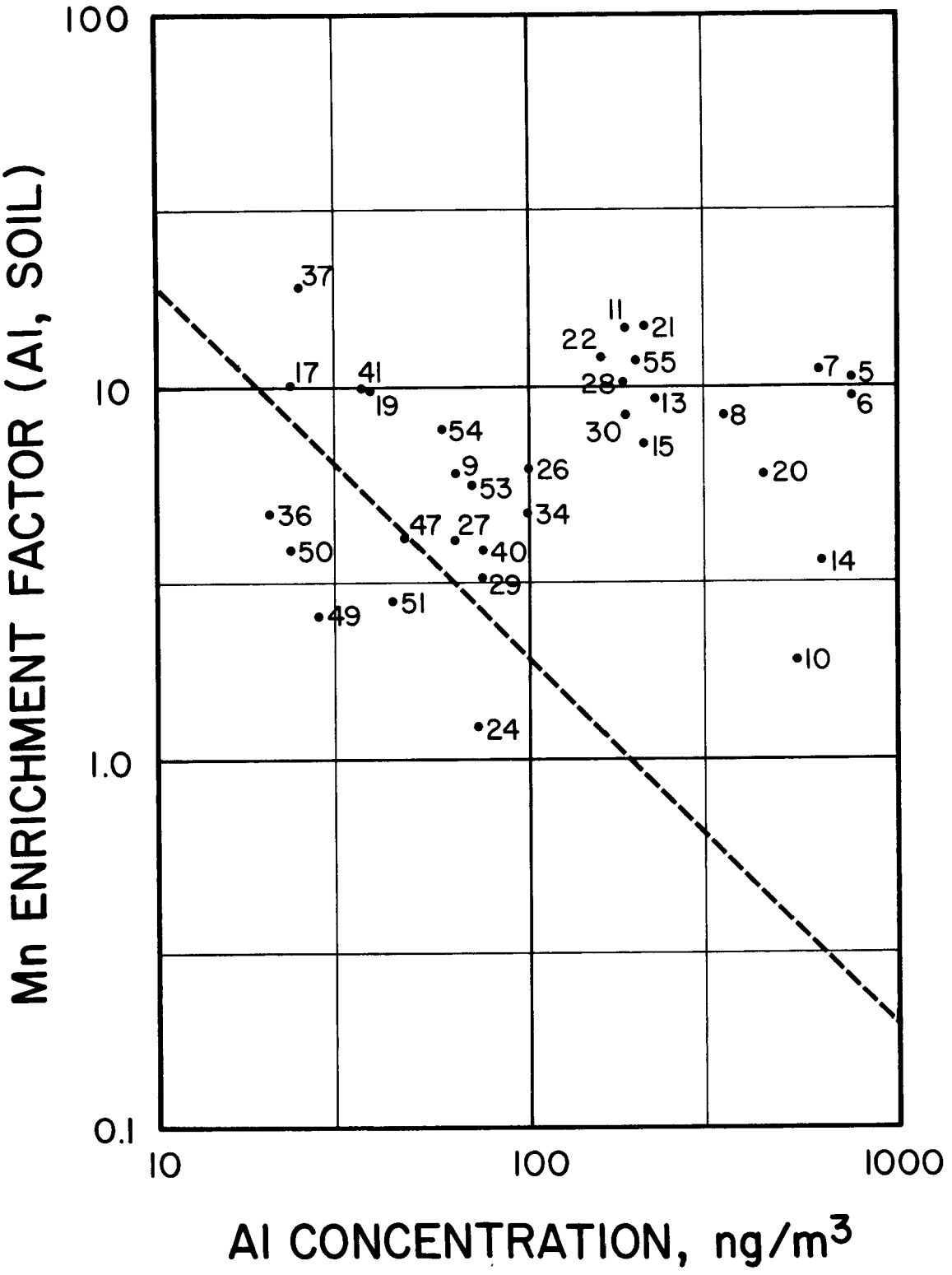

FIGURE 15. Mn Enrichment Factor vs. Al Concentration.

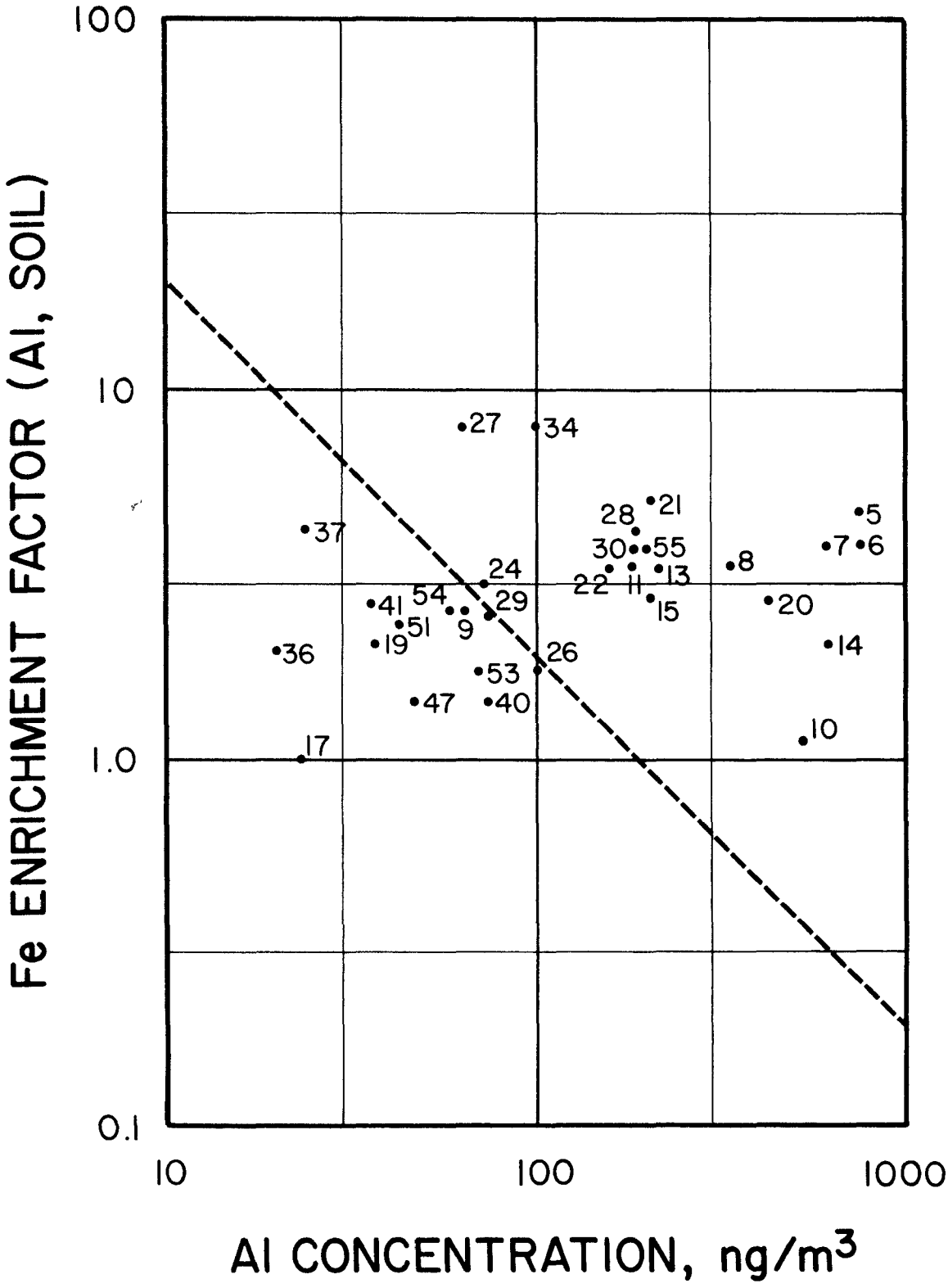

FIGURE 16. Fe Enrichment Factor vs. Al Concentration.

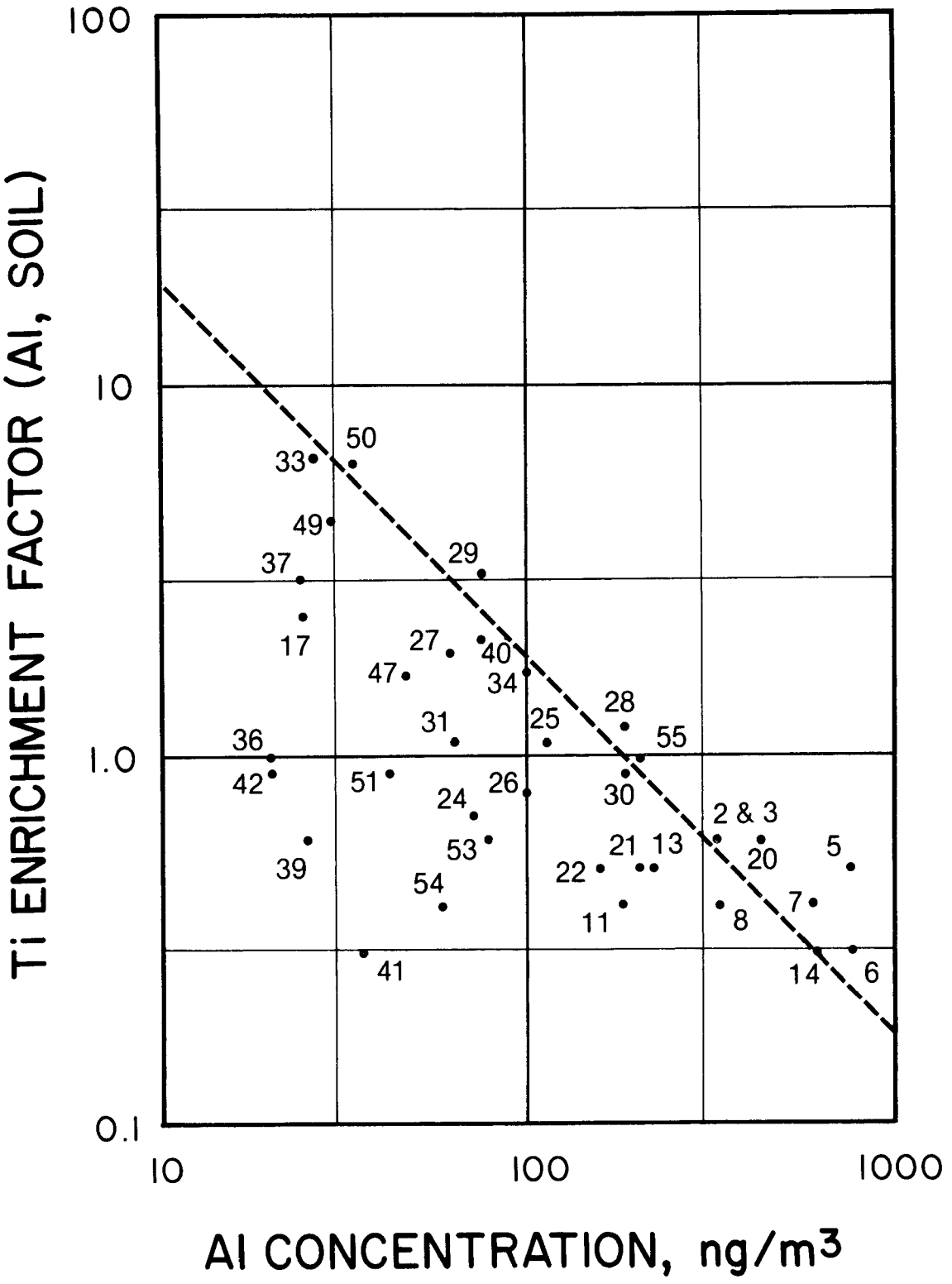

FIGURE 17. Ti Enrichment Factor vs. Al Concentration.

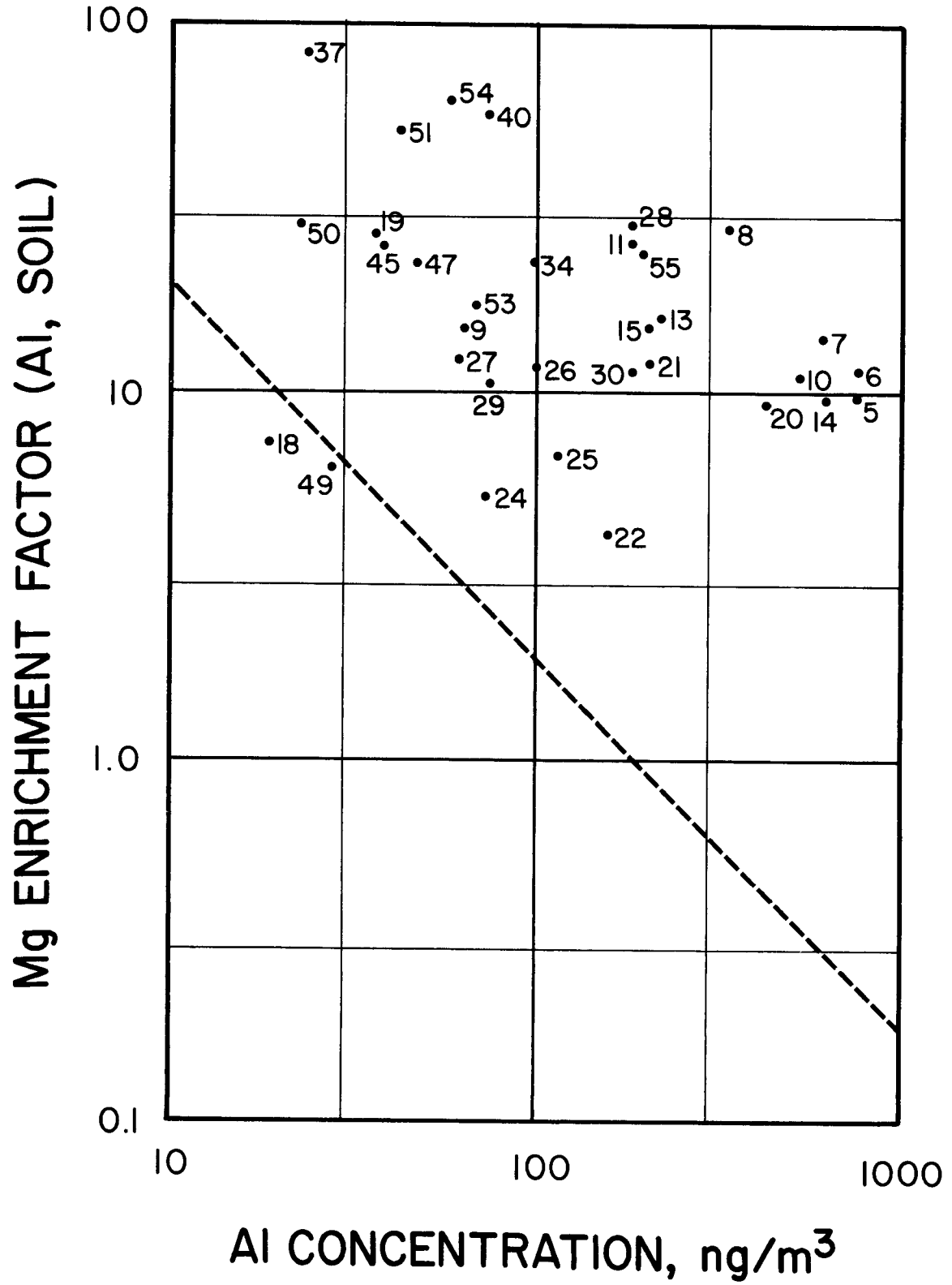

FIGURE 18. Mg Enrichment Factor vs. Al Concentration.

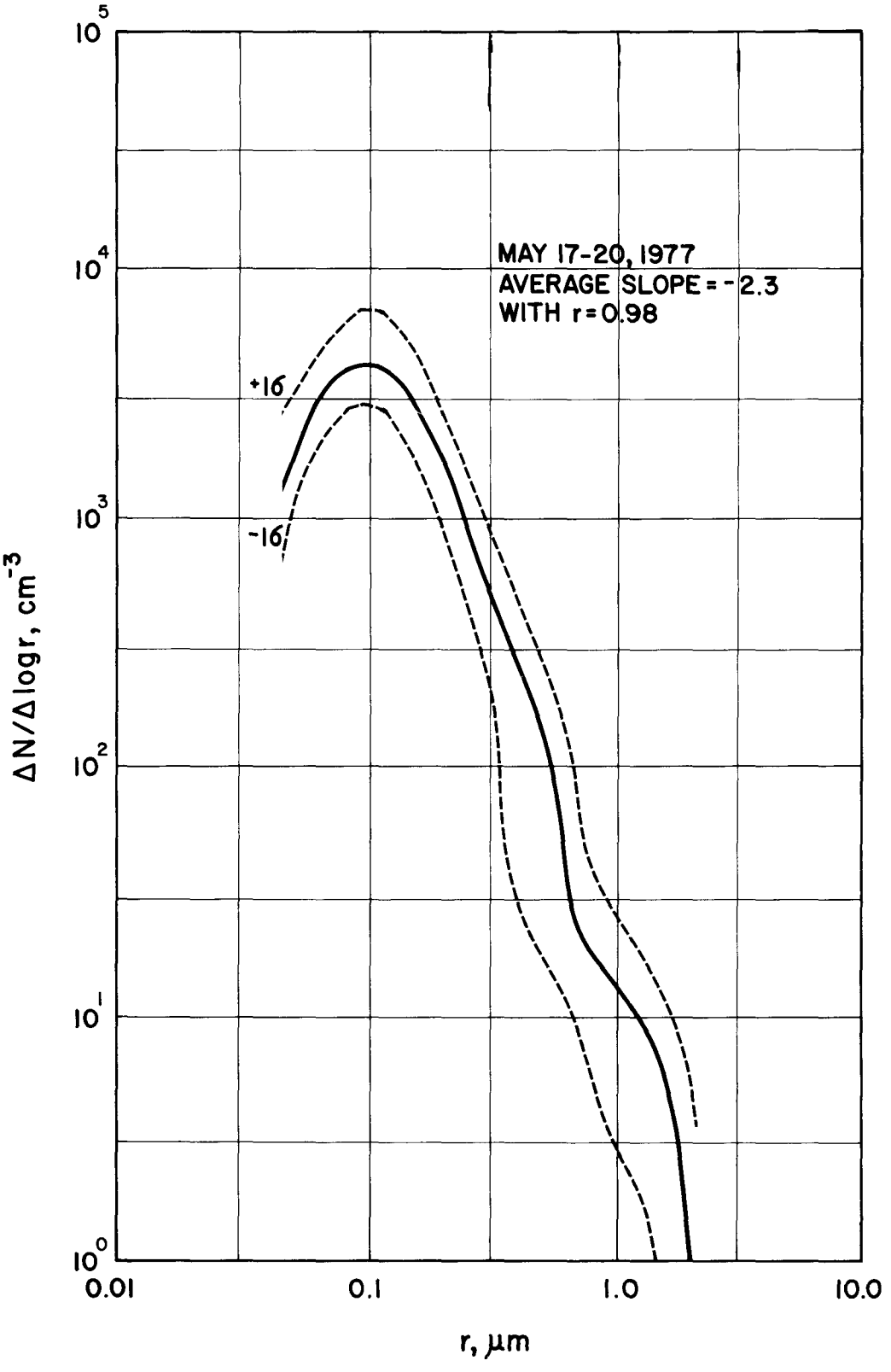

FIGURE 19. ΔN/Δ (log r) vs. log r for 17-20 May 77.

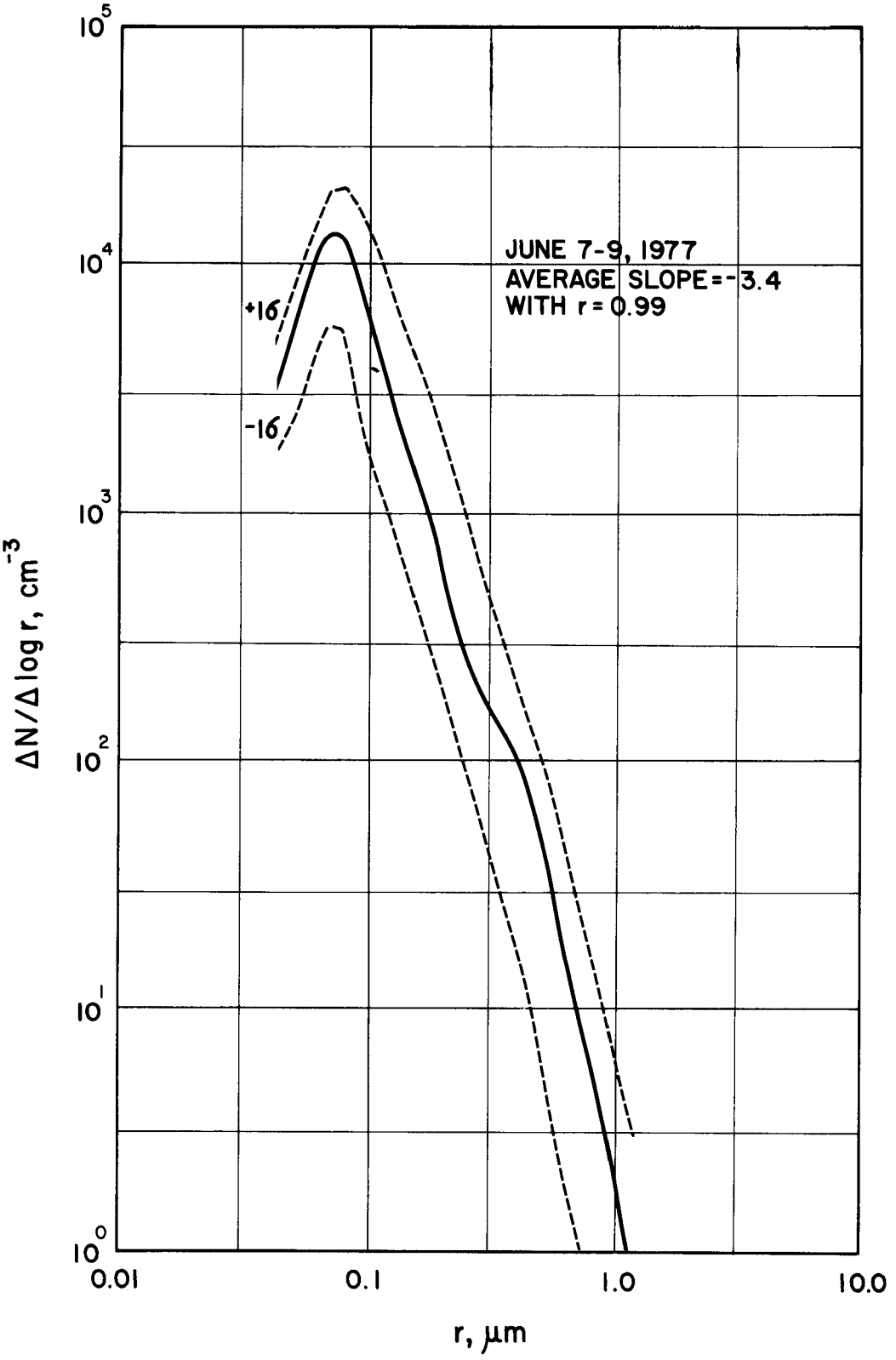

FIGURE 20. $\Delta N/\Delta$ (log r) vs. log r for 7-9 June 77.

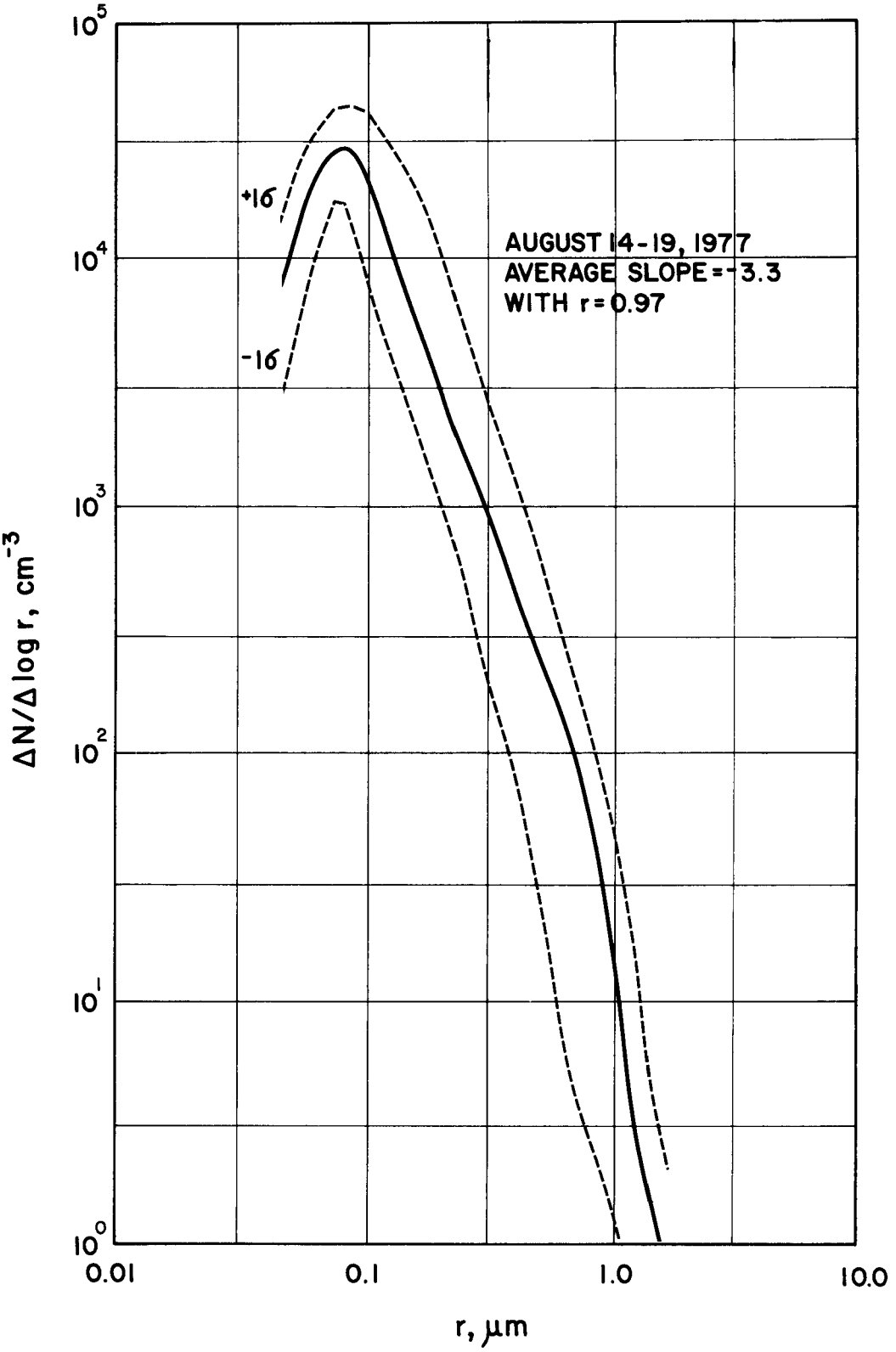

FIGURE 21. ΔN/Δ (log r) vs. log r for 14-19 Aug 77.

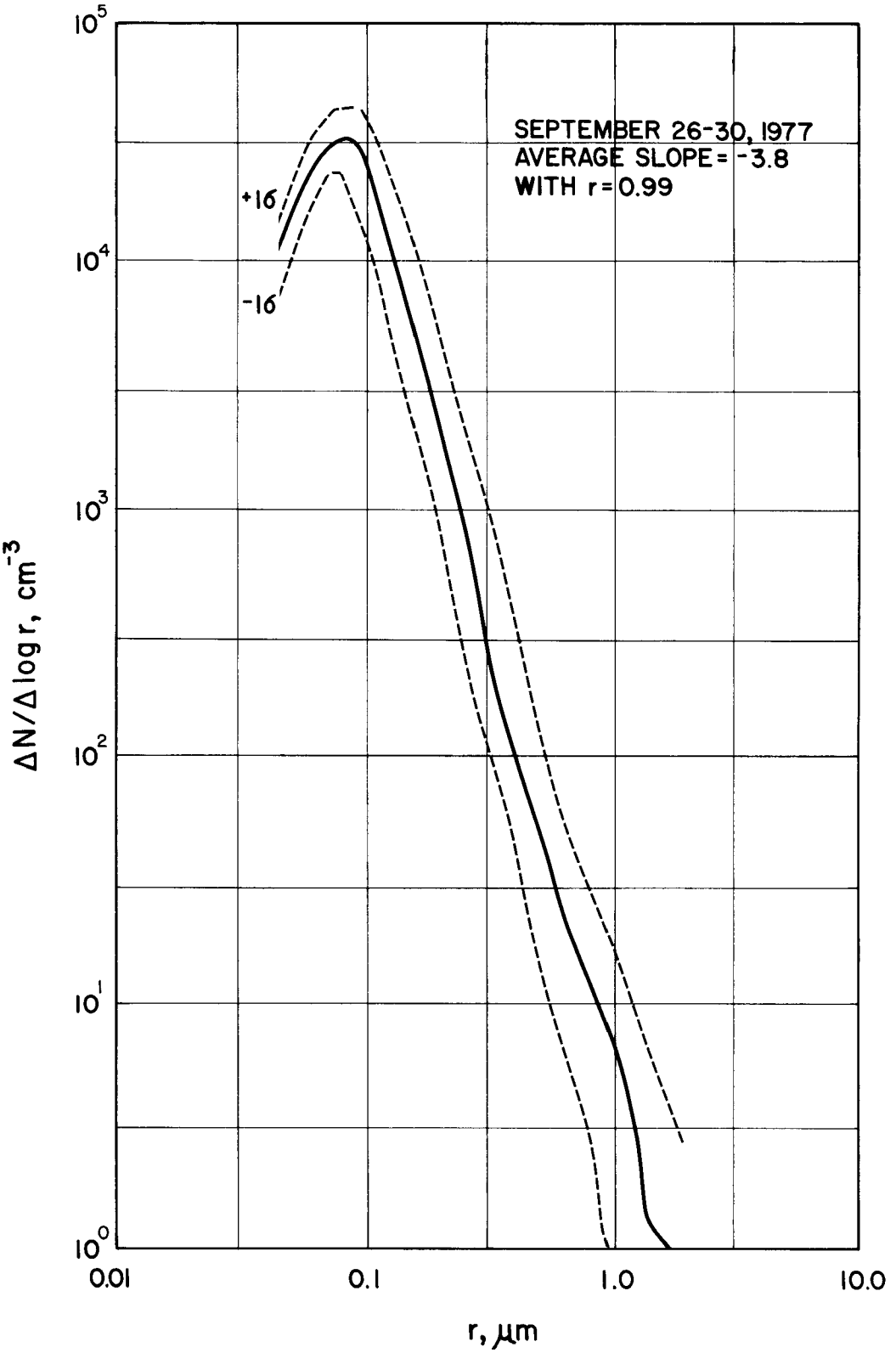

FIGURE 22. ΔN/Δ (log r) vs. log r for 26-30 Sept 77.

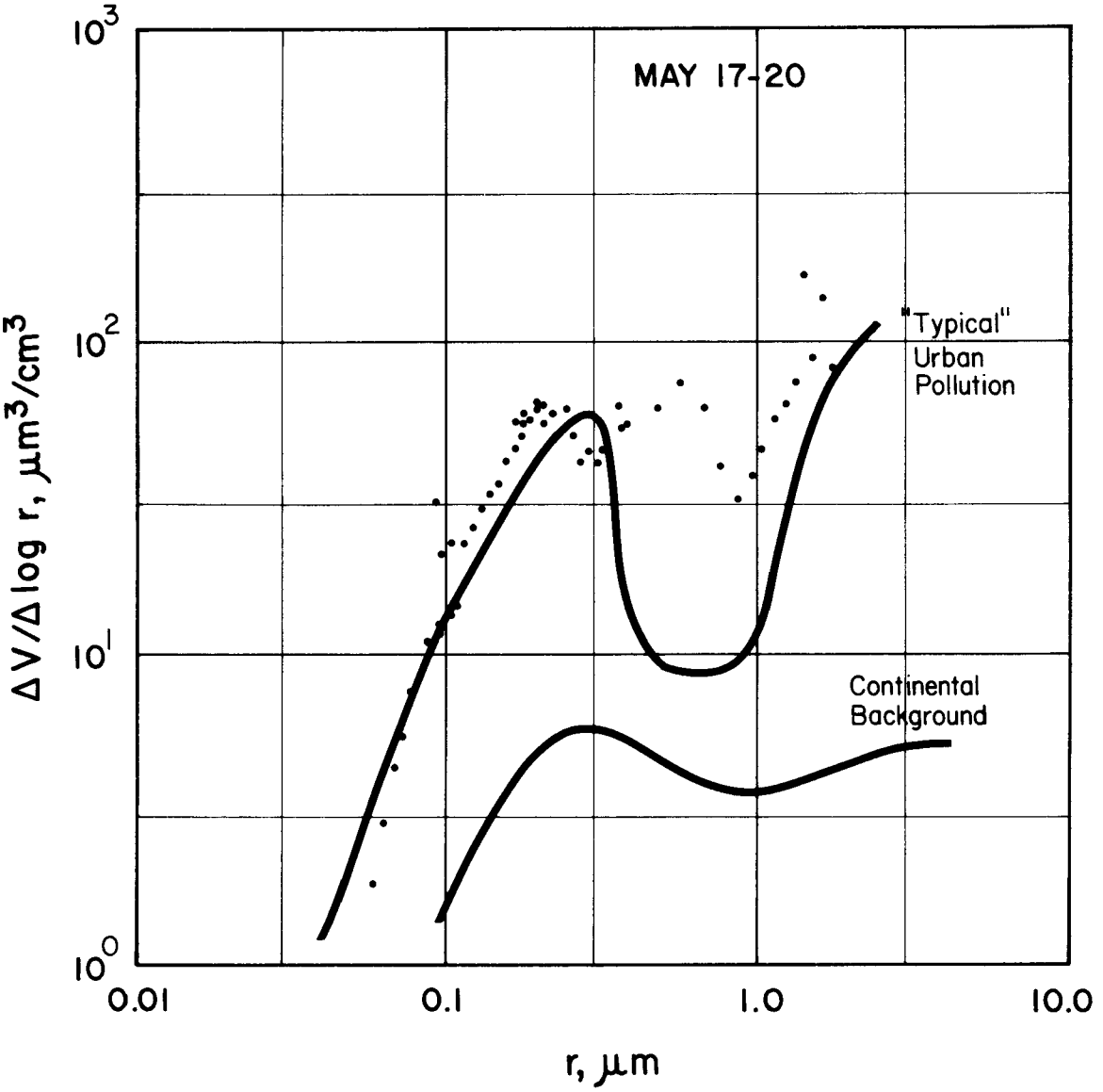

FIGURE 23. $\Delta V/\Delta$ (log r) vs. log r for 17-20 May 77.

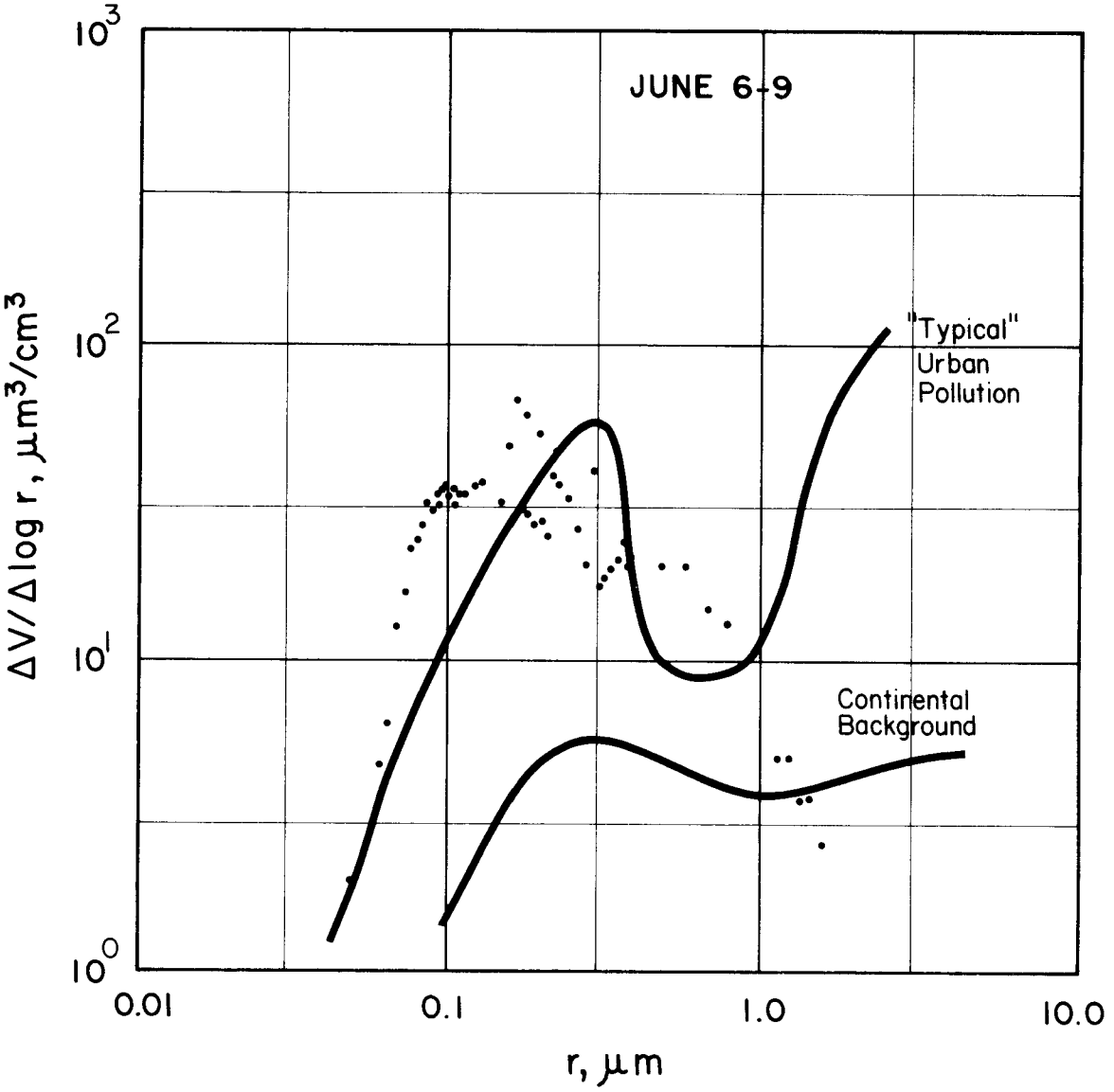

FIGURE 24. $\Delta V/\Delta$ (log r) vs. log r for 6-9 June 77.

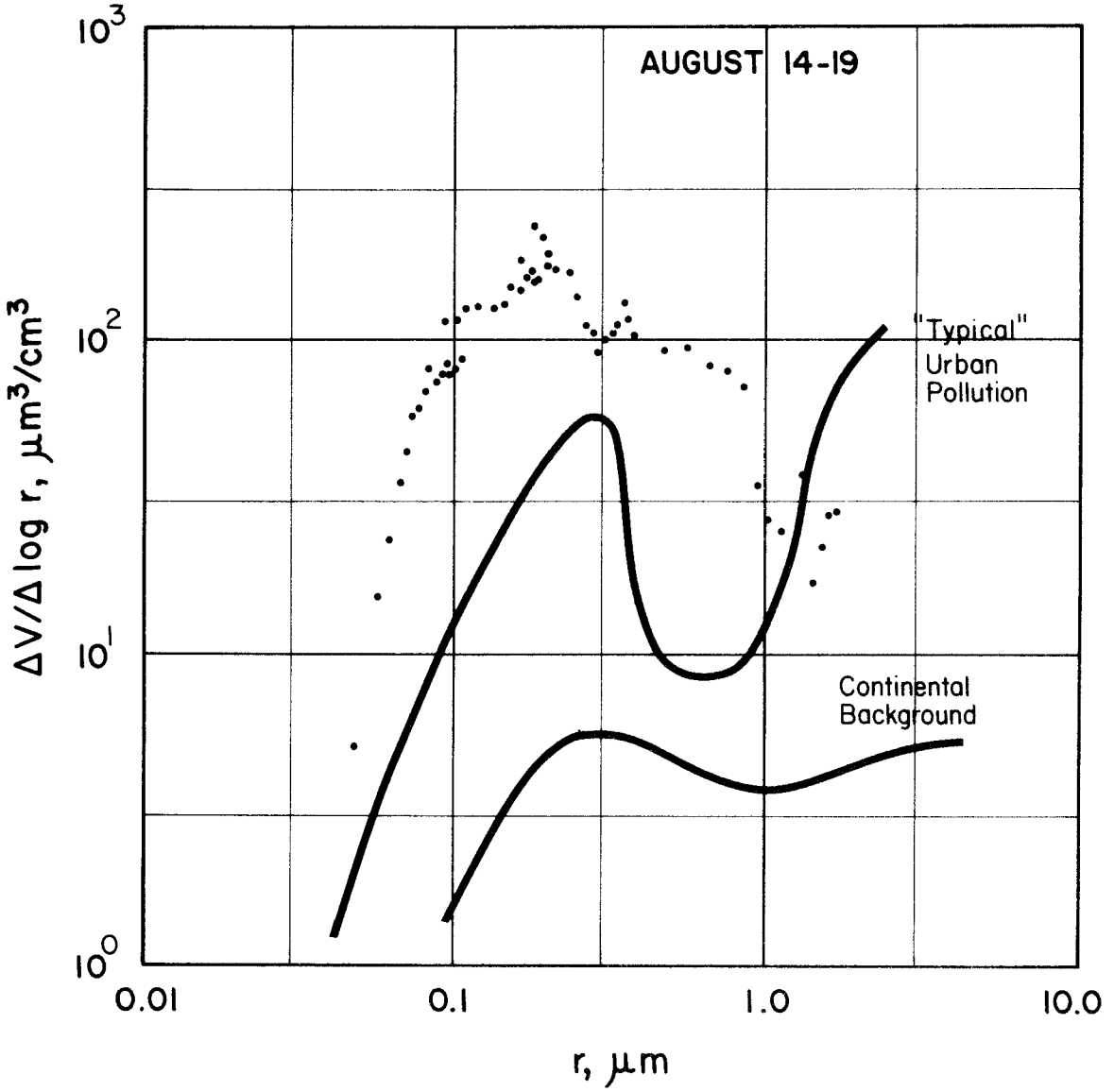

FIGURE 25. ΔV/Δ (log r) vs. log r for 14-19 Aug 77.

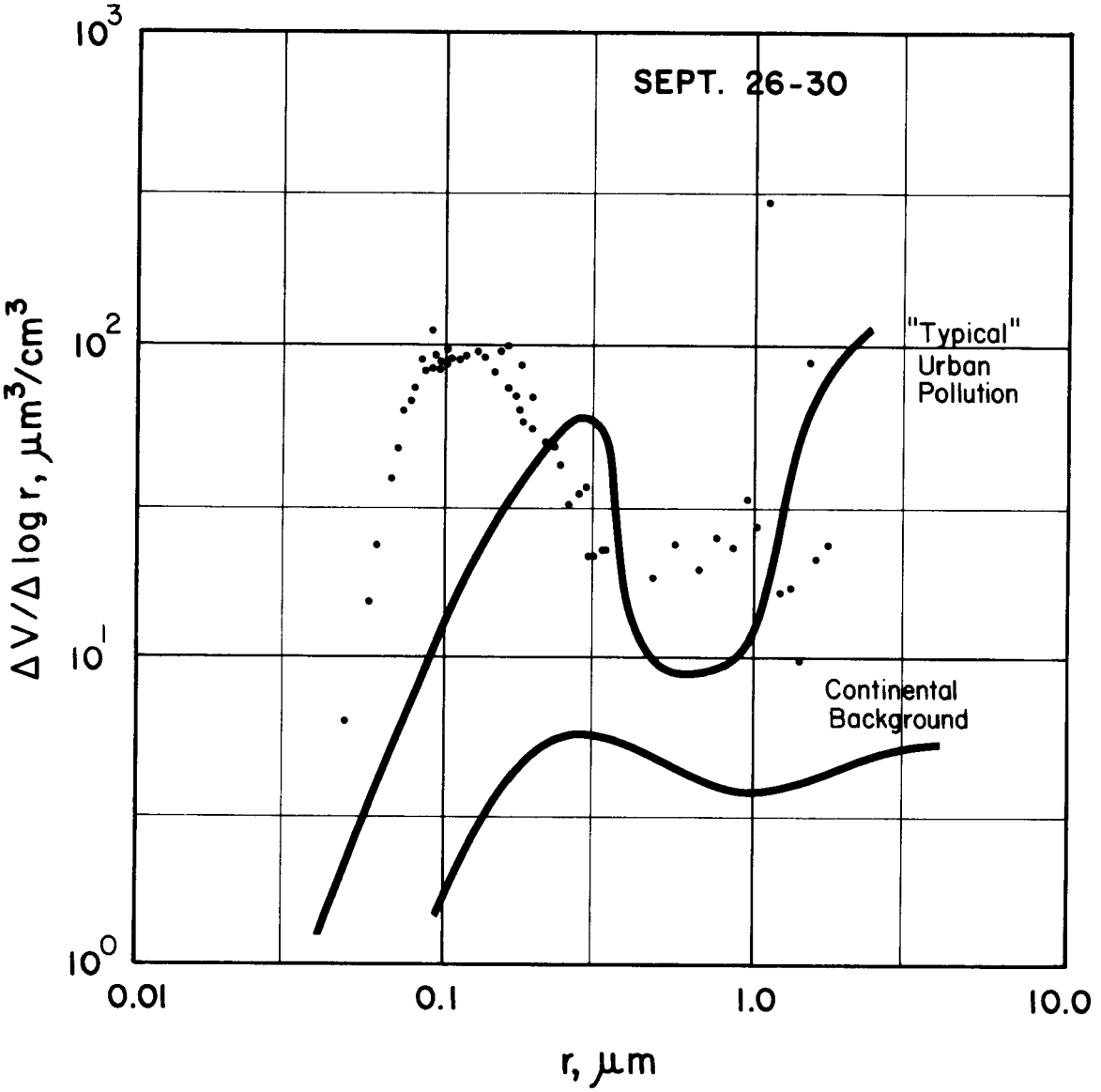

FIGURE 26. $\Delta V/\Delta$ (log r) vs. log r for 26-30 Sept 77.

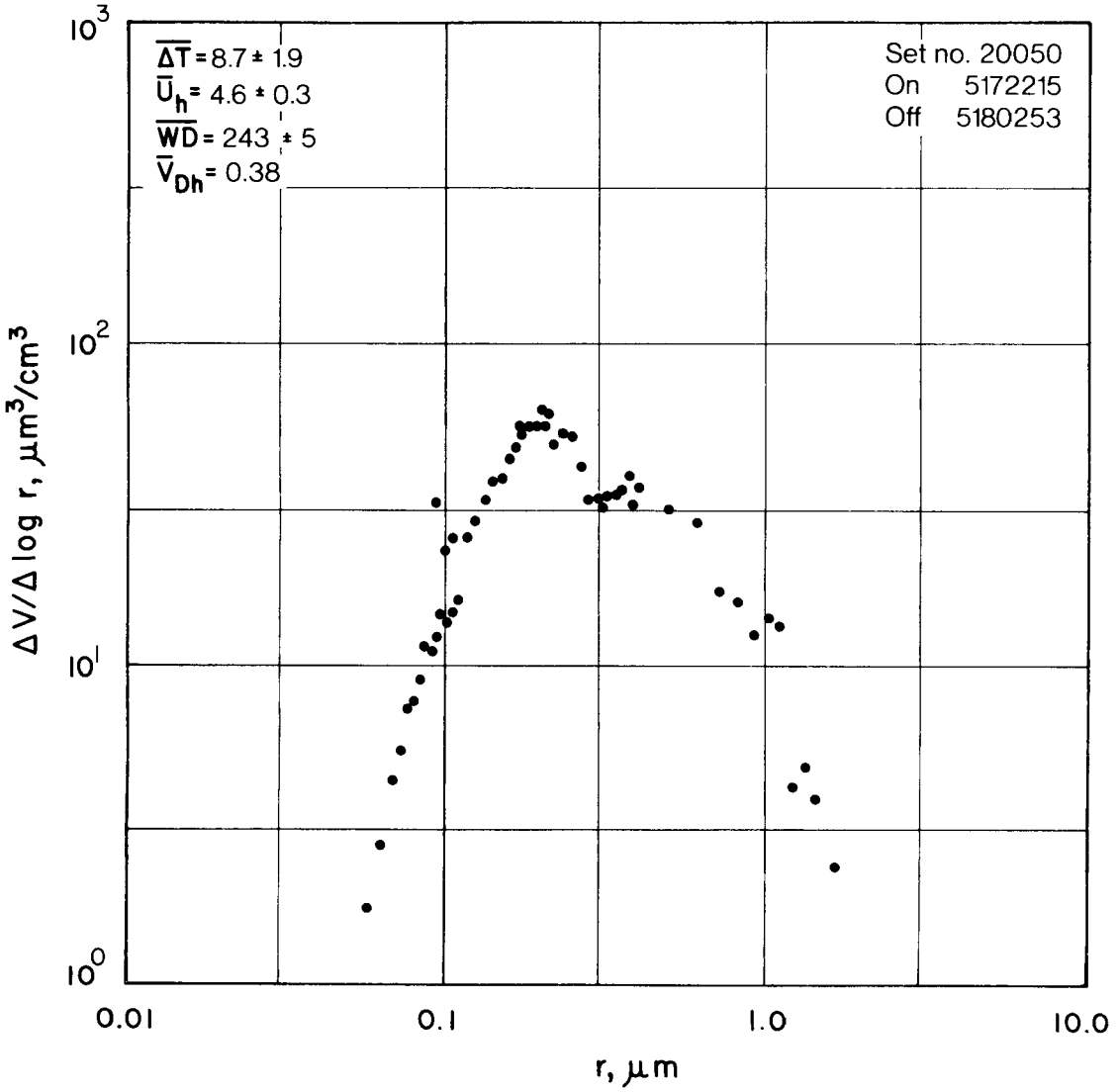

FIGURE 27. ΔV/Δ (log r) vs. log r for 22:15 CDT, 17 May 77 to 02:53 CDT 18 May 77.

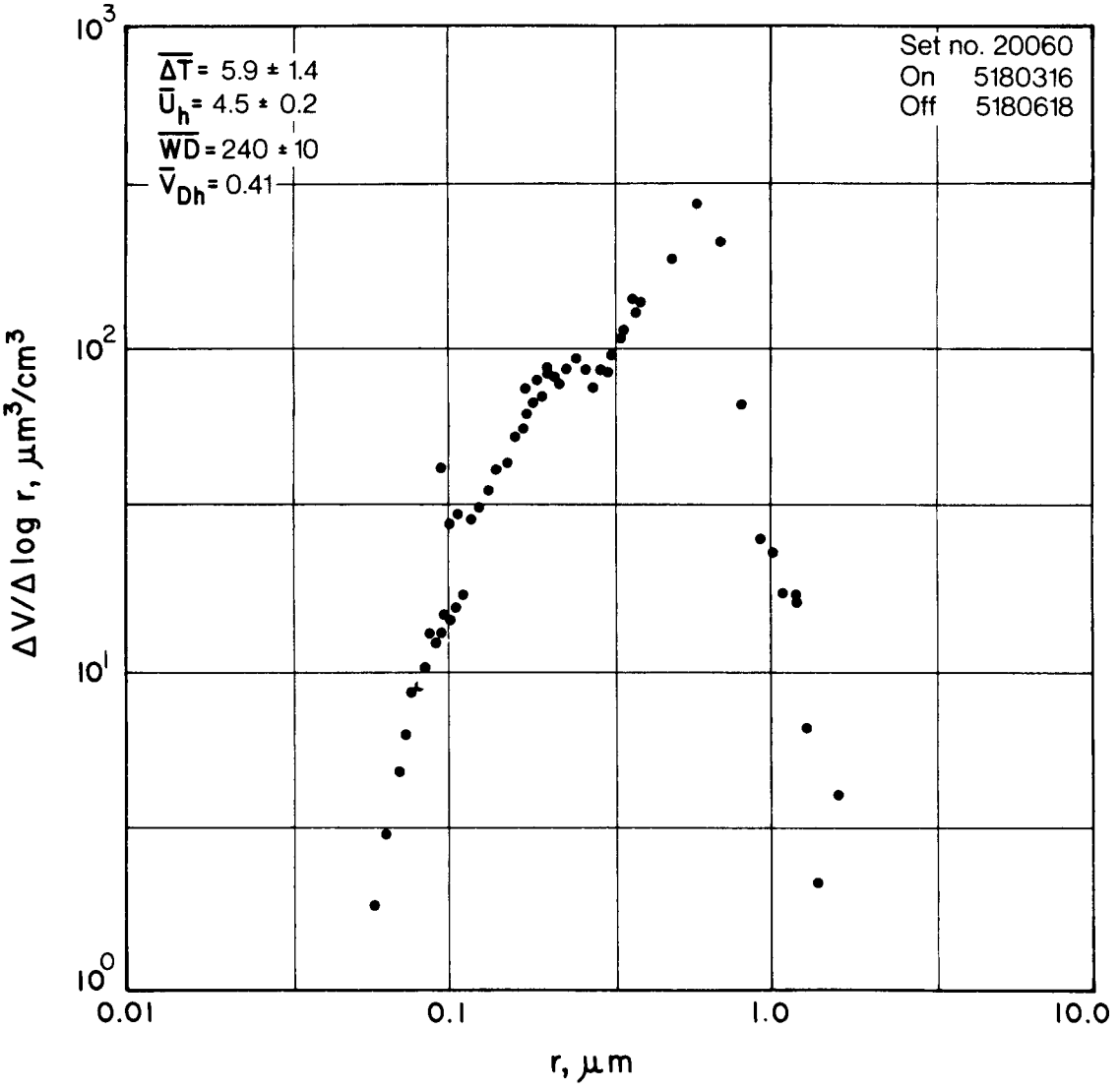

FIGURE 28. $\Delta V/\Delta$ (log r) vs. log r for 03:16 CDT, 18 May 77 to 06:18 CDT 18 May 77.

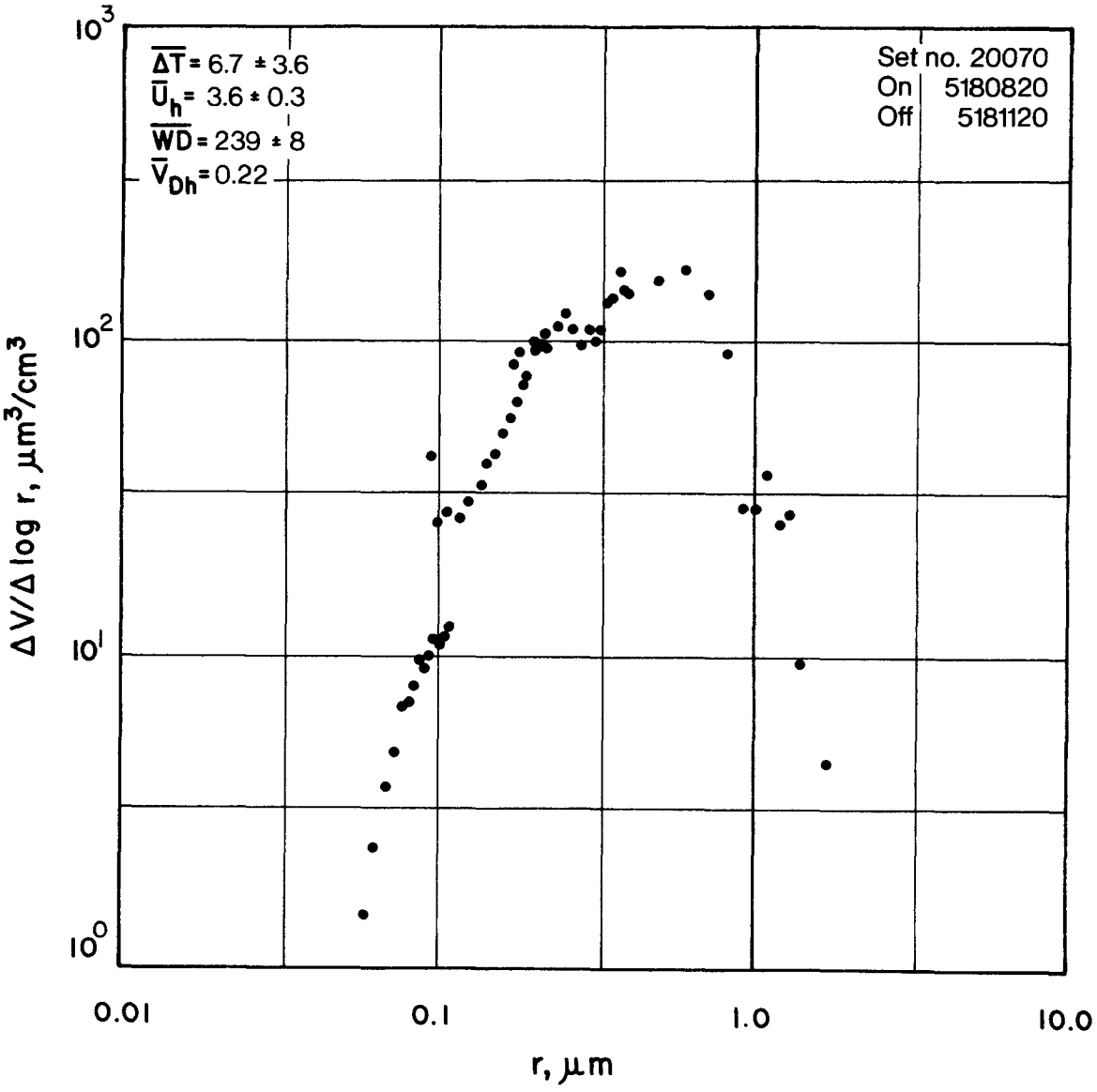

FIGURE 29. $\Delta V/\Delta$ (log r) vs. log r for 08:20 CDT, 18 May 77 to 11:20 CDT 18 May 77.

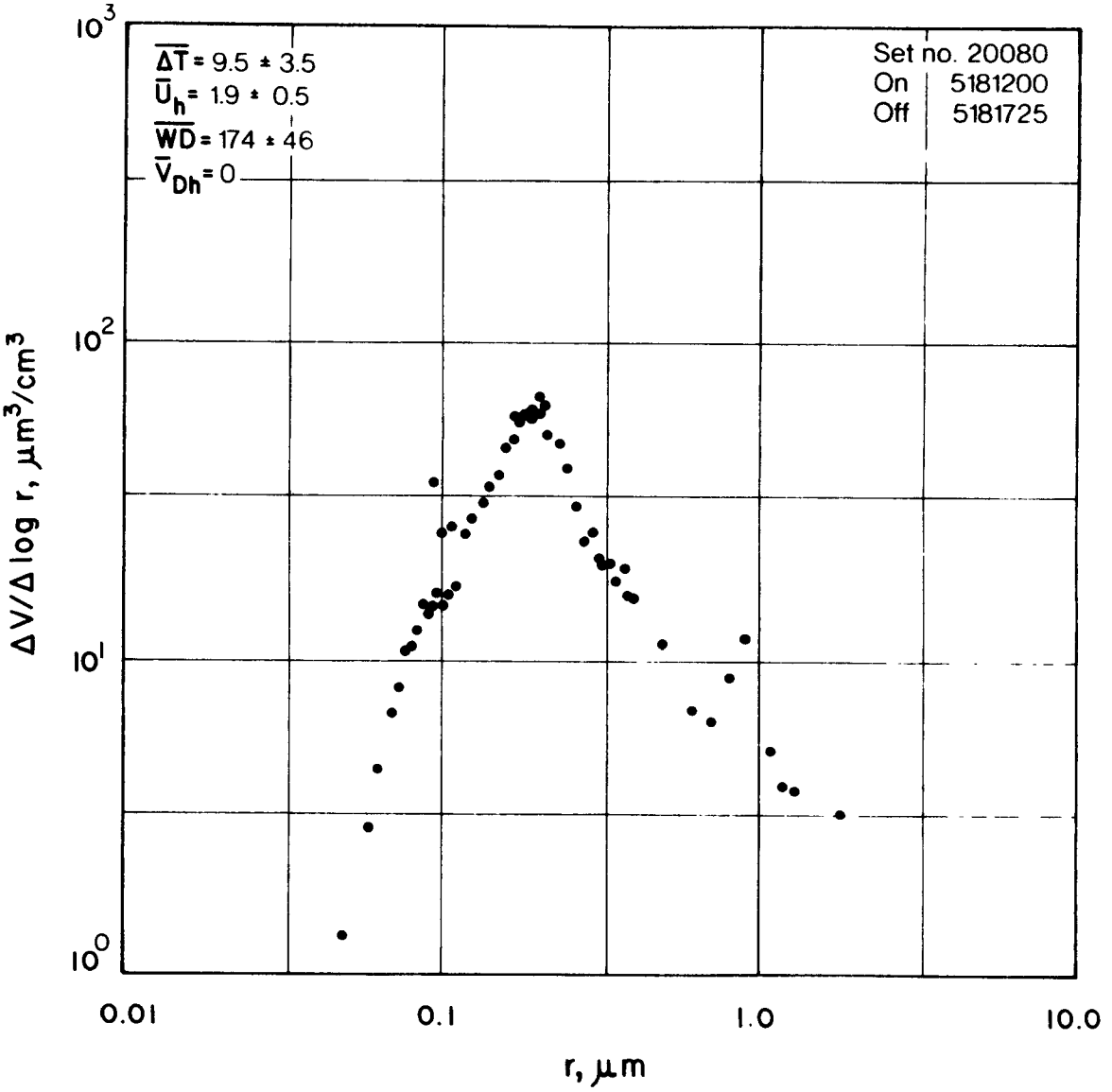

FIGURE 30. $\Delta V/\Delta$ (log r) vs. log r for 12:00 CDT, 18 May 77 to 17:25 CDT 18 May 77.

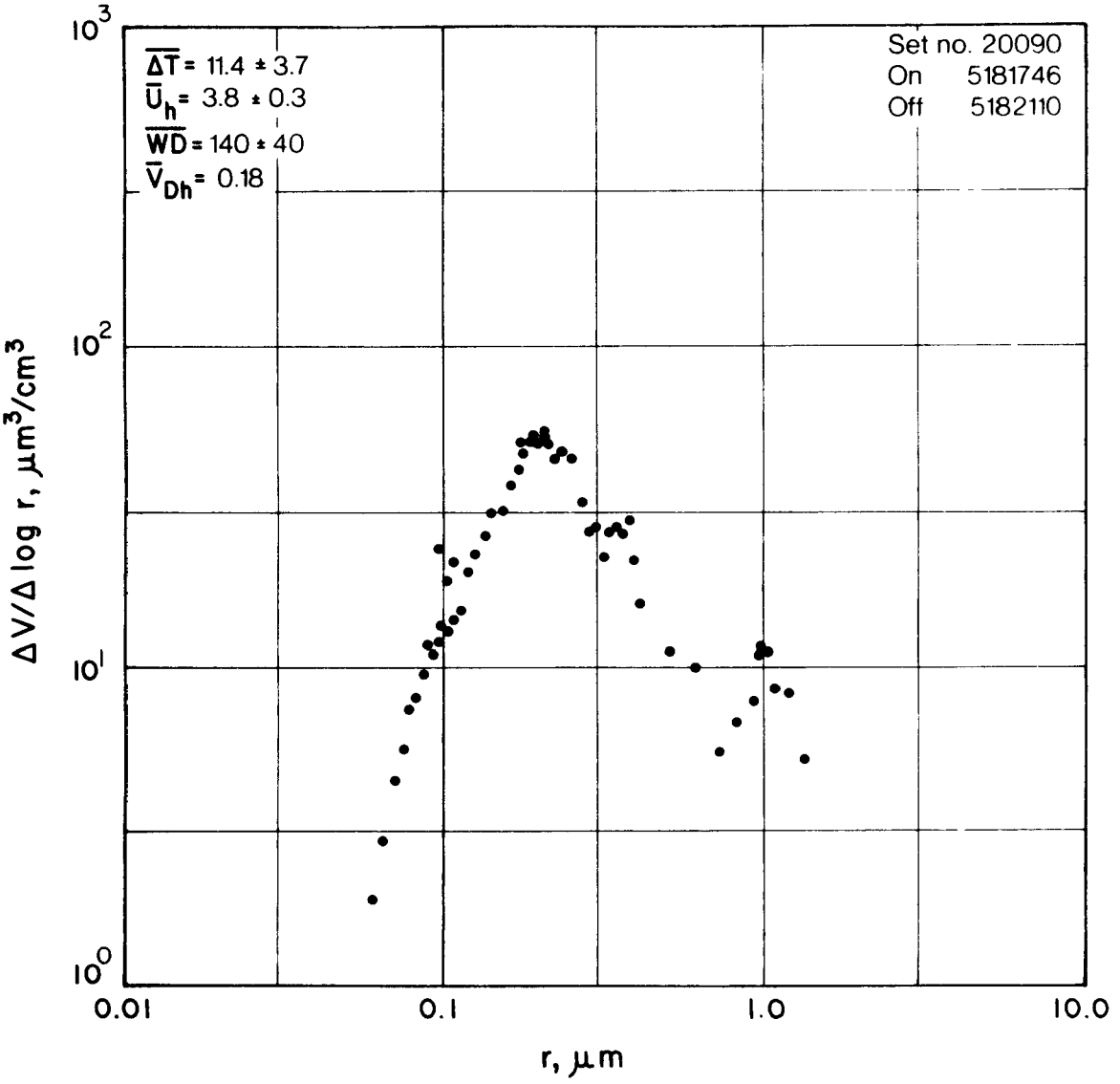

FIGURE 31. $\Delta V/\Delta$ (log r) vs. log r for 17:46 CDT, 18 May 77 to to 21:10 CDT 18 May 77.

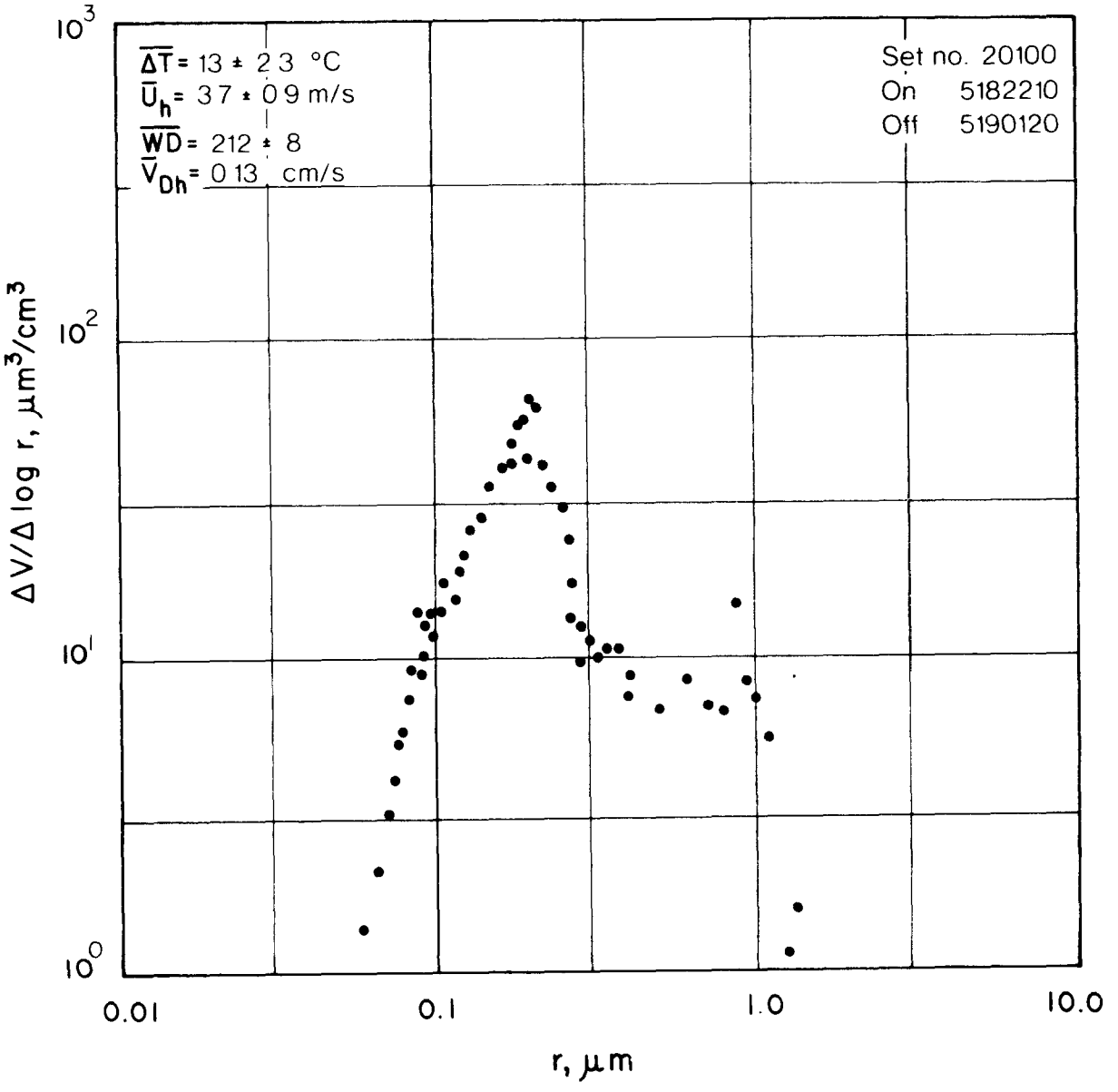

FIGURE 32. ΔV/Δ (log r) vs. log r for 22:10 CDT, 18 May 77 to 01:20 CDT 19 May 77.

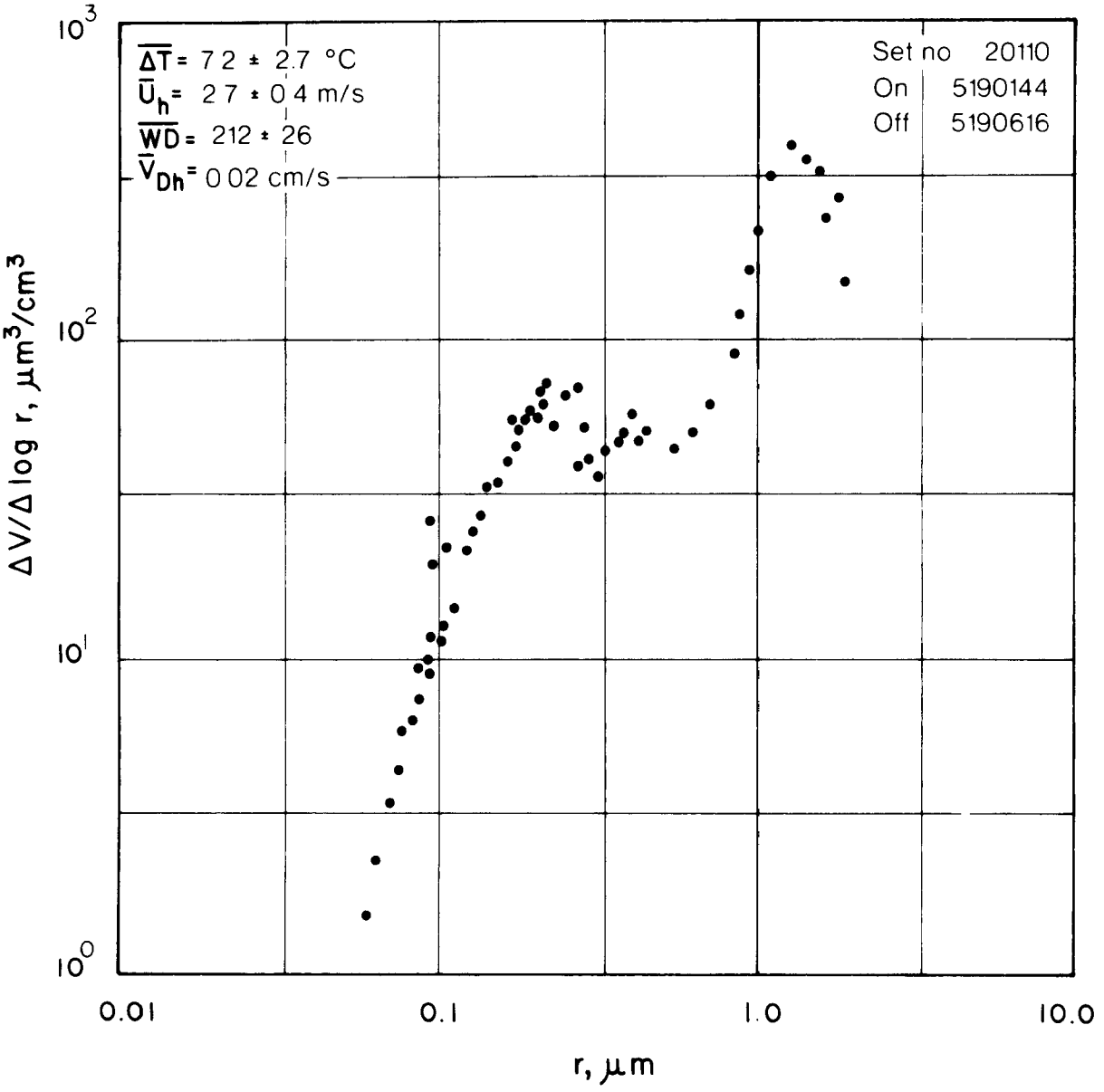

FIGURE 33. ΔV/Δ (log r) vs. log r for 01:44 CDT, 19 May 77 to 06:16 CDT 19 May 77.

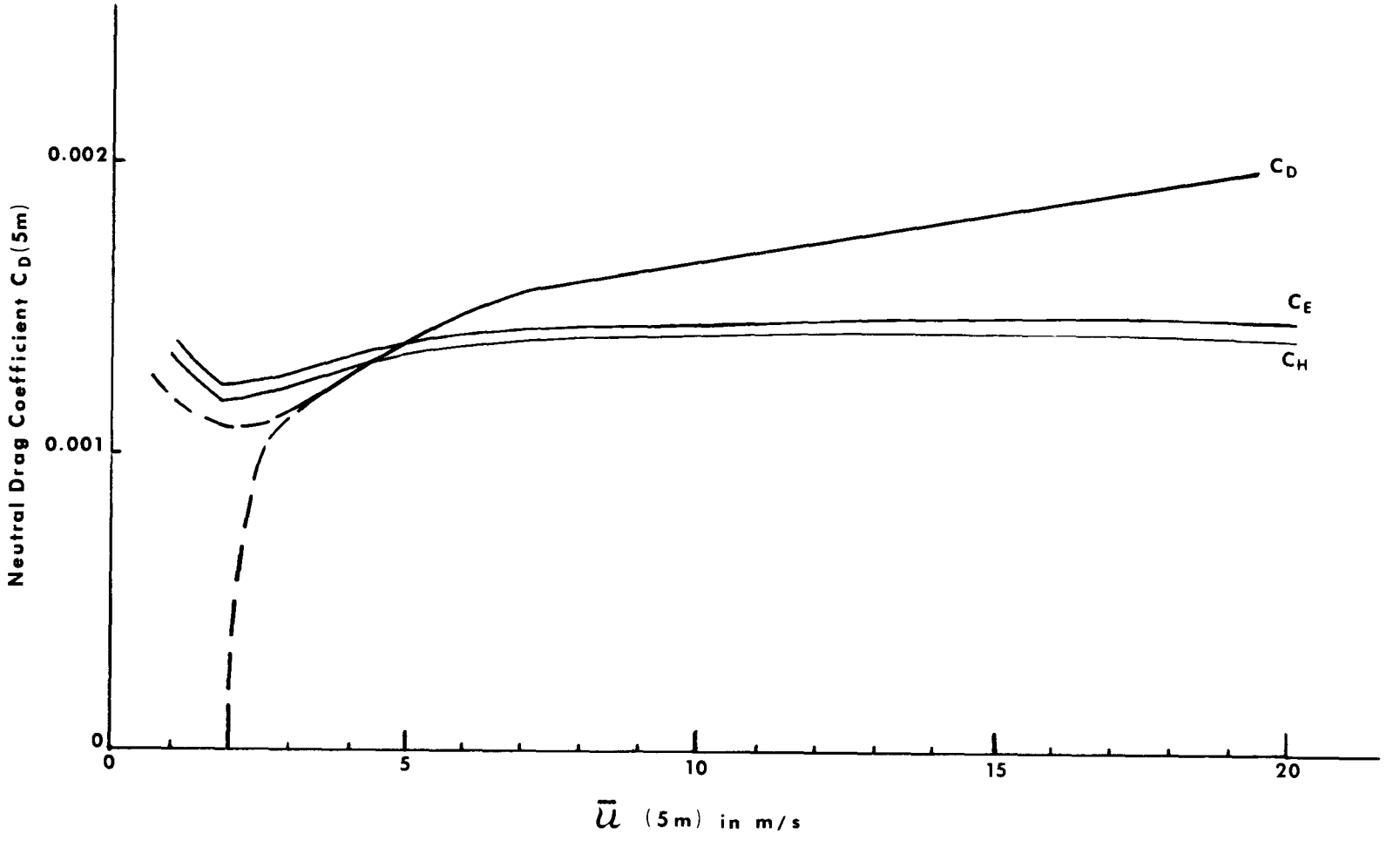

FIGURE 34. C_D, C_H and C_E vs. $\bar{u}$ at 5 m Sampling Height.

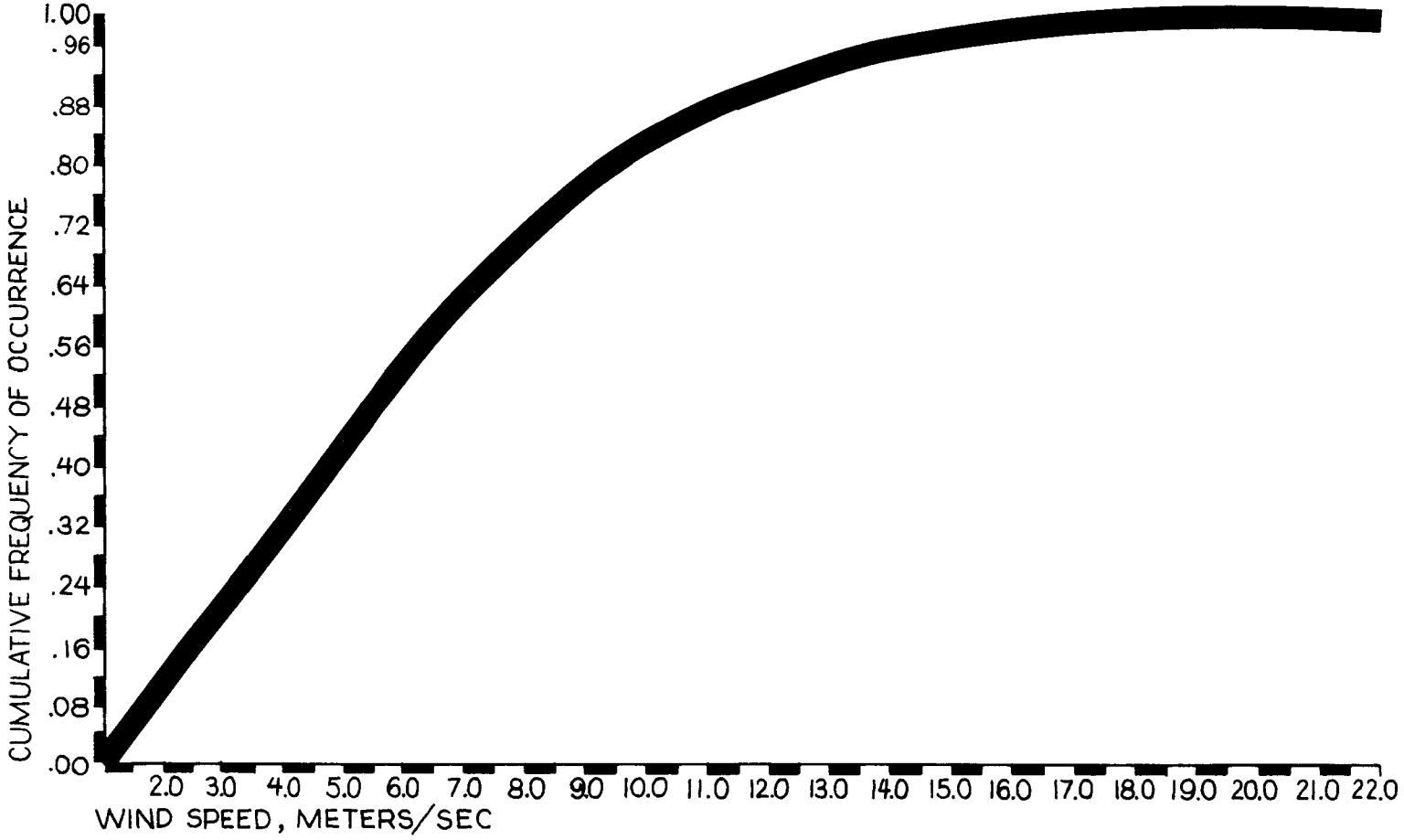

FIGURE 35. Cumulative Frequency of Occurrence of Wind Speed.

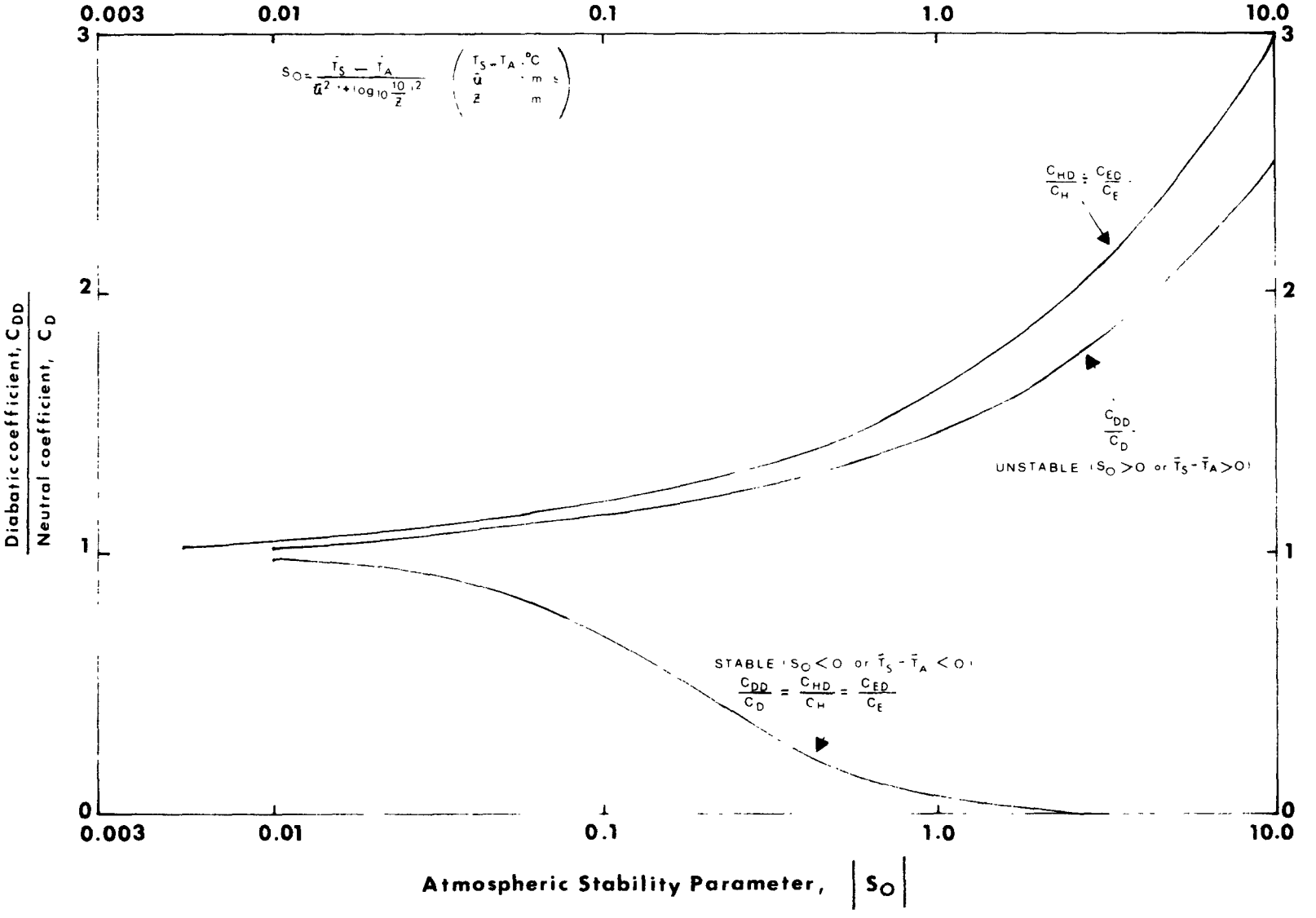

FIGURE 36. Ratio of C_{DD} to C_D vs. $|S_O|$.

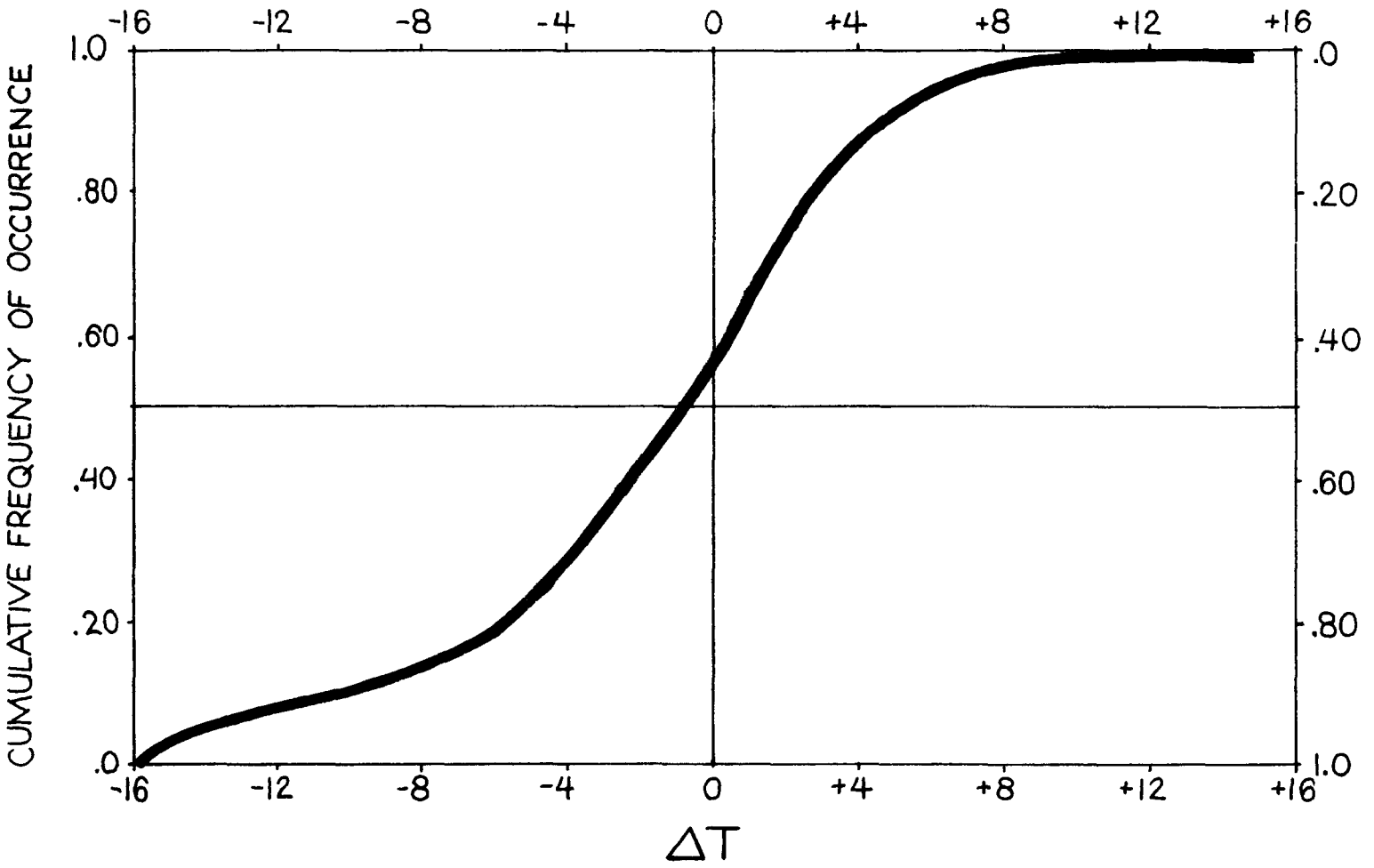

FIGURE 37. Cumulative Frequency of Occurrence of ΔT Over Southern Lake Michigan.

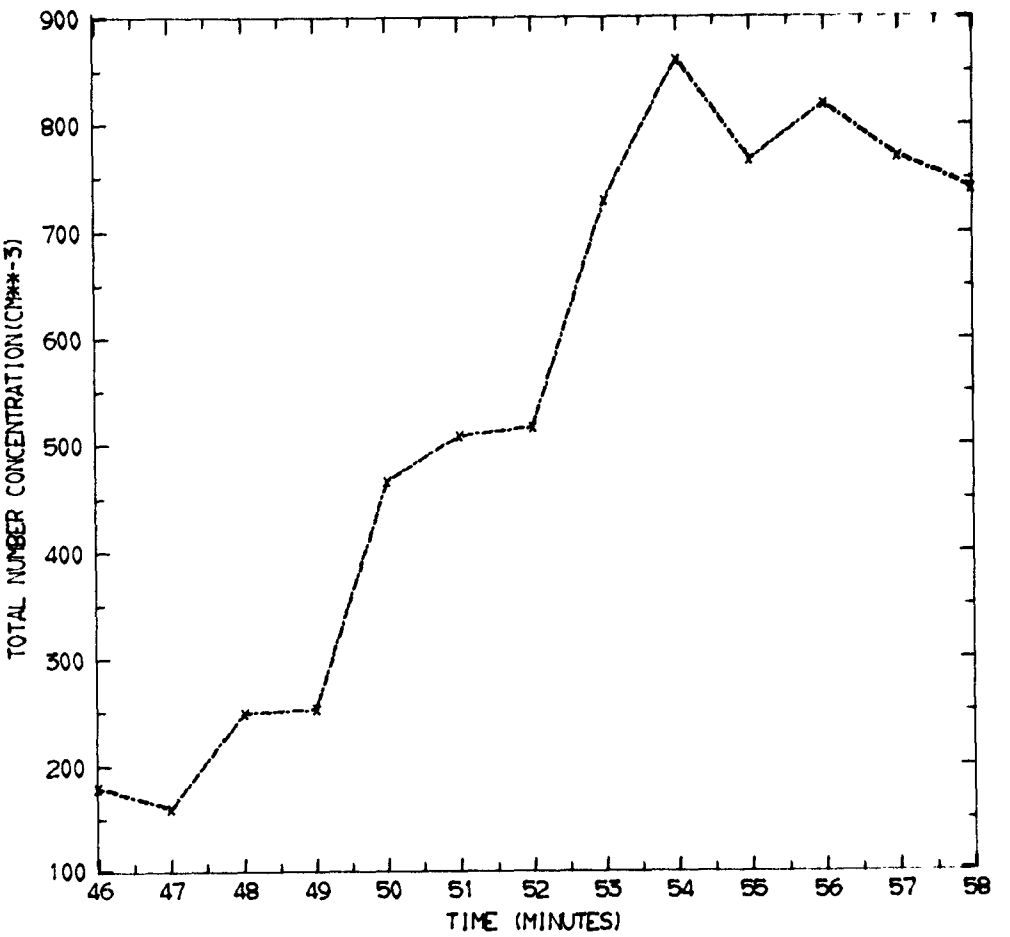

FIGURE 38. Aerosol Number Concentration (cm^{-3}) Measured in Size Range $0.25 < d < 20$ μm for the Midway Airport to Midlake Flight Leg Collected on 30 Sept 77 from 06:46 CDT to 06:58 CDT.

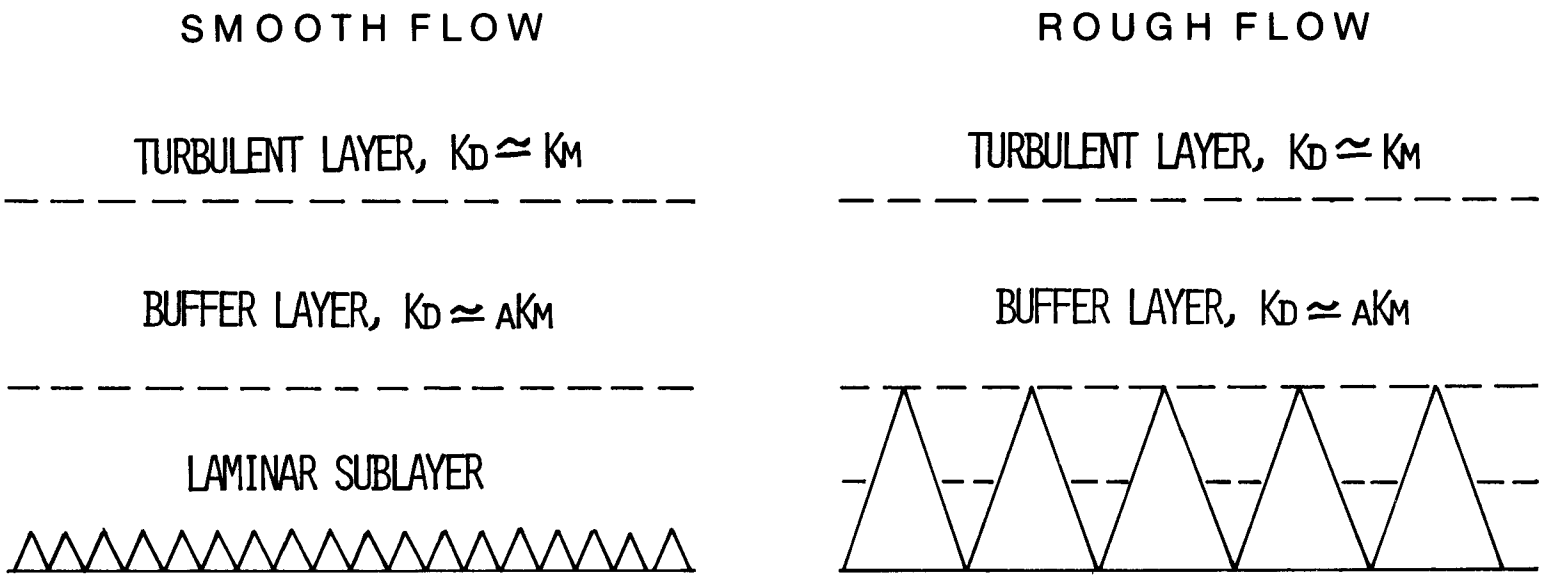

FIGURE 39. Diagramatic Representation of The Air/Water Interface.

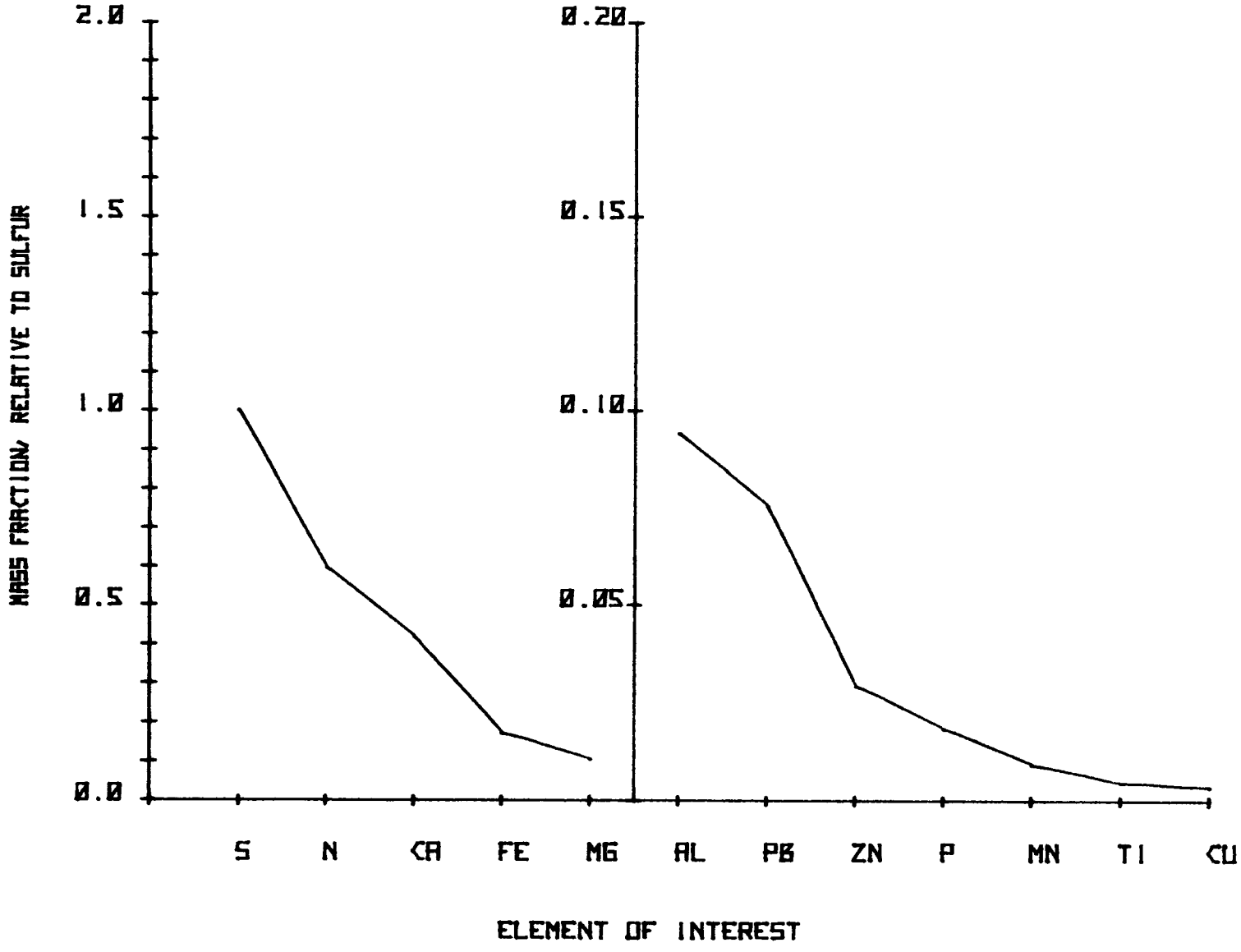

FIGURE 40. Normalized Aerosol Mass Fraction for All 1977 Sampling.

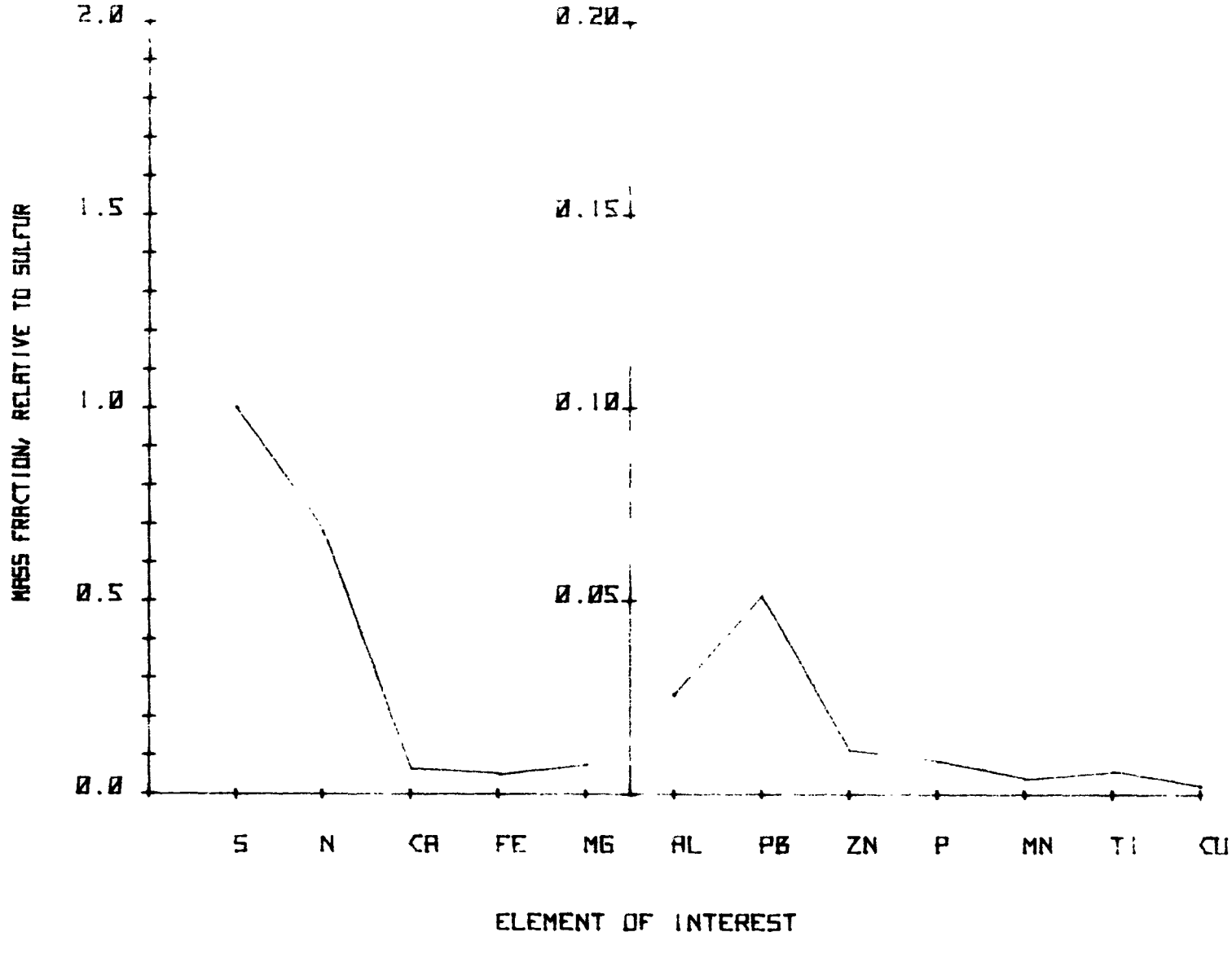

FIGURE 41. Normalized Aerosol Mass Fraction for Overlake Transport Samples.

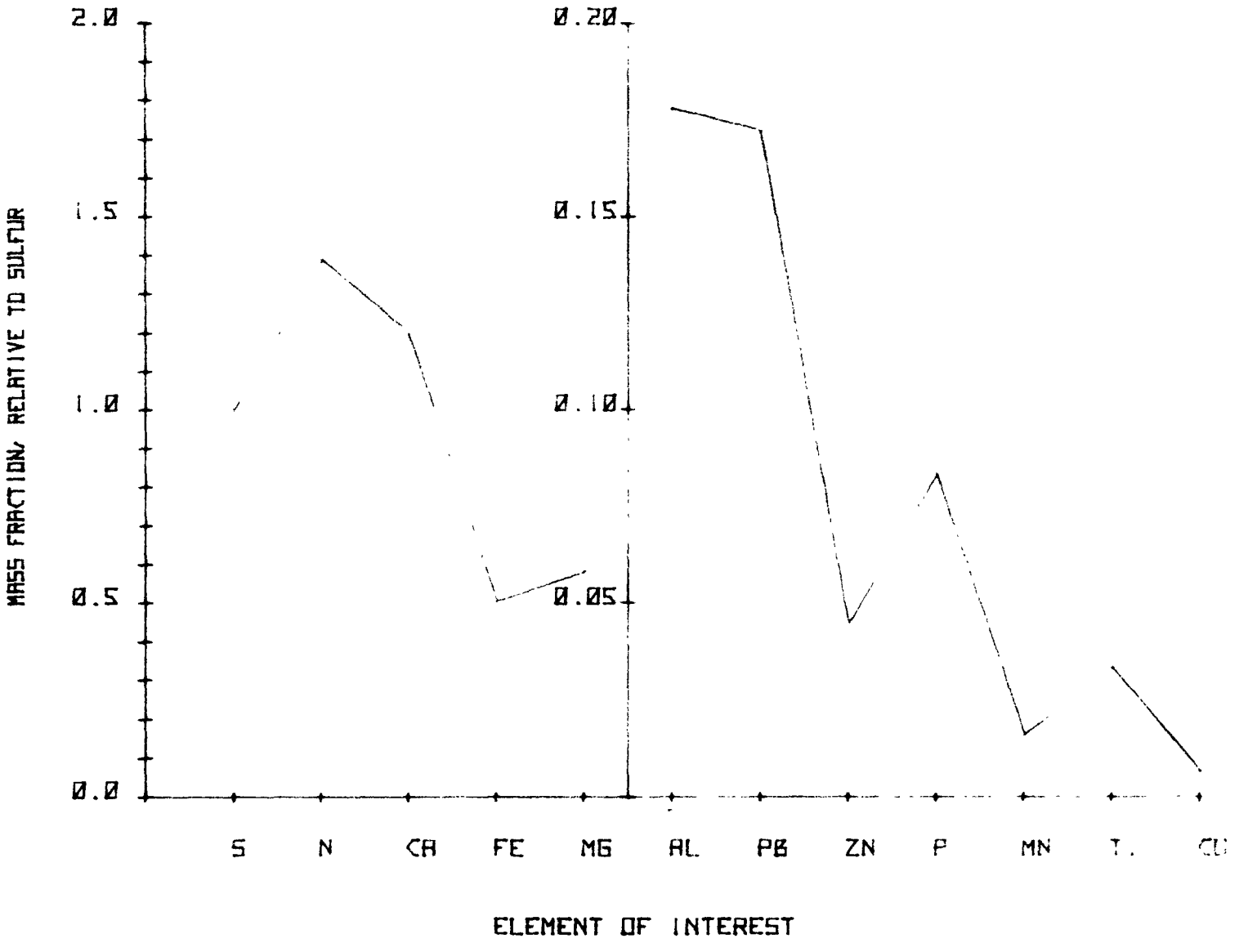

FIGURE 42. Normalized Aerosol Mass Fraction for West Shore Source Samples.

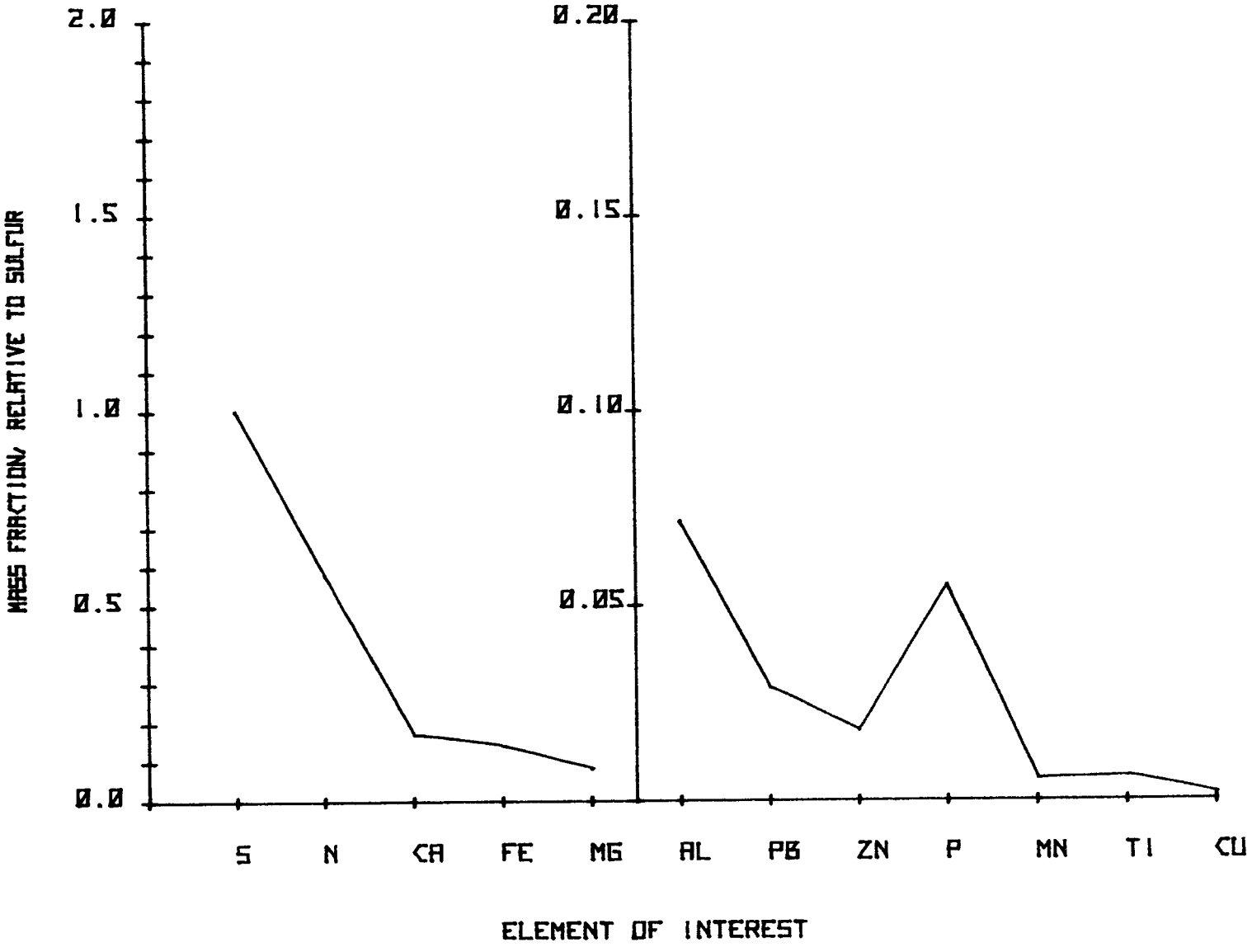

FIGURE 43. Normalized Aerosol Mass Fraction for East Shore Source Samples.

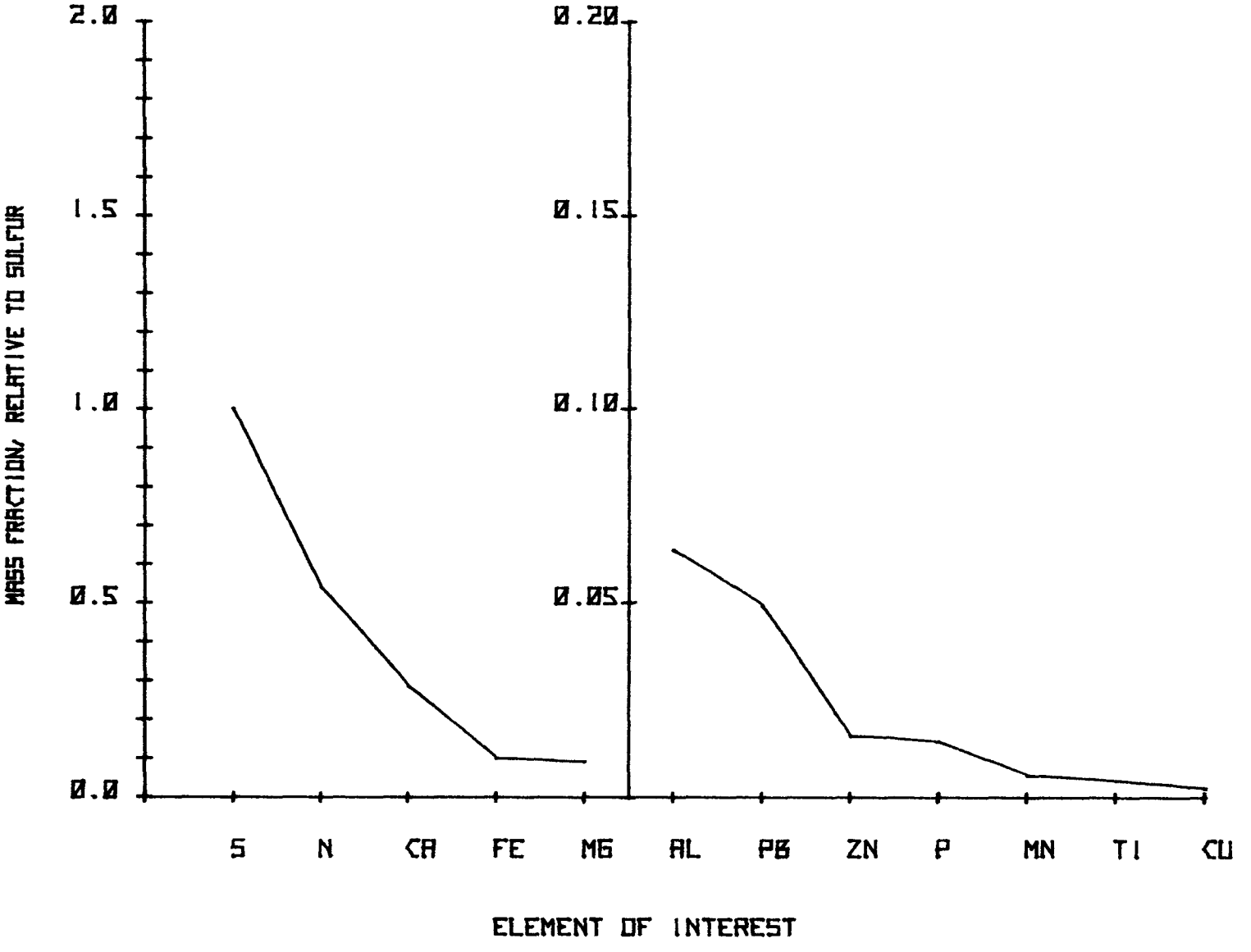

FIGURE 44. Normalized Aerosol Mass Fraction for Southeast Shore Source Samples.

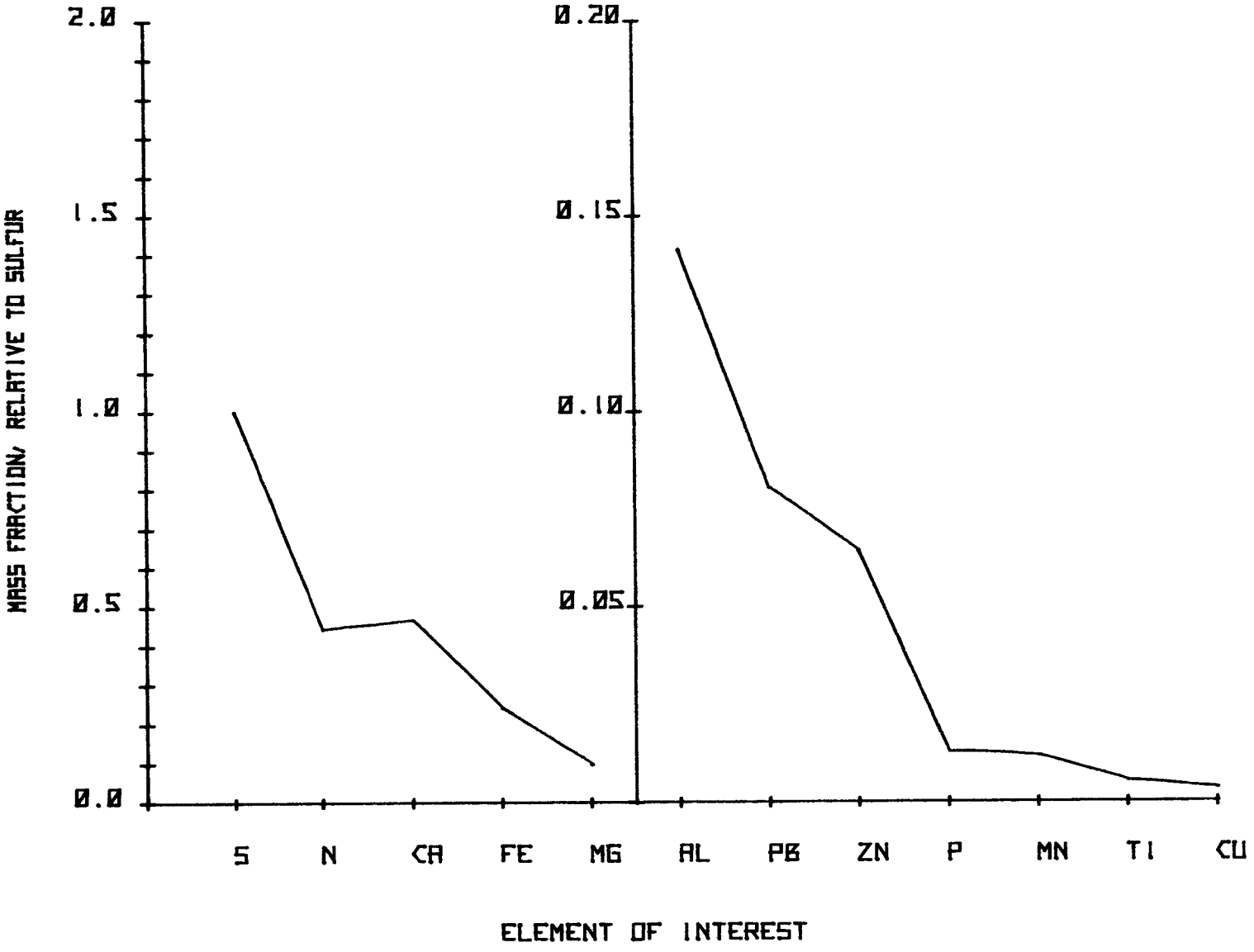

FIGURE 45. Normalized Aerosol Mass Fraction for Chicago/Gary Source Samples.

Table 1. Listing of Meteorological Parameters Measured and Type of Sensors Used in the Lake Michigan Study

Wind Velocity at 5 m height	(u_h)	3-cup anemometer/Weather Measure Grp (WMC) #W103
Ambient Air Temperature	(T_h)	YSI thermistor probe/WMC #IS6/TP621 HF-35
Relative Humidity	(RH)	Capacitance type/WMC#IS/HM-111
Vertical Wind	(W)	Gill propeller anemometer/R. M. Young Co. #27103-21282
Wind Direction	(WD)	Lightweight vane/WMC#W104
		Ship's log of WD, semi-hourly report
Water Surface Temperature	(T_o)	Hand-held Infrared Thermometer/Barnes Engineering Co. #PRT-10
Water Surface Current	(u_o)	Floating drifter; Optical range finder
Bulk Water Temperature	(T_w)	Bucket thermometer

TABLE 2. Detection Limits (L_d) Filter Blank Corrections (β), and Typical Sample Elemental Concentrations (C) in the ICAP-AES Liquid Sample (all $\mu g\text{-}\ell^{-1}$).

Elements	L_d	β	C	Percent of Sets C $>L_d$
Al	50	140	810	97
B	50	1850	†	77
Ba	5	5	*	46
Ca	700	1200	8150	85
Cd	2	2	*	31
Co	5	5	*	5
Cu	6	9	18	88
Fe	170	380	1700	92
Mg	100	240	1890	95
Mn	5	16	110	98
Mo	5	6	*	48
Na	15000	15000	*	10
Ni	5	13	*	40
Pb	20	25	170	97
Ti	15	19	50	90
V	12	12	*	5
Zn	60	125	175	98

* No C value, over 50 percent of sets below L_d.

† Possible contamination of some data sets.

	BULK WATER					SURFACE	
Element	Overall	May	June	August	September	September	$E^{\dagger}_{sb}$
Al	13	*	*	38	*	*	*
B	79	12	13	140	68	55	-0.19
Ba	10	11	10	10	10	10	0.00
Ca	29240	33000	34200	25400	29800	30900	0.04
Cd	0.5	*	*	*	0.9	1.0	0.10
Co	0.4	*	*	0.9	0.2	0.6	2.00
Cu	2.6	*	*	3.0	3.0	4.0	0.30
Fe	29	54	*	25	24	37	0.50
Mg	8710	10200	10300	7700	8590	8870	0.03
Mn	0.8	*	*	1.9	1.0	*	*
Mo	2.2	*	*	2.8	2.9	3.0	0.03
Na	4870	4580	4630	5860	4160	4330	0.04
Ni	3.1	*	*	6.6	1.8	3.0	0.70
Pb	3.5	*	*	2.4	6.2	8.0	0.30
Ti	1.5	*	*	1.0	2.7	3.0	0.10
V	3.8	*	*	11	*	*	*
Zn	17	15	27	17	15	20	0.3

$^{\dagger}E_{sb}$ = (C surface/C bulk) - 1.0

* Less than 3 samples > L_d

pH	8.3	8.2	8.3	8.5	8.2	N/A
$T_w{}^{o}C$	N/A	2.7	10.3	21.9	17.4	N/A

TABLE 3. Geometric Mean Concentrations ($\mu g\text{-}\ell^{-1}$) of Certain Elements in Lake Michigan Water at 87°00'W by 42°00'N

TABLE 4. Geometric Mean Concentrations in Air (ng - m^{-3}) of Certain Elements at 87°00'W by 42°00'N During 1977 Sampling Periods

Element	Overall	May	June	August	September
Al	180	470	190	90	60
Ca	770	1900	1500	340	550
Cu	6	13	4	3	4
Fe	320	790	990	190	90
Mg	200	420	220	150	210
Mn	20	45	25	10	6
Pb	140	350	85	70	60
Ti	8	13	10	8	7
Zn	55	240	95	25	15
Total P	35	40	20	30	30
NO_2/NO_3 - N	1000	2300	1400	560	720
SO_4 - S	1800	3500	1200	1400	1000
Mass	32000	66200	21000	21100	22700

TABLE 5. Characterization of Mid-Lake Michigan Aerosol with Respect to Several Chemical Species

Element	Π*	FC**	EF***
Al	0.56	1.2	≡ 1.0
Ca	2.4	0.43	22
Cu	0.02	3.9	170
Fe	1.0	1.6	3.5
Mg	0.63	0.64	23
Mn	0.06	2.0	10
Pb	0.44	17.3	5200
Ti	0.03	0.69	1.4
Zn	0.17	6.1	530
Total P	0.11	4.2	---
NO_2/NO_3 - N	3.1	8.0	---
SO_4 - S	5.6	27.5	---

* Π = % of total aerosol mass

** FC = fractional degree of association of element with $d < 1.0$ μm aerosol

*** EF = Al-based enrichment factor, using Bowen's (1966) soil composition

Ca	.44											
Mg	.81	.43										
Al	.88	.85	.49									
Fe	.90	.79	.91	.44								
Mn	.89	.78	.86	.97	.41							
Mo	.35	.25	.33	.38	.41	.03						
Pb	.71	.69	.69	.72	.78	.63	.47					
Ti	.71	.58	.67	.68	.62	.33	.51	.13				
Zn	.84	.73	.79	.90	.95	.49	.88	.68	.45			
C_m	.45	.50	.55	.54	.63	.14	.52	.28	.59	.43		
$\overline{u}_5$	-.13	-.09	-.14	-.10	-.14	-.00	-.12	.29	-.08	-.12	.11	
$\overline{\Delta T}$	.50	.60	.65	.49	.46	.20	.50	.16	.40	.52	-.35	.38
	Ca	Mg	Al	Fe	Mn	Mo	Pb	Ti	Zn	C_m	u_5	$\overline{\Delta T}$

TABLE 6. Correlation Coefficients Matrix Among Trace Element, Total Aerosol Mass, Wind Speed, and Air/Lake Surface Temperature Difference Using 40 Filter Sets' Data.

TABLE 7a. Trace Element Analysis Results for Data Sets Collected at the Nearshore Site in 1978.

Element	$\overline{C}$ (ng-m^{-3})	Π	FC	EF
Al	290	0.41	1.8	≡ 1.00
Ba	12	.02	2.0	6.2
Ca	1800	2.5	0.9	28
Cd	6	.009	14.4	40000
Co	1	.001	6.9	43
Cu	24	.03	6.4	300
Fe	750	1.10	3.3	4.5
Mg	600	.85	2.2	27
Mn	60	.09	3.1	15
Mo	4	.006	6.8	720
Na	250	.36	0.9	12
Ni	10	.01	5.0	50
Pb	450	.64	12.7	11000
Ti	10	.01	1.9	0.5
V	8	.01	7.3	24
Zn	200	.28	4.4	980

	Cu		Fe		Pb		Zn		Mn		
Data Set	% Soluble	Total Recovery	% Soluble	Total Recovery	% Soluble	Total Recovery	% Soluble	Total Recovery	% Soluble	Total Recovery	Wind Direction
60640	0	0	40	40	90	95	19	19	0	0	69
60650	54	109	109	119	62	120	36	129	42	124	91
60670	41	64	86	86	55	97	78	135	46	104	25
60680	45	62	109	115	53	105	28	107	47	126	90
60690	44	77	90	98	48	107	18	81	28	83	105
70700	19	25	96	96	90	109	57	97	43	99	41
70710	41	74	124	124	65	102	29	93	49	98	45
70720	39	74	78	89	39	103	24	91	31	110	203
70740	105	105	104	104	105	105	86	86	83	95	215
70750	146	146	153	153	163	163	135	159	116	155	191
70760	91	92	75	75	96	97	88	92	53	73	271
70770	43	43	22	22	40	40	19	24	19	39	272
70780	62	62	65	65	97	97	52	52	56	57	277
70790	65	65	61	61	96	96	82	87	56	63	290
70800	124	124	141	141	122	122	115	115	163	198	257
70810	86	92	109	109	101	101	88	104	85	111	265
70820	62	77	94	97	87	103	34	108	58	95	220
70830	18	90	51	84	63	97	11	102	25	94	variable
70840	35	84	74	93	47	116	22	96	43	131	variable
70850	36	97	61	90	66	113	20	112	19	110	variable
MEAN	52.8	78.1	84	93	79.2	104	52	94	48.1	98.2	
σ	36.5	32.8	37.7	31	31.2	21	36.7	33	34.3	41.8	
Excluding 70740-70810 MEAN	36.2	69.4	84.6	94	63.8	105.6	31.3	97.5	35.9	97.8	
σ	16.8	30.1	24.5	21.5	17.2	7.8	18.8	29.1	15.9	34	

TABLE 7b. Results of Passive Aqueous Extraction of Nearshore Aerosol Samples.

TABLE 8. 50 percent Collection Efficiency Diameters for Hi-Volume Sampler Integrating Nephelometer and Active Scattering Aerosol Spectrometer (ASAS)

Aerosol Sizing Instrument	Range of Diameter Sampled, μm
Hi-Volume Sampler*	≤ 0.1 to 10 or 20
Integrating Nephelometer**	0.1 or 0.2 to 1.0

ASAS Channel #	SR 0	SR 1	SR 2	SR 3
1	0.67-0.87	0.32-0.35	0.17-0.19	0.09-0.11
2	0.87-1.06	0.35-0.38	0.19-0.21	0.11-0.12
3	1.06-1.26	0.38-0.41	0.21-0.22	0.12-0.13
4	1.26-1.45	0.41-0.44	0.22-0.24	0.13-0.14
5	1.45-1.65	0.44-0.47	0.24-0.25	0.14-0.15
6	1.65-1.85	0.47-0.50	0.25-0.27	0.15-0.15
7	1.85-2.04	0.50-0.53	0.27-0.28	0.15-0.16
8	2.04-2.24	0.53-0.56	0.29-0.30	0.16-0.17
9	2.24-2.43	0.56-0.59	0.30-0.32	0.17-0.17
10	2.43-2.63	0.59-0.62	0.33-0.33	0.17-0.18
11	2.63-2.83	0.62-0.65	0.33-0.35	0.18-0.19
12	2.83-3.02	0.65-0.68	0.35-0.37	0.19-0.19
13	3.02-3.20	0.68-0.71	0.37-0.38	0.19-0.20
14	3.20-3.37	0.71-0.74	0.38-0.40	0.20-0.21
15	3.37-3.53	0.74-0.76	0.40-0.41	0.21-0.22

* Based on 50 percent collection efficiency of glass fiber filter for small aerosol and of Hi-Vol hood for large aerosol

** Charlson, et al. (1968)

Data Set	Run Time (CDT)	Meteorology $\overline{\Delta T}$ (°C)	Meteorology $\overline{\overline{u(5)}}$ (m/s)	Meteorology $\overline{WD}$ (°)	Aerosol Mass (μg/m³) b_{scat} Mass	Aerosol Mass (μg/m³) Hi-Vol Mass	Aerosol Mass (μg/m³) ASAS Mass <1.0 μm	Aerosol Mass (μg/m³) Total
20050	5/17 22:15-5/18 03:00	8.7 ± 1.9	4.6 ± 0.3	243 ± 5	117	↑	46	51
20060	5/18 03:00-5/18 06:00	5.9 ± 1.4	4.5 ± 0.2	240 ± 10	125		160	169
20070	5/18 08:20-5/18 11:20	6.7 ± 3.6	3.6 ± 0.3	239 ± 8	226		174	193
20080	5/18 12:00-5/18 17:25	9.5 ± 3.5	1.9 ± 0.6	174 ± 46	141	132	29	31
20090	5/18 17:45-5/18 21:00	11:4 ± 3.7	3.8 ± 0.3	140 ± 40	110		29	34
20100	5/18 22:00-5/19 01:30	13.3 ± 2.1	3.7 ± 0.9	212 ± 8	47		19	23
20110	5/19 01:45-5/19 06:15	7.2 ± 2.9	2.7 ± 0.4	212 ± 26	141	↓	133	333

TABLE 9. Sample Time, Meteorological Parameters, and Aerosol Data for Data Sets 20050 - 20010.

Profile Set	$\bar{u}(5)$ (m/s)	Wind Direction (^{o})	$\overline{\Delta T}$ (^{o}C)	Ratio of High to Low Position Aerosol Counts	Size Range (μm)	Ri_B	α	$\left(\frac{h_1}{5}\right)^{\alpha} - \left(\frac{h_2}{5}\right)^{\alpha}$	$\bar{v}_{dp}/\tilde{v}_d$
23 June 78 13:40-14:30	4.0	45	2.0	1.34 ± 0.19	0.6 < d < 1.5	0.02	0.4	0.38	0.7 ± 0.3
	±	±	±	1.19 ± 0.17	0.3 < d < 0.6		±	±	0.2 ± 0.1
$\tilde{v}_d$ = 0.6 cm/s	0.2	5	0.3	1.72 ± 0.24	0.1 < d < 0.2		0.1	0.11	0.4 ± 0.1
crib site									
16 August 77 20:45-21:30	7.9	355	2.4	1.30 ± 0.18	0.6 < d < 2.0	0.0037	0.2	0.11	1.2 ± 0.5
	±	±	±	1.30 ± 0.14	0.3 < d < 0.6		±	±	1.2 ± 0.5
$\tilde{v}_d$ = 1.3 cm/s	0.3	10	0.2	1.47 ± 0.13	0.2 < d < 0.4		0.05	0.03	1.7 ± 0.6
ship site				1.50 ± 0.18	0.1 < d < 0.2				1.8 ± 0.7
28 September 77 17:00-18:15	1.3	305	2.8	0.95 ± 0.08	0.6 < d < 2.6	0.13	0.6		-
	±	±	±	0.93 ± 0.08	0.3 < d < 0.6		±	- - -	-
$\tilde{v}_d$ = 0	0.3	7	0.3	0.96 ± 0.06	0.2 < d < 0.4		0.15		-
ship site				1.01 ± 0.03	0.1 < d < 0.2				-
19 May 77 13:30-16:30	1.6	105	8.8	0.77 ± 0.11	0.6 < d < 3.2	0.22	0.65		-
ship site	±	±	±	0.94 ± 0.05	0.3 < d < 0.6		±	- - -	-
$\tilde{v}_d$ = 0	0.5	5	1.4	0.79 ± 0.12	0.2 < d < 0.4		0.15		-
- THEN - - -	- -	- -	- -	0.98 ± 0.05	0.1 < d < 0.2				-
19 May 77 17:00-18:30	4.2	105	8.5	1.34 ± 0.08	0.6 < d < 2.6	0.04	0.5	0.28	0.55 ± 0.20
	±	±	±	1.09 ± 0.03	0.3 < d < 0.6		±	±	0.15 ± 0.05
$\tilde{v}_d$ = 0.25 cm/s	0.3	5	0.5	1.07 ± 0.06	0.2 < d < 0.4		0.1	0.06	0.10 ± 0.05
				1.02 ± 0.06	0.1 < d < 0.2				0.05 ± 0.02

TABLE 10. Meteorological and Aerosol Data for the Profile Data Sets

Profile Set	$\bar{u}(5)$ (m/s)	Wind Direction (^{o})	$\overline{\Delta T}$ (^{o}C)	Ratio of High to Low Position Aerosol Counts	Size Range (μm)	Ri_B	α	$\left(\frac{h1}{5}\right)^{\alpha} - \left(\frac{h2}{5}\right)^{\alpha}$	$\bar{v}_{dp}/\tilde{v}_d$
THEN									
19 May 77	3.3	146	8.5	0.8 ± 0.55	0.6 < d < 2.7	0.07	0.55	0.29	0
20:00-21:15				0.95 ± 0.10	0.3 < d < 0.6				0
	±	±	±	1.06 ± 0.05	0.2 < d < 0.4		±	±	0.1 ± 0.04
$\tilde{v}_d$ = 0.2 cm/s	0.6	15	0.9	1.12 ± 0.12	0.1 < d < 0.2		0.15	0.09	0.2 ± 0.05
- - THEN - -	- -	- -	- -	- - - -	- - - -	- -	- -	- - -	- - - - -
19 May 77	3.9	198	8.6	0.8 ± 0.26	0.6 < d < 3.0	0.05	0.55	- - -	0
22:45-24:00				0.85 ± 0.16	0.3 < d < 0.6				0
	±	±	±	0.98 ± 0.04	0.2 < d < 0.4		±		0
$\tilde{v}_d$ = 0.23 cm/s	0.6	25	1.5	0.99 ± 0.04	0.1 < d < 0.2		0.15		0

TABLE 10. Continued.

TABLE 11. Binned Data Sets, Using $\overline{\Delta T}$ as the Defining Parameter

$\overline{\Delta T}$ (°C)	< -0.9	-0.8 - 0.9	+1.0 - 2.7	2.8 - 8.2	> 8.3
F_o (Yr)	.38	.19	.15	.18	.02
$\overline{v}_d$ (cm-s^{-1})	.72	.73	.51	.39	.15
		$\overline{C}$ (ng-m^{-3})			
Al	40	90	100	630	450
Ca	140	620	710	2700	1200
Cu	5	5	5	20	5
Fe	60	210	190	1400	420
Mg	100	300	200	520	340
Mn	5	15	10	80	20
Pb	25	60	80	600	190
Ti	5	10	15	20	10
Zn	10	20	40	300	80
Total P	15	35	35	60	20
NO_2^-/NO_3^-	1200	3800	3000	7900	9500
$SO_4^=$	1400	3700	5000	11400	10300
Mass	13500	27900	22500	58900	68000

TABLE 12. Binned Data Sets, using $\bar{u}_5$ as the Defining Parameter.

$\bar{u}_5$ (m-s^{-1})	< 2.0	2.1 - 3.5	3.6 - 5.2	5.3 - 6.9	> 7.0
F_o (Yr)	.04	.16	.15	.20	.41
$\bar{v}_d$ (cm-s^{-1})	0.0	.23	.47	.76	1.17
		$\bar{C}$ (ng-m^{-3})			
Al	200	140	300	110	50
Ca	790	780	2000	540	320
Cu	10	5	10	5	2
Fe	300	360	550	330	60
Mg	200	460	380	240	70
Mn	20	10	40	20	5
Pb	140	60	230	120	70
Ti	6	0	10	10	10
Zn	50	30	90	40	20
Total P	20	20	45	30	25
NO_2^-/NO_3^-	6950	4300	7400	3300	1800
$SO_4^=$	4850	5800	7900	4050	4100
Mass	32900	28200	37000	30800	18700

TABLE 13. Binned Data Sets, Using Source Region as the Defining Parameter.

SOURCE AREA	OVERLAKE	WEST SHORE	EAST SHORE	S.E. SHORE	CHIC./ GARY
F_o (Yr)	.22	.16	.09	.35	.20
$\bar{v}_d$ (cm-s^{-1})	.50	.72	.62	.50	.42
		$\bar{C}$ (ng-m^{-3})			
Al	25	55	105	150	575
Ca	70	375	255	700	1900
Cu	2	2	2	5	15
Fe	50	160	208	250	980
Mg	80	180	120	215	400
Mn	5	5	8	15	50
Pb	50	55	42	120	325
Ti	6	10	10	10	21
Zn	10	15	27	40	260
Total P	10	30	40	50	40
NO_2^-/NO_3^--N	3750	2400	1700	8750	6200
$SO_4^=$-S	3650	1100	2000	10900	9650
Mass	28600	17300	20100	43200	50300

TABLE 14. Annual Loadings of Certain Trace Elements to the Southern Basin of Lake Michigan (10^3 kg - yr^{-1}).

ELEMENT	DRY DEPOSITION			Precipitation (2)	Run-Off (3)
	Minimum	Mean	% Total		
Al	300	650	$\geq$ 2	560	1300
Ca	1000	2900	< 1		490000
Cu	{10}	{20}	{6}	20	140 (4)
Fe	600	1200	$\geq$ 20	950	1450
Mg	400	730	< 1		134000
Mn	30	60	$\geq$ 10	50	250
Pb	300	520	$\geq$ 60	90	100
Ti	{15}	{30}	{10}	60	100
Zn	100	200	$\geq$ 30	50	180 (4)
Total P	75	150		100 (5)	~3000 (6)
NO_3^-/NO_2^--N	2000	4350			
SO_4-S	3500	7850			

Brackets { } enclosing results indicate caution should be used in interpretation -- see Section 5.

(1) This work.

(2) Gatz, 1975b.

(3) Winchester and Nifong, 1971.

(4) Robbins, et al., 1972.

(5) Murphy and Doskey, 1976.

(6) International Joint Commission on The Great Lakes, 1976.

FACTOR	1	2	3	4	5	6
"LABEL"	Transport of soil, lake and anthropogenically derived aerosol enhanced by temperature stability and Chicago/Gary Source Region	TI ship contaminant, other elements' conc. not significantly contributed to by ship effluent.	Stand Alone Wind Direction Factor	Fine Particulate with Nutrients	Soil and Lake Derived Coarse Particles contributing CA, MG, AL	Temp. Stab. brings out reactive and coarse particulate
PRIMARY MEMBERS	CA, MG, AL, FE, MN, PB, TI, ZN	u_5	C/G SES ES	P, NO_2/NO_3 SO_4 Mass	C/G WS L	NO_2/NO_3 ΔT
SECONDARY MEMBERS	P, NO_2/NO_3, SO_4 C/G ΔT	-TI	-L WS	MN PB ZN	CA MG AL	MG AL SO_4 MASS
VARIATION	41	8	9	20	10	12

TABLE 15. Factor Analysis Results and Interpretation of Factors.

Filter Set#	Source* Region	Time to Reach Shore (hours)	Bulk Richardson Number, R_{iB}	Air Mass Type
5	nC/G	2.7	0.05	-
6	nC/G	3.0	0.04	-
7	nC/G	2.8	0.06	mT
8	-	-	0.32	-
9	L	3.4	0.09	mT
10	nC/G	3.2	0.12	mT
11	nC/G	3.5	0.12	mT
13	nSES	2.5	0.07	mT
14	nSES or nC/G	3.5	0.13	-
15	-	-	0.11	-
17	L	6.5	0.03	cP
18	L	9.9	0.05	cP
19	SES	3.5	0.03	cP
20	nC/G	2.8	0.01	cP
21	nC/G	6.1	0.18	cP
22	-	-	0.09	-
24	ES	4.4	0.01	-
25	ES	3.8	0.01	-
26	ES	2.9	0.013	-
27	ES	5.3	0.03	-
28	ES or nSES	1.5	0.012	-
29	SES	1.2	0.01	mT
30	nC/G	2.6	0.03	mT
31	-	-	0.022	-
33	L	4.1	0.01	cP
34	WS	5.4	0.012	cP
35	L	6.4	0.01	cP
36	L	6.6	0.014	cP
37	-	-	0.016	-
40	WS or nC/G	1.7	0.018	-
41	WS or C/G	3.0	0.023	-
45	WS	2.1	0.008	cP
47	WS	2.0	0.005	cP
49	L	4.0	0.007	cP
50	L	3.6	0.12	cP
51	SES	2.9	0.033	cP
53	SES	1.9	0.022	cP
54	SES	1.5	0.015	-
55	nSES	1.8	0.013	-

* C/G is Chicago/Gary, WS is West Shore, L is Lake, ES is East Shore, SES is Southeast Shore and n refers to nearshore source domination (vs. longer range source domination, for which no prefix is stated)

TABLE 16. Meteorological Influences Upon the 39 Filter Set Data Base.

Table 17. Factor Analysis of Nineteen Filter Sets' Data with $Ri_B \geq 0.03$.

	UNCORRELATED FACTORS			
Variable	1	2	3	4
Al	(.82)	(.54)	.17	.09
Ca	(.86)	.34	.19	.33
Fe	(.93)	.24	.21	.17
Mg	(.76)	(.59)	.07	.28
Mn	(.91)	.22	.12	.34
Pb	(.52)	.27	.09	(.81)
Ti	(.95)	.02	.28	.10
Zn	(.79)	.15	.18	(.56)
Mass	.17	(.93)	.18	.28
u_5	.24	.20	(.95)	.08
ΔT	.16	(.98)	(.09)	.02
% TOTAL VARIATION	52.3	23.5	9.9	12.3

Table 18. Factor Analysis of Twenty Filter Sets' Data with $Ri_B < 0.03$.

	UNCORRELATED FACTORS				
Variable	1	2	3	4	5
Al	(.50)	(.82)	.05	.23	.17
Ca	.22	(.94)	-.06	.22	.15
Fe	(.76)	(.57)	.08	.28	.08
Mg	.22	.24	.01	(.92)	.22
Mn	(.87)	.43	-.02	.24	.01
Pb	(.92)	.18	.07	.08	.34
Ti	.38	(.58)	(.67)	.19	.22
Zn	(.95)	.31	-.01	.05	.03
Mass	(.99)	.06	.01	.09	-.06
u_5	.08	.19	(-.97)	.04	-.11
ΔT	.08	.27	.19	.22	(.91)
% TOTAL VARIATION	36.4	30.2	12.1	9.9	9.4

TABLE 19. Factor Analysis of Fifteen Filter Sets' Data with Travel Time to Shore $\geq$ 3.5 hrs.

	UNCORRELATED FACTORS		
Variable	1	2	3
Al	.35	.07	(.94)
Ca	(.84)	.26	.48
Fe	.30	.11	(.95)
Mg	(.63)	.12	(.77)
Mn	(.63)	.40	(.67)
Pb	(.88)	.04	.48
Zn	(.92)	.12	.37
Mass	(.97)	.08	.22
WS	.12	(.99)	.11
T	(.70)	.32	(.64)
% TOTAL VARIATION	43.9	13.5	38.6

TABLE 20. Factor Analysis of Seventeen Filter Sets' Data with Travel Time to Shore $\leq$ 3.0 hrs.

	UNCORRELATED FACTORS	
Variable	1	2
Al	(.94)	.25
Ca	(.96)	.30
Fe	.98	.18
Mg	(.96)	.21
Mn	.98	.19
Pb	.95	.31
Zn	.97	.23
Mass	(.99)	.08
WS	.19	(.98)
T	(.94)	.37
% TOTAL VARIATION	85.3	13.1

Element	Average Soil Conc.* (ppm)	% Soil Derived	Average Bulk Water Conc.** (ppb)	% Lake Derived***	% Non-natural
Al	71000	100	38	(.08)	-
Ca	13700	3	29900	97	-
Mg	6000	6	8730	94	-
Fe	38000	24	46	0.4 to 10	$\geq$ 65
Mn	850	11	2.6	0.4 to 10	$\geq$ 80
Ti	4700	(134)	2.4	(10)	-
Zn	50	0.2	18	1.0 to 25	$\geq$ 75
Pb	10	0.02	7.5	0.2 to 4.5	$\geq$ 95

* Bowen, 1966.
** Grand average of more than 40 bulk water samples.
*** Assumes a maximum of 25 X enrichment of element of interest over that in bulk water.

TABLE 21. Percentages of Soil, Lake and Non-Naturally Derived Mid-Lake Michigan Atmospheric Surface Layer Metal Concentrations.

REFERENCES

Andren, A.W., A.W. Elzerman, and D.E. Armstrong, 1975, Proc. 1st Spec. Symp. on Atmos. Contribution to the Chemistry of Lake Waters. IAGLR, 101-110.

Batchelor, G.K., 1967, An Introduction to Fluid Dynamics. Cambridge Univ. Press, Cambridge, Mass., 615 pp.

Binkowski, F.S., 1979, Atmos. Env., 13, 247-253.

Blackader, A.K., 1975, Experiments With Simplified Second-Moment Approximations for Use in Regional Scale Models: Second Annual Rep., SRG; CAES, Penn. St. Univ.

Blifford, I.H. and G.O. Meeker, 1967, Atmos. Env., 1, 147-157.

Bloch, M.R., D. Kaplan, V. Kertes and J. Schnerb, 1966, Nature, 209, 802-803.

Bowen, H.J.M., 1966, Trace Elements in Biochemistry. Academic Press, N.Y.

Brtko, W.J. and R.L. Kabel, 1976, Water, Air, Soil Poll., 6, 71-79.

Businger, J.A., J.C. Wyngaard, Y. Izumi and E.F. Bradley, 1971, J. Atmos. Sci., 28, 181-189.

Cadle, R.D., 1975, The Measurement of Airborne Particles. Wiley, N.Y., p. 81 ff.

Chamberlain, A.C., 1968, Quart. J. of the Royal Meteor Soc., 94, 318-324.

Davé, M., D. Dolske and H. Sievering, 1979, Atmospheric Aerosol Mass Concentration and Scattering Coefficient in a Midlake Region: Accepted for publication in Atmos. Env.

Davidson, C.I. and S.K. Friedlander, 1978, J. Geophys. Res., 83, 2343-2352.

Deacon and Webb, 1962, in M.N. Hill (ed.) The Sea, Interscience, N.Y., pp. 43-87.

Deardorff, J., 1968, J. Geophysical Res., 93, 2549-2554.

Delumyea, R.G. and R.L. Petel, 1977, Atmospheric Inputs of Phosphorus to Southern Lake Huron, April-October 1975. EPA-600/3-77/038.

Donelan, M.A., 1977, Manuscript Rept. Series #43 Symp. On Modeling of Transport Mechanisms in Oceans and Lakes. Available from the Marine Sciences Directorate, Dept. of the Environment, Ottawa, Canada.

Donelan, M.A., K.N. Birch and D.C. Beesley, 1974, Proc. 17th Conf. Great Lakes Res. Int. Great Lakes Assoc., 369-388.

Dyer, A. and B.B. Hicks, 1970, Quart. J. of the Royal Meteor. Soc., 715-721.

Eisenreich, S.T., P.J. Emmling and A.M. Beeton, 1977, J. Great Lakes Res., 3, 291-304.

Eisenreich, S.T., A.W. Elzerman and D.E. Armstrong, 1978, Env. Sci. and Tech., 12, 413-417.

Elzerman, A.W., 1976, Surface Microlayer - Microcontainment Interactions in Freshwater Lakes. Ph.D. Thesis, U. of Wisconsin.

Elzerman, A.W., and D.E. Armstrong, 1979, Limnol. and Oceanog., 8, 133-139.

Friedlander, S.K., 1977, Smoke, Dust and Haze: Fundamentals of Aerosol Behavior, Wiley-Interscience, New York, N.Y., 317 pp.

Gaarenstroom, P.D., S.P. Perone and J.L. Moyers, 1977, Env. Sci. and Tech., 11, 795-800.

Garland, J.A., D. Atkins, C. Readings and S. Caughey, 1974, Atmos. Env., 8, 75-79.

Garrett, W.D., 1965, Limnol. Oceanog., 10, 602-605.

Gartrell, G., Jr. and S.K. Freidlander, 1975, Atmos. Env., 9, 279-288.

Gatz, D.F., 1975a, Atmos. Env., 9, 1-18.

Gatz, D.F., 1975b, Water, Air and Soil Poll., 5, 239-251.

Gatz, D.F., 1978, J. Appl. Meteor, 17, 600-608.

Gillette, D.A. 1972a, J. Appl. Meteor., 19, 1977-1985.

Gillette, D.A. 1972b, Atmos. Env., 6, 451-462.

Gillette, D.A. and J.W. Winchester, 1972, Atmos. Env., 6, 443-450.

Hall, C.D., 1954, Bull. Amer. Meteor. Soc., 35, 105-107.

Harmon, H.H., 1967, Modern Factor Analyses, 2nd Ed., U. of Chicago Press, 389 pp.

Hess, G.D. and B.B. Hicks, 1975, Interagency Comm. on Marine Science and Engineering Report: 2nd Conf. on the Great Lakes, 238-247.

Hicks, B.B., 1972, Boundary Layer Meteor., 3, 201-213.

Holzworth, G.C., 1972, Mixing Height Wind Speeds and Potential for Air Pollution in the Contiguous United States. Office of Air Programs Publ. No. AP-101. United States Environmental Protection Agency, Washington, D.C.

Hopke, P.K., 1976, J. Environ. Sci. Health, 6, 367-383.

Hunt, J.C.R., 1973, J. Fluid Mechanics, 61, 625-635.

Hunt, J.C.R. and P.J. Mulhearn, 1973, J. Fluid Mechanics, 61, 245-254.

International Joint Commission, 1976, Water Quality Board Report, App. B., Surveillance Subcom. Rep.

International Joint Commission, 1973, Environmental Management Strategy for the Great Lakes System., Final PLUARG Report IJC, Windsor, Ont.

Irwin, J.S., 1979, Atmos. Env., 13, 191-194.

Izumi, Y. and J.S. Caughey, 1976, Minnesota 1973 Atmospheric Boundary Layer Experiment Data Report. Air Force Cambridge Laboratory, AFCRL-TR-76-0038.

Jirka, A., M.J. Carter, D. May, and F. Fuller. Ultra-Micro Semi-Automatic Method for the Simultaneous Detection of Total Kjeldahl Nitrate in Waste Water. USEPA Central Regional Laboratory, Chicago, Ill.

Kondo, J., 1975, Boundary Layer Meteor., 9, 91-112.

Kondo, J., Y. Fujinawa and G. Naito, 1973, J. Phys. Oceanog., 3, 197-209.

Kraft, R.L., 1977, Predictions of Mass Transfer to Air-Land and Air-Water Interfaces. Penn. St. Univ., CAES Publ. #472-77.

Kramer, J.R., June 1976, "Atmospheric Chemical Loading of the Great Lakes" Annual Meeting of Great Lakes Chapter, AICHE, Northwestern Univ.

Lyons, W.A., 1972, J. Appl. Meteor., 11, 1259-1270.

Lyons, W.A. and L.E. Olsson, 1973, Monthly Weather Review, 101, 387-403.

Lyons, W.A., C.S. Keen and R.A. Northouse, 1974, Symposium on Atmospheric Diffusion and Air Pollution, Sept. 9-13, 1974. American Meteorological Society, Boston, Mass., 273-280.

Meszaros, A., 1977, Atmos. Env., 11, 1075-1081.

Montieth, J.L., 1973, Principles of Environ. Physics. Amer. Elsevier Publ. Co., New York, N.Y., 241 pp.

Moyers, J.L., R.A. Duce and G.L. Hoffman, 1972, Atmos. Env., 6, 551-556.

Murphy, T.J. and P.V. Doskey, 1976, J. Great Lakes Res., 2, 60-70.

Nageb, 1978, personal communication.

National Oceanic and Atmospheric Administration (NOAA), 1975, Summary of Synoptic Meteorological Observations for Great Lakes Areas, Vol. 3, Lake Michigan. Nat'l Climatic Center, Asheville, N.C.

Owen, P.R. and W.R. Thomson, 1963, J. Fluid Mechanics, 15, 321-334.

Owen, R.M., P.A. Meyers, and J.E. Mackin, 1979, Geophy. Res. Letters, 6, 147-150.

Panofsky, H., 1963, Quart. J. Roy. Meteor. Soc., 89, 85.

Pena, J.A., J.M. Norman and D.W. Thomson, J. of the Air Poll. Control Assoc., 27, 337-341.

Priestly, C., 1959, Turbulent Transfer in the Lower Atmosphere, U. of Chicago Press, 130 pp.

Rahn, K., 1976, The Chemical Composition of the Atmospheric Aerosol. Grad. School of Oceanography, Univ. of Rhode Island, Kingston, R.I., 265, pp.

Robbins, J.A., 1972, Proc. 15th Conf. Great Lakes Res. Inter. Assoc. Great Lakes Res., 270-290.

Robbins, J.A. and D.N. Edgington, 1975, Proc. 2nd ICMSE Conf. on Great Lakes. Interagency Committee on Marine Science and Engineering, Argonne, Ill., 378-390.

Raynor, G., P. Michael, R. Brown, and S. SethuRamon (1974) Symp. on Atmos. Diff. and Air Poll., Santa Barbara, Cal., Sept. 9-13, pp. 289-294.

Rummel, R.J., 1970, Applied Factor Analyses, Northwestern Univ. Press, 404 pp.

Schlichting, H., 1968, Boundary-Layer Theory, 6th ed., McGraw-Hill, New York, 747 pp.

Schmict, J., 1977, Selected Metals in Air Particulates Over Lake Michigan. M.S. Thesis, U. Wisc. Madison.

Sehmel, G.A., 1971, J. of Colloid and Interface Science, 37, 891-898.

Sehmel, G.A. and S.L. Sutter, 1974, Pacific NW Lab. Annual Rep. for 1971, Vol. II, Part 1. Atmos. Sciences, Battelle NW Labs, Richland, Wa. 99352.

Sehmel, G.A. and S.L. Sutter, 1975, J. Rech. Atm., III, 911-918.

SethuRaman, S., 1976, Monthly Weather Rev., 104, 1040-1045.

SethuRaman, S. and J. Tichler, 1977, J. Appl. Meteor., 16, 455-461.

Sheperd, J.G., 1974, Atmos. Env., 8, 69-73.

Sheppard, P.A., 1963, Abst. in Proc. 135th Assembly, IUGG-IAMAP, Berkeley, Ca., pp. 117-121.

Sievering, H., 1976, Water, Air and Soil Poll., 5, 343-351.

Sievering, H., 1979, Proc. 4th Symp. Turbulence, Diffusion and Air Pollution. Reno, Nev., 518-521.

Sievering, H. and C. Williams, 1975, Potential Loading of Southern Lake Michigan in Proc. of Workshop on Atmospheric Transport and Removal Processes. 2nd ICMSE Conf. on Great Lakes, Argonne, Ill., pp. 265-275.

Sievering, H., M. Davé, P.G. McCoy, K. Walther, 1978, Env. Sci. and Tech., 12, 1435-1437.

Sievering, H., M. Davé, D. Dolske, P. McCoy, 1979a, Trace Element Concentrations Over Mid-Lake Michigan as a Function of Meteorology and Source Region: Accepted for publication in Atmos. Env.

Sievering, H., M. Dave, D.A. Dolske, H.A. Roberts, 1979b, Deposition and Transformation of $SO_4^=$ During Stable Atmosphere Transport Over Lake Michigan: Accepted for publication in Atmos. Env.

Skibin, D., 1973, Water, Air and Soil Poll., 2, 405-407.

Slinn, W.G.N., 1975, Atmos. Env., 9, 763-765.

Slinn, W.G.N., L. Hasse, B.B. Hicks, A.W. Hogan, D. Lal, P.S. Liss, K.O. Munnich, G.A. Sehmel and O. Vittori, 1978, Atmos. Env., 12, 2055-2087.

Stolzenburg, T.R. and A.W. Andren, 1979, Spatial and Temporal Concentration Variations of Certain Aerosol Constituents in a Mixed Urban-Rural Watershed. 22nd Conf. on Great Lakes Res., May, 1979, Rochester, N.Y.

Stulov, L.D., F.I. Murashkevich and N. Fuchs, 1978, J. Aerosol Sci., 9, 1-7.

Sutton, N., 1977, Lake Michigan Lab Manual - unpublished data.

Taneda, S., 1956, J. Phys. Soc. Japan, 11, 302-309.

Technicon Instruments Corp., Automated Methyl-Thymol Blue Auto-Analysis Procedure Method #CRL453. Technicon Instruments Corporation, Chicago, Ill.

Torrey, M., 1976, Chemistry of Lake Michigan; Vol. 3 of Environmental Status of the Lake Michigan Region. ANL/ES-40, Argonne Natl. Labs, Argonne, Ill.

Twomey, S., 1977, Atmospheric Aerosols. Elsevier Publ. Co., Amsterdam, 302 pp.

USEPA, 1974, Methods for Chemical Analysis of Water and Waste. USEPA Office of Technology Transfer, Washington, D.C., 78-144 (metals), 207-214 (NO_2/NO_3).

Vugts and Businger, 1977, Boundary Layer Meteor., 11, 295-305.

Wieringa, J., 1974, Comparison of Three Methods for Determining Strong Wind Stress Over Lake Fleva, Boundary Layer Meteor., 7, 3-19.

Winchester, J.W. and G.D. Nifong, 1971, Water, Air and Soil Poll., 50-64.

Windom, H.L. and R.A. Duce, 1976, Marine Pollutant Transfer, Lexington Books, Lexington, Mass., 391 pp.

Whelpdale, D.M. and R.W. Shaw, 1975, Tellus, 26, 196-199.

Wu, J., 1969, J. Geophys. Res., 74, 444-455.

Wu, J., 1972, Phys. Fluids, 15, 741-747.

APPENDIX A

FACTOR ANALYSIS - A TECHNIQUE FOR INTERPRETING ENVIRONMENTAL DATA

INTRODUCTION

Factor analysis, initially developed to explain intelligence test scores, is widely used in the social sciences. There have been a few and limited applications in the environmental field. Gaarenstroom (1977) has applied both pattern recognition and factor analysis techniques to characterize atmospheric particulate composition. Gatz (1978) has used factor analysis in the identification of aerosol sources using the large METROMEX project data base. Hopke (1976) has used the technique to interpret chemical and physical analyses of lake sediments. Finally, Blifford (1967) has used the National Air Sampling Network data to produce a pollution model with the use of factor analysis.

All efforts thus far in applying factor analysis have been "results" rather than "user" oriented. The primary aim of this paper is to introduce factor analysis in a way that will help the researcher understand the scope and dimension of this technique. The explanation is conveyed through an application to an ongoing research project. Several conclusions are drawn using the factor analysis results. The technique is applied to the data base to exemplify the procedures one must follow in order to perform a factor analysis on any data base. The same data base has been considered in a "results" oriented approach to interpret trace metal and meteorological data (Sievering et al., 1979a).

The basic mathematical concepts are presented in conjunction with examples to clarify understanding. The data base used here is part of a study to determine atmospheric dry deposition to Lake Michigan. The data consist of several trace metal, nutrient, micro- and meso-meteorological, and total suspended particulate mass parameters. The trace symbols used in the tables are self-explanatory. The symbols P, NO_3, and SO_4 stand for total phosphorus, nitrate, and sulfate respectively. MASS represents the total suspended particulate mass. The symbols WS, WD1, WD2, WD3 and DELT represent various meteorological parameters. WS stands for the wind speed monitored at a 5 m height above the water surface. The WD1, WD2, and WD3 symbols stand for three wind direction sectors. Figure A-1 shows the wind direction sectors along with the ship location with respect to Lake Michigan. DELT is a measure of the temperature stability. It is the air temperature at the 5 m height above the water surface less the water surface temperature.

THE METHOD OF FACTOR ANALYSIS

Factor analysis is a technique which provides a way of recognizing and aiding in the interpretation of the underlying patterns of interrelationships in any multiple-parameter data base. It differentiates the separate patterns of relationships in the data matrix by factoring the matrix into its basic dimensions. Aside from ascertaining the relationships, it condenses large sets of data into uncorrelated sets of factors. These factors represent the total variability in the data and may be interpreted in place of the data matrix. These factors can then be labeled or classified with a physical significance attached to the group of variables that constitute that factor. Each factor or characteristic is assigned a weighting that shows to what degree a factor represents the variation in the data base. This weighting may be used to quantitatively compare one factor with another.

The basic outline of a factor analysis is shown in Figure A-2. The following sections are numbered with Roman numerals corresponding to appropriate blocks of the flow chart.

Block I - The Data Matrix

One starts with a data matrix, Dm, n, with m being the number of data points or sets and n the number of variables or parameters.

Block II - Standardize Data Matrix

The first step in any statistical analysis of non-compatible variables is to standardize the data matrix. By standardizing the data matrix one eliminates scale differences between measured variables. Equation (1) is used to standardize the data.

$$Z_i = \frac{X_i - \overline{X}}{\sigma} \qquad (1)$$

where, X_i = ith data value

$\overline{X}$ = average of all data values

σ = standard deviation

Z_i = standardized value of X_i

The standardized data values are then used to calculate a matrix of correlation coefficients.

Block III - Correlation Coefficient Matrix

The coefficient of correlation expresses the degree of relationship between any two variables. The correlation coefficient matrix of the 40 data sets, each with 17 variables from the Lake Michigan data base, is shown in Table A-1. The principal diagonal contains the squared multiple correlation coefficient. This number times 100 measures the percentage of linear variation that can be produced (predicted, generated, explained) for one variable from the others. The squared multiple correlation (SMC) for MN is 0.49. This indicates that 49 percent of the linear variation in MN is dependent on the other 16 variables. WD1, WD2, and WD3 are fairly linearly independent of the other variables (Rummel, 1970).

Block IV - Does One Do A Factor Analysis?

One must now make a decision whether or not to proceed with a factor analysis. There are three major considerations which influence that decision. First, one must have approximately twice as many data points as there are variables. There are, however, certain exceptions, discussed in the section on the Factor Score Matrix, for which one may use as few data points as there are variables. Second, the squared multiple correlation of about half the variables should be approximately 0.40 or greater. This is a good indication of linearity in the data. Finally, since the factor analysis routine only detects interrelationships in the correlation matrix, if one can decipher all the possible relationships directly from the correlation matrix, the need to do a factor analysis does not arise. Based on these three points, one should be able to decide whether or not to perform a factor analysis.

Block V - Common Factor Matrix

If one decides to go ahead with the factor analysis, the next step is to calculate the common factor matrix. The correlation matrix is used to extract initial factors. The common factor model and the principal axes technique is used to calculate the factors. Later, the results of this factor matrix are used to rotate the factors. To avoid confusion, this initial factor matrix will be referred to as the "unrotated factor matrix." Equation (2) shows the common factor model. The basic assumption is that each variable can be described as a linear combination of factors.

$$
\begin{aligned}
V_1 &= \alpha_{11} F_1 + \alpha_{12} F_2 + \cdots + \alpha_{1p} F_p + \alpha_{1u} F_{1u} \qquad (2)\\
V_2 &= \alpha_{21} F_1 + \alpha_{22} F_2 + \cdots \quad \alpha_{2p} F_p + \alpha_{2u} F_{2u}\\
&\vdots\\
V_n &= \alpha_{n1} F_1 + \alpha_{n2} F_2 + \cdots \quad \alpha_{np} F_p + \alpha_{nu} F_{nu}
\end{aligned}
$$

where, F_p = pth common factor

α_{np} = a loading measuring the contribution of F_p to the common variance of V_n

p = number of common factors ($p \leq n$)

n = number of variables

V_n = variable n

F_{nu} = a unique factor contributing to the unique variation of V_n

α_{nu} = a scalar weight for F_{nu}

The aim here is to solve for the α_{np}'s. The factors (F_p's) can then be determined. To do this, the unique factors (F_{nu}'s) must first be omitted. The first stage of the principal axes method involves the selection of the first factor coefficients (α_{n1}'s) in order to make the sum of the contributions to that factor a maximum. This sum is given by:

$$S_1 = \alpha_{11}^2 + \alpha_{21}^2 + \alpha_{31}^2 + \cdots \alpha \qquad (3)$$

Using the method of Lagrange multipliers, one may determine the values of the α_{n1}'s. This may be continued until all the α_{np}'s are obtained. The first common factor accounts for the most general pattern of relationship in the data; the second factor delineates the next most general pattern that is uncorrelated with the first; the third represents the third most general pattern uncorrelated with the first two; and so on (Harman, 1967).

The Lake Michigan data base is used to obtain the common factor loading matrix shown in Table A-2. The number of factors can be as many as the number of variables, but not all factor loadings are calculated.

Block VI - Number of Significant Factors

The number of significant factors are considered to be the factors having an eigenvalue of greater than or equal to 0.6. They are the number of uncorrelated patterns of relationships between the variables. In Table A-2, the first six factors are considered to be significant.

Block VII - Interpretation of Communality

The factor loadings, α's, measure which variables are involved in what factor and to what degree. They are the "correlation coefficients" between the variables and each factor. The communality of each variable, or the measure of the common

variance of a variable, is the sum of the squared loadings for that variable. By subtracting the communality from one, the uniqueness of a variable is determined. For CA, the communality indicates that 92% of its variation has been accounted for. The remaining 8% is either unique and/or is explained by the remaining nine factors which have not been extracted. The eight factors in Table A-2 account for 96% of the variation in the data base.

Block VIII - Rotate Common Factors

Since most of the variability in the data base is accounted for by the first factor and the amount of variability accounted decreases in descending order from the first factor to the last, it is difficult to interpret the factors. Using factor one, F1, and factor two, F2, of Table A-2 as the x and y axes respectively, the common factor loadings may be plotted for all the variables.

This graphical representation is shown in Figure A-3. As one can see, several clusters are formed, and if the axes can be orthogonally rotated, the variance on a factor can be maximized. This is done simultaneously for all six factors that are to be rotated. The varimax criterion is used to orthogonally transform (rotate) the common matrix. The varimax criterion is a function of the variation of the column of factor loadings. As there are more high and low loadings on a factor, the variance of the squared factor loadings is larger. Therefore, an orthogonal rotation can be computed by maximizing the variance of the squared factor loading. By rotating the common factor space, the adequacy of the solution is not affected. Once the rotated factor matrix is calculated, one may proceed to interpret factors and the variables constituting each factor.

The rotated factor matrix, as presented in Table A-3, is the most important since it is used for interpreting the factor loadings and identifying the factors. The factor loadings convey the same meaning as in the unrotated factor matrix. At the bottom of the table the percent variation explained by each factor is shown.

Block IX - Interpret Factor Loadings

As a rule of thumb, absolute loadings of less than 0.5 are not considered to be a member of a particular factor, though they may be considered as subordinate or secondary members. For example, in Table A-3, factor two is made up of WS as a primary member and TI as a secondary inverse member. The various primary and secondary members constituting each of the six factors are shown in Table A-4.

The "labels" attached to the six factors in Table A-4 are based on the combination of primary and secondary members making up that factor. This is where the researcher needs to draw on his experience to properly label the factors.

In factor one, the trace metals CA, MG, AL, FE, MN, PB, TI, and AN are primary members; WD1, DELT, and the nutrients P, NO_3, and SO_4 are secondary members. The trace metals and nutrients represent anthropogenic, soil, and lake-derived sources. The presence of WD1 indicates that these sources are from the Chicago and Gary wind direction sector. DELT being a secondary member shows that

temperature stability enhances the transport of aerosol over the lake's surface and to the midlake region. Based on this interpretation, factor one is then appropriately labeled.

The two members of factor two form a very interesting combination. The most likely cause for the TI concentration to rise with low wind speeds or the TI concentration to decrease with high wind speed is ship contamination. With low wind speeds, the ship effluent may very likely be carried up to the bow sampling site by turbulent eddies. With high wind speed, and given the ship pointing into the wind, there would be little possibility for the ship effluent to contaminate the sampling site. Therefore, TI is seen as a ship contaminant. Other constituents have an inverse loading of no more than one-third displayed by TI on factor two, so TI is isolated in this regard.

Factor three is made up of the three wind direction sectors only and thus no dominant effect of source regions is present in the data base.

Factor four is the most interesting of all factors. The constituents that comprise this factor are associated with fine particles (particle diameter $\leq$ 1 μm) and yet total suspended particulate mass (TSP) is also a member of this factor. In urban and land-based environments, the opposite is usually the case, with coarse particulates (particle diameter $\geq$ 1 μm) contributing the majority of the mass. The physical explanation for this is that coarse particles are lost to the lake prior to reaching the midlake sampling location.

In factor five, WD1 and WD2 wind direction sectors are co-members with CA, MG, and AL. Calcium and magnesium are quite abundant in the lake and can be considered as lake sources as well as soil-derived, which explains the WD2, lake, and wind direction sector presence. Aluminum is abundant in soil and can therefore be considered as a soil-derived source contributed to by the WD1 wind direction sector.

Factor six is made up of the reactive constituents NO_3 and SO_4 associated with temperature stability. Total suspended particulate mass is a secondary member. This suggests that temperature stability is needed to bring coarse particulate MG and AL to the midlake region and thus contribute to TSP.

Block X - Determine "Odd" Variables

Looking at the results of the rotated factor matrix, three variables -- WD1, WD2, and WD3 do not seem to lend added information. In fact, they form to make up a factor, namely factor 3, on their own. It would appear warranted to perform the factor analysis by omitting these "odd" variables.

Block XI - Factor Score Matrix

There may be concern that a single or a few data points may skew the factor analysis results, or one may want to evaluate the relation between the data points and factors. The factor score matrix provides a scale on which one may compare data points with each other. Equation (4) is the basis for calculating the factor score matrix.

$$G = (B'B)^{-1}B'Z \qquad (4)$$

Where, G = factor score matrix

B = rotated factor loading matrix

Z = standardized data matrix

B' = transpose of matrix B

$(B'B)^{-1}$ = inverse of product of B and B'

The factor score matrix presented in Table A-5 gives a score for every case or data point for every factor. The score shows how each data point has affected the factor. The mean, standard deviation, minimum, and maximum values for each factor are shown at the bottom of the table.

Block XII - Plot Factor Scores

The factor scores have been normalized and plotted in Figure A-4 showing the mean and standard deviation. The plots are a much clearer representation of the factor scores. The figure actually represents six separate plots; one for each factor with the factor scores being the abscissa and the data points the ordinate.

Block XIII - Determine "Odd" Data Points

A data point would be considered "odd" if its factor scores consistently lie outside the standard deviation for each factor. In Figure A-4, the data points starting with the number 20050 to 20150 inclusive were all collected in the month of May. With the exception of number 50560, the May data set is consistently skewed away from the remainder of the data points. Therefore, it would be wise to break the data base in two parts -- one consisting of the 10 data points collected in May, and the other consisting of the remainder of the data sets excluding data point 50560. Data point 50560 is clearly an "odd" data point.

Block XIV - Re-do Factor Analysis

Three "odd" variables -- WD1, WD2, and WD3 -- and one "odd" data point -- 50560 -- have been determined. The factor score plots suggest breaking the data into two parts. One must now decide whether or not to re-do the factor analysis based on these results. If one does decide to do so, the "odd" data points and variables must be deleted and the procedure must be started again at Block I.

Block XV - Delete "Odd" Data and Variables

The three wind direction sectors and the data point 50560 have been eliminated from the data base. The data base is then broken up into two parts -- one with the May data and the other with the remaining data. The following sections are results of these two parts.

RESULTS FOR THE MAY DATA

The May data consists of 10 data points and 14 variables. Statistically, it is not valid to perform a factor analysis since one needs at least as many data points as variables. The correlation coefficient matrix is shown in Table A-6. The squared multiple correlation for all the variables is well below the necessary 0.40 mentioned earlier. This indicates that the data is not well related on a linear basis and it is not justified to do a factor analysis. Based on these arguments, a factor analysis of the May data is not pursued.

RESULTS OF THE REMAINING DATA

This data set is made up of 29 data points and 14 variables. There are just enough data points and variables showing a squared multiple coefficient above 0.40 to justify a factor analysis. The correlation coefficient matrix is shown in Table A-7. WS is the only variable displaying a very low squared multiple correlation. The unrotated common factor matrix is shown in Table A-8. The eigenvalues suggest that only the first five factors are viable and, thus, to be considered for rotation. The seven factors explain 93% of the variation in the data. The communality of the variables varies between 84 and 99 percent. The results of transforming the first five factors are shown in Table A-9. primary and secondary members of each factor are outlined in Table A-10.

Looking at the first factor, CA, MG, AL, FE, MN, TI, ZN, and NO_3 represent pollutant, soil, and lake-derived sources. DELT being a secondary member, it enhances the transport of land-based aerosols to the midlake region.

Factor two is made up of two parts. The first is the inverse relationship between wind speed and TI, which again suggests that TI is a ship contaminant. The second is temperature stability related with nitrate. This relation suggests that higher temperature (and thus temperature stability over the colder summertime lake) contributes to the formation of nitrates.

The conclusion that fine particulates contribute to TSP is again reflected in factor three. There is, however, the added component of temperature stability necessary to transport those fine particulates to midlake. A second dominant aspect of factor three is the higher temperature creation of NO_3 and SO_4.

A combination of coarse and fine particulates contributing to TSP is present in factor four. The coarse aerosols associated with MG may be largely lake-derived.

The least weighted factor, factor five, shows a two-fold relation. Only FE, TI, and P very likely represent soil-derived sources. The temperature dependence of the chemical transformation to produce SO_4 is secondarily present.

CONCLUSIONS

Factor analysis is a powerful technique to aid in the interpretation of large data bases. The method is not limited to any particular field and is widely adaptable to a broad range of applications. Using the Lake Michigan data base, several

relationships evolved that would not have been detected without the use of factor analysis: the inverse relationship between titanium and wind speed leading to the conclusion that titanium must be a ship contaminant; and the important conclusion that fine particulates primarily contribute to TSP in the midlake region.

There is, however, concern in using factor analysis. The common factor model is a linear model and therefore assumes linearity in the data. This may be an incorrect assumption, and the researcher must consider this problem carefully. The relationship within the factors themselves, however, may be non-linear and still allow the use of factor analysis.

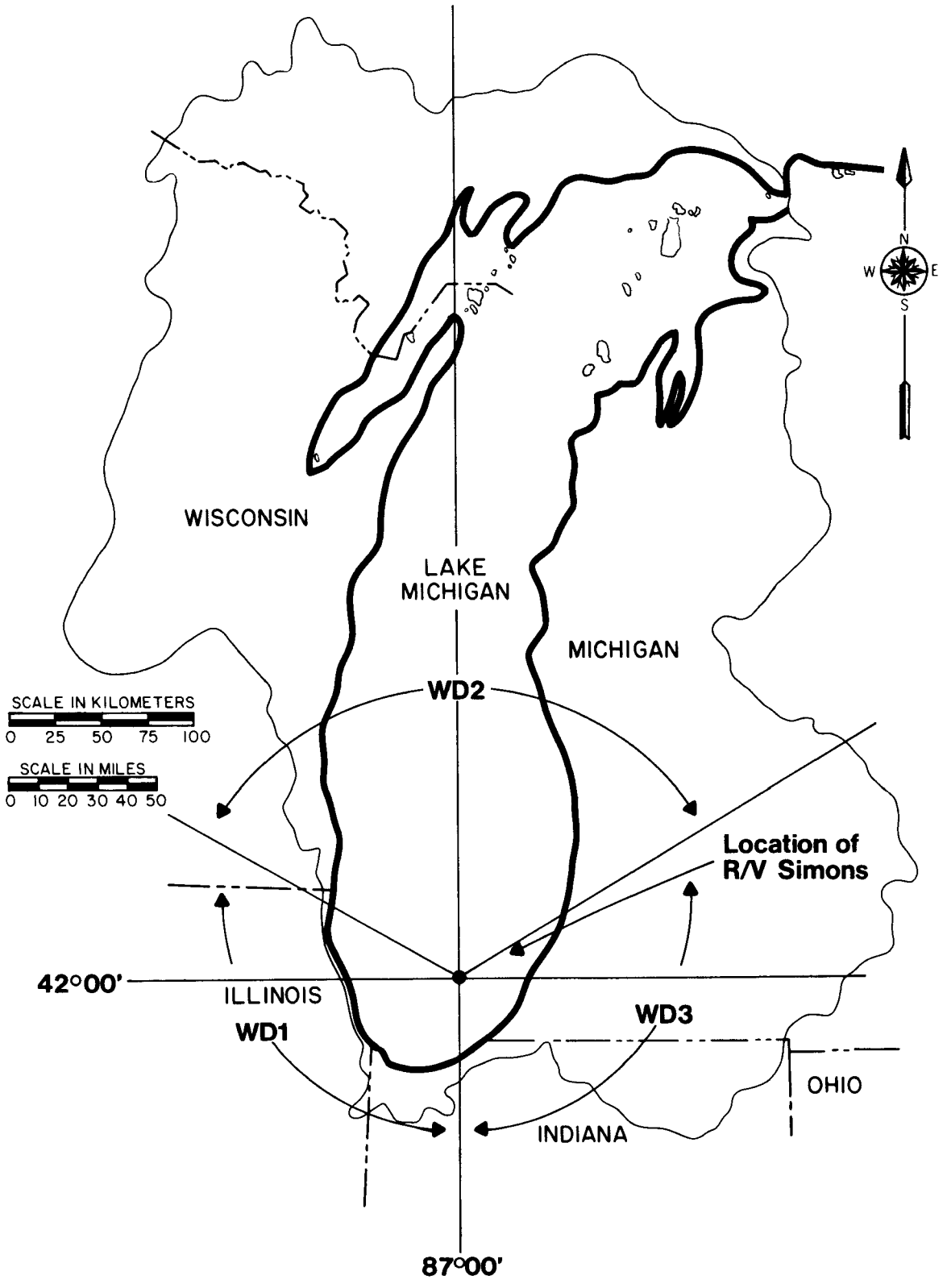

FIGURE A-1. Wind Direction Sectors Over Southern Lake Michigan.

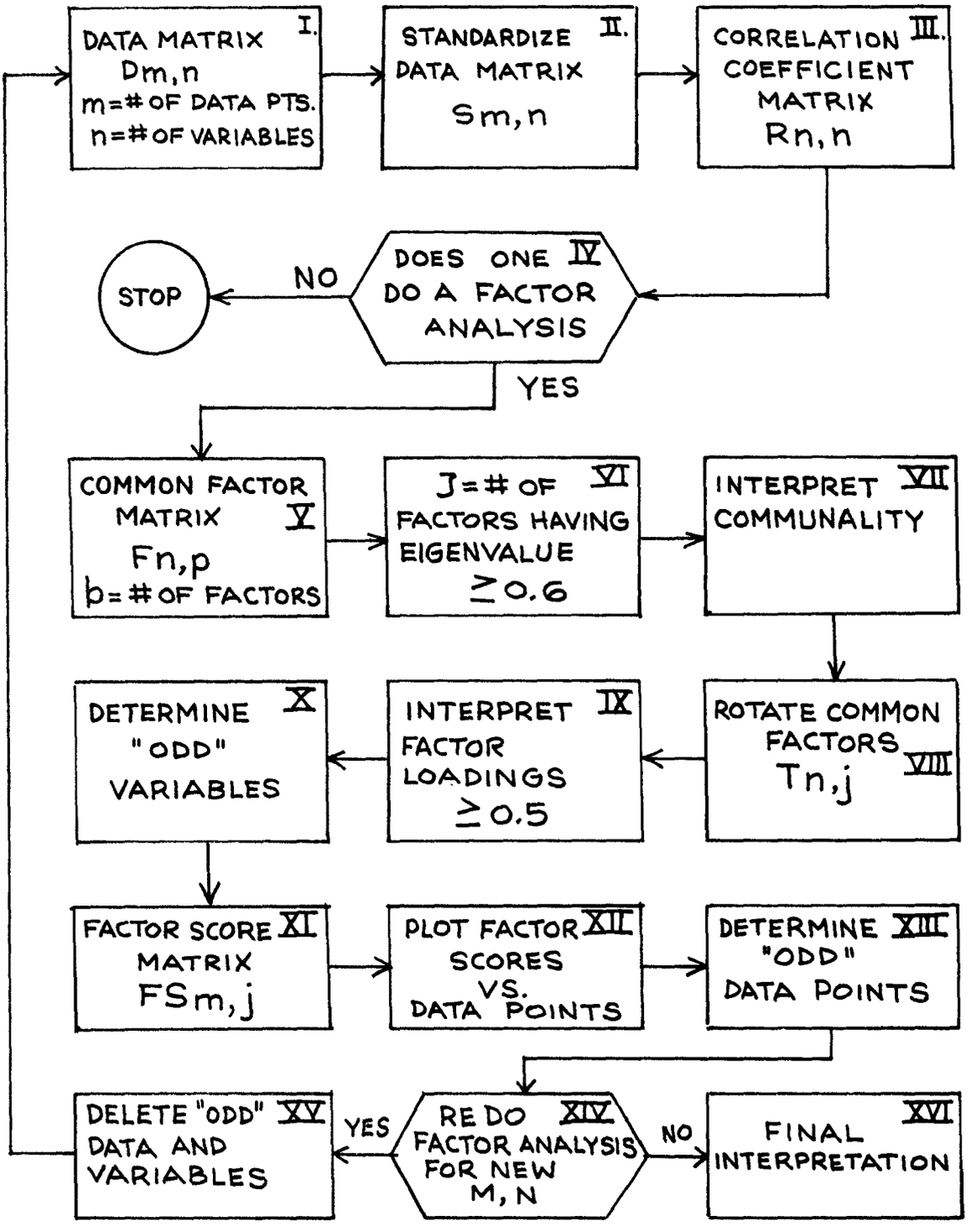

FIGURE A-2. Basic Outline of Factor Analysis.

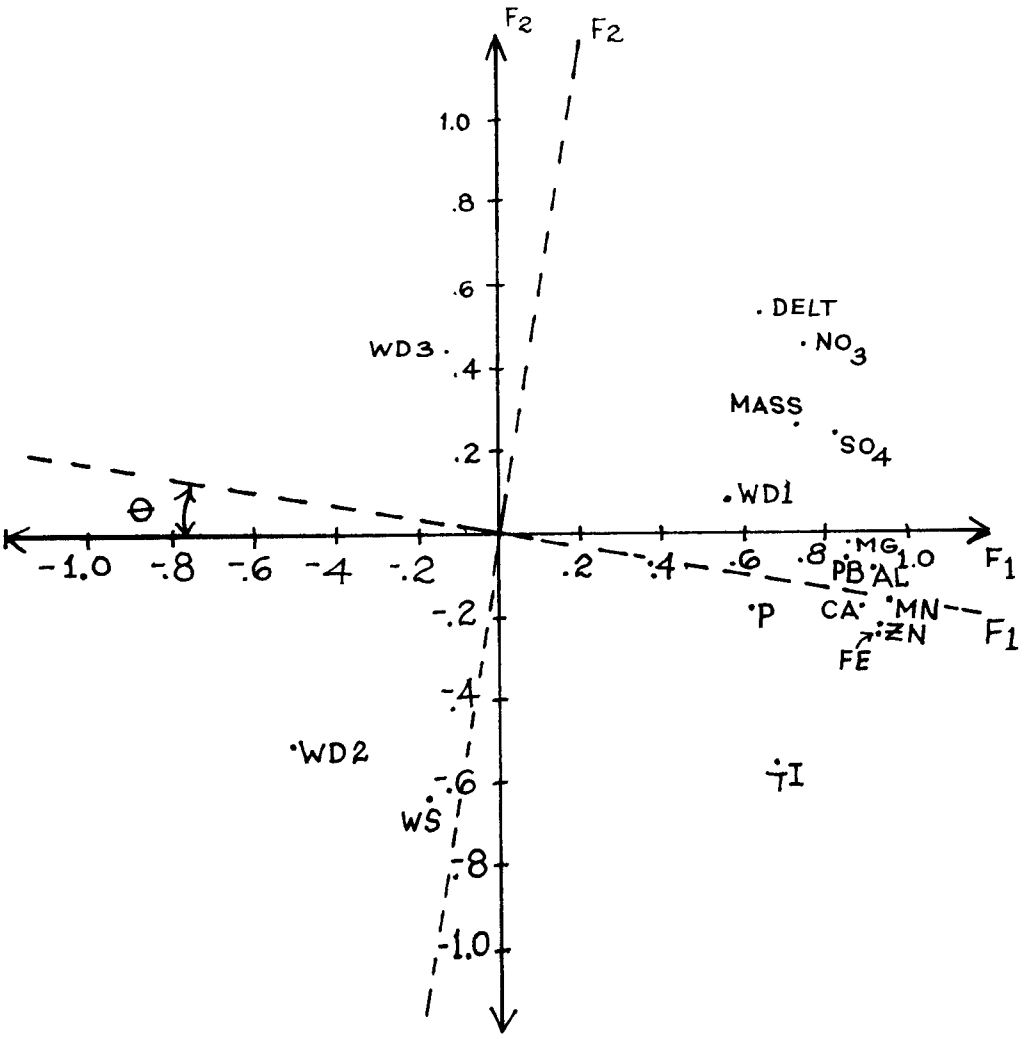

FIGURE A-3. Rotation of Co-ordinates.

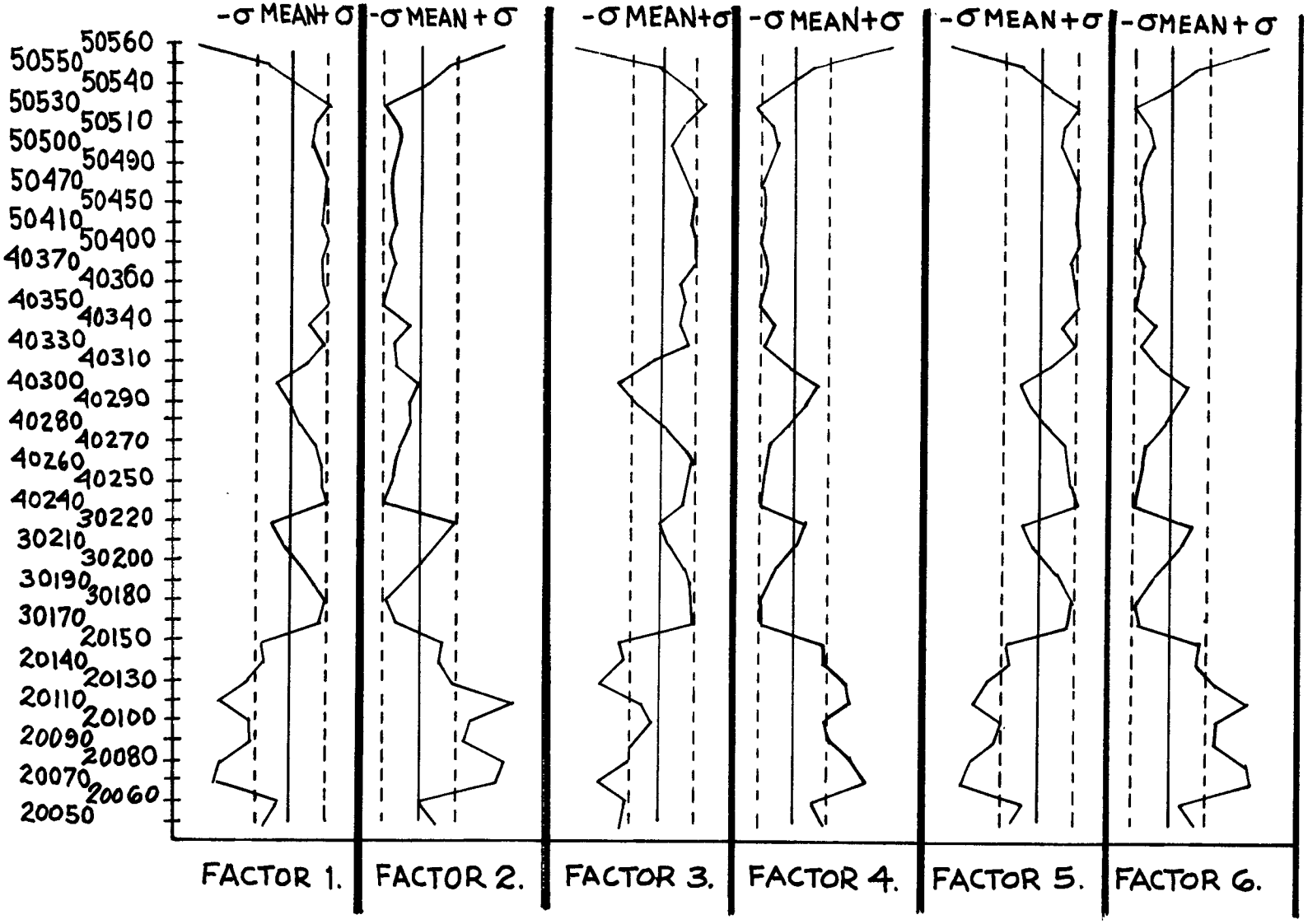

FIGURE A-4. Plot of Factor Scores.

CA	.33																
MG	.81	.37															
AL	.88	.85	.40														
FE	.90	.79	.91	.39													
MN	.89	.78	.86	.97	.49												
PB	.71	.69	.69	.72	.78	.49											
TI	.71	.58	.67	.78	.72	.51	.16										
ZN	.84	.73	.79	.90	.95	.88	.68	.46									
P	.37	.35	.40	.53	.59	.47	.51	.62	.36								
NO_3	.53	.59	.55	.52	.61	.64	.24	.57	.49	.63							
SO_4	.55	.56	.63	.65	.70	.68	.46	.70	.62	.79	.63						
MASS	.45	.50	.55	.54	.63	.52	.28	.59	.71	.79	.79	.69					
WS	-.13	-.09	-.14	-.10	-.14	-.12	.29	-.8	.11	-.34	-.18	-.12	.09				
WD1	.53	.46	.53	.48	.50	.37	.28	.43	.20	.33	.31	.39	-.31	.12			
WD2	-.41	-.45	-.41	-.34	-.39	-.31	-.19	-.31	-.18	-.43	-.41	-.38	.29	-.61	.20		
WD3	-.17	-.5	-.18	-.19	-.17	-.10	-.12	-.18	-.04	-.06	.8	-.05	-.07	-.51	-.37	.01	
DELT	.50	.60	.65	.49	.46	.50	.16	.40	.09	.70	.63	.52	-.35	.32	-.43	.09	.50
	CA	MG	AL	FE	MN	PB	TI	ZN	P	NO_3	SO_4	MASS	WS	WD1	WD2	WD3	DELT

TABLE A-1. Correlation Coefficient Matrix.

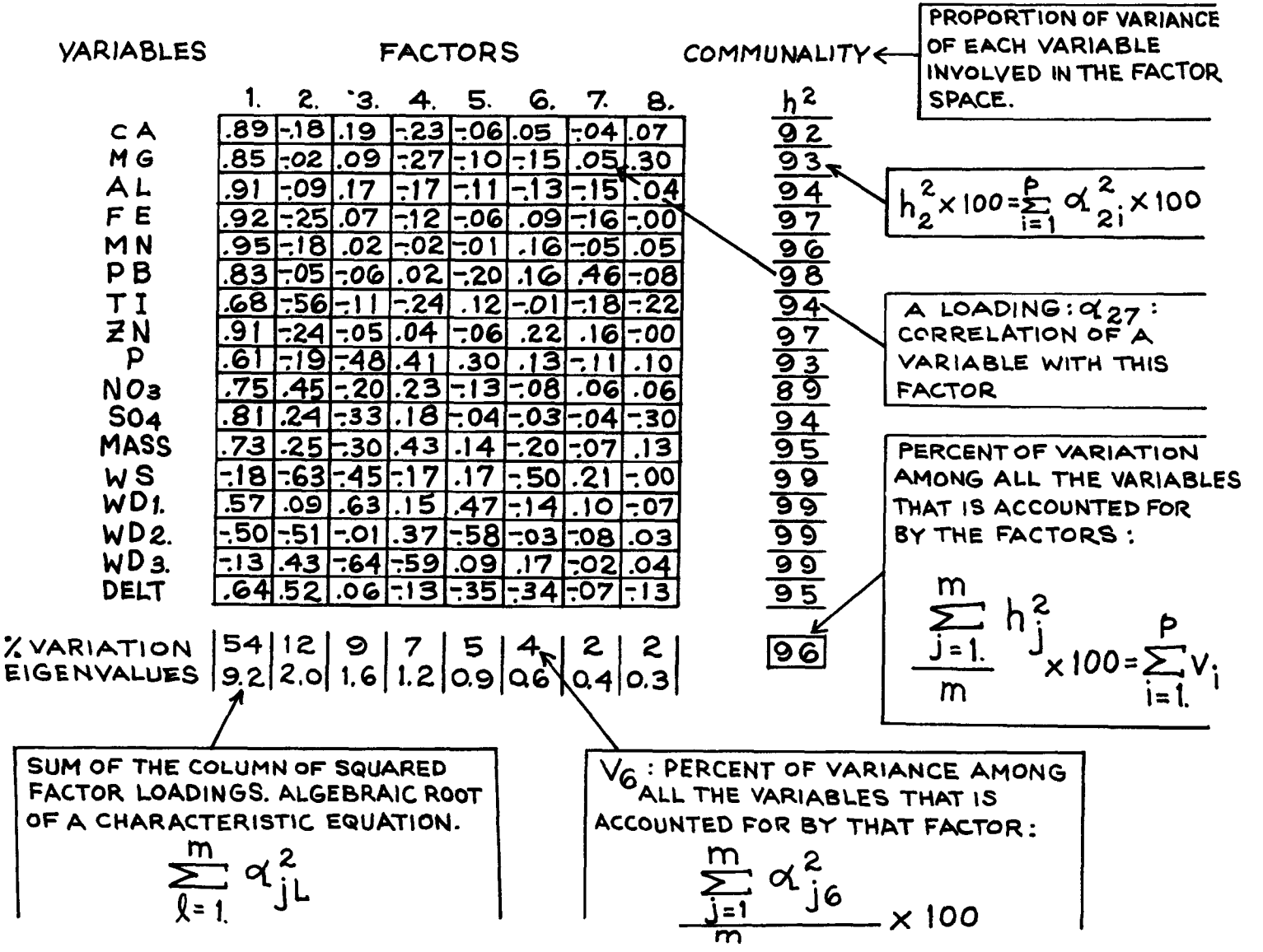

VARIABLES	1.	2.	3.	4.	5.	6.	7.	8.	h^2
CA	.89	-.18	.19	-.23	-.06	.05	-.04	.07	92
MG	.85	-.02	.09	-.27	-.10	-.15	.05	.30	93
AL	.91	-.09	.17	-.17	-.11	-.13	-.15	.04	94
FE	.92	-.25	.07	-.12	-.06	.09	-.16	-.00	97
MN	.95	-.18	.02	-.02	-.01	.16	-.05	.05	96
PB	.83	-.05	-.06	.02	-.20	.16	.46	-.08	98
TI	.68	-.56	-.11	-.24	.12	-.01	-.18	-.22	94
ZN	.91	-.24	-.05	.04	-.06	.22	.16	-.00	97
P	.61	-.19	-.48	.41	.30	.13	-.11	.10	93
NO3	.75	.45	-.20	.23	-.13	-.08	.06	.06	89
SO4	.81	.24	-.33	.18	-.04	-.03	-.04	-.30	94
MASS	.73	.25	-.30	.43	.14	-.20	-.07	.13	95
WS	-.18	-.63	-.45	-.17	.17	-.50	.21	-.00	99
WD1.	.57	.09	.63	.15	.47	-.14	.10	-.07	99
WD2.	-.50	-.51	-.01	.37	-.58	-.03	-.08	.03	99
WD3.	-.13	.43	-.64	-.59	.09	.17	-.02	.04	99
DELT	.64	.52	.06	-.13	-.35	-.34	-.07	-.13	95
% VARIATION	54	12	9	7	5	4	2	2	96
EIGENVALUES	9.2	2.0	1.6	1.2	0.9	0.6	0.4	0.3	

TABLE A-2. Common Factor Loading Matrix.

TABLE A-3. Rotated Factor Matrix.

VARIABLES	FACTORS					
	1	2	3	4	5	6
CA	.93	.06	.10	.12	.23	.23
MG	.83	-.04	.00	.16	.26	.47
AL	.85	-.00	.14	.18	.23	.41
FE	.94	.02	.11	.27	.13	.15
MN	.89	.10	.09	.39	.15	.11
PB	.84	.21	.01	.44	-.02	.25
TI	.89	-.41	.02	.17	.10	-.11
ZN	.89	.11	.08	.43	.04	.05
P	.38	-.15	.01	.88	.04	-.23
NO_3	.33	.27	-.07	.69	.13	.57
SO_4	.48	.11	-.12	.76	.10	.40
MASS	.25	.00	.09	.88	.20	.35
WS	.00	.97	.06	.02	.18	.16
WD1	.32	.16	.54	.13	.74	.10
WD2	.22	.16	-.33	.17	.87	.17
WD3	.13	.04	.98	-.02	-.09	-.07
DELT	.32	.20	-.07	.19	.16	.89
% VARIATION	41	8	9	20	10	12

FACTOR	1	2	3	4	5	6
"LABEL"	Transport of soil, lake, and anthropogenically derived aerosol enhanced by temperature stability and Chicago/Gary Source Region	TI ship contaminant, other metals' conc. not significantly contributed to by ship effluent	Stand Alone Wind Direction Factor	Fine Particulate with Nutrients	Soil and Lake Derived Coarse Particles contributing CA, MG, AL	Temp. Stab brings out reactive and coarse particulates
PRIMARY MEMBERS	CA, MG, AL FE, MN, PB TI, ZN	WS	WD1 WD3	P, NO_3, SO_4 Mass	WD1 WD2	NO_3 DELT
SECONDARY MEMBERS	P, NO_3, SO_4 WD1 DELT	-TI	-WD2	MN PB ZN	CA MG AL	MG AL SO_4 MASS
PERCENT VARIATION	41	8	9	20	10	12
HIERARCHY	1	6	5	2	4	3

TABLE A-4. Interpretation of Factors.

SAMPLE SET NUMBER	FACTORS					
	1	2	3	4	5	6
20050	-.781	.038	-.443	1.668	-.730	1.162
20060	-.670	-.021	-.427	1.405	-.634	.906
20070	-1.243	.260	-.535	2.839	-1.129	2.166
20080	-1.183	.284	-.422	2.470	-1.054	2.082
20090	-.932	.144	-.397	1.912	-.863	1.524
20100	-.922	.170	-.337	1.719	-.788	1.511
20110	-1.206	.317	-.376	2.408	-1.036	2.137
20130	-.952	.096	-.521	2.226	-.933	1.534
20140	-.804	.051	-.444	1.718	-.754	1.218
20150	-.825	.062	-.459	1.782	-.781	1.268
30170	-.308	-.102	-.184	.091	-.244	.177
30180	-.269	-.129	-.191	.036	-.228	.091
30190	-.366	-.073	-.197	.239	-.296	.305
30200	-.501	-.008	-.229	.595	-.416	.601
30210	-.646	.047	-.284	1.026	-.561	.915
30220	-.747	.106	-.309	1.243	-.636	1.138
40240	-.251	-.136	-.218	.009	-.204	.038
40250	-.292	-.113	-.199	.096	-.256	.142
40260	-.310	-.103	-.182	.131	-.282	.184
40270	-.358	-.082	-.230	.264	-.297	.275
40280	-.498	-.051	-.306	.778	-.467	.566
40290	-.583	-.055	-.401	1.196	-.589	.726
40300	-.697	-.016	-.464	1.534	-.677	.971
40310	-.442	-.101	-.363	.731	-.420	.434
40330	-.294	-.111	-.209	.085	-.236	.145
40340	-.411	-.049	-.233	.367	-.334	.402
40350	-.241	-.141	-.223	-.021	-.195	.026
40360	-.279	-.127	-.239	.094	-.232	.107
40370	-.300	-.109	-.186	.096	-.255	.162
50400	-.262	-.124	-.178	-.013	-.206	.071
50410	-.289	-.105	-.194	.037	-.223	.135
50450	-.279	-.114	-.188	.029	-.223	.115
50470	-.261	-.119	-.207	-.017	-.203	.076
50490	-.307	-.109	-.238	.150	-.253	.170
50500	-.383	-.090	-.269	.404	-.333	.330
50510	-.353	-.096	-.227	.292	-.312	.271
50530	-.221	-.140	-.156	-.118	-.202	-.002
50540	-.511	-.001	-.215	.620	-.454	.633
50550	-.745	.080	-.316	1.321	-.658	1.117
50560	-1.389	.269	-.649	3.429	-1.285	2.422
AVERAGE	-.558	-.012	-.301	.872	-.497	.706
SIGMA	.323	.130	.122	.939	.304	.690
MINIMUM	-1.389	-.141	-.649	-.118	-1.285	-.002
MAXIMUM	-.221	.317	-.156	3.429	-.195	2.422

TABLE A-5. Factor Score Matrix.

CA	.05													
MG	.85	.01												
AL	.77	.87	.17											
FE	.94	.80	.86	.17										
MN	.98	.80	.77	.97	.11									
PB	.64	.62	.44	.56	.68	.30								
TI	.90	.75	.80	.97	.94	.53	.16							
ZN	.94	.78	.66	.87	.96	.83	.83	.17						
P	.84	.75	.55	.69	.81	.87	.62	.93	.11					
NO_3	-.16	-.03	-.41	-.37	-.22	.27	-.32	-.07	.14	.00				
SO_4	.23	.10	.02	.24	.32	.57	.33	.43	.35	-.05	.00			
MASS	.04	.06	.09	-.09	-.04	.11	-.21	-.00	.18	.34	-.56	.29		
WS	.50	.20	.49	.57	.53	.22	.50	.45	.29	-.56	.06	.30	.31	
DELT	-.50	-.30	-.15	-.41	-.53	-.37	-.38	-.58	-.57	.15	-.48	.36	.05	.19
	CA	MG	AL	FE	MN	PB	TI	ZN	P	NO_3	SO_4	MASS	WS	DELT

TABLE A-6. Correlation Coefficient Matrix for the May Sample Sets.

	CA	MG	AL	FE	MN	PB	TI	ZN	P	NO_3	SO_4	MASS	WS	DELT
CA	.19													
MG	.51	.14												
AL	.90	.54	.35											
FE	.75	.56	.87	.44										
MN	.73	.57	.86	.89	.58									
PB	.38	.34	.56	.52	.64	.76								
TI	.52	.43	.65	.62	.48	.47	.27							
ZN	.60	.43	.81	.74	.81	.82	.54	.58						
P	.12	.26	.34	.39	.26	.30	.59	.37	.16					
NO_3	.49	.42	.64	.73	.83	.72	.38	.69	.24	.34				
SO_4	.24	.18	.39	.42	.49	.82	.51	.66	.42	.58	.34			
MASS	.18	.39	.22	.29	.40	.53	.34	.28	.28	.54	.45	.31		
WS	-.06	.18	-.02	-.08	-.21	.08	.44	-.02	.26	-.19	.04	.10	.05	
DELT	.30	.13	.44	.47	.51	.56	.16	.52	.22	.53	.45	.19	-.29	.30

TABLE A-7. Correlation Coefficient Matrix.

VARIABLE	FACTORS							COMMUNALITY
	1	2	3	4	5	6	7	
CA	.73	-.16	-.52	-.02	.15	.11	-.20	91
MG	.60	.20	-.37	.45	-.12	-.38	.26	96
AL	.89	-.10	-.37	-.14	.06	.05	-.07	97
FE	.89	-.11	-.28	-.06	-.14	.05	-.01	90
MN	.91	-.26	-.14	.10	-.04	.05	.07	94
PB	.81	.04	.45	.02	.30	-.09	.06	96
TI	.69	.56	-.16	-.19	.01	.18	-.15	90
ZN	.89	-.07	.07	-.19	.20	-.04	.22	92
P	.46	.53	.13	-.33	-.57	.02	.11	97
NO_3	.83	-.23	.20	.23	-.04	.08	.01	84
SO_4	.68	.15	.56	-.14	.16	.15	.14	89
MASS	.50	.24	.38	.64	-.16	.14	-.25	97
WS	.00	.87	-.11	-.01	.32	-.23	-.14	94
DELT	.57	-.39	.35	-.27	-.15	-.44	-.32	99
% VARIATION	51	13	11	7	5	4	3	93
EIGENVALUES	7.2	1.8	1.5	1.0	.7	.5	.4	

TABLE A-8. Unrotated Common Factor Matrix.

VARIABLE	FACTORS				
	1	2	3	4	5
CA	.99	-.02	.13	.02	-.04
MG	.73	-.20	-.08	.64	.12
AL	.94	.00	.31	.01	.17
FE	.89	.14	.29	.16	.29
MN	.82	.24	.41	.29	.08
PB	.31	-.07	.91	.28	.04
TI	.57	-.52	.33	.11	.53
ZN	.68	.01	.72	.03	.14
P	.13	-.12	.19	.13	.96
NO_3	.55	.30	.61	.48	.06
SO_4	.13	-.08	.94	.19	.25
MASS	.06	-.06	.36	.92	.13
WS	.06	.98	-.02	-.05	-.18
DELT	.30	.60	.69	-.05	.26
% TOTAL VARIATION	37	13	27	13	11

TABLE A-9. Rotated Factor Matrix

FACTORS	1	2	3	4	5
"LABEL"	Transport of soil, lake and anthropogenically derived aerosol enhanced by temp. stability	TI - ship contaminant	Fine particulate transport by temp. stability enhances mass conc. at mid-lake. Higher temp. enhances SO_4, NO_3 conc.	Coarse particulate as well as fine particulate mass.	Soil derived sources and DELT reaction of SO_4.
PRIMARY MEMBERS	CA, MG, AL, FE, MN, TI, ZN, NO_3	-TI, WS DELT	PB, ZN, NO_3, SO_4, DELT	MG, MASS	TI, P
SECONDARY MEMBERS	DELT	NO_3	MN, MASS	MN, PB, NO_3	FE, SO_4, DELT
% VARIATION	37	13	27	13	11
HIERARCHY	1	3	2	4	5

TABLE A-10. Meteorological and Aerosol Data for the Profile Data Sets.

APPENDIX B

MICROMETEOROLOGY RELATED TO DIABATIC DRAG COEFFICIENT DETERMINATION

Results of modeling efforts to date clearly point to the flux of aerosol across the air/water interface and its discrimination by aerosol size as the most crucial parameter needing experimental measure. Other researchers (Andren, 1976; Gatz, 1976; Hess and Hicks, 1975; Kramer, 1976) also have identified this flux or deposition rate as the major unknown quantity needed to resolve the question of atmospheric contribution to Great Lakes loading. The deposition velocity, v_d, is given by

$$v_d = \frac{\text{Flux of constituent of interest}}{\text{Concentration of that constituent}} \qquad (1a)$$

and, more specifically for atmospheric aerosol

$$v_d(r) = \frac{\text{Flux of aerosol as a function of radius}}{\text{Concentration of aerosol as a function of radius}} \qquad (1b)$$

$v_d(r)$ was used to approximate fluxes into Lake Michigan. Using wind tunnel data of Sehmel and Sutter (1974) for aerosol $v_d(r)$ and having $C(r)$ of aerosols at or near the water surface, the flux can be approximated by

$$\text{Aerosol Flux} = v_d(r) \cdot C(r) \qquad (2)$$

It is clear that a field measurement of $v_d(r)$ under varying meteorological conditions and for constituents of interest such as the trace metals and phosphorus is the most crucial piece of field data to resolving the controversy over lake loading by atmospheric aerosols.

Defining a tractable experiment is not a simple task. In general, the flux of a constituent S can be related to the mass fraction of the constituent S per unit mass of air (s), as well as the vertical velocity of s (W_s) and the density of air (ρ). The rate of vertical transport, i.e. the flux, is expressed by $\rho W_s s$. If this transport is measured a few meters above a horizontal rigid surface, upward and downward currents are found to be distributed in space and time in the chaotic and random fashion we know to be turbulence. The net vertical transport of air, however, must be zero if the total mass at the surface is constant (as we know it to be at the earth-atmosphere interface).

However, the average value of $\rho w_s s$ is not zero, for the downward currents may systematically carry larger amounts of s than the upward currents. The rate of average vertical transport of S, the flux $\overline{F}_S$, is then dimensionally given by

$$\overline{F}_S = \frac{\mu g \text{ of air}}{m^3 \text{ of air}} \left(\frac{m}{sec}\right) \frac{\mu g \text{ of S}}{\mu g \text{ of air}} = \frac{\mu g \text{ of S}}{m^2 \text{ sec}} \tag{3}$$

It can be shown that the flux of aerosol A is given by

$$\overline{F}_A = -\rho K_A \frac{\partial \overline{a}}{\partial z} \tag{4}$$

where a is the mass fraction of aerosol A, and K_a is the aerosol mass transfer coefficient. Priestly (1959) and others have pointed out that the sheer stress, τ, can be related both to the change in u with height through the momentun transfer coefficient K_m, as well as to wind speed at one height alone (u_1) through the momentum drag coefficient, C_D, i.e.

$$\tau = \rho K_m \frac{\partial u}{\partial z} = \rho C_D u_1^2 \tag{5}$$

Because we are concerned with aerosols of radius $\leq$ 10 μm in all cases, the terminal velocity is less than the vertical velocity fluctuations ($\overline{W'_a}$) for all aerosols $\leq$ 1 μm radius. This is also true for most aerosols $\leq$ 6 μm radius and for some in the size range $6 < r < 10$ μm, depending on their shape, surface and density. For this case

$$K_A \simeq K_m \tag{6}$$

so that

$$\overline{F}_A = -\rho K_m \frac{\partial \overline{a}}{\partial z} = -\rho \left(\frac{C_D u_1^2}{\frac{\partial u}{\partial z}}\right) \frac{\partial a}{\partial z} \tag{7a}$$

or, in finite difference form

$$\overline{F}_A = -\rho \frac{C_D u^2 \left(a_2 - a_1\right)}{u_2 - u_1} \tag{7b}$$

where u_2 is the wind speed at the height for which the second aerosol concentration a_2 has been determined.

Gilette et al. (1972) have used this equation to study wind erosion with some success. If C_D can be well specified and if high enough winds prevail, statistical significance in $u_2 - u_1$ and $a_2 - a_1$ over a soil surface can be demonstrated. It was for these narrow meteorological conditions on certain "days of opportunity" that Gillette obtained $\overline{F}_A$ for four different size ranges of aerosol, using cascade impactors.

The problem in using the above equation for $\overline{F}_A$ generally comes in achieving statistical significance in $a_2 - a_1$ and $u_2 - u_1$ over soil surfaces. Over a water surface $a_2 - a_1$ is relatively easier to measure because one has essentially no re-entrainment (until wave whitecapping) but the measurement of $u_2 - u_1$ becomes more difficult. Since a water surface presents less wind resistance, the difference between u_2 and u_1, no matter what the height separation (remembering to confine our attention to the surface layer of 30-50 m) will be even less than it is over land. The measurement of $u_2 - u_1$ over land has been accomplished on a number of occasions, usually with difficulty and requiring sophisticated equipment. For example, Businger et al. (1971) obtained $u_2 - u_1$ for a wide range of wind speeds and stability. That experiment required the use of eight cup anemometers at 2, 4, 5.7, 8, 11.3, 16, 22 and 32 meters in a stationary position for three months of once per second data. Given the still more difficult task of obtaining statistically significant $u_2 - u_1$ measurements over a water surface, the use of equation (7) for $\overline{F}_A$ determination appears infeasible. The good fortune of a "meteorological day of opportunity" with relatively high winds of sufficiently sustained steadiness to obtain characteristic mass loadings does not suffice for the expensive and thus relatively few sampling occasions afforded by EPA shipboard sampling.

If the sampled portion of the surface layer (here, the first 10 m) can be assumed to be a constant flux layer, one can integrate equation (7) from the surface to any one height of interest (i.e., a single sampling height) and thereby obviate the measurement of $u_2 - u_1$. Several indirect flux experiments, that of Dyer and Hicks (1970) chief among them, have convincingly shown the surface layer to be a constant flux layer.

Integration of equation (7) with constant $\overline{F}_A$ gives

$$\int_1^2 \overline{F}_A dz = \rho \int_1^2 K_m \frac{\partial a}{\partial z} d_z \qquad (8a)$$

or

$$\overline{F}_A = -\rho |B_m| (\overline{a}_2 - \overline{a}_1) \qquad (8b)$$

where B_m is the bulk turbulent transfer coefficient for momentum. Priestly (1959) has shown that B_m can be related to the momentum drag coefficient, C_D, by

$$B_m = C_D(\overline{u}_z - \overline{u}_0) \qquad (9)$$

where $\bar{u}_z$ is the average of the horizontal wind speed at any one height in the atmosphere and $\bar{u}_0$ is the average speed at the roughness length height (i.e., we specify the lower height for integration $z_1 \equiv z_0$). The roughness length height over a lake surface is less than 0.05 cm.

Considering the lake surface to be an efficient sink for aerosols, $a_1 = \bar{a}_0$ is approximately equal to 0. This should hold as long as whitecapping of waves (requiring $u \geq 12$ m/s) does not occur, for then one might expect significant aerosol release from the surface. Given the above considerations, equation (8b) results in

$$\bar{F}_A = -\rho \bar{a} C_D (\bar{u} - \bar{u}_0) \qquad (10)$$

Measurement of $\bar{u}$ and $\bar{a}$ is relatively simple. (Size fractionating $\bar{a}$ by using a cascade impactor will, of course, give $\bar{F}_A$ as a function of aerosol size.) A value of $\bar{u}_0$ can be obtained by measuring the time it takes a spherical object floating half in/half out of the water to pass from stem to stern of the sampling ship. A value for C_D is all that remains to be determined.

When the roughness elements of the surface are greater than the roughness length and for neutral conditions, Deacon and Webb (1962) approximate C_D to be

$$C_D = [1 + 0.07(\bar{u}_{10} - \bar{u}_0)] \times 10^{-3} \qquad (11)$$

Experimentally, the neutral case certainly seems to give a tractable solution. One needs only to measure $\bar{u}_{10}$ and $\bar{u}_0$. These measurements can be done fairly easily.

However, equation (11) assumes the water surface to be fully rough. We need to relax this assumption as well as the assumption of neutral stability, so that both mechanical and thermal stability variations can be considered. This is so because neutral thermal stability and mechanical instability of the surface occurs less than 5 percent of the time over Lake Michigan.

Incorporating smooth, transition, and rough surface conditions has already been done in the micrometeorological literature of the 1960's. The resultant curve is the heavy line of Figure 34 with the straight line portion being given by equation (11). The diabatic case (thermal instability) is much more difficult to resolve.

Deardorff (1968) proposed a way to handle stability effects on drag coefficients. However, he had to assume the drag coefficient for momentum, C_D, to be equal to C_H and C_E, the analogous coefficients for heat and water vapor. Further, his method raises the problem of determining the Monin-Obukhov length -- a very difficult parameter to obtain in field experiments. Thus, a derivation of the drag coefficient for the diabatic case (C_{DD}) in terms of measurable quantities is essential.

A basic definition of C_{DD} in terms of the ψ functions of Panofsky (1963) is

$$C_{DD} = k^2/\psi_M^2 \tag{12}$$

where k is the von Karmen constant and ψ_M is the dimensionless momentum ψ function given by

$$\psi_M(b_1,b_0) = \int_{b_0}^{b} \frac{\phi_M}{b}\, db, \tag{13}$$

where $b_0 = z_0/L$, and $b = z/L$. Dyer and Hicks(1970) have found, for the unstable case,

$$\phi_M = (1 - 16b)^{-1/4} \tag{14}$$

For the stable case

$$\phi_M = 1 + 6\,\frac{b}{1 + b} \tag{15}$$

Integration of ϕ_M/b for $b < 0$ (the unstable case) yields:

$$\psi_M = \int_{b_0}^{b} \frac{db}{b} - \int_{x_0}^{x} 2\left(\frac{1}{1 + x} + \frac{x}{1 + x^2} + \frac{1}{1 + x^2}\right) dx \tag{16a}$$

$$= \ln\frac{b}{b_0} + \ln\frac{(x_0^2 + 1)\,(x_0 + 1)^2}{(x^2 + 1)\,(x + 1)^2} + 2\,(\tan^{-1}x - \tan^{-1}x_0) \tag{16b}$$

where

$$x = (1 - 16b)^{1/4} \qquad x_0 = (1 - 16b_0)^{1/4} \tag{17}$$

Integration of ϕ_M/b for $b > 0$ (the stable case) yields

$$\psi_M = \ln b/b_0 + 6 \ln\left(\frac{1 + b}{1 + b_0}\right) \tag{18}$$

These expressions for ψ_M (and for ψ_H and ψ_E, calculated in a similar way) can then give the diabatic transfer coefficients. Details of the calculation are:

1. Take an arbitrary value of neutral wind speed u(n). A friction velocity is calculated by

$$u^* = C_D\, u(n) \tag{19}$$

2. Take arbitrary values of the characteristic temperature and specific humidity Values for b, b_0 and ψ_M can then be calculated from equation (13).

3. C_{DD} can then be obtained from

$$C_{DD} = k^2/\psi_M^2 \,. \tag{20}$$

By this procedure a set of values of u, $T_0 - T_1 + 0.61\theta(q_0 - q_1)$ and C_{DD} is obtained. For conditions over Lake Michigan, $T_0 - T_1 + 0.61\theta(q_0 - q_1) \simeq T_0 - T_1$. Calculations were made for several score sets and values plotted. A sketch is shown in Figure 36 where the ratio of C_{DD} to C_D is plotted against S_0, a stability parameter defined by

$$S_0 = \frac{T_0 - T_1}{u^2\left[1 + \log_{10}\left(\frac{10}{z}\right)\right]^2} \tag{21}$$

Experimentally, one needs to measure T_0 and T_1 (in addition to $\bar{u}$, $\bar{u}_0$ and $\bar{a}$). The surface temperature can be obtained through use of an infrared sensing thermometer. The 10 m height temperature is a standard measurement. The difference between the two must, however, be measured with at least 0.5^0 C accuracy. The IR thermometer used in this experiment is accurate to $\pm\ 0.2^0$ C and the thermistor to $\pm\ 0.1^0$ C.

APPENDIX C

TRACE ELEMENT LOADING OF SOUTHERN LAKE MICHIGAN BY DRY DEPOSITION OF ATMOSPHERIC AEROSOL

INTRODUCTION

The densely populated and heavily industrialized southwestern shore of Lake Michigan represents a significant and expanding source of anthropogenic aerosol to the atmosphere. The combustion of fossil fuels in residential, industrial, and transportation activities, as well as manufacturing processes such as steel-and cement-making, are principal sources. Pollutant aerosol emitted in nearshore urban/industrial areas provides an input potential for loading of Lake Michigan via wet and dry fallout. Fifty percent or more of the time, prevailing winds give rise to greater than 80 km long trajectories over the lake for air masses passing through the Chicago/Gary area (Williams and Sievering, 1975). Not only the health of the urban population, but also the health of the lake ecosystem, may therefore be linked to atmospheric pollution by wet and dry deposition.

Earlier workers sought to quantify the extent of atmospheric route loadings for several elements by estimation schemes which were based on assumed transfer efficiency (E_t) values, where:

$$E_t = \frac{\text{pollutant loaded to lake}}{\text{pollutant emitted at source}} \qquad (1)$$

Winchester and Nifong (1971) estimated loadings by calculating an emission inventory for the southwest shore source region and assuming an E_t value of 0.10. It was soon pointed out, however, that this value of E_t may be too low. In consideration of mesoscale circulation effects on aerosol trajectories, as well as temperature stability and wind speed effects on deposition, Skibin (1973) suggested that an E_t of 0.25 or larger would be appropriate. Gatz (1975a) presented a refined characterization of Chicago source region aerosol composition, which was used in loading estimates (Gatz, 1975b). Sievering (1976) described a model of the transport and deposition of aerosol over the lake, and proposed an E_t of 0.20 to 0.40, dependent upon season, for combined wet and dry deposition. All of these studies, however, were based upon extrapolation of shore-collected aerosol chemistry data and, at best, wind-tunnel measurements of aerosol dry deposition rate (Sehmel and Sutter, 1974). Very little has appeared in the literature regarding overlake aerosol composition and the deposition rate of that aerosol. Eisenreich, Emmling, and Beeton (1977) used primarily shore-

collected bulk preparation samples to estimate lake loading from field measurements of deposition rates. The bulk samples, i.e., wet and dry fallout combined, give no better than an order of magnitude accuracy for the dry depositional component of total loading (Cadle, 1974). The objective of the research presented here is to consider the dry deposition contribution to lake loading separately. By the collection of an aerosol composition and deposition rate data base at midlake, the annual dry route loading rate to southern Lake Michigan can be better estimated.

In order to approach this objective, three aspects of concurrent investigation were pursued at a midlake site (87°00'W by 42°00'N), about 55 km ENE of Chicago. First, the concentration and composition of atmospheric aerosol were determined. Data describing the chemical makeup (for certain trace lements) and the physical nature of the aerosol were collected. Second, surface-layer meteorological data were obtained for the estimation of aerosol deposition velocity (v_d). Values for v_d based upon midlake data not only improve upon wind-tunnel v_d data (because all lake-surface effects cannot adequately be duplicated in the laboratory), but also can be determined as a general function of meteorological parameters and changes in those parameters. Through climatological information, v_d results from limited sampling periods may be extrapolated into an estimation of the entire year's loading rate. Third, meteorological observations were utilized in the calculation of mesoscale aerosol trajectories. These collection site-to-shore back trajectories provide information on the lake's effect on transport and deposition of aerosol, as well as provide identification of general source regions on shore for the aerosol.

METHODS

During four several-day-long periods in the summer and autumn of 1977, aerosol samples and meteorological data were collected from the U.S. Environmental Protection Agency (USEPA) R/V Roger R. Simons, anchored at a mid-Lake Michigan station (see Figure 1). This site was chosen to be fairly representative of most of the southern basin lake surface. The nearest shore is 40 km distant, so that effects upon loading rates due to point sources and the land-water boundary zone are minimized. The 40 km or greater upwind fetch allows a 10 to 30 m thick "surface layer" of air, just above the water, to reach equilibrium with respect to surface effects. As long as the lake surface appears constant to the air passing over it, the mass flux within the surface layer is constant throughout its vertical extent (Kraft, 1977). Thus, under most conditions, the aerosol is well-mixed within the atmospheric surface layer by the time it is transported to the sampling site (Gillette and Winchester, 1972). The site is also well away from heavily travelled shipping lanes. Reports from several National Weather Service and U.S. Coast Guard stations were added to R/V Simons, Governors State University, and Argonne National Laboratory meteorological data, forming a network of data points around the southern end of the lake.

Aboard the R/V Simons, meteorological instruments (Table 1) were mounted at the tip of a 6 m aluminum boom which extended forward of the bow horizontally at a mean height of 5 m above water. With the ship bow-anchored on station, the boom faced upwind; this allowed for measurement of ambient conditions. The results

of Hunt and Mulhearn (1973) show that even a 3.5 to 4.0 m boom length would have been sufficient to avoid turbulence effects due to the ship's structure. During very light winds (u_5 < 2.0 m-s^{-1}) or periods of quickly changing WD, which made the windward orientation of the boom questionable, sampling was halted. Analog output from the u_5, WD, T_5, and RH sensors was sampled once per second by a data acquisition system (Weather Measure Corp., #SC601/M733). For each 15 minutes of the 1 Hz data, arithmetic mean and standard deviation (σ) values were calculated by the system. These mean and σ values were hardcopy printed and stored on digital magnetic tape (Texas Instruments, Inc., #ASR733). The vertical wind (W_5) analog output was continuously monitored on a strip chart recorder as a check on the vertical motion of the boom. The infrared thermometer was operated manually by an observer standing on the upper foredeck.

Shipboard data collection was done around the clock. In order to divide each sampling period into manageable time segments, data collection was done within 3 to 6 hour periods, referred to as "data sets". Each data set, because of its limited duration, corresponds to a period of fairly constant meteorological conditions. The occurrence of rain or fog events precluded any sampling, since this study was directed at dry deposition only. At the beginning of each data set, aerosol sampling media were replaced. Thus, aerosol samples can be classified according to values of meteorological parameters which prevailed during each set. In general, a minimum three hours elapsed time for a data set was required to provide: 1) statistically meaningful definition of prevailing meteorological conditions, and 2) sufficient loading of the Hi-Volume filters to be above detection limits of the chemical analysis procedure. Past that minimum time, rapid and persistent changes in u_5, WD, T_5, or T_0 were cause for the termination of a data set. Such changes were defined as two successive 15 minute mean values for a given parameter being > 1σ removed from the running mean. A maximum run time of about 8 hours was allowed so that no data set was biased by a widely differing run time.

Aerosol was collected on three-part cellulose filters (Sierra/Misco #P252A, P810A) in a three-stage cascade impactor. The impactor utilized the first, third, and backup stages of a Sierra Series 230 Cascade. This configuration provided resolution of the aerosol analyses results into fine particulate (diameter D < 1.0 μm) and coarse particulate (D > 1.0 μm) fractions (Sievering, et al., 1978). The filters were exposed at a flow-controlled (Sierra #310) rate of 1.13 m^3-min^{-1} (40 ft^3-min^{-1}), on a standard Hi-Volume sampler (General Metal Works, #GMW1000). The Hi-Vol was located 4.5 m ahead of the bow, on the instrumentation boom. This location, and the addition of a 4 m long exhaust tubing to the Hi-Vol motors, helped reduce contamination of aerosol samples (Schmidt, 1977; Moyers, Duce, and Hoffman, 1972). An additional Hi-Vol was operated on the upper foredeck with 20 X 25 cm glass-fiber filters (Sierra #C305) for gravimetric analysis of total aerosol mass concentration.

Aerosol samples on the three-part cellulose filters were analyzed for trace elements at the USEPA Central Region Laboratory in Chicago. The filters were placed in acid-washed fused quartz trays and low temperature ashed in O_2 at 75 watts. The residue was then dissolved in HNO_3 and distilled deionized water. Trace element analysis was done by Inductively Coupled Argon Plasma atomic

emission spectroscopy (ICAP-AES) (Jarrell-Ash, Plasma AtomComp 750). In more than 85 percent of the data sets, concentrations of Ca, Mg, Cu, Fe, Mn, Pb, Ti, and Zn were above ICAP-AES instrumental detection limits (L_d). The limited 3 to 8 hour exposure time of the filters resulted in concentrations of Na, Ba, Cd, Co, Mo, Ni, and V which were below L_d for 50 percent of the data sets (Table 2). Therefore, loading calculations will not be done for these metals. Post-analysis statistical review of the data revealed contaminant or otherwise anomalous data for B, so that this element was not used in loading estimates. Filter blanks were carried throughout the handling and analysis procedures, except the collection of ambient aerosol. The blank correction (β_i) applied to the ICAP-AES results for the exposed filters was defined as:

$$\beta_i = C_{bi} + 1\sigma \qquad (2)$$

where: C_{bi} is the mean concentration of the element i in filter blanks,

σ is the standard deviation in that mean value.

(both ng - ℓ^{-1})

For those elements which were above L_d in > 85 percent of the data sets, concentrations are reported here within the < 20 percent expected reproducibility confidence for ICAP-AES analyses.

Several optical particle-measuring instruments were also used at the ship site to collect information on the physical character of midlake aerosol. An Integrating Nephelometer (IN) (Meteorology Research, #1550) was operated on the upper foredeck to continuously monitor aerosol light scattering coefficient and thus, variations in total aerosol mass concentration (Davé, Dolske, and Sievering, 1979). An Active Scattering Aerosol Spectrometer (ASAS) (Particle Measuring Systems, #ASAS 300-PMT) was mounted at the proximal end of the sampling boom. The ASAS counts aerosol number concentration in 60 adjacent size channels in the range $0.1 < D < 3.5$ μm. The size distribution of midlake aerosol was thus recorded, generally at 15 minute counting intervals during each data set. Size and volume plots yield much qualitative information regarding aerosol transport and depositional processes (Slinn, 1974; Sievering, 1979). ASAS counts were usually taken at the 5 m mean height above water. When vertical ship motion was minimal, attempts were made to measure vertical gradients in the aerosol number concentration. The instrument's intake was alternately placed at heights of 3.6 and 6.4 m during successive counting periods of from 6 to 15 minutes. In a limited number of cases, the measurement of number concentration difference between the two heights was statistically significant (Sievering, 1979).

Aerosol deposition velocity (v_d) was estimated for each data set by means of a diabatic drag coefficient, C_{dd}, and the relation:

$$v_d \simeq C_{dd} \cdot (\bar{u}_5 - \bar{u}_0) \qquad (3)$$

where: v_d = deposition velocity

$\bar{u}_5$ = mean wind speed at 5 m height

$\bar{u}_0$ = water surface current

(all in $cm\text{-}s^{-1}$)

Note that v_d, as given by this method, is independent of aerosol size. The limited results of ASAS-measured number concentration gradients indicate that v_d may not vary strongly with aerosol size in the range $0.1 < D < 2$ μm. Theoretical models of deposition processes and wind tunnel data predict as much as an order of magnitude variability in v_d across this size range. The ASAS vertical gradient measurements suggest the size dependent variability of v_d is somewhat less than a factor of three for this size range of aerosol (Sievering, 1979). These vertical gradient measurements further suggest the v_d determined by relation (3) has an uncertainty of roughly 2-to 3-fold, which is the same order as the size-dependent variability. Aerosol size distribution and total mass concentration data from the midlake site indicate that most of the aerosol mass was accounted for by the the $0.1 < D < 2$ μm size range (Davè, Dolske, and Sievering, 1979). A bulk estimate of v_d from relation (3) is therefore a reasonable value, although not size dependent, for use in loading calculations.

The value of C_{dd} used in (3) is itself a function of surface layer wind speed and atmospheric thermal stability ($\Delta\bar{T} = \bar{T}_5 - T_0$). The v_d determined for each data set is thus strongly dependent upon meteorological conditions prevailing during that period of time. From the most stable cases ($\Delta T > 8.3^{o}C$) to the most unstable cases ($\Delta T < -0.9^{o}C$), mean $\bar{v}_d$ from (3) varies from 0.15 to 0.72 $cm\text{-}s^{-1}$ (Table 11). For very low wind speeds ($\bar{u}_5 < 2.0$ $m\text{-}s^{-1}$), aerosol deposition is impeded by a continuous laminar sublayer immediately above the air/water interface. For such cases, the v_d estimate of (3) is no longer physically reasonable and a $\bar{v}_d$ of zero is assumed. For the highest wind speed cases ($\bar{u}_5 > 7.0$ $m\text{-}s^{-1}$), a mean $\bar{v}_d$ of 1.17 $cm\text{-}s^{-1}$ was determined (Table 12). The great variability in $\bar{v}_d$ due to changing meteorological conditions must then be considered in the estimation of annual loading rates for the lake. At present, techniques for direct measurement of aerosol deposition, such as eddy-flux correlation and concentration-profile methods, require much development before v_d can be routinely determined (Hicks, 1979; Sievering, 1979). Until the direct measurement methods become reliable for over-water field sampling, the C_{dd} method yields meaningful estimates of lake loading via dry deposition, within the approximate factor of two accuracy indicated. While this may seem to be a rather large uncertainty, it represents a significant refinement in the estimation of the dry route loading component over previous estimates given by extrapolation of shore-collected data or bulk sampling results.

Two approaches were followed in the calculation of estimated annual dry loadings to the southern basin of Lake Michigan. The most basic approach is the overall-average method:

$$\lambda = \bar{v}_d \cdot \frac{C_i}{v_d} \cdot A \cdot t \qquad (4)$$

where: λ_i is loading to lake of element i ($kg\text{-}yr^{-1}$)

$\bar{v}_d$ is mean bulk deposition velocity for all data sets ($m\text{-}s^{-1}$)

$\bar{C}_i$ is mean concentration of element i ($kg\text{-}m^{-3}$)

A is total water surface area of southern basin of Lake Michigan ($2.9 \times 10^{10}\ m^2$)

t is part of the year when no precipitation occurs overlake ($s\text{-}yr^{-1}$)

Equation (4), although straightforward, entails an underlying assumption that deposition at the midlake point represents deposition over the entire southern basin. For single-site sampling, this is an unavoidable assumption. However, the surface layer conditions at midlake are certainly more similar to the majority of the lake surface than are conditions on shore or near to shore. Moreover, (4) assumes that the data sets which made up the mean $\bar{v}_d$ and $\bar{C}_i$ values were representative of the entire year's variability in v_d and C_i. The values of v_d and C_i are, however, strongly dependent upon surface layer meteorological conditions and aerosol source region. Overlake climatology is thus an important factor in the determination of annual loading rates. In order to relate the limited number of sampling hours (approximately 2 percent of the year) to the annual total loading, data sets taken in periods of similar surface layer conditions are computationally grouped into "bins". Each bin is defined by a range of values for one of three parameters: temperature stability, ΔT, wind speed, u_5, or source region, identified through back-trajectory construction. For each bin, the annual frequency of occurrence, F_o, is determined for the range of the defining parameter from climatological data (NOAA, 1975). Annual loadings which account for the climatological dependence of v_d and C_i are then calculated from:

$$\lambda = \sum_j \bar{v}_{dj} \cdot \bar{C}_{ij} \cdot F_{oj} \cdot A \cdot \frac{t}{\sum_j F_{oj}} \qquad (5)$$

where: λ_i is loading of element i ($kg\text{-}yr^{-1}$)

$\bar{v}_{dj}$ is mean v_d for data sets in j^{th} bin ($m\text{-}s^{-1}$)

$\bar{C}_{ij}$ is mean concentration for i for sets in the j^{th} bin ($kg\text{-}m^{-3}$)

F_o is annual frequency of occurrence for defining range of parameter (ΔT, u_5, or source) - (yr)

t is time without precipitation overlake ($s\text{-}yr^{-1}$)

In applying equation (5), it is assumed that the year in which sampling is done is a climatologically representative one. How well the data fits prevailing climatology is at least partially accounted for by the inclusion of the F_{oj} values. It is assumed, however, that the $\bar{v}_{dj}$ and $\bar{C}_{ij}$ values for each bin do indeed represent the conditions of that bin averaged over a year. Even so, (5) is a refinement over (4) in that the variations in v_d and C_i due to surface layer meteorology and source region are taken into consideration.

RESULTS

The geometric mean aerosol mass concentration, $\bar{C}_m$, observed at the midlake site was 32. $\mu g\text{-}m^{-3}$. The range of values measured was $10. < C_m < 94. \mu g\text{-}m^{-3}$. Trace element composition of midlake aerosol is expressed in Table C-1 by three ratios of concentrations:

$$P_i = \frac{\bar{C}_i}{\bar{C}_m} \cdot 100 \qquad (6)$$

$$A_i = \frac{\bar{C}_i \ (D < 1.0 \ \mu m)}{\bar{C}_i \ (D < 1.0 \ \mu m)} \qquad (7)$$

$$EF_i = \frac{\bar{C}_i / C_{std} \ \text{(in aerosol)}}{C_i / C_{std} \ \text{(in soil)}} \qquad (8)$$

In (6), P_i gives the mass percentage contributed by the concentration of element i and is useful for comparison to the data of Gatz (1975a). Two values of P_i and A_i are tabulated from the midlake data. The first is for the mean of all data sets collected at midlake, while the second P_i and A_i values are based only on those data sets for which the Chicago/Gary area was indicated as the probable aerosol source region. From (7), A_i is a measure of how significant the fine particulate ($D < 1.0 \mu m$) component of C_i is in relation to the coarse particulate ($D > 1.0 \mu m$) fraction. A rough comparison between the composition of midlake aerosol and source area aerosol is indicated by a transport composition ratio, R_{tc}, which is the ratio between P_i for the Chicago-source midlake data and P_i from Gatz' (1975a) composite model Chicago area aerosol data. For the majority of the elements R_{tc} appears to be close to 1.0, which suggests that the trace element composition of the aerosol is not drastically altered during overlake transport.

Enrichment factors, $\overline{EF}_i$, from (8), relate the concentration of an element to the concentration which might be attributed to a reference natural source material. In this work, the composition of midwestern soil described by Bowen (1966) is used, with Al concentration defined as the source standard, C_{std}. EF_i values close to unity indicate that element is present in soil-derived proportions; large EF_i values indicate other major sources for that element in aerosol (Rahn, 1976). It appears that at least Cu, Zn, and especially Pb are greatly enriched in midlake aerosol, i.e. come from other than natural sources.

The dependence of trace element concentrations at midlake upon surface layer meteorology and aerosol source region is discussed in detail by Sievering, et al.(1979a). The data "binned" in Tables 11, 12, and 13 can clearly show that midlake meteorology and source region strongly affect $\overline{C}_{ij}$. Values of $\overline{v}_{dj}$ are also quite strongly dependent upon ΔT and u_5. The variability of $\overline{C}_{ij}$ and $\overline{v}_{dj}$ are of particular importance to the loading rates, because these two parameters are producted in λ_i calculations (4) and (5). For example, although the Chicago/Gary-source data sets give higher $\overline{C}_i$ results than the Southeast shore sets, λ_i values for the two source regions are about equal, due to the compensating effect of lower $\overline{v}_d$ and F_0 values for the Chicago/Gary sets. Both the ΔT (Table 11) and u_5 (Table 12) data set aggregations reveal that meteorological conditions which lead to high v_d values were not sampled. The most unstable bin F_0 accounts for the 0.38 year with $\Delta T < -0.9^oC$; yet, the single most unstable case sampled was $\Delta T = -2.0^oC$. C_{dd}, and thus v_d from (3) increases markedly as ΔT becomes more negative. If more unstable ($\Delta T < -2.0^oC$) data had been collected, the v_d for this bin would likely have been somewhat higher. Similarly, the bin for high u_5 values has an F_0 which accounts for the 0.41 year with $u_5 < 7.0$ m-s^{-1}. The highest u_5 case sampled was $u_5 = 8.3$ m-s^{-1}. Again, the available data sets miss the cases where higher v_d values might have been determined. The F_0 values used in the most extreme-case bins thus apply the available data to parts of the year when loading rates would be greater. Because of this, the λ_i values calculated here likely underestimate annual λ_i. Given this consideration and the 2-to 3-fold uncertainty in the C_{dd} based v_d determination, the least λ_i estimate from the overall-mean (4) and bin-method (5) calculations is divided by two and reported as a "minimum" loading estimate.

DISCUSSION

Two factors in the loading estimate calculations, (4) and (5), were quantified through field observations and related to overlake meteorological variability: v_d and C_i. Because all sampling was done at a single site, temporal variations within data-set-mean $\overline{v}_d$ and $\overline{C}_i$ are important factors in veiwing the resultant λ_i estimates. The time-scale resolution afforded by the 3 to 6 hour data set lengths eliminates short-term "patchiness" in the observed parameters, yet provides definition of the prevailing surface-layer meteorological regime. The data set initiation/termination criteria give priority consideration to the constancy of meteorological observations. As the consequence, the sets used in λ_i estimations generally had standard deviations about the data set means of: $\sigma WD < 15^o$, $\sigma u_5 < 1$ m-s^{-1}, and $\sigma\Delta T < 1^oC$. However, this degree of steadiness does not conclusively point to a similar aerosol concentration steadiness. Although a detailed analysis of ASAS ambient aerosol counts is as yet incomplete, preliminary results indicate

that aerosol number concentration remained fairly constant within each data set. Variation about the overall set mean was generally less than 20 percent. The IN-monitored aerosol mass concentration also showed a similar degree of steadiness. Each data set thus represents a period of fairly homogeneous meteorological and aerosol concentration conditions. The data set mean v_d and $\bar{C}_i$ were then used as input values for the calculations of this work.

The emphasis, during sampling, upon constancy of parameters within each set necessitated relatively short Hi-Vol filter run times. The gross amount of aerosol collected was thus such that 7 elements which were analyzed for by ICAP-AES failed to appear above L_{di} in many data sets (Table 2). Contamination, probably introduced by the analytical procedure, makes the data for B unreliable. This leaves 9 elements as candidates for the λ_i calculation; however, data for 2 of these elements must be used with caution. Because the Hi-Vol sampler pumps use Cu-alloy commutators which are known to produce Cu-aerosol (Moyers, Duce, and Hoffman, 1972), precautions were taken in setting up the samplers to avoid re-entrainment of the pump exhaust. At the 1.18 m^3 - min^{-1} flow rate, given the short run times and low filter matrix load, back-pressure contamination through the sampler head is unlikely. There is nothing in the Cu results to directly suggest any significant contamination actually occurred. To the contrary, P_{Cu}, A_{Cu}, and R_{tc} results appear to be consistent with other elements (Table C-1). Even so, any Cu data from Hi-Vol sampling should be used with caution, and the λ_{Cu} results are so indicated. Finally, the Ti data shows some anomalous behavior that suggests probable contamination. Sievering, et al. (1979a) showed that while all other elements in this data base correlated inversely with u_5, Ti was weakly positively correlated. In Table C-1, the R_{tc} results clearly set Ti apart. By plotting Ti enrichment factors versus Al concentration (Figure 17), Ti is seen to tend somewhat towards constant concentration (dashed diagonal line). All this suggests the probability of contamination for Ti in collecting, handling, or analyzing the aerosol samples. The possibility is not conclusive, however, and the λ_{Ti} results are still presented, with caution in interpretation suggested. For the remaining 7 elements (Al, Ca, Fe, Mg, Mn, Pb, and Zn), the uncertainty introduced to the λ_i calculation by the C_i factor is expected to be the ICAP-AES instrumental reproducibility confidence of < 20 percent.

It should be emphasized that the v_d used in loading calculations (4) and (5) is derived from meteorological data through the C_{dd} method and relation (3). This derivation is based upon an analogy between momentum transfer and mass transfer. The resultant v_d is a parameterized bulk estimate of the aerosol deposition rate and not a direct measurement. Methods which may, after further technique development, lead to directly-measured v_d's (such as the concentration-profile method, or the eddy correlation method) are not yet suitable for routine over-water use (Hicks, 1979; Shepherd, 1974). The C_{dd} method was used here in order to reduce the order-of-magnitude uncertainty in dry deposition loading estimates from E_t-based modeling (Winchester and Nifong, 1971; Gatz, 1975b) and bulk precipitation sampling (Eisenreich, Emmling, and Beeton, 1977) results. As stated in a preceding section, the v_d's used in this work should be viewed in the context of the stated 2-to 3-fold uncertainty. Still, there are some data highly supportive of the C_{dd}-based results. Limited ASAS aerosol number concentration profiles taken on board the R/V Simons indicate v_d's close, i.e. within a factor of two, to the C_{dd}-based

v_d values (Sievering, 1979). Delumyea and Petel (1977), using a simple mixing-box aerosol depletion model in a study of phosphorus deposition over Lake Huron, found that v_d for $D \approx 1$ μm aerosol to be 0.6 cm-s^{-1}. Sievering, et al. (1979b) used a similar depletion model and sulfate-aerosol data taken during May 1977 at the midlake site and in Chicago to calculate a v_d of 0.3 cm-s^{-1}. For those midlake samples, 90 percent of the sulfate was associated with the $D < 1.0$ μm aerosol. These results agree well with the overall mean C_{dd}-based v_d of 0.5 cm-s^{-1}.

Another apparent shortfall of the C_{dd} method is that v_d is given as a bulk estimate and not as a function of aerosol size. Theoretical consideration of aerosol deposition points to as much as an order of magnitude variation in v_d in the particle size range $0.1 < D < 3.5$ μm; wind tunnel studies of deposition to a water surface also indicate strongly size-dependent v_d (Sehmel and Sutter, 1974). Not all mechanisms of aerosol deposition are adequately accounted for in theoretical models or wind tunnel studies, however, and field measurements of aerosol v_d suggest a much weaker size dependent variability. ASAS profile results suggest that the maximum change in v_d in the $0.1 < D < 2$ μm size range is no more than a factor of two. The R_{tc} results in Table C-1 may also suggest a lack of strong size dependence in v_d. If v_d were size-dependent, then one might expect the composition of aerosol to change during over water transport. Trace metals in urban aerosol are generally associated with the fine particulate fraction. If the fine particulates had a much reduced relative v_d, one might then expect the R_{tc} values to be much greater than unity. This is not observed; in fact, the R_{tc} values fall quite close to 1.0, with the exception of Ti with an R_{tc} of 6.0, which may be an indication of probable Ti contamination. Ca, with an R_{tc} of 2.5, seems also to be an exception, but uncertainty in the composition model (Gatz, 1975a) makes the difference probably not unsignificant. It appears that the size-dependent variability in v_d for the $0.1 < D < 2$ μm aerosol is very probably less than the overall uncertainty in the C_{DD}-based v_d from (3). Because nearly all aerosol mass at the midlake site was attributable to the $0.1 < D < 2$ μm size range, no attempt was made to include a size-dependent v_d factor in the loading calculations.

The binned data sets of Tables 11 and 12 demonstrate clearly that both v_d and C_i are functions of the prevailing meteorological regime overlake. As much as a 6-fold range in v_d and an order of magnitude range in C_i for most elements were observed during the conditions sampled from May to September. Using the overall mean $\overline{v_d}$ and $\overline{C_i}$, estimates of λ_i were calculated from equation (4). That calculation, however, does not take into account the wide range of observed v_d and C_i. A better approach, in which the range and concurrent variability of both factors are applied, is the use of (5) to estimate λ_i. Also, from trends observed in the binned v_d and C_i data, on can infer some qualitative information about the bias in λ_i resulting from the summer-season only sampling. The F_o values provide a simple weighting factor for each bin in the averaging process of (5), relating observed data to southern basin climatology (NOAA, 1975). All λ_i results are normalized to $t = 2.7 \times 10^7$ s-yr^{-1}, i.e., the 85 percent of a year when no precipitation occurs overlake (Sievering and Williams, 1975). F_o values for the bins with the greatest v_d values ($\overline{\Delta T} < -0.9^{o}C$; $\overline{u_5} > 7.0$ m-s^{-1}) extrapolate the data to more unstable-air and high wind speed periods which were not sampled in the summer season. If winter season data had been available, the v_d's for these

extreme-case bins would likely have been somewhat larger. The extrapolation through the F_0 values thus tends to make λ_i values apparent underestimates of annual loadings. At the other end of the bins, an assumption of $\bar{v}_d$ = zero for all cases with $\bar{u}_5 < 2.0$ m-s^{-1} also leads to underestimation of annual loadings. For such low wind speed cases (which include some very stable-air cases), a laminar sublayer exists at the interface which impedes, but probably does not completely block (Sievering, 1979) aerosol deposition. The dependence of $\bar{C}_i$ and $\bar{v}_d$ on u_5, ΔT, and source region is discussed by Sievering, et al. (1979a). The influence of these dependencies upon λ_i results is significant. In Table 10, $\bar{C}_i$ tends to generally increase as ΔT becomes more stable (positive); $\bar{v}_d$ tends to be reduced. Because λ_i depends upon the product of these two factors, a "self-protection" mechanism of the lake surface from high stable-air $\bar{C}_i$ levels is implied. For the fall-winter, unstable-air season this mechanism is reversed. even though lower $\bar{C}_i$ values might be expected, higher $\bar{v}_d$'s would likely result in significant winter loadings. In Table 12 , similar trends appear, although weakly defined for $\bar{C}_i$. Again, the winter season overlake being the high wind speed season (NOAA, 1975), summertime "self-protection" of the lake is reversed in winter. The source region bin data in Table 13 points to another aspect of the dry deposition loading situation. Although $\bar{v}_d$ is only weakly variable with source sector, a $\bar{C}_i$ maximum is clearly indicated from the Southeast Shore and Chicago/Gary areas (Figure 1), not an unexpected result. The sum of F_0 values show that 53 percent of the year these two high-air pollution regions are sources of increased $\bar{C}_i$ at the midlake site. As a consequence, the Chicago/Gary and Southeast Shore areas contribute from 60 to 65 percent of the total dry deposition λ_i to the southern basin. Table C-2 gives these dry deposition λ_i values in the context of the precipitation loadings estimated by Gatz (1975b) from about the same general source region. It appears that wet and dry route λ_i values are about equal, except for Pb and Zn, where the dry route λ_i are somewhat larger than for precipitation. Transfer efficiencies, based on the total atmospheric route loading and source strength model (Gatz, 1975b), range from 4 percent (Cu) to 14 percent (Zn). The dry deposition λ_i's of this work agree well with the source strength E_t results of Gatz (1975b), again excepting Pb and Zn where loadings are larger than Gatz predicted.

The transfer of trace elements from the lake water surface to the atmosphere is assumed, in (4) and (5), to be very small compared to the downward flux of aerosol to the lake. For over 90 percent of the year, wind speed over the lake is less than 10 m-s^{-1} (NOAA, 1975) and aerosol generation at the surface is minimal. At the highest $\bar{u}_5$ cases observed in the 1977 sampling, no increase in Ca or Mg content of the aerosol was observed (Table 12). Also, Ca and Mg levels are much reduced in the overlake-source data sets (Table 13). Ca and Mg are present in fairly high levels in lake water and one might then expect to see an increase relative to other elements if lake surface generated aerosol were present. The R_{tc} value of 2.5 for Ca in Table C-1 is probably not a significant indication of increased relative Ca; if the "all data sets" P_i value had been used, R_{tc} for Ca would fall in line with the other elements' values. Although some lake-surface aerosol generation does occur, it seems reasonable to expect the trace element flux to be small relative to the atmospheric input on a long term average.

The significance of atmospheric inputs of trace elements to the Lake Michigan ecosystem is not well known (IJC, 1978). Dry deposition appears to be a major contributing source of at least four elements on a percentage of total loading basis (Table 14). 10 percent of Mn, 20 percent of Fe, 30 percent of Zn, and as much as 60 percent of Pb inputs to the lake are by dry deposition of atmospheric aerosol. Only for those elements which have very large natural land run-off inputs are atmospheric loadings seen to be negligible. More important to consider than the gross total loadings, however, is the fact that all atmospheric route loadings are deposited directly to the surface zone of maximal biological activity. The impact of this upon the well being of the biota must surely be an object of future research, as must be the continuation of the task of precisely quantifying atmospheric route loadings to Lake Michigan, other large lakes, and the oceans.

	Mid-Lake Michigan						Chicago	
	All Data Sets			Chicago Source Sets			Composite Aerosol †	
ELEMENT	$P_{i(\%)}$	A_i	EF_i	$P_{i(\%)}$	A_i	EF_i	$P_{i(\%)}$	R_{tc}
Al	0.6	1.3	≡1.0	2.	0.6	≡1.0	2.	1.0
Ca	3.	0.5	22.	5.	0.4	11.	2.	2.5
Cu	0.02	3.9	170.	0.09	2.9	280.	0.1	0.9
Fe	1.	1.7	3.5	3.	1.3	3.2	3.	1.0
Mg	0.8	0.7	23.	1.	0.6	8.6	0.9	1.1
Mn	0.05	2.2	10.	0.1	1.2	6.0	0.1	1.0
Pb	0.5	21.	5200.	0.9	13.	3300.	0.6	1.5
Ti	0.03	0.7	1.4	0.06	0.8	0.9	0.01	6.0
Zn	0.2	6.4	530.	0.7	5.8	560.	0.6	1.1

† Gatz, 1975a

TABLE C-1. Aerosol Trace Element Composition and Enrichment Factor.

	Percent of Dry Loading Total due to Chicago/N. W. Indiana	Atmospheric Route Loading, (10^3 kg - yr^{-1}) Dry Deposition	Precipitation*	Total	E_t* Percent
Al	80	480	560	1040	13
Ca	80	1600			
Cu	{65}	{12}	20	{32}	{4}
Fe	75	750	750	1500	7
Mg	60	440			
Mn	80	50	50	100	13
Pb	75	370	90	460	8
Ti	{60}	{20}	60	{80}	{9}
Zn	85	170	50	220	14

* Precipitation Loadings and Area Source Strengths from Gatz (1975b)

** Results in brackets { } indicate caution in interpretation - see Discussion

TABLE C-2. Atmospheric Route Loadings to the Southern Basin of Lake Michigan Due to the Chicago Shore/Northwest Indiana Source Region.

APPENDIX D

AEROSOL SAMPLE PREPARATION PROCEDURE FOR EMISSION SPECTROSCOPY ANALYSIS

EQUIPMENT

1 Plasmod Low Temperature Asher
1 D2A Vacuum Pump, 61 l/min
1 Oxygen Cylinder with Two-Stage Regulator
1 Hot Plate
1 Top Loading Balance
4 or 8 Quartz Combustion Podats, each with a permanent identifying mark

SUPPLIES

1 pair Teflon Coated or Plastic Scissors (dedicated)
1 Oxford Pipet, 5 ml, with disposable pipet tips
1 Eppendorf Pipet, 50 λ (μl) with disposable pipet tips
1 Graduated Cylinder, 50 ml
60 ml Polyethylene Bottles with caps (Monsanto), 5 for each filter set
Disposable Plastic Funnels, 1 for each bottle
Petri Dishes, 100 X 100 X 15 mm square style, 1 for each filter set
Glass Rods, 3 mm diameter, "L" shape, 2 for each petri dish
1 Glass Plate
2 Pair Forceps, Teflon coated or plastic
Disposable Plastic Gloves and ruler are also needed

REAGENTS

Yttrium Nitrate, Purified Crystals
Deionized Water or Doubly-Distilled-in-Glass Water
Redistilled-in-Glass Nitric Acid or Spectrograde Nitric Acid
Spectrograde Hydrochloric Acid

PREPARATION OF YTTRIUM STOCK SOLUTION: 1000 ppm

1. Acid wash a 1 liter volumetric flask. Rinse several times with deionized water. Dry flask in oven and let cool to room temperature.

2. Weigh a clean, dry weighing boat or bottle to the nearest 0.1 mg. Weigh out 4.3080 g of $Y(NO_3)_3 \cdot 6H_2O$. Quantitatively transfer the Yttrium Nitrate to the 1 liter volumetric flask using a cleaned powder funnel and a wash bottle of deionized water. Dissolve all of the $Y(NO_3)_3 \cdot 6H_2O$ and

then dilute to mark with deionized water. Store the 1000 ppm Yttrium stock solution in a labeled, clean (acid washed) bottle.

REDISTILLED ~ 6N HNO_3

1. Clean and assemble an all glass distillation set-up. Use an electric heating mantle to heat the distillation flask.

2. Add a 50 percent solution of concentrated reagent grade HNO_3 in distilled water until the flask is half filled.

3. Adjust the current to the mantle until the nitric acid solution just begins to boil. Collect the condensate in a cleaned, labeled reagent bottle. Distill the solution down to approximately one-fourth of the original volume. Add more of the 50 percent solution of nitric acid and distill.

PROCEDURE I-A. PREPARATION OF INERTIAL CASCADE IMPACTOR FILTERS

The cascade and backup filters are stamped with a five digit filter identification number. The trace metal samples for ICAP analysis will be identified by a six digit number. The samples from the cascade impactor filters will be identified by the filter number plus a zero (0). The backup filter will be divided into three samples. The undisturbed portion of the backup filter will be numbered with the filter number plus a "-1". The samples from the portion of the backup filter used in the extraction procedure will be numbered with the filter number plus a "-2" and the soluble portion from the extraction will be identified as the filter number plus a "-3".

The cascade filters and backup filter are stored in a filter set container. Each filter within the filter set is numbered. The cascade filters are approximately 5½" X 6" with 11 impaction strips. 10 of the strips are impacted with atmospheric particulates. The narrower end strip will be eliminated, since it is not impacted on. The 10 impacted strips are to be cut and ashed. It is imperative that the cutting procedure be performed in a clean work area. A pair of Teflon coated scissors should be kept <u>solely</u> for use on this procedure.

1. Clean the quartz boats by adding ~5 ml of 6N HNO_3 to each. Place boats on the hot plate and heat until acid begins to fume. Gently (and carefully) swirl acid around inside surfaces. Pour acid out and rinse several times with deionized water. Wipe inside dry with Kimwipes. Do not touch inner surfaces of boats after cleaning.

2. Clean the pair of scissors with acetone prior to cutting a sample.

3. Record, along one row of the Plasma Asher Log, the date and, in the column designated for the quartz boat, the filter number (see Figure D-1).

4. Wearing disposable plastic gloves, cut the filter along lines as indicated in Figure D-2.

a) Cut the filter along dashed line marked "cut 1". Dispose of the numbered end strip.

b) Cut along the dashed lines marked "cut 2 and cut 3". Dispose of the two side strips.

c) Cut along the dashed line marked "cut 4". 10 impacted strips and a numbered end strip will remain.

d) Cut the 10 impacted strips in half.

5. Place the 20 impacted strips in the appropriate quartz boat. Dispose of the numbered end strip.

6. Repeat steps 2 through 5 for the other cascade filter within the set. NOTE: If the ashing chamber can accommodate four quartz boats, repeat steps 2 through 5 for the cascade filters in the next filter set.

7. Proceed to Procedure II - Low Temperature Ashing. After ashing all of the inertial cascade impactor filters, proceed to Procedure I-B.

PROCEDURE I-B. PREPARATION OF HI-VOLUME BACKUP FILTERS

The backup filters are 8" X 10". The exposed area is approximately 7" X 9". A 3-5/16" X 7" portion (cut into two equal pieces) of the backup filter is used in a soluble aerosol extraction procedure. The extraction is performed and then the extracted portion and the undisturbed portion of the backup filter are prepared for ashing.

1. Write the filter number and "-3" on the external surfaces of the top and bottom of an unused square petri dish. Use a grease pencil to write number. Cover the number with an adhesive label. (The numbers should be readible and legible when the two halves of the dishes are resting on their external surfaces.)

2. Acid clean (using diluted HNO_3) the "L" shaped glass rods. Rinse thoroughly with deionized water and allow to dry in a clean environment. Put two of the rods in each of the larger half of the labeled petri dishes. Arrange the rods so that they form a square. Set aside the smaller half of the petri dish.

3. Add 29 ml of deionized water to each dish. NOTE: pH can be measured on a dish set up as a blank.

4. Clean the pair of scissors prior to cutting the filters.

5. Measure along both sides of the exposed area of the filter a distance of 3-5/16" (see Figure D-3). Cut along the line connecting the two points.

6. Put the larger piece (with number intact) back in the filter set container.

7. Measure 3-1/2" along the bottom edge of the exposed area of the smaller piece. Cut the piece of filter in half at that point.

8. Cut off the borders. Two 3-5/16" X 3-1/2" pieces should remain.

9. Put one of the 3-5/16" X 3-1/2" pieces of the backup filter back in the filter set container.

10. Using two pair of forceps, gently place the other 3-5/16" X 3-1/2" piece and filter onto the surface of the water in the petri dish correspondingly numbered to the backup filter. NOTE: The filter should just rest upon the glass rods and should not be submerged nor should the edges of the filter touch or drape over the side of the petri dish.

11. Repeat steps 4-10 for the remaining backup filters.

12. Cover the array of petri dishes with a glass plate and let them remain undisturbed for 24 hours.

13. Carefully remove the piece of filter paper after 24 hours. Use the two pair of forceps. Place the wet piece or filter in the correspondingly numbered smaller half of the petri dish.

14. Repeat step 13 for the remaining samples. Set them aside to dry in a clean area. If possible, cover filters without touching them.

15. Remove from the filter set container the other 3-5/16" X 3-1/2" section of the backup filter. Carefully place it on the surface of the liquid in the correspondingly numbered petri dish.

16. Repeat step 15 for the remaining filters.

17. Cover the array of petri dishes with a glass plate and let them remain undisturbed for 24 hours.

18. Place the dry filter sections from step 14 into their correspondingly numbered filter set containers.

19. Repeat steps 13, 14 and 18 after the second 24-hour extraction.

20. Number a sample bottle corresponding to the first petri dish.

21. Tare the bottle on the top loading balance.

22. Carefully pour the contents of the petri dish into the bottle through a clean, unused plastic funnel. The glass rods will adhere to the surface of the petri dish. Carefully remove them with the forceps and knock in the last drops from the dish.

23. Set the bottle back on the balance. Wash down with deionized water any residual drops from the funnel, (NOTE: do not weigh the funnel -- hold it up from contact with the bottle) and add water until the weight registers 25 g, i.e. 25 ml of solution. Measure and record the pH (be careful not to contaminate the sample).

24. Cap the bottle and set aside.

25. Repeat steps 20-24 for the remaining liquid samples.

26. Record the filter number and "-2" in the plasma asher log for the first backup filter.

27. Remove the two (dry) extracted portions of the backup filter and cut them into strips small enough to fit into quartz boats.

28. Put all of the strips in a clean (see Step 1 of Procedure I-A), identified quartz boat.

29. Record in the plasma asher log the backup filter number and "-1". Remover from the filter set container the undisturbed portion of the backup filter. Cut off and dispose of the borders. Cut into strips small enough to fit into quartz boats. Put all strips in a clean, identified quartz boat.

30. Proceed to Procedure II - Low Temperature Ashing.

PROCEDURE II - LOW TEMPERATURE ASHING IN TEGAL PLASMOD ASHER

1. Place two or four boats into the inner glass chamber of the low temperature asher.

2. Make sure that the oxygen tank, regulator, vacuum pump, and low temperature asher are properly connected.

3. Turn on the oxygen supply and regulate to 10 psi.

4. Turn on vacuum pump.

5. Turn on the asher (push in AC button) making sure that the RF power switch is OFF (OFF is the down position).

6. While holding the glass chamber up against its casing, turn on (switch up) the vacuum switch. A tight vacuum must be obtained for the asher to operate properly.

7. Shut the screen door, turn on the RF power switch, and set RF level to 75 watts. Adjust the tuning knob until a minimum reading is obtained on the RF power meter. A faint blue or pink hue of excited oxygen will appear in the chamber. Turn RF power to maximum value and retune to obtain a minimum signal.

8. Ashing times are related to the amount of filter paper being ashed. Complete destruction of all organic material is required for proper sample preparation. Complete ashing can be identified by a very faint blue glow after a period of a bright blue glow (the bright blue corresponds to excited CO_2).

9. When the filter has been ashed, turn the RF level down to zero and switch the RF power to OFF. The door may now be opened to inspect the filter. If the filter has not been completely ashed, repeat step 7.

10. Turn off the vacuum switch. Allow the purge line to fill the chamber with air and then take out the inner glass chamber. If no more filters are to be ashed, turn off vacuum pump, asher, and oxygen supply.

11. Place quartz boats on a clean asbestos square that is resting on a hot plate (in hood). Using an oxford pipette, add to each boat 5 ml of redistilled 6N HNO_3. Heat for approximately 10 minutes. Do not let solution spatter. Insure contact of all surfaces by gently (and carefully) swirling the acid. Let the boats cool. Insure that all of the material is solubilized.

12. Label 2 or 4 bottles with the appropriate filter identification numbers.

13. Tare the first bottle on the top loading balance.

14. Quantitatively transfer the contents of the first boat into the first bottle. Be sure to rinse the underside of the lip of the boat.
NOTE: Many small rinses are better than one large rinse. Use a clean, unused plastic funnel in the transferring process.

15. Set the bottle back on the balance and wash down the funnel until a weight of 25 g is registered. Again note that the funnel should be held out of contact with the bottle.

16. Repeat steps 13-15 for the remaining boats.

PROCEDURE III. YTTRIUM SPIKE

When all of the filters from one outing -- cascade and backup -- have been ashed and dissolved and all extractions completed, the Yttrium spike can be added.

1. Arrange the bottles according to filter sets (5 bottles per set).

2. Open the first bottle.

3. Pipette 50 λ (μl) of the 1000 ppm Yttrium stock solution into the bottle.

4. Cap the bottle and place identifying mark to note fact that Yttrium spiking was done.

5. Repeat steps 2 through 4 for the remaining bottles.

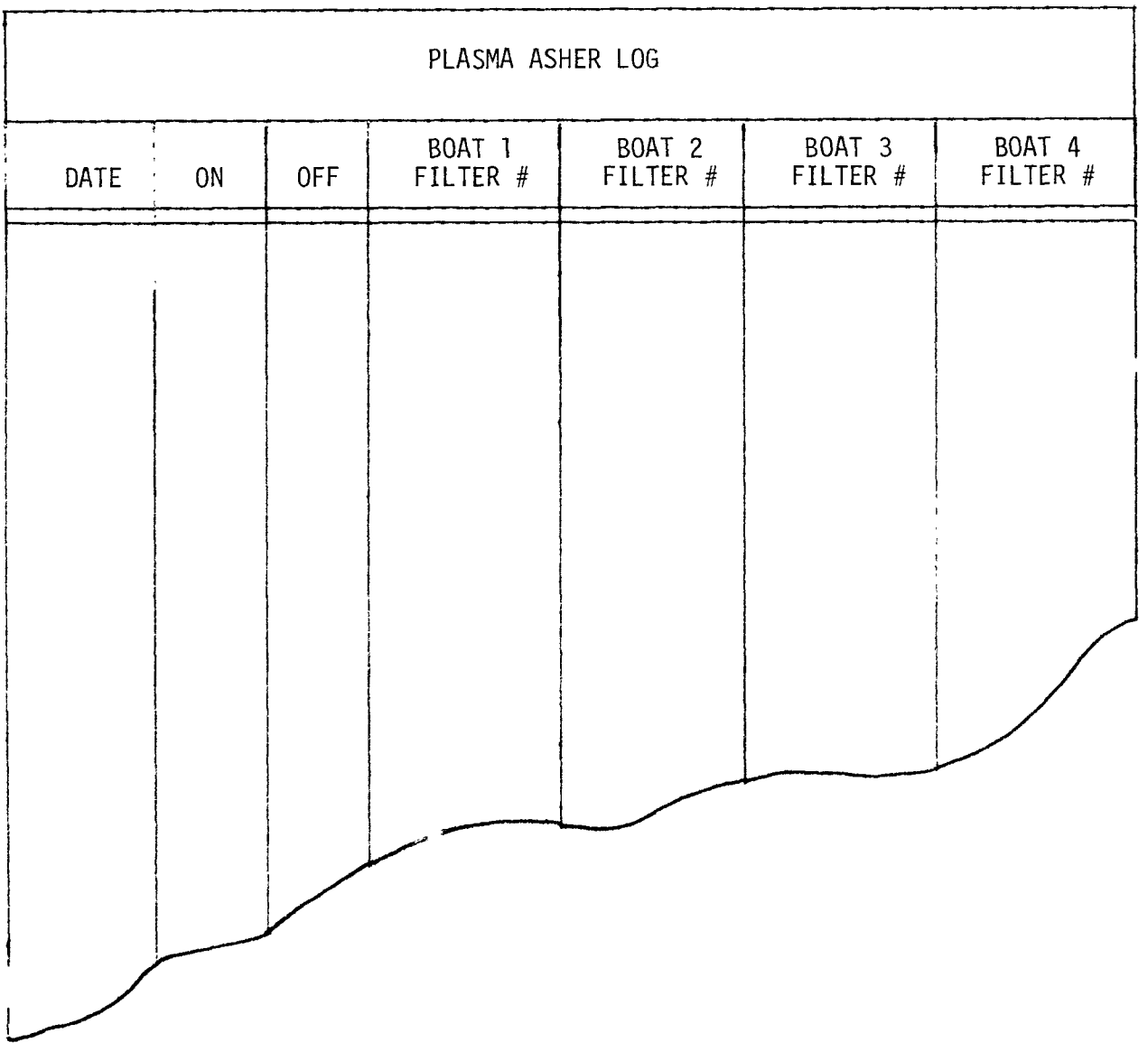

FIGURE D-1. Example of Plasma Asher Log.

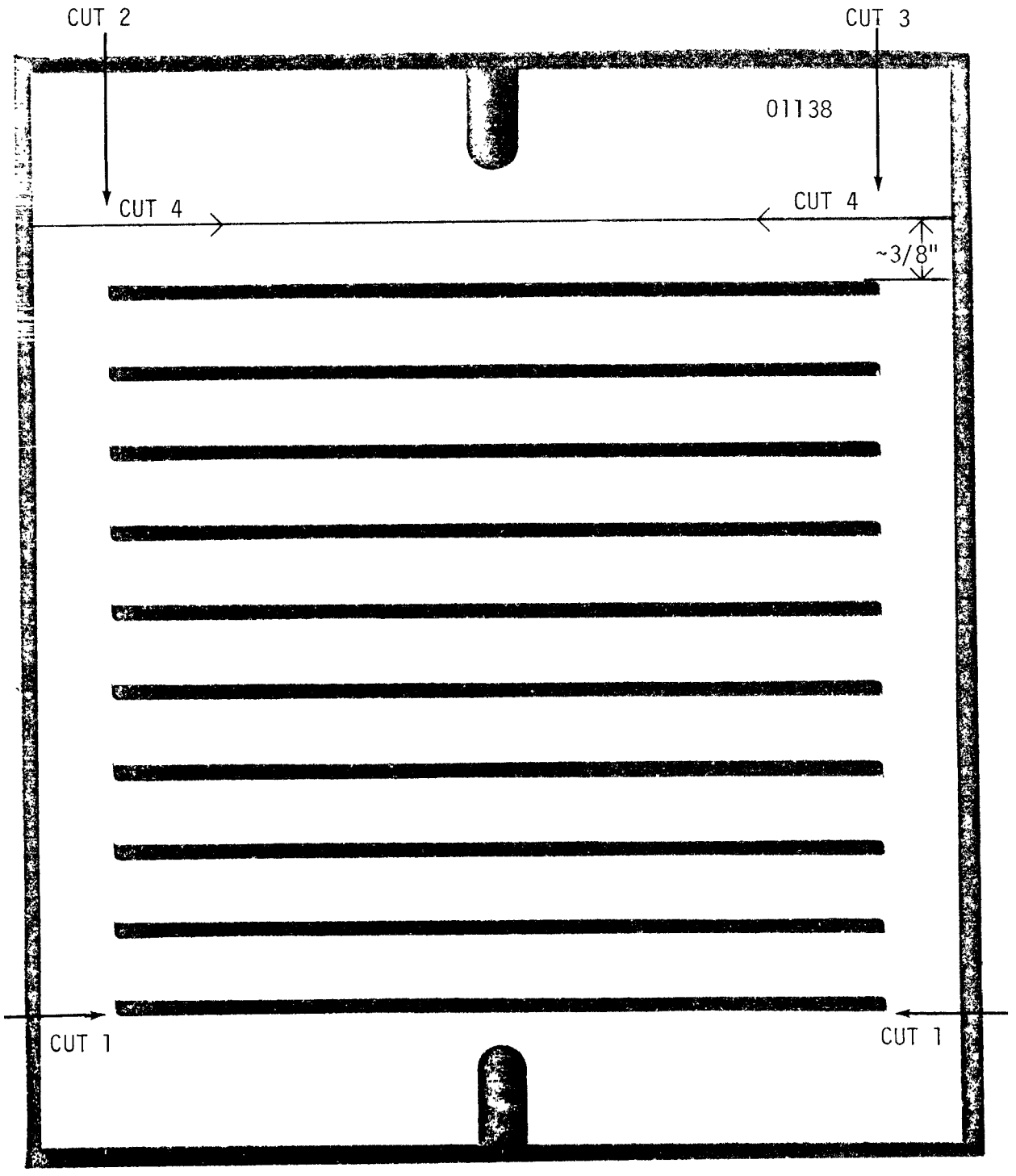

FIGURE D-2. Cuts Made During Preparation of Inertial Cascade Impactor Filter.

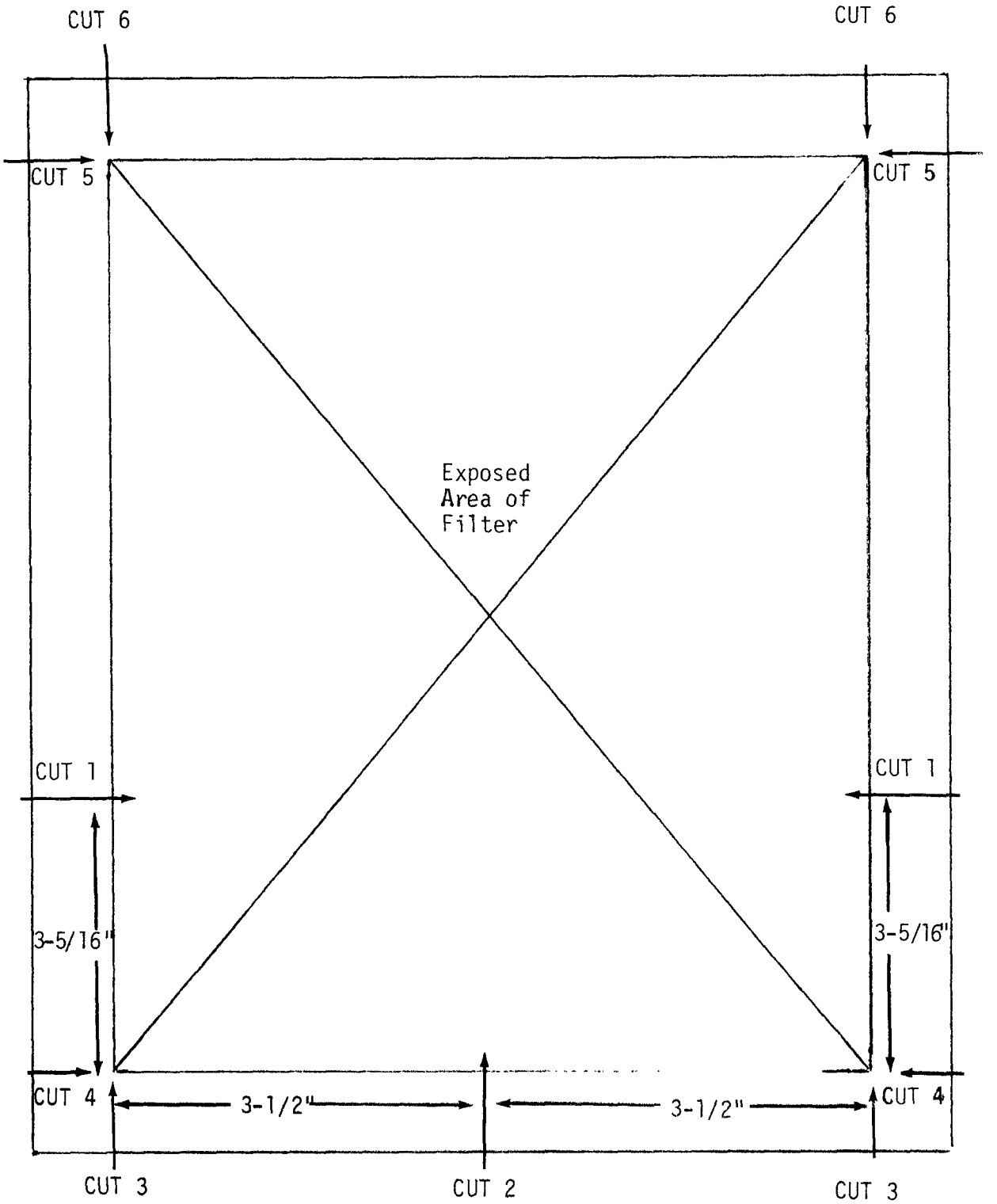

FIGURE D-3. Cuts Made During Preparation of Hi-Volume Filter.

TECHNICAL REPORT DATA
(Please read Instructions on the reverse before completing)

1. REPORT NO. 905/4-79-016	2.
3. RECIPIENT'S ACCESSION NO.	
4. TITLE AND SUBTITLE An Experimental Study of Lake Loading by Aerosol Transport and Dry Deposition in the Southern Lake Michigan Basin	5. REPORT DATE Date of Preparation: July 1979
	6. PERFORMING ORGANIZATION CODE
7. AUTHOR(S) Herman Sievering, Mehul Davé, Donald A. Dolske, Richard L. Hughes, Patric McCoy	8. PERFORMING ORGANIZATION REPORT NO.
9. PERFORMING ORGANIZATION NAME AND ADDRESS College of Environmental & Applied Sciences Governors State University Park Forest South, Illinois 60466	10. PROGRAM ELEMENT NO. 2BA645
	11. CONTRACT/GRANT NO. R00530101
12. SPONSORING AGENCY NAME AND ADDRESS Great Lakes National Programs Office U.S. Environmental Protection Agency, Region V 536 South Clark Street Chicago, Illinois 60605	13. TYPE OF REPORT AND PERIOD COVERED Final 6/1/76 - 7/31/79
	14. SPONSORING AGENCY CODE EPA-OGLNP Office of Great Lakes National Programs

15. SUPPLEMENTARY NOTES
Additional support received from the National Center for Atmospheric Research, Research Aircraft Facility, Boulder, Colorado 80307

16. ABSTRACT

A Lake Michigan experimental program to assess the contribution to Great Lakes loading by atmospheric transport and dry deposition of aerosol was conducted. A midlake and nearshore trace element and nutrients data base with associated meteorology capable of establishing a climatology for mass transfer to Lake Michigan was collected during 1977 and 1978. Significant data for Al, Ca, Cu, Fe, Mg, Mn, Pb, Ti, Zn, total P, NO_3 and SO_4 were obtained. A strong linear dependence upon atmospheric thermal stability in the variability of all twelve aerosol constituents was found, but no linear dependence upon wind speed was found. Source region and wind direction dependence are cause for as much as an order of magnitude variation in concentrations. Aircraft-based meteorological and aerosol data were collected in June and September, 1977 and May, 1978.

Bulk deposition velocities as a function of overlake climatology were used to calculate dry deposition atmospheric loadings to Lake Michigan. Limited aerosol number profile measurements of the deposition velocity confirmed a three-fold or smaller uncertainty in the bulk deposition velocity estimates. Minimum dry deposition loading estimates compared to precipitation and surface runoff show that atmospheric inputs by dry loading are at least 60% for Pb, 30% for Zn and over half the total sulfate and nitrate input. Dry loading of total P is approximately equal to precipitation loading.

17. KEY WORDS AND DOCUMENT ANALYSIS

a. DESCRIPTORS		b. IDENTIFIERS/OPEN ENDED TERMS	c. COSATI Field/Group
GREAT LAKES		Atmospheric Loading	12A
Aerosols	Water Pollution	Dry Deposition	07D
Meteorology	Lake Breeze	Aerosol Spectrometry	10B
Lake Michigan		Nutrients	13B
Trace Elements		ASAS/Knollenberg	
Fallout			
Air Pollution			

18. DISTRIBUTION STATEMENT Release Unlimited	19. SECURITY CLASS *(This Report)* Unclassified	21. NO. OF PAGES
	20. SECURITY CLASS *(This page)* Unclassified	22. PRICE

EPA Form 2220-1 (9-73)

☆ U. S. GOVERNMENT PRINTING OFFICE: 1980-653-168